Modeling, Analysis, and Optimization of Multi-Tier Cellular Networks

by

Ahmed Hamdi Sakr

A Thesis submitted to The Faculty of Graduate Studies of

The University of Manitoba

in partial fulfillment of the requirements for the degree of

Doctor of Philosophy

Department of Electrical and Computer Engineering

University of Manitoba

Winnipeg

January 2017

Abstract

Multi-tier cellular networks have led to a paradigm shift in the deployment of base stations (BSs) where macrocell BSs are overlaid with smaller and lower power BSs such as microcells, picocells, and femtocells. Stochastic geometry has been proven to be an effective tool to capture such heterogeneity and uncertainties in deployment of cellular BSs. In stochastic geometry, random spatial models are used to model multi-tier cellular networks where the locations of BSs is each tier is assumed to be drawn from a point process with the appropriate spatial density. This thesis proposes stochastic geometry-based approaches to analyze, model, and optimize multi-tier cellular networks under several setups and technologies. First, I propose a novel location-aware cross-tier cooperation scheme that aim at improving the performance of users with low signal-to-interference-plus-noise ratio (SINR). Second, I study the performance of cognitive device-to-device (D2D) communication in multi-channel downlink-uplink cellular network with energy harvesting. For the coexistence between cellular and D2D transmissions, I propose a spectrum access policy for cellular BSs to avoid using D2D channels when possible. Third, I investigate the feasibility of energy harvesting from ambient RF interference in multi-tier uplink cellular networks. For this setup, I capture randomness in the network topology and the battery dynamics. Fourth, I extend multi-tier uplink cellular networks to consider the case when users do not necessarily associate with the nearest BS (i.e., flexible cell association). Finally, I compare between different cell association criteria including coupled and decoupled cell association for uplink and downlink transmissions in multi-tier full-duplex cellular networks. For all network setups, I use stochastic geometry to derive simple and

closed-form expressions to evaluate the performance in terms of several metrics, e.g., outage probability, mean rate, transmission probability, success probability, and load per BS. I also highlight main tradeoffs in different networks and provide guidelines to optimize different performance metrics by carefully tuning fundamental network design parameters.

Acknowledgements

All praise and thanks be to Almighty Allah who bestowed upon me guidance and benevolence to complete this work.

First and foremost, I would like to express my sincerest gratitude to my advisor Prof. Ekram Hossain for his continuous support throughout my research. I attribute the level of my work to his patience, encouragement, enthusiasm, and immense knowledge without which this thesis would not have been possible. I could not wish for a better or friendlier advisor and mentor.

Special thanks go to the members of my examination committee, Prof. Sherif Sherif, Prof. Pourang Irani, and Prof. Ben Liang, for their encouragement and insightful comments.

I thank my fellow graduate students in Wireless Communications, Networks, and Services (WiCoNS) research group, specially Hesham ElSawy, for the fruitful discussions and precious suggestions. I thank the staff at Department of Electrical and Computer Engineering, specially Amy Dario. I also thank my friends in Winnipeg for the warmth everyone has shown that made my stay more pleasurable.

I would like to express my gratitude to my mother, father, and brother for allowing me to realize my own potential and supporting me throughout my entire life. I also thank my family and friends for their love and encouragement.

Last but not the least, I must acknowledge my lovely wife and best friend, Eman, without whose love and encouragement I would not have finished this thesis. I also express my gratitude to my son, Ziyad, who added a great value for everything.

Table of Contents

List of Figures

List of Tables

List of Abbreviations

2NT	Two-node topology
3NT	Three-node topology
BS	Base station
CCA	Coupled cell association
CDF	Cumulative distribution function
CoMP	Coordinated multipoint
CSI	Channel state information
D2D	Device-to-device
DCA	Decoupled cell association
DL	Downlink
FC	Full cooperation
FD	Full-duplex
HD	Half-duplex
i.i.d.	Independent and identically distributed
LAC	Location-aware cross-tier cooperation
MAC	Medium access control
MIMO	Multiple-input multiple-output
OFDMA	Orthogonal frequency division multiple access
PDF	Probability density function

PMF	Probability mass function
PPP	Poisson point process
PSA	Prioritized spectrum access
QoS	Quality-of-service
RE	Range expansion
RF	Radio frequency
RSA	Random spectrum access
SI	Self-interference
SIC	Self-interference cancellation
SINR	Signal-to-interference-plus-noise ratio
SIR	Signal-to-interference ratio
UL	Uplink
ZFBF	Zero-forcing beamforming

Publications

- **Book Chapters:**

  1. **A. H. Sakr**, H. Tabassum, and E. Hossain, "Ambient Wireless Energy Harvesting in Small Cell Networks: Performance Modeling and Analysis," book chapter in Wireless-Powered Communication Networks: Architectures, Protocols, and Applications, (Eds. D. Niyato, E. Hossain, D. I. Kim, V. Bhargava, and L. Shafai), Cambridge University Press, 2017.

- **Journal and Magazine Publications:**

  1. **A. H. Sakr**, and E. Hossain, "Location-Aware Cross-Tier Coordinated Multipoint Transmission in Two-Tier Cellular Networks," in *IEEE Transactions on Wireless Communications,* vol. 13, no. 11, pp. 6311–6325, Nov. 2014.

  2. **A. H. Sakr**, and E. Hossain, "Cognitive and Energy Harvesting-Based D2D Communication in Cellular Networks: Stochastic Geometry Modeling and Analysis," in *IEEE Transactions on Communications,* vol. 63, no. 5, pp. 1867–1880, May 2015.

  3. **A. H. Sakr**, H. Tabassum, E. Hossain, and D. I. Kim, "Cognitive Spectrum Access in Device-to-Device (D2D)-Enabled Cellular Networks," in

IEEE Communications Magazine, vol. 53, no. 7, pp. 126–133, July 2015.

4. **A. H. Sakr**, and E. Hossain, "Analysis of K-tier Uplink Cellular Networks with Ambient RF Energy Harvesting," in *IEEE Journal on Selected Areas in Communications,* vol. 33, no. 10, pp. 2226–2238, Oct. 2015.

5. H. Tabassum, **A. H. Sakr**, E. Hossain, and D. I. Kim, "Analysis of Massive MIMO-Enabled Downlink Wireless Backhauling for Full-Duplex Small Cells," in *IEEE Transactions on Communications,* vol. 64, no. 6, pp. 2354–2369, April 2016.

6. **A. H. Sakr** and E. Hossain, "On Cell Association in Multi-Tier Full-Duplex Cellular Networks," submitted to *IEEE Transactions on Communications*.

- **Conference Publications:**

1. **A. H. Sakr**, and E. Hossain, "Energy-Efficient Downlink Transmission in Two-Tier Network MIMO OFDMA Networks," in *Proc. of IEEE International Conference on Communications (ICC) 2014,* Sydney, Australia, 10-14 June 2014, pp. 3652–3657.

2. **A. H. Sakr**, H. ElSawy, and E. Hossain, "Location-Aware Coordinated Multipoint Transmission in OFDMA Networks," in *Proc. of IEEE International Conference on Communications (ICC) 2014,* Sydney, Australia, 10-14 June 2014, pp. 5166–5171.

3. **A. H. Sakr**, and E. Hossain, "Analysis of Multi-Tier Uplink Cellular Networks with Energy Harvesting and Flexible Cell Association," in *Proc. of IEEE Global Communications Conference (Globecom) 2014,* Austin, TX, USA, 8-12 Dec. 2014, pp. 4712–4717.

4. H. Tabassum, **A. H. Sakr**, E. Hossain, and D. I. Kim, "Massive MIMO-enabled wireless backhauls for full-duplex small cells," in *Proc. of IEEE Global Communications Conference (Globecom) 2015, San Diego, CA, USA, 6-10 Dec. 2015, pp. 1–6.*

Chapter 1

Introduction

In modern wireless cellular networks, the data traffic demand is increasing exponentially especially as the number of advanced devices such as smartphones, tablets, laptops, etc. is expected to exceed more than 50 billions by 2020 [1]. At the same time, the link spectral efficiency is approaching its theoretical limit and there is an urgent need for new solutions to address this major challenge. One of the most promising solutions to improve the spectral efficiency (bit/sec/Hz) is the densification of the network by deploying more base stations (BSs) to use the gain of cell splitting and frequency reuse. Unfortunately, deploying more macrocell BSs is infeasible due to high cost and infrastructure complexity. Therefore, several possible approaches have recently attracted significant attention as an alternative to densifying macrocell networks and meet the ever-increasing users' demand. For example, deploying small cells, multi-cell cooperation, device-to-device (D2D) communication, and full-duplex (FD) communication have been proposed to improve the spectral efficiency of the cellular networks. This however poses an important challenge to properly model and analyze modern cellular networks to cope with this paradigm shift in network design. From now on, I refer to networks with both macrocell BSs and small cells or D2D communi-

cation as multi-tier cellular networks in which each class of BSs represents a different tier [2]. In this thesis, I use tools from stochastic geometry to develop tractable yet accurate comprehensive frameworks to better model, analyze, and optimize the key performance metrics in multi-tier cellular networks.

The rest of this chapter is organized as follows. Section 1.1 presents several solutions that aim at improving the spectral efficiency of cellular networks. Section 1.2 summarizes different approaches for modeling and analyzing multi-tier cellular networks. The motivation and key contributions of this thesis are summarized in Sections 1.3 and 1.4. In Section 1.5, mathematical preliminaries on statistical modeling using stochastic geometry are provided. Finally, the organization of the thesis is presented in Section 1.6.

1.1 Solutions to Improve Spectral Efficiency in Cellular Networks

In the last few years, the world has witnessed a rapid evolution of the cellular networks and an increase in the need for higher data rates. This is mainly due to the emergence of several services such as video calling and streaming of high definition videos which require very high data rates to provide mobile users with a satisfying experience. Several solutions have been proposed to meet these requirements by reducing the frequency reuse distance and improving the spectral efficiency of cellular networks. In the following, some of these solutions are presented.

1.1.1 Network Densification

Due to the infeasibility of deploying more macrocell BSs, the introduction of small cells has recently attracted significant attention to densify cellular networks. Typ-

Table 1.1: Comparison among different classes of cells/base stations

Attributes	**Macrocell**	**Picocell**	**Femtocell**
BS Installation	Mobile Operator	Mobile Operator	Mobile Subscriber
Transmission Range	300-2000 m	40-100 m	10-30 m
Transmission Power	40 W (approx.)	200mW- 2 W	10-100 mW
Band License	Licensed band	Licensed band	Licensed band
Transmission Rate	up to 1 Gbps	up to 300 Mbps	100 Mbps-1 Gbps
Power Consumption	High	Moderate	Low

ically, small cells such as femtocells, picocells, and microcells have lower transmit power and deployment cost compared to macrocell BSs. Small cells can achieve high data rates and better coverage and reliability by reducing the distance between a user and the serving BS and eliminating coverage holes. The different network tiers operate simultaneously in the same geographical area and may differ in transmit power, coverage range, supported data rate, channel access protocol, and spatial density. Hence, referred to as multi-tier cellular networks.

Figure 1.1 shows an example for a multi-tier network consisting of three different tiers with macrocell, picocell, and femtocell BSs. It can be seen that the coverage area varies from one BS to another due to the differences in transmission power where in typical scenarios the transmit power of a macrocell BS can be up to 1000 times higher than that of a small cell. Note also that, in practical scenarios, macrocell BSs are deployed by the operator in a planned manner while small cells with irregular coverage areas such as femtocell BSs are deployed randomly by the end user. Table 1.1 provides a comparison between the different classes of BSs including macrocell, picocell, and femtocell BSs.

The motivations of using small cells such as femtocells and picocells in a multi-tier network architecture can be providing high data rate and improved quality-of-services to subscribers, eliminating coverage holes in macrocell footprint, improving energy efficiency of communication and extend the battery life of mobile phones, reduce

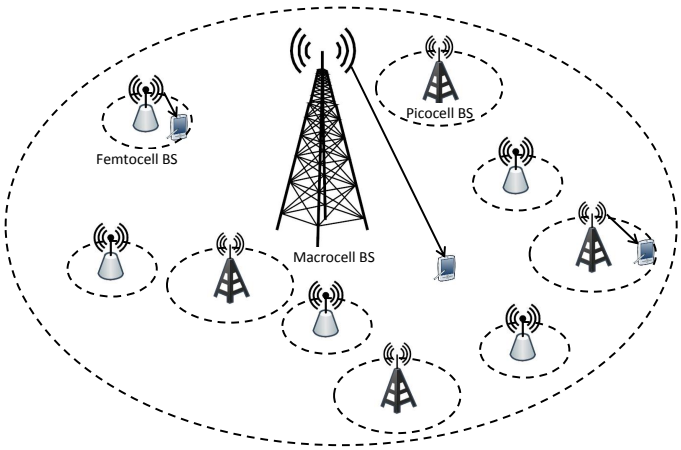

Figure 1.1: A multi-tier cellular network with a macrocell network which is overlaid with lower power and denser picocell and femtocell BSs where dashed lines show the coverage area of each cell.

traffic load in macrocell BSs, hence more resources are available for for macrocell users, and mitigating spectrum underutilization problem.

1.1.2 Multi-Cell Cooperation

With the deployment of multiple network tiers, many fundamental challenges that affect the network performance in terms of coverage and throughput are arising. Interference management (i.e., development of methods to mitigate co-tier and cross-tier interference) is one of the major challenges in multi-tier networks. For example, macrocell users located in the close vicinity of a small cell may be victimized by transmissions to small cell users and vice versa. The concept of multi-cell cooperation among multiple tiers has been proposed as a solution to mitigate the cross-tier interference resulting from the deployment of small cells and to improve the spectral efficiency of the multi-tier cellular networks [3, 4]. For example, coordinated multipoint (CoMP) transmission (also referred to as network MIMO) is a form of cooperation in which multiple BSs communicate with each other to cancel out the

interference and improve the overall system performance by jointly transmitting the users' data concurrently [5–8]. In multi-tier cellular networks, CoMP can be exploited to achieve high gain of the universal frequency reuse. For example, Figure 1.2 shows a scenario in which a macrocell BS and a picocell BS are cooperating to simultaneously serve a macrocell user who is very close to the coverage area of the picocell in order to mitigate the effect of the cross-tier interference resulting from that picocell BS.

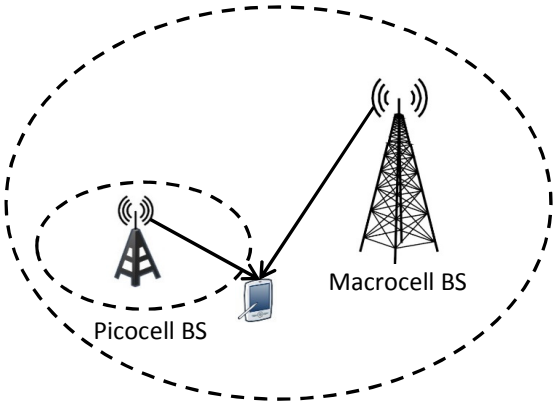

Figure 1.2: An example of multi-cell cooperation with a macrocell BS and a picocell BS cooperating to jointly serve a single user.

1.1.3 Device-to-Device Communication

Device-to-device (D2D) communication is another promising concept to maximize the utilization of radio resources in cellular networks and improve the overall spectral efficiency of the system. In D2D communication, devices in proximity of each other can establish a direct communication link without connecting through their corresponding BS [9, 10]. In other words, D2D communication enables single-hop communication instead of dual-hop uplink and downlink communication. This also enhances the latency and power consumption of D2D users. In addition, it improves the cellular networks performance in terms of coverage and spectral efficiency by im-

proving the spectrum reuse and reduce the load per BS by offloading users to the D2D mode. For example, Figure 1.3 shows an illustration of a cellular network with a macrocell BS that is overlaid with D2D network in which D2D users form pairs or clusters to exchange data. D2D communication underlaying a cellular network can be seen as another network tier, hence, constitutes a multi-tier cellular network.

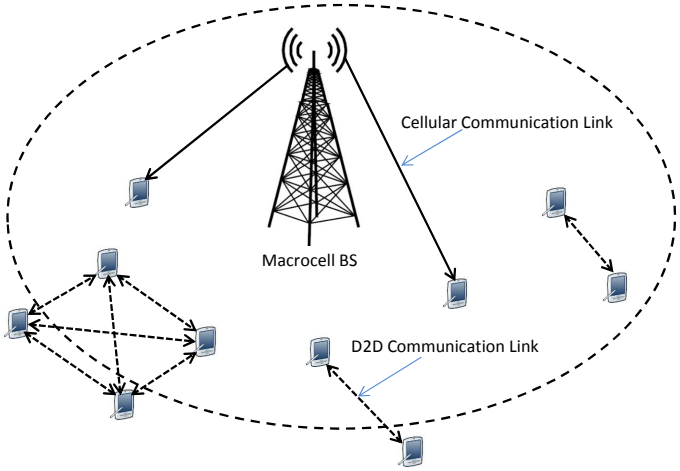

Figure 1.3: An example of a D2D-based networks as an underlay to a cellular network.

One of the main challenges in D2D communication is channel and power allocations especially when the radio resources are shared between the D2D devices and cellular BSs. In addition, both D2D and cellular networks should be protected from interfering to each other to achieve high performance gains. In general, D2D communication can be enabled in a cellular network in three possible ways, namely, D2D-unaware, D2D-aware, and network-controlled D2D transmissions [11]. In D2D-unaware transmissions, D2D users exchange control and data packets between each other with no intervention from the cellular BS. That is, the cellular BS does not have any supervision over the radio resources used by the D2D pairs (e.g., power control and spectrum allocation) and no coordination exists between D2D and cellular transmissions. On the other hand, in D2D-aware transmissions, the cellular BS

perform limited supervision of D2D transmissions for better coordination with the concurrent cellular transmissions. Nonetheless, this supervision is limited in terms of information exchange and signaling overheads. D2D users can possibly decide their mode of operation (i.e., D2D or cellular mode) and the radio resources for data transmission. In network-controlled D2D transmissions, a cellular fully controls the radio resources management of all cellular and D2D users in a cell. This scenario enables the network to make perfect coordination between cellular and D2D users which may require large amount of information exchange and signaling overheads. Moreover, a D2D pair cannot establish a communication link without initiating a request and the approval of request from the cellular BS. The aforementioned scenarios offer trade-offs in terms of performance and complexity of implementation.

1.1.4 Full-Duplex Communication

In-band full-duplex (FD) communication has recently attracted significant attention as a potential enabler for modern cellular networks to support higher data rates and meet the ever-increasing user demand for broadband wireless services. In contrast to half-duplex (HD) communications in which a time-frequency resource block is only used for either transmission or reception, in-band FD communication implies simultaneous transmission and reception of information in the same frequency band [12, 13]. The main challenge for this solution is that it introduces extra interference between uplink and downlink networks which affects the network performance gains especially for uplink transmissions that suffer from excessive downlink-to-uplink interference [14]. The performance of FD networks is also limited by the capability of network terminals (e.g., user devices and BSs) to cancel self-interference (SI), which results from their own transmitter to their own collocated receiver. Fortunately, this

technology is becoming feasible thanks to the recent advancements in antenna and digital baseband technologies where SI can be reduced close to the level of noise floor in low-power devices [15].

1.2 Modeling of Multi-Tier Cellular Networks

The signal-to-interference-plus-noise ratio (SINR) is one of most important performance metrics for the analysis of wireless networks. For example, in order to correctly decode received information, the SINR is required to exceed some predefined threshold. In addition, the SINR is directly related to most of many of the main performance metrics such as coverage probability, spectral efficiency, and energy efficiency. The coverage probability of a network is defined as the probability that the SINR at the receiver is greater than a predefined threshold. Note that coverage is the complementary event of the outage. On the other hand, spectral efficiency is defined as the number of data bits that can be successfully transmitted in a certain communication link per second per unit bandwidth (i.e., bit/sec/Hz or bps/Hz). Energy efficiency is defined as the number of data bits that can be successfully transmitted per unit energy or equivalently the data rate per unit power (i.e., bit/Joule or bps/Watt).

Based on the aforementioned relation, it is crucial during the modeling phase of a cellular network to obtain expressions for the SINR that take into account the system characteristics while being tractable and simple as possible. Therefore, different approaches have been considered in the literature to address this challenge under different assumptions. For example, Wyner model has been used in the literature to model single-tier networks and provide expressions for the different system performance metrics [16]. In this model, the network geometry (i.e., locations of BSs) is completely ignored such that the interference level is constant over the entire cell.

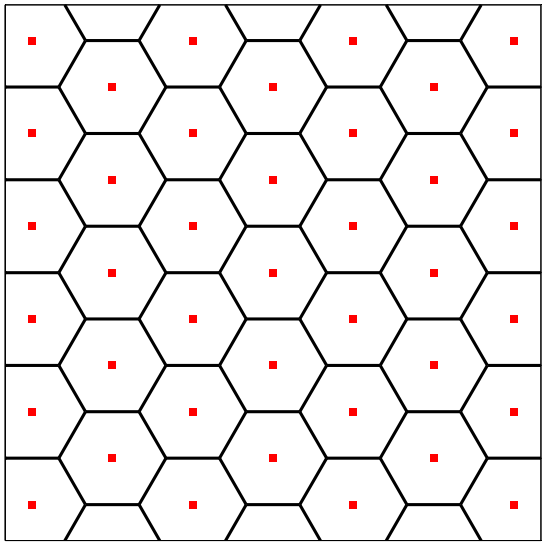

Figure 1.4: A single-tier macrocell network with hexagonal grid model. Solid black lines show the coverage area of each cell.

Due to these very simplistic assumptions, the resulting expressions are not accurate in general and not many insights can be obtained.

Another popular model in the literature for modeling cellular networks is the hexagonal grid model. In this model, the coverage areas of all BSs are assumed to be regular and the distance between neighboring BSs are equal as shown in Figure 1.4. It can be seen that this model does not capture the network topology where the assumption made for the locations of the BSs is too idealistic. In addition, closed-form expressions for the different network performance metrics are very hard to obtain when adopting such model. In most cases, the deterministic grid-based models are only used for system-level simulation.

Even for single-tier networks, both models deviate from the actual deployment of BSs in which BSs do not follow a regular model. In addition, models such as hexagonal grid and Wyner models are not suitable in the context of multi-tier networks due to the uncertainties and randomness of the network topology. This is especially due to

the increase in the spatial density of network elements brought by the deployment of small cells such as picocells and femotcells. Motivated by the impact of randomness of the network topology on the accuracy of the obtained insights, the main challenge now is to adopt other modeling tools that are topology-aware and able to capture this randomness while providing simple, accurate, and tractable expressions of the performance metrics.

Stochastic geometry has been extensively used to model multi-tier cellular networks while capturing the uncertainties in the locations of the BSs of different networks tier by modeling each tier by an appropriate spatial point process [17–28]. Most importantly, it has been shown that stochastic geometry-based modeling can provide tractable and accurate expressions with closed-form expressions for many performance metrics such as coverage, data rate, and energy efficiency compared to deterministic and grid-based models. For example, Figure 1.5 shows a realization of a single-tier cellular network where the locations of macrocell BSs are drawn from a Poisson point process (PPP). Furthermore, Figure 1.6 illustrates how stochastic geometry is powerful tool to model multi-tier cellular networks. Without loss of generality, Figure 1.6 shows a two-tier cellular network where the macrocell network shown in Figure 1.5 is overlaid with a denser and lower power picocell network tier where each tier is modeled by an independent PPP.

1.3 Motivation and Objective

The deployment of small cells and D2D communication to improve cellular networks performance has introduced one of the main challenges which is the spectrum allocation and interference management [29]. For example, different network tiers in a multi-tier cellular network can use different spectrum bands (i.e., orthogonal or non-

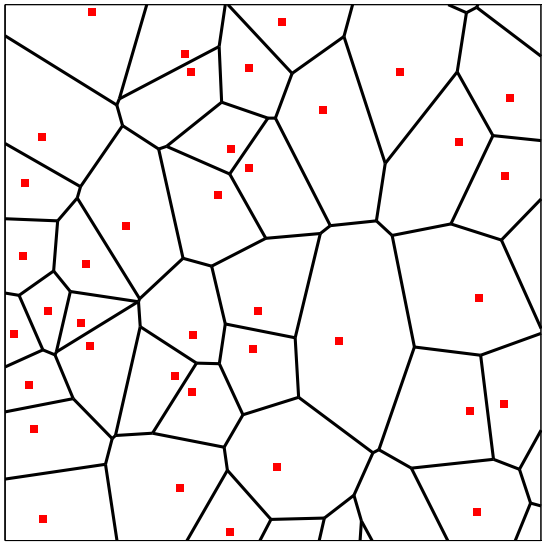

Figure 1.5: A single-tier macrocell network with random spatial model. Solid black lines show the coverage area of each cell.

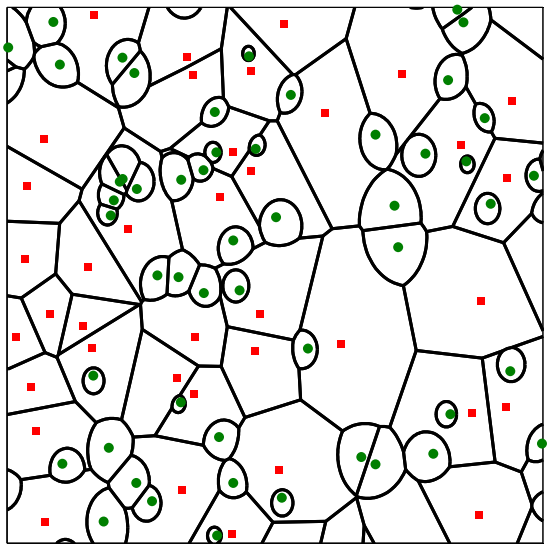

Figure 1.6: A two-tier cellular network with the macrocell network shown in Figure 1.5 overlaid with lower power and denser picocell BSs (green circles). Solid black lines show the coverage area of each cell.

overlapping spectrum allocation). Although this option for small cell deployment can eliminate interference among the different network tires, it is not efficient from the

viewpoint of radio spectrum utilization. On the other hand, with a co-channel deployment (i.e., overlapping spectrum allocation) where different network tiers use the same spectrum band, the utilization of radio spectrum can be improved. However, intelligent interference management methods will be required in this case. A partially overlapping spectrum allocation can also be used to provide a balance between spectrum utilization and other network performance measures such as coverage and throughput.

Another challenge in multi-tier cellular networks is the increase in energy consumption due to the deployment of more BSs to satisfy the ever-increasing user demand. This increase significantly contributes to the global greenhouse gas emissions [30]. Therefore, energy efficiency is considered as important as system spectral efficiency and needs to be considered during the design phase for cellular networks. To improve energy efficiency of multi-tier cellular networks, several solutions such energy harvesting has recently emerged as a promising technology. In energy harvesting, different network elements such as the mobile phones and the small cell BSs are enabled to harvest energy from nontraditional sources such as solar power, wind, and ambient RF interference to power wireless communication devices [31–33]. Such a novel scheme can be used by the operator in order to maximize the energy efficiency and minimize the power consumption in cellular networks. While energy harvesting is a potential solution to improve energy efficiency of cellular networks, techniques such as multi-cell cooperation and D2D communication have emerged as promising solution that improve both spectrum efficiency and energy efficiency.

Modeling, analysis, and optimization of multi-tier networks in presence of these new technologies and interference management methods is fundamental for practical design and deployment of such networks. With the large-scale deployment of many

tiers of BSs, the number and locations of small cells become random and irregular, hence, the models of modern cellular networks shift from the conventional regular grid-based models such as the hexagonal grid model as shown in the previous sections. Since modeling is required for analysis and design of cellular networks, a network operator should use a proper modeling tool that can capture the randomness and irregularity of BS deployment. After the modeling phase, a network designer needs to analyze and optimize the network parameters in order to provide a quality-of-service (QoS) guarantee to the users while meeting certain constraints imposed by either the operator policy, national regulations, or any other requirements. This can be done by carefully tuning the different network parameters to balance the tradeoffs between different key performance metrics such as coverage, data rate, delay, interference, etc. and observe how these metrics change in response to such variations.

Therefore, the main focus of this thesis is to develop accurate yet tractable frameworks to model multi-tier cellular networks while taking into account the topological randomness and network geometry. Throughout this work, I use stochastic geometry as the tool for statistical modeling of multi-tier cellular networks [34–38]. I consider different setups and technologies for multi-tier cellular networks such as multi-tier cooperation, cognitive channel access, energy harvesting, D2D communication, and FD communication. In addition, I aim at using the developed system models to analyze the network performance in terms of different performance metrics in order to optimize the network design process to satisfy different users' requirements.

1.4 Scope and Contributions

In this thesis, I develop novel models for performance analysis and optimization of multi-tier cellular networks in presence several emerging technologies to improve the

overall spectral efficiency. I use a statistical approach based on stochastic geometry to capture the uncertainties and irregularity of multi-tier networks and to develop comprehensive analytical frameworks to model these technologies. The frameworks enable us to evaluate the performance of the proposed system models in terms of coverage probability, achievable data rate, network load, etc. The results from the analysis help us to understand the impact of varying network parameters (such as spatial densities of BSs and user, transmit power, number of channels, receiver sensitivity, etc.) on the performance measures and provide insightful guidelines for system design. The main contributions are summarized as follows.

- **Multi-tier cooperation:** I propose a novel interference management location-aware cross-tier cooperation (LAC) scheme between BSs in different tiers for downlink CoMP transmission in multi-tier cellular networks in Chapter 2. On one hand, the proposed scheme allows cooperation only to enhance the performance of users who suffer from high cross-tier interference due to the co-channel deployment of small cells. On the other hand, users with good SINR conditions are served directly by a single BS. Thus, the data exchange between the cooperating BSs can be reduced. I evaluate the performance of the proposed scheme in terms of the outage probability, average rate, and load per BS as the key performance metrics. Using stochastic geometry, I derive closed-integral form expressions for these metrics. I also compare the proposed scheme with other schemes in the literature such as range expansion, full cooperation, as well as non-cooperative transmission. I study the performance of different schemes under different system setups by varying the BS spatial density, amount of cooperation, and required QoS. I show that the proposed LAC scheme improves the network coverage and achievable spectral efficiency while considering the

load of macrocell BSs.

- **D2D communication with energy harvesting and cognitive radio access:** In Chapter 3, I study D2D communication as an additional network tier when underlaying a multi-channel cellular network. I address two main challenges in such networks which are interference management and energy efficiency. For the first challenge, D2D users are proposed to use cognitive spectrum access such that each D2D transmitter performs spectrum sensing before transmission to opportunistically access a predefined channel and to make sure that this channel is not being used for cellular communication. In a multi-channel environment, I also propose two different spectrum access policies for the macrocell BSs, namely, random spectrum access (RSA) and prioritized spectrum access (PSA) policies, to enable the coexistence of the cellular and D2D users. In addition, I propose D2D users to be restricted to use only the harvested RF energy from the ambient interference that results from the concurrent cellular uplink and downlink transmissions. This in turn improves the energy efficiency which is now seen as important as system spectral efficiency in order to reduce the global greenhouse gas emissions. For a general path-loss exponent, I provide a tractable analytical framework for statistical analysis of the proposed system and I derive simple and closed-form expressions for the probability of harvesting sufficient energy, the probability that the channel to be used by D2D users is free, the SINR outage probability for both D2D and cellular users, and the overall outage probability for D2D users. I discuss several variations of the proposed system such as (i) both cases when D2D transmissions take place in a channel assigned for downlink cellular transmissions or uplink cellular transmissions, (ii) macrocell BSs are adopting RSA or PSA access policies. I define the

operation conditions in which uplink channels are preferable to downlink channels and vice versa. More specifically, I derive a closed-form expression for the value of the BS density after which uplink channels should be used to achieve a better performance when compared to using downlink channels. Finally, I show that provisioning of multiple channels can be used along with cognition by D2D users to protect the cellular transmissions while enabling D2D communication.

- **Energy harvesting for cellular uplink users:** Due to the limited battery of mobile devices, I study the feasibility of harvesting energy from the ambient RF interference in multi-tier uplink cellular networks in Chapters 4 and 5. Under channel inversion power control, I derive a closed-form expression for the coverage probability of cellular users who have no other sources of energy except energy harvesting. In Chapter 4, I use the steady-state probability analysis of Markov chains to derive simple expressions for the probability of successful transmission while capturing battery dynamics. In Chapter 5, I extend the results on energy harvesting to consider flexible cell association in multi-tier uplink cellular networks. Then, the proposed framework is used to derive several special cases and models in the literature. I highlight different tradeoffs in the system by showing the effect of varying network parameters such as spatial densities of BSs, sensitivity of the receivers, and bias factors on the system performance. Finally, I show that energy harvesting is a feasible solution to power up cellular devices while providing an acceptable performance for uplink cellular networks.

- **Optimal cell association in FD cellular networks:** In Chapter 6, I present an analytical framework to analyze multi-tier FD cellular networks with decoupled cell association. I derive the mean interference received at both uplink

and downlink under weighted path-loss cell association. I also derive the mean transmission rates in FD, HD downlink, and HD uplink networks as well as the mean transmission rate of legacy nodes with only HD capabilities in a multi-tier FD network. I formulate and solve an optimization problem to maximize the mean rate of the FD network by jointly optimizing the uplink and downlink cell association criteria. Furthermore, I investigate the effect of imperfect self-interference cancellation (SIC) and show that there exist minimum required SIC capabilities for BSs and users for which FD networks are preferable to HD networks. In addition, I discuss several special cases and provide guidelines on the possible extensions of the proposed framework. Finally, I show that decoupled cell association outperforms coupled cell association in which users associate to the same BS for both uplink and downlink transmissions.

1.5 Mathematical Preliminaries

Throughout this work, I use stochastic geometry to model the multi-tier networks under consideration. In particular, the locations of BSs belonging to a specific tier are assumed to be drawn from an independent and homogeneous Poisson point process (PPP) in the two-dimensional Euclidean space $\mathbb{R}^2$. Homogenous PPP is one of the simplest point processes and can be characterized by two properties:

- For any two disjoint areas, the numbers of points falling within the two regions are independent random variables.
- The expected number of points N falling within a region $\mathbf{A} \subset \mathbb{R}^2$ is distributed according to a Poisson random variable, i.e.,

$$\mathbb{P}\{\mathbf{A} = k\} = \frac{(\lambda L(\mathbf{A}))^k \exp\left[-\lambda L(\mathbf{A})\right]}{k!} \tag{1.1}$$

where λ is the spatial density of the PPP measured in number of points in unit area and $L(\mathbf{A})$ is the Lebesgue measure which is equivalent to the area of $\mathbf{A}$.

For example, Figure 1.6 shows a two-tier network where the locations of both macrocell and picocell BSs are sampled from two independent PPPs with spatial densities $(0.5^2\pi)^{-1}$ and $2 \times (0.5^2\pi)^{-1}$ BS/km^2, respectively. That is, the locations of BSs in the k-th tier are modeled by a PPP $\mathbf{\Phi}_k = \{x_i : i = 1, 2, \dots\} \in \mathbb{R}^2$ with certain spatial density λ_k where x_i denotes the location of the i-th BS.

1.5.1 Analysis of SINR

For the network in Figure 1.6, it is assumed that each tier has different transmit powers such that BSs belonging to the same tier $k \in \{1, 2\}$ have the same transmit power P_k. For a communication link in the network, a signal transmitted by a network node (i.e., BS or user) is subject to both large-scale and small-scale fading. Large-scale fading results from the signal attenuation over distance and is modeled as a distance-dependent path-loss with a rate of $r^{-\alpha}$ where $\alpha > 2$ is the path-loss exponent and r is the propagation distance. As for small-scale fading, transmitted signals are assumed to experience independent Rayleigh fading where the channel power gains are modeled by independent exponential random variables with some arbitrary mean.

Hence, for a user located at a generic point $y \in \mathbb{R}^2$ and served by BS $x_\circ$ from tier k, the SINR of the downlink (i.e., transmission link from the BS down to the user) can be expressed as

$$\mathrm{SINR}(y) = \frac{P_k h(x_\circ, y) \|x_\circ - y\|^{-\alpha}}{\sum_{i=1}^{2} P_i \sum_{x \in \mathbf{\Phi}_i \setminus \{x_\circ\}} h(x, y) \|x - y\|^{-\alpha} + \sigma^2} \tag{1.2}$$

where $h(x, y) \sim \mathrm{Exp}(1)$ is an exponential random variable with unit mean to model

the fading over each channel between two locations x and y, and $\|\cdot\|$ denotes the Euclidean distance. Note that the numerator in (1.2) represents the useful power received at the user. One the other hand, the first term in the denominator represents the aggregate interference resulting from both tiers excluding the serving BS while the second term σ^2 is the variance of the additive noise at the receiver.

As can be seen in (1.2), channel gains as well as distances between a user and BSs are random variables, hence, SINR is also a random variable. Therefore, the coverage probability $\mathcal{C}$ defined in Section 1.2 for a user located at y can be expressed as follows

$$\mathcal{C}(\tau) = \mathbb{E}\left[\mathbb{P}\left[\mathrm{SINR}(y) > \tau\right]\right] \tag{1.3}$$

where a user is said to be in outage when the received SINR falls below a given threshold τ. Note that the expectation in (1.3) is taken with respect to the channel gains and locations of users and BSs (i.e., network geometry). Note also that τ is a design parameter and it should be chosen carefully to satisfy certain QoS requirements of users. Consequently, the outage probability can be expressed as

$$\begin{aligned}\mathcal{O}(\tau) &= \mathbb{E}\left[\mathbb{P}\left[\mathrm{SINR}(y) \leq \tau\right]\right] \\ &= 1 - \mathcal{C}(\tau).\end{aligned} \tag{1.4}$$

Furthermore, the SINR in (1.2) and Shannon formula can be used to obtain the average spectral efficiency (or data rate) of a user located at y as follows

$$\begin{aligned}\mathcal{R} &= \mathbb{E}\left[\mathbb{E}_{\mathrm{SINR}}\left[\log_2(1+\mathrm{SINR}(y))\right]\right] \\ &= \mathbb{E}\left[\int_{\mathbb{R}^+} \mathbb{P}\left[\log_2(1+\mathrm{SINR}(y)) > t\right]\, \mathrm{d}t\right]\end{aligned}$$

$$= \mathbb{E}\left[\int_{\mathbb{R}^+} \mathbb{P}\left[\text{SINR}(y) > 2^t - 1\right] \, \mathrm{d}t\right]$$
$$\stackrel{(a)}{=} \mathbb{E}\left[\int_{\mathbb{R}^+} \mathcal{C}(2^t - 1) \, \mathrm{d}t\right] \tag{1.5}$$

where the spectral efficiency is measured in bit/sec/Hz (or bps/Hz) and data rate is measured in bit/sec.

An alternative definition for the rate coverage is

$$\begin{aligned}\mathcal{R}(\tau) &= \mathbb{P}[\text{SINR}(y) > \tau] \log_2(1+\tau) \\ &= \mathcal{C}(\tau) \log_2(1+\tau)\end{aligned} \tag{1.6}$$

which corresponds to a fixed data rate transmission when the SINR of the communication link exceeds the predefined thresholds τ, otherwise, the transmission rate is zero. It is also measured in bit/sec/Hz.

In addition, the system energy efficiency in bit/Joule (or equivalently bps/Watt) can be defined as follows

$$\mathcal{E} = \frac{\mathcal{R}}{P_T} \tag{1.7}$$

where $\mathcal{R}$ is the average spectral efficiency given in (1.5) and P_T is the total power consumption.

1.5.2 Analysis of Coverage Probability

From (1.5)(a) and (1.7), it is clear that several metrics are directly related to the coverage probability expressed in (1.3). Therefore, deriving the coverage probability is of a great interest in order to provide insights about the performance of cellular

networks. Let us rewrite the SINR in (1.2) as follows

$$\mathrm{SINR}(y) = \frac{P_k h(x_\circ, y) R_\circ^{-\alpha}}{\mathcal{I} + \sigma^2} \tag{1.8}$$

where $R_\circ = \|x_\circ - y\|$ is the length of the communication link between the generic user and her serving BS and $\mathcal{I}$ is the aggregate interference received at the user, i.e.,

$$\mathcal{I} = \sum_{i=1}^{K} P_i \sum_{x \in \mathbf{\Phi}_i \setminus \{x_\circ\}} h(x, y) \|x - y\|^{-\alpha}. \tag{1.9}$$

Under Rayleigh fading assumption, using (1.3), the coverage probability can be derived as follows

$$\begin{aligned}
\mathcal{C}(\tau) &= \mathbb{P}\left[\frac{P_k h(x_\circ, y) R_\circ^{-\alpha}}{\mathcal{I} + \sigma^2} > \tau\right] \\
&= \mathbb{P}\left[h(x_\circ, y) > \frac{\tau(\mathcal{I} + \sigma^2)}{P_k R_\circ^{-\alpha}}\right] \\
&\overset{(b)}{=} \int_{\mathbb{R}_+} \exp\left[-\frac{\tau(i + \sigma^2)}{P_k R_\circ^{-\alpha}}\right] f_{\mathcal{I}}(i) di \\
&= \mathbb{E}_{\mathcal{I}}\left[\exp\left[-\frac{\tau(i + \sigma^2)}{P_k R_\circ^{-\alpha}}\right]\right] \\
&\overset{(c)}{=} \exp\left[-\frac{\tau\sigma^2}{P_k R_\circ^{-\alpha}}\right] \mathcal{L}_{\mathcal{I}}\left(\frac{\tau}{P_k R_\circ^{-\alpha}}\right)
\end{aligned} \tag{1.10}$$

where (b) follows from $h(x_\circ, y) \sim \mathrm{Exp}(1)$ and $f_{\mathcal{I}}(\cdot)$ is the PDF of the aggregate interference and (c) follows from the definition of Laplace transform. Using the independence assumption across interfering network tiers in (1.9), Laplace transform of the PDF of the interference in (1.10)(c) can be expressed as

$$\mathcal{L}_{\mathcal{I}}\left(\frac{\tau}{P_k R_\circ^{-\alpha}}\right) = \prod_{i=1}^{K} \mathcal{L}_{\mathcal{I}_i}\left(\frac{\tau}{P_k R_\circ^{-\alpha}}\right) \tag{1.11}$$

where $\mathcal{L}_{\mathcal{I}_i}(\cdot)$ is the Laplace transform of the PDF of the interference resulting from downlink transmissions of tier i.

Assume that each user associates with the BS that results in the maximum average received power, i.e., $P_k R_\circ^{-\alpha} \geq P_i R_i^{-\alpha}$ for $i \in \{1, 2, \ldots, K\}$ where R_i is the distance to a BS from the i-th tier. Without loss of generality, I calculate the Laplace transform $\mathcal{L}_{\mathcal{I}_i}(s)$ as follows

$$\begin{aligned}
\mathcal{L}_{\mathcal{I}_i}(s) &= \mathbb{E}_{\mathcal{I}_i}\left[\exp\left[-s\mathcal{I}_i\right]\right] \\
&\overset{(d)}{=} \mathbb{E}_{\mathbf{\Phi}_i,\{h\}}\left[\exp\left[-sP_i \sum_{x\in\mathbf{\Phi}_i\setminus\{x_\circ\}} h(x,y) R_i^{-\alpha}\right]\right] \\
&\overset{(e)}{=} \mathbb{E}_{\mathbf{\Phi}_i}\left[\prod_{x\in\mathbf{\Phi}_i\setminus\{x_\circ\}} \mathbb{E}_{\{h\}}\left[\exp\left[-sP_i h(x,y) R_i^{-\alpha}\right]\right]\right] \\
&\overset{(f)}{=} \mathbb{E}_{\mathbf{\Phi}_i}\left[\prod_{x\in\mathbf{\Phi}_i\setminus\{x_\circ\}} \frac{1}{1+sP_i R_i^{-\alpha}}\right] \\
&\overset{(g)}{=} \exp\left[-2\pi\lambda_i \int_z^\infty \left(1 - \frac{1}{1+sP_i r^{-\alpha}}\right) r\,\mathrm{d}r\right]. \qquad (1.12)
\end{aligned}$$

In (1.12), (d) follows from defining $R_i = \|x - y\|$, (e) follows from the independence across channel fading gains of interfering links, (f) follows from the moment generating function of an exponential random variable with parameter 1, while (g) follows from (i) the PPP assumption and the probability generating functional of a PPP [28] and (ii) the maximum received power association criteria such that $z = \left(\frac{P_i}{P_k}\right)^{\frac{1}{\alpha}} R_\circ$ is the minimum distance to an interfering BS from tier i.

Combining (1.10)-(1.12), the coverage probability can be expressed as follows

$$\mathcal{C}(\tau) = \mathbb{E}\left[\exp\left[-\frac{\tau\sigma^2}{P_k R_\circ^{-\alpha}}\right] \exp\left[-2\pi \sum i = 1^K \lambda_i \int_{\left(\frac{P_i}{P_k}\right)^{\frac{1}{\alpha}} R_\circ}^\infty \frac{sP_i u^{1-\alpha}}{1+sP_i u^{-\alpha}}\,\mathrm{d}u\right]\right] \quad (1.13)$$

where the expectation is with respect to $R_\circ$, distance of a generic user to the serving BS, whose PDF $f_{R_\circ}(r)$ can be derived based on the association criteria and PPP assumption. Throughout this thesis, variations of the procedure described above are used to derive performance metrics under several network setups.

1.6 Organization

In Chapter 2, I present a novel location-aware cooperation scheme that incorporates the locations of both users and BSs in the selection of users' mode of operation in multi-tier cellular networks. In Chapter 3, I study the performance of D2D-based cellular networks with energy harvesting from the ambient RF interference power and cognitive spectrum access. Chapter 4 investigates the feasibility of exploiting energy harvesting in multi-tier uplink cellular networks where users are solely powered by harvesting energy. In chapter 6, I present a modeling framework for FD communication in multi-tier networks with focusing on the problem of cell association. Finally, the thesis is concluded in Chapter 7 where the key contributions are summarized.

Chapter 2

Location-Aware Cross-Tier Cooperation in Multi-Tier Cellular Networks

In this chapter, I propose a novel scheme for location-aware cross-tier cooperation (LAC) between BSs in different tiers for downlink transmissions. The proposed scheme aim at mitigating the impact of cross-tier interference that rises due to the co-channel deployment of multiple tiers of BSs. In the multi-tier network under consideration, high power base stations (BSs) such as macrocell BSs are overlaid by another tier of lower power small cells such as femtocells or picocells. Coordinated multipoint (CoMP) transmission has been used as a multi-cell cooperation solution to enhance the coverage and data rate offered by multi-tier cellular systems. In addition, I propose a user-centric location-based policy in which each user independently chooses her mode of operation through or without cooperation. On one hand, the proposed scheme uses CoMP transmission only to enhance the performance of users who suffer from high cross-tier interference due to the co-channel deployment of small cells. On

the other hand, users with good signal-to-interference-plus-noise ratio (SINR) conditions are served directly by a single BS from any of the two tiers. Thus, data exchange between cooperating BSs over the backhaul network can be reduced when compared to the traditional CoMP transmission scheme. I use tools from stochastic geometry to quantify the performance gains obtained by using the proposed scheme in terms of outage probability, achievable data rate, and load per BS. I also compare the performance of the proposed scheme with that of other schemes in the literature such as schemes that use cooperation to serve all users and schemes that use range expansion to offload users to the small cell tier.

2.1 Introduction

Deployment of multi-tier networks is an attractive solution to satisfy the ever-increasing users' demand for higher data rates and network coverage. Unlike traditional single-tier networks, multi-tier networks consist of different classes of BSs such as macrocell, picocell, and femtocell BSs. These BSs operate simultaneously in the same geographical area and differ in transmit power, coverage range, and spatial density [2]. However, with co-channel deployment of multiple network tiers, cross-tier interference degrades network performance in terms of coverage and throughput. For example, a macrocell user who is located in the close vicinity of a small cell may receive high level of cross-tier interference resulting from transmissions from that small cell BS to its users. Therefore, multi-cell cooperation has been proposed to address this problem [3, 4]. Coordinated multipoint (CoMP) transmission (also referred to as network MIMO) is a form of cooperation in which interference between multiple BSs can be canceled out by allowing these BSs to communicate with each other to exchange users' data and coordinate their transmissions. That is, BSs cooperate to

jointly transmit users' data concurrently [5–8]. In CoMP, BSs use backhaul links to exchange users' data and/or control information where these links are capacity-limited in practice and affect the performance of the wireless system [39].

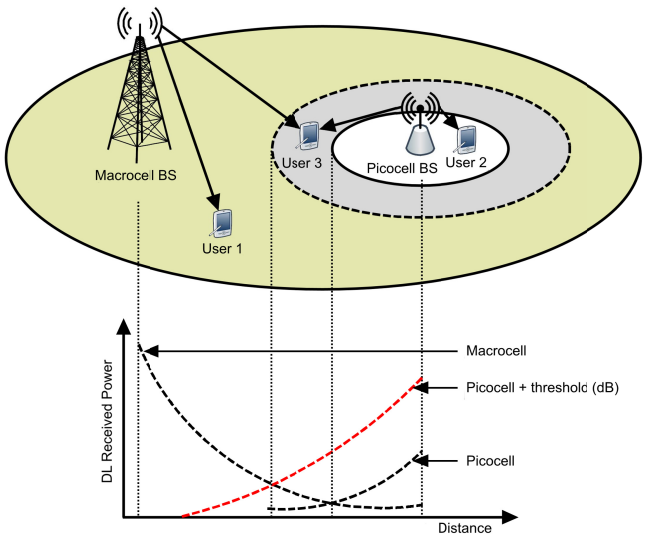

Figure 2.1: A two-tier cellular network with a macrocell and a picocell where the range of cooperation is defined by a positive threshold. While each of User 1 and User 2 is served by only one BS that results in the maximum received power from any of the two tiers, User 3 is connected to more than one BS – one BS from each tier that results in the maximum received power from that tier.

Multi-cell cooperation solutions such as CoMP could be effective to mitigate the effect of cross-tier interference in multi-tier networks. For example, in the two-tier macrocell-picocell network shown in Figure 2.1, although the power received at User 3 from the serving macrocell BS is higher than that of the interference resulting from the closest picocell BS, the interference power can be comparable to the useful signal power which results in a low level of SINR. Therefore, the macrocell BS can cooperate with the interfering picocell BS to serve User 3 jointly. This will not only eliminate the strongest interference signal, but also increase the useful received signal power by taking the advantage of the user's proximity to that interferer thus improving the SINR. However, using cooperation might be unnecessary in some cases. For

example, in Figure 2.1, the useful signal power received at User 1 and User 2 from the serving macrocell BS and picocell BS, respectively, is sufficiently higher than the power received from the strongest interferer, i.e., the picocell BS for User 1 and the macrocell BS for User 2. For these two users, the gain of cooperation may not be high compared to the costs of joint processing and using the backhaul network to exchange users' data especially when the capacity of the backhaul links is limited.

In this chapter, in order to improve coverage and spectral efficiency in a two-tier macrocell-picocell network, I propose a novel location-aware cross-tier cooperation (LAC) scheme in which macrocell BSs and small cells can cooperate to serve a user jointly only if the user suffers from high interference due to the co-channel deployment of small cell BSs. This user is then referred to be served in CoMP mode. Otherwise, if the power received from the interfering BS at the user is not high enough to cause severe interference, direct link transmission is used to serve the user without cooperation and the user is referred to be served in non-CoMP mode. Note that the main focus of this chapter is on mitigating the effect of cross-tier interference.

As shown in Figure 2.1, a cooperation region is defined around the small cell in which a user is served by CoMP transmission, otherwise, the user is connected directly to one BS, i.e., macrocell BS or small cell BS. That is, when the ratio of the received power from the macrocell BS at any user to the received power from the small cell BS exceeds a predefined threshold (greater than 1), this implies that the useful signal is sufficiently higher than the interference, and thus, cooperation is unnecessary and the user (e.g. User 1) is served by the macrocell BS only. The predefined threshold is referred to as cooperation threshold which will be defined later in Section 2.3.2. On the other hand, if the ratio is less than the cooperation threshold and still greater than 1, cooperation is beneficial since the interference power is comparable to the

useful signal power (e.g., for User 3). Finally, if the ratio is less than 1, the user (e.g., User 2) is directly connected to the small cell since the received signal from the small cell is stronger than that from macrocell in this case.

The main motivation of the proposed scheme is to provide better coverage in multi-tier networks and protect macrocell users from excessive cross-tier interference while considering the limitation of the backhaul network. For example, assume a macrocell-picocell network where each macrocell has p randomly-located picocell BSs within its coverage area. Since cooperation in LAC scheme is only possible between BSs belonging to different tiers, only p backhaul links per macrocell are required to enable cooperation between a macrocell BS and picocell BSs in its coverage (a star-connected backhaul network). Now consider another scheme where cooperation is also allowed between BSs belonging to the same tier. In this case both macrocell and picocell BSs are required to exchange users' data in order to perform joint transmission (a fully-connected mesh backhaul network). For example, when cooperation is limited between picocell BSs within the same macrocell, this requires $\binom{p}{2}$ backhaul links to connect any two picocell BSs. In addition, each macrocell BS should be able to exchange users' data with at least its first q neighbors as well as the p picocell BSs in its coverage. In total, at least $0.5p^2 + 0.5p + q$ backhaul links are required to enable cooperation between BSs. Although the latter scheme offers a better coverage when compared to LAC scheme, only p backhaul links are needed for LAC scheme. Therefore, with LAC scheme, there is a significant saving in the number of backhaul links when the number of picocell BSs per macrocell is large.

Note that other techniques, such as range expansion (also referred as flexible cell association), have also been proposed to improve the performance of multi-tier networks and balance the load for all tiers. For example, in a two-tier network with

range expansion, users from the macrocell network tier are offloaded to the small cell tier, where the association to the small cells is biased. That is, a positive bias factor is added to the power of the pilot signals of the small cell BSs to convince macrocell users who are close to a small cell coverage boundary to connect to that small cell even if the power received from the macrocell BS is stronger than that received from the small cell BS [40–42].

2.1.1 Contributions

In this chapter, I analyze the performance of the proposed LAC scheme for downlink transmission in a two-tier cellular network. I use tools from stochastic geometry to model the network where locations of BSs in each tier are distributed according to a two-dimensional independent PPP [20]. Each tier of BSs is characterized by its available transmit power, spatial density, and path-loss exponent value. In order to evaluate the performance of the proposed scheme, I derive closed-form expressions for the outage probability and data rate. Furthermore, I use the analytical model to derive expressions for outage probability for (i) range expansion scheme, (ii) scheme with full cooperation where all users are served by cross-tier CoMP transmission, as well as (iii) traditional scheme where neither cooperation nor range expansion is used. The performance metrics of different schemes are compared in terms of outage probability, average achievable data rate, and load per BS. The results show that the proposed cooperation scheme outperforms both traditional and range expansion schemes for multi-tier networks in terms of both outage and data rate, while it has higher load per BS. Compared to the full cooperation scheme, the proposed scheme reduces the amount of users' data exchange over the backhaul network as measured by the load per BS. In addition, the outage performance of the proposed scheme approaches that

with full cooperation for a wide range of values of cooperation threshold.

The contributions of the chapter are summarized as follows.

- I propose a novel user-centric location-aware cross-tier cooperation (LAC) scheme that uses CoMP transmission for users who experience high level of interference power compared to the power level of the useful signal received from the serving BS. I define a range of interference power based on which the transmission mode (i.e., CoMP or non-CoMP transmission) is decided by each user individually.

- I use stochastic geometry to evaluate the performance of the proposed scheme in terms of the outage probability, average data rate, and load per BS as the key metrics. I compare the proposed scheme with other schemes such as range expansion scheme, full cooperation scheme, as well as a non-cooperative scheme in which a user is served by the strongest BS only. The derived expressions are in the closed-integral form.

- I analyze the performance of different schemes under different system parameters by varying the spatial densities of BSs, path-loss exponents, cooperation threshold, and required SINR thresholds. Then, I highlight the insights obtained from the analysis and show the impact of the aforementioned parameters on the network behavior.

- I show that the proposed LAC scheme is promising for improving the network outage and achievable data rate while considering the load of macrocell BSs and the performance of macrocell users. Furthermore, I show that the performance of LAC scheme lies in the middle between the performance of the traditional range expansion-based networks and full cooperation networks.

2.1.2 Organization

The rest of this chapter is organized as follows. A review of the related work is presented in Section 2.2. The system model, different modes of operation of the users, probability of a user to operate in a certain mode, as well as the distance analysis for the users in different modes are presented in Section 2.3. In Section 2.4, the outage probability and ergodic rate are obtained for the users in different modes. Finally, the performance evaluation results are presented in Section 2.5 and the chapter is summarized in Section 2.6.

2.2 Related Work

Previous works on multi-tier networks and multi-cell cooperation can be divided into two general groups. In the first group, statistical modeling techniques, such as stochastic geometry, are used to analyze network performance and obtain statistically-optimal decision parameters [20, 42–47]. In the second group, instantaneous optimal decisions are obtained by using the instantaneous information of the network based on some objective function [48–51]. Note that the statistically-optimal parameters might not be optimal on a short time-scale, however, obtaining instantaneous optimal parameters costs more signaling and computations.

In [20] the authors provide a general framework to analyze and evaluate the performance of a cellular network with K tiers of BSs. In this model, independent PPPs are used to capture the randomness of the locations of BSs as well as the differences in transmit power, propagation environment, and BS spatial density. In addition, analytical expressions for outage probability, achievable data rate, and load per BS are obtained. In [42], the model is extended where the association to different tiers is biased (range expansion). It shows that range expansion degrades the overall network

performance in terms of outage and data rate. On the other hand, in the context of multi-cell cooperation, the authors in [43] propose two clustering schemes for CoMP transmission in multi-tier networks where clustering is performed on a per-user basis and the performance is evaluated in terms of outage probability. It is assumed that the backhaul network is ideal and the number of cooperating BSs in each cluster is constant. While the first clustering scheme forms a group of N BSs which results in the reception of the N strongest signals at the receiver, the second clustering scheme selects the N closest BSs to the receiver where one BS is chosen from each tier.

In [44], the authors propose a cooperation scheme to mitigate the co-tier interference in a single-tier network in which a user-centric decision criterion is used to decide whether to be served with or without cooperation. The decision is based on the distance between the user and her first two neighboring BSs and some decision parameters. All BSs are assumed to be able to exchange users' data to perform joint transmission with power splitting. The authors use stochastic geometry to investigate the effect of limited channel state information (CSI) at the transmitter. The authors in [45] propose another clustering scheme for single-tier networks where the clusters are formed in a random manner by grouping BSs that lie in the same Voronoi cell of an overlaying PPP with low spatial density. In this paper, BSs that belong to the same cluster cooperate to nullify the interference by exchanging the CSI data. In [46], the authors use stochastic geometry to evaluate the impact of the overhead delay on the performance of CoMP transmission in multi-tier networks while using zero-forcing beamforming (ZFBF) as a precoding scheme. In [47], a macrocell-femtocell network with single macrocell user and macrocell BS is considered where all femtocell BSs are cognitive. To mitigate cross-tier interference, the macrocell user is assumed to generate a busy tone such that femtocell BSs defer their transmissions if the received

power is greater than a predefined threshold. The authors use stochastic geometry to obtain the outage probability and average data rate.

The authors in [48] derive closed-form expressions for the bias factor of range expansion in a macrocell-picocell network for downlink and uplink. Furthermore, a cooperative scheduling scheme between macrocell and picocell BSs is proposed to mitigate the effect of high interference in the expanded regions where simulations are used to evaluate the network and the proposed scheme. In [49], a game-theoretic approach is used to study the impact of backhaul constraints on the performance of femtocell networks with CoMP transmissions. A cooperative game is formulated such that each femtocell BS chooses the cooperation strategy and exchanges users' data to its cooperative partner over either wired or wireless backhaul. The objective of the proposed game is to balance the tradeoff between the achievable spectral efficiency and delay. The authors in [50, 51] use fractional programming to obtain the optimal power, channel, and precoding coefficients allocation for CoMP transmissions in single-tier and two-tier cellular networks, respectively. In both works, the optimization problem aims at maximizing the energy efficiency (bit/Joule) under co-tier or cross-tier interference, power budget, and backhaul link capacity constraints.

To the best of my knowledge, the concepts of cross-tier BS cooperation along with location-aware BS cooperation, which are introduced in this chapter, have not been explored previously in the literature. The term "location-aware" is used in the sense that the locations of both users and BSs are considered to make a decision on whether cooperative transmission will be used or not. Note that, I have proposed a similar location-aware BS cooperation scheme for single-tier cellular networks in [51] to mitigate the effect of the co-tier interference.

2.3 System Model and Assumptions

2.3.1 Two-Tier Cellular Network Model

I consider downlink transmission in a multi-tier network which consists of K tiers that are independent with different spatial densities, path-loss exponents, and transmit powers. BSs belonging to the same network tier $k \in \{1, \ldots, K\}$ have the same transmit power P_k. Locations of BSs in the k-th tier are modeled according to a two-dimensional homogeneous PPP $\mathbf{\Phi}_k \in \mathbb{R}^2$ with spatial density λ_k. The users are spatially distributed according to some independent stationary point process $\mathbf{\Psi}_u \in \mathbb{R}^2$ (e.g., a homogenous PPP) with spatial density λ_u which is assumed high enough (compared to $\sum_{k=1}^{K} \lambda_k$) such that each BS has at least one user to serve. For statistical analysis, without any loss of generality, I consider a typical user at the origin [17]. During a transmission interval, a user served by a certain network tier in a particular channel experiences interference from the all other BSs including (i) other BSs from the same network tier and (ii) BSs from other network tiers. However, there will be no intra-cell interference assuming that different users in a cell are served using orthogonal time-frequency resources (e.g. OFDMA). A BS from any tier can use the same channels (i.e., a co-channel deployment scenario is considered). All transmitters and receivers are equipped with a single antenna.

Without loss of generality, I consider a two-tier macrocell-picocell cellular network, i.e., $K = 2$. Figure 2.2 shows a realization of a two-tier cellular network where a macrocell network tier is deployed as tier 1 and overlaid with a denser and lower power picocell network tier as tier 2. For a generic point $y \in \mathbb{R}^2$, let x_k denote the BS belonging to the k-th tier that results in the strongest long-term average received

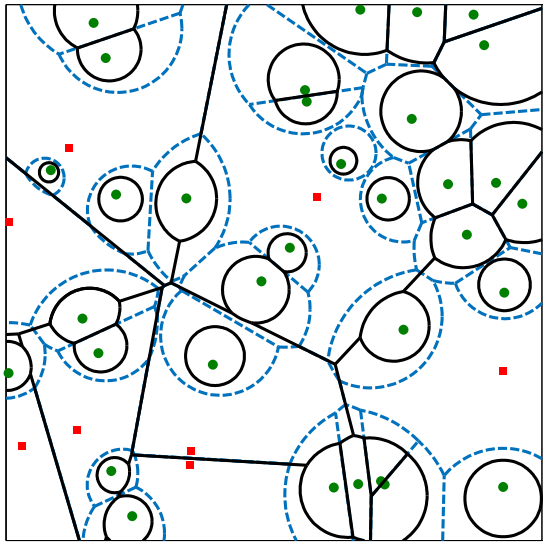

Figure 2.2: A two-tier cellular network with a macrocell network tier (red squares) overlaid with lower power and denser picocell network tier (green circles). Solid black lines show the coverage area of each cell for a traditional two-tier network, while the dashed lines show the cooperation regions that surround each picocell in which cooperation is performed between the macrocell and picocell BSs.

power at this point. That is,

$$x_k = \arg\max_{x \in \mathbf{\Phi}_k} \{P_k \|x - y\|^{-\alpha_k}\} \tag{2.1}$$

where different path-loss exponents $\{\alpha_k\}_{k=1,2}$ are used for downlink modeling at each network tier and $\|\cdot\|$ denotes the Euclidean distance.

2.3.2 Mode of Operation and Cell Association

Based on the received power from each tier, each user independently chooses her mode of operation through or without cooperation. In this context, I define two modes of operation: non-CoMP and CoMP transmission modes. In the non-CoMP mode of operation, the user is connected to the BS that results in the maximum long-term

average received power regardless of the corresponding network tier, i.e., macrocell network tier or picocell network tier. In the CoMP mode of operation, the user is served by two BSs that cooperate with each other to jointly transmit data to this user. In this mode, one BS is selected from each tier based on the maximum received power at the user. That is, the users are split into three disjoint groups: non-CoMP macrocell users, non-CoMP picocell users, and CoMP users.

To elaborate, if the received signal power from the strongest BS at the user is sufficiently higher than that received from the highest interferer, the user operates in the non-CoMP mode since the cooperation between the serving BS and this interfering BS is not necessary in this case. On the other hand, if the received signal power at the user from the strongest interfering BS is comparable to the useful signal power received from the strongest BS, the user operates in the CoMP mode. In this case, the network takes advantage of the proximity of the interfering BS to the user and assigns it to cooperate with the user's serving BS to jointly transmit data to the user. This not only mitigates the effect of the highest interferer, but also increases the power level of the useful signal.

Let $\mathcal{B}$ denote the set of BSs that serve a typical user, which can be written as follows

$$\mathcal{B} = \begin{cases} \{x_1\}, & \text{if } \frac{P_1 R_1^{-\alpha_1}}{P_2 R_2^{-\alpha_2}} \geq \beta & \text{“non-CoMP macrocell”} \\ \{x_2\}, & \text{if } \frac{P_1 R_1^{-\alpha_1}}{P_2 R_2^{-\alpha_2}} \leq 1 & \text{“non-CoMP picocell”} \\ \{x_1, x_2\}, & \text{if } 1 < \frac{P_1 R_1^{-\alpha_1}}{P_2 R_2^{-\alpha_2}} < \beta & \text{“CoMP”} \end{cases} \tag{2.2}$$

where x_k ($k \in \{1, 2\}$) is defined in (2.1) and R_k ($k \in \{1, 2\}$) is the distance from the typical user to the strongest BS in the k-th tier. β is the cooperation threshold which represents the ratio between the powers received from the serving macrocell

BS and the strongest picocell BS, respectively. This threshold defines the level of cross-tier interference beyond which the user switches to the CoMP mode. That is, if the strongest interference power received from the picocell network tier $P_{\text{int}} = P_2 R_2^{-\alpha_1}$ at some macrocell user is in the range $\frac{1}{\beta} P_1 R_1^{-\alpha_1} < P_{\text{rm}} < P_1 R_1^{-\alpha_1}$, this user switches her mode to be served via cooperation.

As shown in Figure 2.1, User 1's received power from the macrocell BS is stronger than that from the picocell BS plus the threshold (dB) and User 2's received power from the picocell BS is stronger than that from the macrocell BS. Therefore, Users 1 and 2 operate in the non-CoMP mode where they are associated with the macrocell BS and picocell BS, respectively. On the other hand, although User 3's received power from the macrocell BS is higher than that from the picocell BS, the received power from the picocell BS plus the threshold (dB) is higher. Therefore, User 3 operates in the CoMP transmission mode where she is served by both BSs.

For the proposed LAC scheme, cooperation threshold β is an important design parameter and plays a key role in controlling the gains obtained by using this scheme. That is, the higher the cooperation threshold, the larger is the cooperation region which improves the overall system performance while increasing the amount of data exchange over the backhaul network as well as the load per BS. On the other hand, the lower the cooperation threshold, the smaller is the cooperation region which reduces the backhaul signaling between BSs and the load per BS while sacrificing some overall performance gain in terms of outage and data rate.

2.3.3 Distance Analysis

Let q_M, q_P, and q_C denote the probability that a typical user is in non-CoMP mode and served by the macrocell BS (i.e., non-CoMP macrocell user), in the non-CoMP

mode and served by the picocell BS (i.e., non-CoMP picocell user), and in the CoMP mode, respectively. Conditioned on each event, in the following lemma, I derive the probability density functions (PDFs) of the distance between a typical user at the origin and her serving BS(s) in different modes of operation.

For a typical user in the CoMP mode, let $f_{R_C}(\mathbf{r})$ denote the joint PDF of the distances between the typical user and her two serving BSs x_1 and x_2, i.e., macrocell BS and picocell BS, respectively. For a non-CoMP macrocell user, let $f_{R_1}(r)$ denote the PDF of the distance between a macrocell user and her serving macrocell BS x_1. Finally, $f_{R_2}(r)$ is the PDF of the distance between a non-CoMP picocell user and her serving picocell BS x_2.

Lemma 2.1. The PDFs of the distances between a typical user and her serving BS(s) are

$$f_{R_C}(\mathbf{r}) = \frac{4\pi^2\lambda_1\lambda_2}{q_C} r_1 r_2 \exp\left[-\pi\left(\lambda_1 r_1^2 + \lambda_2 r_2^2\right)\right] \tag{2.3}$$

$$f_{R_1}(r) = \frac{2\pi\lambda_1}{q_M} r \exp\left[-\pi\left(\lambda_1 r^2 + \lambda_2 \left(\frac{\beta P_2}{P_1}\right)^{\frac{2}{\alpha_2}} r^{\frac{2\alpha_1}{\alpha_2}}\right)\right] \tag{2.4}$$

$$f_{R_2}(r) = \frac{2\pi\lambda_2}{q_P} r \exp\left[-\pi\left(\lambda_2 r^2 + \lambda_1 \left(\frac{P_1}{P_2}\right)^{\frac{2}{\alpha_1}} r^{\frac{2\alpha_2}{\alpha_1}}\right)\right] \tag{2.5}$$

where $r_1 \in \mathbb{R}^+$ and $\left(\frac{P_2}{P_1}\right)^{\frac{1}{\alpha_2}} r_1^{\frac{\alpha_1}{\alpha_2}} < r_2 < \left(\frac{\beta P_2}{P_1}\right)^{\frac{1}{\alpha_2}} r_1^{\frac{\alpha_1}{\alpha_2}}$, and

$$q_M = 2\pi\lambda_1 \int_{\mathbb{R}_+} r \exp\left[-\pi\left(\lambda_1 r^2 + \lambda_2 \left(\frac{\beta P_2}{P_1}\right)^{\frac{2}{\alpha_2}} r^{\frac{2\alpha_1}{\alpha_2}}\right)\right] \mathrm{d}r \tag{2.6}$$

$$q_P = 2\pi\lambda_2 \int_{\mathbb{R}_+} r \exp\left[-\pi\left(\lambda_2 r^2 + \lambda_1 \left(\frac{P_1}{P_2}\right)^{\frac{2}{\alpha_1}} r^{\frac{2\alpha_2}{\alpha_1}}\right)\right] \mathrm{d}r \tag{2.7}$$

$$q_C = 1 - q_M - q_P. \tag{2.8}$$

Proof. See **Appendix A.1**. □

For the special case when $\alpha_1 = \alpha_2 = \alpha$, q_M and q_P can be expressed in a closed-form as

$$q_M = \frac{\lambda_1 P_1^{\frac{2}{\alpha}}}{\lambda_1 P_1^{\frac{2}{\alpha}} + \lambda_2 (\beta P_2)^{\frac{2}{\alpha}}}, \quad q_P = \frac{\lambda_2 P_2^{\frac{2}{\alpha}}}{\lambda_1 P_1^{\frac{2}{\alpha}} + \lambda_2 P_2^{\frac{2}{\alpha}}}. \tag{2.9}$$

Furthermore, it can be seen that when the cooperation threshold β is set to 1 (no cooperation), the probability that a typical user operates in the CoMP mode reduces to zero, i.e., $q_M + q_P = 1$. That is, a user associate only with the strongest BS in terms of received power.

2.4 Analysis of SINR Outage Probability and Average Rate

In this section, I characterize the SINR for downlink transmission to a typical user in different modes of operation. Then, I derive closed integral-forms for the outage probability and ergodic rate of downlink transmission for the proposed LAC scheme.

2.4.1 SINR

Based on the mode selection criteria in (2.2), the received signal power at a typical user can be written as

$$\underbrace{\sum_{x_k \in \mathcal{B}} \frac{\sqrt{P_k} h(x_k, 0)}{\|x_k\|^{\frac{\alpha_i}{2}}} X}_{\text{useful signal}} + \underbrace{\sum_{j=1}^{2} \sum_{x_i \in \mathbf{\Phi}_j \setminus \mathcal{B}} \frac{\sqrt{P_j} h(x_i, 0)}{\|x_i\|^{\frac{\alpha_j}{2}}} Y_{j,i}}_{\text{inter-cell interference}} + Z \tag{2.10}$$

where $h(x,0)$ is the small-scale fading coefficients for a link from a BS located at $x \in \mathbb{R}^2$ to the typical user at the origin, i.e., $(0,0)$. $\{h(x,y)\} \sim \mathcal{CN}(0,1)$ are independent and identically distributed (i.i.d) circular complex Gaussian random variables. That is, $|h(x,y)|$ is a Rayleigh-distributed random variable, hence, channel power envelope is exponentially-distributed as Exp(1), and the phase shift in uniformly distributed in $[0, 2\pi]$. X and $Y_{j,i}$ are two zero-mean and unity-variance random variables that represent the jointly transmitted data by set $\mathcal{B}$ of the serving BSs and the data sent by the interfering BSs, respectively. $Z \sim \mathcal{CN}(0,\sigma^2)$ is the additive white noise at the receiver. No CSI is assumed at BSs and that the channel coherence time is greater than or equal to the frame duration.

Note that, ideally, the interference signals received at a user are dependent since interferers could be cooperating as well. However, as can be seen in (2.10), $\{Y_{i,j}\}$ are independent. The rationale behind this assumption is as follows. Given that two BSs (at distance z_1 and z_2 from a location y) are cooperating and interfering to a certain user located at y, it is a fact that: (i) the received interference power from two cooperating BSs is $|\sqrt{P_1}g_1 z_1^{-0.5\alpha_1} + \sqrt{P_2}g_2 z_2^{-0.5\alpha_2}|^2$ whose PDF has a Laplace transform of $\mathcal{L}_{\text{actual}}(s) = (1 + (\theta_1^2 + \theta_2^2)s)^{-1}$ where $\theta_i = \sqrt{P_i} z_i^{-0.5\alpha_i}$, (ii) the received interference power is assumed to be $|\sqrt{P_1}g_1 z_1^{-0.5\alpha_1}|^2 + |\sqrt{P_2}g_2 z_2^{-0.5\alpha_2}|^2$ with a PDF that has a Laplace transform of $\mathcal{L}_{\text{assump}}(s) = (1 + \theta_2^2 s)^{-1}(1 + \theta_1^2 s)^{-1}$, and (iii) the outage probability is a decreasing function of the Laplace transform of the PDF of the interference. (i) follows because the received power from any two cooperating BSs is exponentially-distributed where more details about the distribution are given in **Appendix A.2**. After the assumption, (ii) follows because the received power from any two cooperating BSs becomes a sum of two independent exponentially-distributed random variables with different means which is equivalent to a hyperexponential

random variable with mean $\theta_1 + \theta_2$ and variance $\theta_1^2 + \theta_2^2$. (iii) follows as will be presented in **Appendix A.2**. Hence, $\mathcal{L}_{\text{actual}}(s) \geq \mathcal{L}_{\text{assump}}(s)$ and the independence assumption gives a lower bound on the outage probability.

Thus, the received SINR at a typical receiver is given by

$$\text{SINR}(\mathcal{B}) = \frac{\left| \sum\limits_{x_k \in \mathcal{B}} \sqrt{P_k} h(x_k, 0) \|x_k\|^{-\frac{\alpha_i}{2}} \right|^2}{\sum\limits_{j=1}^{2} P_j \sum\limits_{x_i \in \mathbf{\Phi}_j \setminus \mathcal{B}} |h(x_i, 0)|^2 \|x_i\|^{-\alpha_j} + \sigma^2}. \tag{2.11}$$

Note that in (2.11), the effect of the user's mode of operation is reflected in $\mathcal{B}$. That is, different modes of operation lead to different levels of the useful signal power (higher/lower) and aggregate interference power (lower/higher).

To show the important role that the proposed mode of operation policy plays in improving the level of the received SINR at the typical user, let us present the following scenario. Considering the no-cooperation case (i.e., when $\beta = 1$) and the cell association based on the strongest signal power regardless of the BS tier, the serving BS x is selected as follows

$$x = \arg \max_{x \in \mathbf{\Phi}_1 \cup \mathbf{\Phi}_2} \{P_k \|x\|^{-\alpha_k}\}. \tag{2.12}$$

In this case, macrocell users, who are close to the boundaries of the deployed picocells coverage, experience high interference, and consequently low SINR. In the proposed scheme, these users are likely to change their mode of operation to use CoMP transmission instead of single cell transmission. The proposed scheme increases the power level of the useful signal and reduces the total interference power by forcing the strongest interferer to cooperate with the original transmitter. The reduction in the interference power level along with the increase of the useful signal power enhances

the received SINR at the CoMP user.

2.4.2 Outage Probability

Using the instantaneous SINR given in (2.11), the outage probability $\mathcal{O}$ of the overall system can be obtained. Here, outage probability is defined as the probability that the received SINR is less than a predefined threshold τ. Note that τ is a design parameter and it is chosen to satisfy certain quality-of-service requirements of users. Let $\mathcal{O}_M(\tau)$, $\mathcal{O}_P(\tau)$, and $\mathcal{O}_C(\tau)$ denote the outage probability of a randomly located user conditioned on her mode of operations, i.e., non-CoMP macrocell user, non-CoMP picocell user, and CoMP user, respectively. That is, the outage probability of a randomly located user given that she operates in the non-CoMP macrocell mode is obtained by

$$\mathcal{O}_M(\tau) = \mathbb{E}\left[\mathbb{P}\left[\text{SINR}(\mathcal{B} = \{x_1\}) \leq \tau\right]\right] \tag{2.13}$$

while that of a randomly located user given that she operates in the non-CoMP picocell mode is given by

$$\mathcal{O}_P(\tau) = \mathbb{E}\left[\mathbb{P}\left[\text{SINR}(\mathcal{B} = \{x_2\}) \leq \tau\right]\right]. \tag{2.14}$$

Finally, the outage probability of a randomly located user who is served by two BSs simultaneously in the CoMP mode is given by

$$\mathcal{O}_C(\tau) = \mathbb{E}\left[\mathbb{P}\left[\text{SINR}(\mathcal{B} = \{x_1, x_2\}) \leq \tau\right]\right]. \tag{2.15}$$

Since the three modes, i.e., non-CoMP macrocell mode, non-CoMP picocell mode,

and CoMP mode, are mutually exclusive, the overall outage probability in the network can be obtained by using the law of total probability as follows

$$\mathcal{O}(\tau) = q_M \mathcal{O}_M(\tau) + q_P \mathcal{O}_P(\tau) + q_C \mathcal{O}_C(\tau) \tag{2.16}$$

where q_M, q_P, and q_C are given in **Lemma 2.1**. The following theorem gives the outage probabilities for a typical user under different modes of operation.

Theorem 2.1. The outage probabilities for a typical user given that this user operates as a non-CoMP macrocell user, or as a non-CoMP picocell user, or as a CoMP user are

$$\mathcal{O}_M(\tau) = 1 - \int_{\mathbb{R}_+} \exp\left[\frac{-\tau\sigma^2}{P_1 r^{-\alpha_1}}\right] \prod_{j=1}^{2} \mathcal{L}_{\mathcal{I}_j}\left(\frac{\tau}{P_1 r^{-\alpha_1}}\right) f_{R_1}(r)\,\mathrm{d}r \tag{2.17}$$

$$\mathcal{O}_P(\tau) = 1 - \int_{\mathbb{R}_+} \exp\left[\frac{-\tau\sigma^2}{P_2 r^{-\alpha_2}}\right] \prod_{j=1}^{2} \mathcal{L}_{\mathcal{I}_j}\left(\frac{\tau}{P_2 r^{-\alpha_2}}\right) f_{R_2}(r)\,\mathrm{d}r \tag{2.18}$$

$$\mathcal{O}_C(\tau) = 1 - \int_{\mathcal{A}} \exp\left[\frac{-\tau\sigma^2}{\sum_{k=1}^{2} P_k r_k^{-\alpha_k}}\right] \prod_{j=1}^{2} \mathcal{L}^{\star}_{\mathcal{I}_j}\left(\frac{\tau}{\sum_{k=1}^{2} P_k r_k^{-\alpha_k}}\right) f_{R_C}(\mathbf{r})\,\mathrm{d}\mathbf{r} \tag{2.19}$$

where $\mathcal{A}$ is defined in (A.8), $f_{R_1}(r)$, $f_{R_2}(r)$ and $f_{R_C}(\mathbf{r})$ are given in **Lemma 2.1**, and

$$\mathcal{L}_{\mathcal{I}_j}\left(\frac{\tau}{P_k r^{-\alpha_k}}\right) = \exp\left[-2\pi\lambda_j \left(\tau\frac{P_j}{P_k}\right)^{\frac{2}{\alpha_j}} r^{\frac{2\alpha_k}{\alpha_j}} \mathcal{F}\left(\left(\frac{a_{kj}}{\tau}\right)^{\frac{1}{\alpha_j}}, \alpha_j\right)\right]$$

$$\mathcal{L}^{\star}_{\mathcal{I}_j}(s) = \exp\left[-2\pi\lambda_j (sP_j)^{\frac{2}{\alpha_j}} \mathcal{F}\left(\left(\frac{1}{sP_j}\right)^{\frac{1}{\alpha_j}} r_j, \alpha_j\right)\right]$$

$$a_{kj} = \begin{cases} \beta, & k = 1 \text{ and } j = 2 \\ 1, & \text{otherwise} \end{cases}$$

$$\mathcal{F}(y,\alpha)=\int_{y}^{\infty}\frac{u}{1+u^{\alpha}}\,\mathrm{d}u. \tag{2.20}$$

Proof. See **Appendix A.2**. □

Theorem 2.1 provides general closed integral-form expressions for the outage probabilities for a randomly located user. Note that the function $\mathcal{F}(y,\alpha)$ can be evaluated numerically. Furthermore, in some special cases $\mathcal{F}(y,\alpha)$ reduces to simple closed-form expressions (see **Appendix A.3**). The expressions in **Theorem 2.1** can be used to obtain the performances for some special cases by varying β, α_k, and cross-interference mitigation scheme.

In the following, I introduce several network setups which will be compared to the proposed LAC scheme, namely,

1. Non-cooperative two-tier cellular network with range expansion (RE).
2. Fully-cooperative two-tier cellular network (FC).
3. Non-cooperative traditional two-tier cellular network (Tr).

2.4.2.1 Non-cooperative two-tier cellular network with range expansion (RE)

RE is a non-cooperative scheme in which the association to the picocell network tier is biased such that some macrocell users are offloaded to the strongest picocell BS even though the received power from this picocell BS is less than that from the macrocell BS, hence, the range of the picocell is expanded. To elaborate, in Figure 2.2, the cooperation regions of the proposed scheme become a part of the picocell BSs'

coverage areas and users in these regions become picocell users. In other words, it can be seen that RE offloads each CoMP user to her strongest picocell BS where these users switch to the non-CoMP mode. That is, the positive bias to the picocell network tier association becomes β. Note that, β refers to both cooperation threshold of LAC scheme and bias factor of RE scheme depending on the context. For the described scheme, according to **Theorem 2.1**, the outage probability of the macrocell network tier (as given in (2.17)) remains unchanged, where the outage probability of the picocell network tier can be obtained as in the following corollary.

Corollary 2.1. (*Range expansion*) In the special case of a non-cooperative two-tier network with a biased association to the picocell network tier, the outage probability of a randomly located picocell user is given by

$$\mathcal{O}_P^{\mathrm{RE}}(\tau) = 1 - \int_{\mathbb{R}_+} \exp\left[\frac{-\tau\sigma^2}{P_2 r^{-\alpha_2}}\right] \prod_{j=1}^{2} \mathcal{L}_{\mathcal{I}_j}\left(\frac{\tau}{P_2 r^{-\alpha_2}}\right) f_{R_2}^{\mathrm{RE}}(r)\,\mathrm{d}r \tag{2.21}$$

where

$$f_{R_2}^{\mathrm{RE}}(x) = \frac{2\pi\lambda_2}{q_P^{\mathrm{ER}}} r \exp\left[-\pi\left(\lambda_2 r^2 + \lambda_1\left(\frac{P_1}{\beta P_2}\right)^{\frac{2}{\alpha_1}} r^{\frac{2\alpha_2}{\alpha_1}}\right)\right]$$

in which $\mathcal{L}_{\mathcal{I}_j}(\cdot)$ is given in **Theorem 2.1** with $a_{kj} = \beta^{j-k}$ and $q_P^{\mathrm{ER}} = q_P + q_C$.

Proof. I follow the same proofs as in **Appendix A.2** and **Appendix A.1**, respectively, while replacing P_2 by βP_2. □

Hence, the overall outage probability of the non-cooperative two-tier cellular network with RE is given by

$$\mathcal{O}^{\mathrm{RE}}(\tau) = q_M \mathcal{O}_M(\tau) + q_P^{\mathrm{RE}} \mathcal{O}_P^{\mathrm{RE}}(\tau) \tag{2.22}$$

where $\mathcal{O}_M(\tau)$ is given by (2.17), $q_P^{\mathrm{RE}} = q_P + q_C$, and q_P and q_C are given in **Lemma 2.1**.

In this case, the closest interferer from the macrocell network tier to a typical picocell user is at least at a distance of $z = \left(\frac{P_1}{\beta P_2}\right)^{\frac{1}{\alpha_1}} r_2^{\frac{\alpha_2}{\alpha_1}}$ instead of r_2. That is, the macrocell BS corresponding to which the received power at the picocell user is the highest is considered as the closest interferer. Furthermore, for the picocell user in the expanded picocell coverage area, cf. Figure 2.2, the highest interference signal from the macrocell network tier is even higher than the useful signal received from the serving picocell BS. This means that the SINR of this user is less than 1. This implies that the RE scheme degrades system performance compared to the proposed scheme.

2.4.2.2 Fully-cooperative two-tier cellular network (FC)

In this scheme, any typical user, regardless of her location, connects to the strongest BS from each tier, i.e., all users operate in the CoMP mode. The outage probability in this case is provided in the following corollary.

Corollary 2.2. (*Full cooperation*) In the special case of a fully-cooperative two-tier cellular network, the overall outage probability of the network is given by

$$\mathcal{O}^{\mathrm{FC}}(\tau) = 1 - \int_{\mathbb{R}_+^2} \exp\left[\frac{-\tau\sigma^2}{\sum_{k=1}^{2} P_k r_k^{-\alpha_k}}\right] \prod_{j=1}^{2} \mathcal{L}_{\mathcal{I}_j}^{\star}\left(\frac{\tau}{\sum_{k=1}^{2} P_k r_k^{-\alpha_k}}\right) \prod_{j=1}^{2} f'_{R_j}(r_j)\, \mathrm{d}\mathbf{r} \qquad (2.23)$$

where $f'_{R_j}(r_j)$ is given in (A.6) and $\mathcal{L}_{\mathcal{I}_j}^{\star}(\cdot)$ is given in **Theorem 2.1**.

Proof. I use the fact that the BS with the strongest received signal at the typical user from the k-th tier is the nearest BS to this typical user among all BSs in this

tier. That is, the distance to the strongest BS is Rayleigh distributed, i.e., $f'_{R_j}(r) = 2\pi\lambda_j r \exp[-\pi\lambda_j r^2]$ and the joint PDF of the distance is the multiplication of the two distributions because of the independence between the two random variables. By plugging the PDF of the distance in (A.18) and following the proof of $\mathcal{O}_C(\tau)$ in **Appendix A.2**, I obtain the results in (2.23) where $q_C = 1$ and $q_M = q_P = 0$. □

In this case, the closet interferers from the macrocell network tier and the picocell network tier to any user is at least at a distance of r_1 and r_2, respectively. Hence, the performance of all users is improved and the overall outage performance is better compared to the LAC scheme, however, this enhancement comes at the expense of the extra overhead due to data exchange between each two cooperating BSs.

2.4.2.3 Interference-limited traditional two-tier cellular network (Tr)

In this case, each user associates with the strongest BS from either macrocell network tier or picocell network tier as defined in (2.12). The outage probability can be obtained from **Theorem 2.1** as in the following corollary.

Corollary 2.3. (*No cooperation with strongest BS association*) In the special case of a two-tier cellular network when each user associates with the BS that results in the highest average received power, the total outage probability simplifies to

$$\mathcal{O}^{\mathrm{Tr}}(\tau) = 1 - \frac{1}{1 + 2\tau^{\frac{2}{\alpha}} \mathcal{F}\left(\tau^{-\frac{1}{\alpha}}, \alpha\right)} \tag{2.24}$$

where the network operates in the interference-limited regime and $\alpha_1 = \alpha_2 = \alpha$.

Proof. By using the results in **Theorem 2.1** and substituting $\alpha_1 = \alpha_2 = \alpha$, $\beta = 1$, and $\sigma^2 = 0$, I obtain $\mathcal{O}_M^{\mathrm{Tr}}(\tau) = \mathcal{O}_P^{\mathrm{Tr}}(\tau)$ (cf., (2.17)), $q_C = 0$, and q_M and q_P are as given in (2.9). Then, the overall outage probability is obtained as in (2.24). □

In this scheme, the closest interferer from the picocell network tier to a typical macrocell user is at least at a distance r_1 compared to $\left(\frac{\beta P_2}{P_1}\right)^{\frac{1}{\alpha_2}} r_1^{\frac{\alpha_1}{\alpha_2}}$ in the case of LAC scheme. That is, the strongest interferer is closer to the user which degrades the overall performance compared to the proposed scheme. It can be seen that, in this case, the outage probability is independent of the spatial density and transmit power of BSs. That is because the association is based on the highest signal received from any BS which means that the outage probability does not change when more BSs are deployed or the transmit power is increased while assuming the same path-loss exponent.

Note that the results presented in **Corollaries 2.1**, **2.2**, and **2.3** are consistent with the previous results in [20, 42, 43] on multi-tier cellular networks. Furthermore, the same result in **Corollary 2.3** can be obtained for the non-cooperative single-tier cellular case by substituting $\lambda = \lambda_1 + \lambda_2$ and assuming that both tiers are identical in powers ($P_k = P$) and path-loss exponents ($\alpha_k = \alpha$), or simply substituting $\lambda_2 = 0$. This result is consistent with the previous results on single-tier networks in [19].

2.4.3 Average Ergodic Rate

Based on the conditional outage probabilities defined in **Theorem 2.1**, I derive expressions of the ergodic rates for a typical user when she operates in different modes. The ergodic rate is measured in nats/sec/Hz where it represents the spectral efficiency of transmission to a user. Using the independence property used in (2.16), the average ergodic rate for a user is given by

$$\mathcal{R} = q_M \mathcal{R}_M + q_P \mathcal{R}_P + q_C \mathcal{R}_C \tag{2.25}$$

where $\mathcal{R}_M$, $\mathcal{R}_P$, and $\mathcal{R}_C$ are the ergodic rate of a typical user given that she operates in the non-CoMP mode and served by a macrocell BS, in the non-CoMP mode and served by a picocell BS, and in the CoMP mode and served by both macrocell and picocell network tiers, respectively. The association probabilities are given in **Lemma 2.1**.

In the following theorem, I derive an expression for the ergodic rate of a randomly located CoMP user. Note that the rate of non-CoMP users, i.e., macrocell or picocell users, can be obtained following the same procedure and the overall average ergodic rate for a user in the network can be obtained from (2.25) and are presented without a proof. The expressions for the ergodic rate of downlink transmission for the RE, FC, and Tr schemes follow the same procedure.

Theorem 2.2. The ergodic rate for a typical user operating in the non-CoMP mode and served by a macrocell BS is

$$\mathcal{R}_M = \int_{\mathbb{R}_+} 1 - \mathcal{O}_M(e^t - 1)\,\mathrm{d}t. \tag{2.26}$$

The ergodic rate for a typical user operating in the non-CoMP mode and served by a picocell BS is

$$\mathcal{R}_P = \int_{\mathbb{R}_+} 1 - \mathcal{O}_P(e^t - 1)\,\mathrm{d}t. \tag{2.27}$$

The ergodic rate for a typical user operating in the CoMP mode and served by a macrocell BS and a picocell BS is

$$\mathcal{R}_C = \int_{\mathbb{R}_+} 1 - \mathcal{O}_C(e^t - 1)\,\mathrm{d}t. \tag{2.28}$$

where $\mathcal{O}_M(\tau)$, $\mathcal{O}_M(\tau)$, and $\mathcal{O}_C(\tau)$ are given in (2.17)-(2.19).

Proof. Following a similar procedure as in Section 1.5.1, the ergodic rate for a randomly located CoMP user is defined as

$$\mathcal{R}_C = \mathbb{E}_{\mathbf{r}} \left[\mathbb{E}_{\text{SINR}} \left[\ln(1 + \text{SINR}(\mathcal{B} = \{x_1, x_2\})) \right] \right]$$

where the expectation is taken with respect to the distance between the user and her serving BSs. That is, the ergodic rate can be rewritten as

$$\begin{aligned}
\mathcal{R}_C &= \int_{\mathcal{A}} \mathbb{E}_{\text{SINR}} \left[\ln(1 + \text{SINR}(\mathcal{B})) \right] f_{R_C}(\mathbf{r}) \, \mathrm{d}\mathbf{x} \\
&= \int_{\mathbb{R}_+} \left[\int_{\mathcal{A}} \mathbb{P} \left[\ln(1 + \text{SINR}(\mathcal{B})) > t \right] f_{R_C}(\mathbf{r}) \, \mathrm{d}\mathbf{r} \right] \, \mathrm{d}t \\
&= \int_{\mathbb{R}_+} \left[\int_{\mathcal{A}} \mathbb{P} \left[\text{SINR}(\mathcal{B}) > e^t - 1 \right] f_{R_C}(\mathbf{r}) \, \mathrm{d}\mathbf{r} \right] \, \mathrm{d}t
\end{aligned}$$

and by using the the definition of $\mathcal{O}_C(\tau)$ given in (A.18), I obtain the result in (2.28). □

2.5 Numerical Results and Discussion

2.5.1 Performance Metrics and System Parameters

In this section, I compare the proposed LAC scheme with three schemes in the literature discussed in Sections 2.4.2.1, 2.4.2.2, and 2.4.2.3. The first scheme is the flexible cell association, which is referred to as range expansion (RE), where its overall outage probability, i.e., $\mathcal{O}^{\text{RE}}(\tau)$, is defined in **Corollary 2.1**. In the second scheme, referred to as full cooperation (FC), each user in the network is served by two BSs. That

is, each user is connected to one BS from the macrocell network tier and one BS from the picocell network that result in the strongest average received power. The overall outage probability for this scheme, i.e., $\mathcal{O}^{\mathrm{FC}}(\tau)$, is given in **Corollary 2.2**. Finally, the third scheme is the traditional scheme (Tr) for a two-tier cellular network in which a typical user is served only by the strongest BS and no biasing is used (i.e., $\beta = 0$ dB). The overall outage probability for this scheme, i.e., $\mathcal{O}^{\mathrm{Tr}}(\tau)$, is given in **Corollary 2.3**.

Table 2.1: Load per BS for the considered schemes: LAC, Range Expansion, Full Cooperation, and Traditional

Scheme	**macrocell BS**	**picocell BS**
LAC	$\frac{\lambda_u}{\lambda_1}(q_M + q_C)$	$\frac{\lambda_u}{\lambda_2}(q_P + q_C)$
RE	$\frac{\lambda_u}{\lambda_1}q_M$	$\frac{\lambda_u}{\lambda_2}(q_P + q_C)$
FC	$\frac{\lambda_u}{\lambda_1}$	$\frac{\lambda_u}{\lambda_2}$
Tr	$\frac{\lambda_u}{\lambda_1}(q_M + q_C)$	$\frac{\lambda_u}{\lambda_2}q_P$

The comparison is performed in terms of outage probability, spectral efficiency, and load per BS. While the first two metrics have been defined before, the load per BS is defined as the average number of users connected to a BS in any tier. Using the independence assumption between point processes of BSs and users, the load per BS for the four schemes can be obtained as given in Table 2.1.

For the numerical evaluation, the transmit powers of a macrocell BS and a picocell BS are assumed to be 37 dBm and 20 dBm, respectively, while the thermal noise power σ^2 is -104 dBm. i.i.d circular complex random variables with zero mean and unit variance are considered to simulate the channels. The macrocell network tier has a spatial density of $\lambda_1 = (0.5^2\pi)^{-1}$ BS/km^2. Unless otherwise stated, the spatial density of BSs in the picocell network tier is 5 times that of the macrocell network

Table 2.2: Simulation Parameters

Parameter	**Value**
Transmit powers of BSs	37, 20 dBm
Spatial density of BSs ($\times(0.5^2\pi)^{-1}$)	1, 5 BS/km^2
Spatial density of users	$10(0.5^2\pi)^{-1}$ user/km^2
SINR threshold	1

tier, i.e., $\lambda_2 = 5(0.5^2\pi)^{-1}$ BS/km^2 and the spatial density of users $\lambda_u = 10(0.5^2\pi)^{-1}$ user/km^2. For the evaluation of outage probability, SINR threshold τ is set to 0 dB. Simulation parameters are summarized in Table 2.2.

2.5.2 Validation of Analysis

In Figure 2.3, I validate the proposed analytical model by comparing the overall outage probability (i.e., CCDF of SINR evaluated at τ) for the LAC scheme obtained from both analysis (2.16) and simulation. Monte Carlo simulations via MATLAB are used where the simulation area is 10km $\times$10km and the results are averaged over 10^6 iterations. In each realization, the performance is evaluated for a typical user at the origin where the BSs are deployed according to two independent PPPs. It can be seen that the analytical results (see the expressions given in (2.16) and **Theorem 2.1**) match exactly with the simulation results for all SINR thresholds which reflects the accuracy of the expressions derived above. Therefore, from now and on, I use the analytical expressions to evaluate the system performance.

2.5.3 Outage Probability

Figure 2.4 shows the effect of varying both path-loss exponents and spatial densities of BSs on the overall outage probabilities for the LAC and RE schemes. From this figure, it can be seen that the proposed LAC scheme has two advantages over the RE

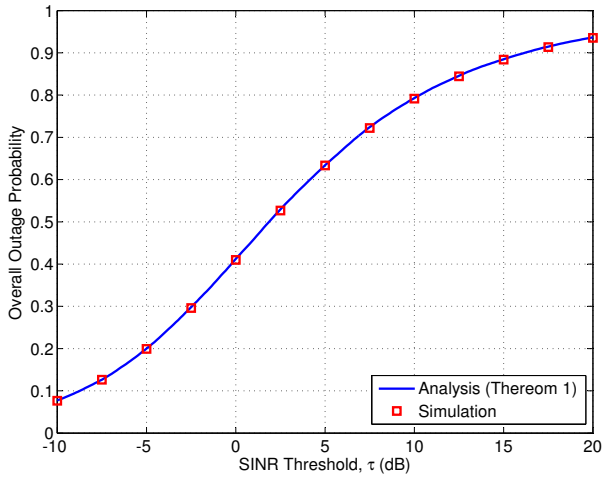

Figure 2.3: Analysis vs. simulation: Overall outage probability for the LAC scheme where $\lambda_1 = (0.5^2\pi)^{-1}$ BS/km^2, $\lambda_2 = 5(0.5^2\pi)^{-1}$ BS/km^2, $P_1 = 37$ dBm, $P_2 = 20$ dBm, $\beta = 4$ dB, $\alpha_1 = \alpha_2 = 4$, and $\sigma^2 = -104$ dBm.

scheme:

1. The overall outage probability for the LAC scheme is better than that for RE scheme for all the different values of path-loss exponents.

2. In some cases, e.g., when $\alpha_1 = \alpha_2$, with the RE scheme, the outage probability deteriorates with increasing the spatial density of picocell BS, while with the LAC scheme the outage probability improves under the same conditions.

The proposed scheme outperforms the RE scheme since for a macrocell user it eliminates the highest interferer from the picocell network tier when the highest received interference power is within a predefined range, i.e.,

$$\frac{1}{\beta} P_2 R_2^{-\alpha_2} < P_{\text{int}} < P_2 R_2^{-\alpha_2}.$$

Moreover, it uses this interfering BS as a cooperation partner along with the original serving macrocell BS to serve this user.

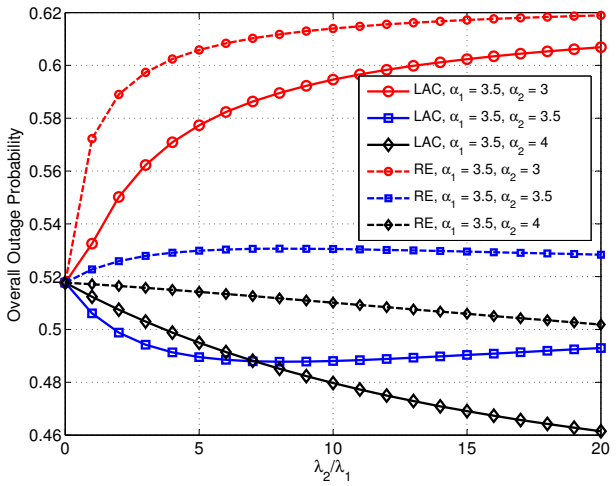

Figure 2.4: LAC vs. Range Expansion: Overall outage probability for different path-loss exponents vs. the ratio of the spatial densities of BSs where $\lambda_1 = (0.5^2\pi)^{-1}$ BS/km^2, $P_1 = 37$ dBm, $P_2 = 20$ dBm, $\beta = 4$ dB, and $\sigma^2 = -104$ dBm.

For the case when $\alpha_1 = \alpha_2$, while using the RE scheme, increasing the spatial density of picocell BSs limits the effect of the thermal noise and the network operates in the interference-limited regime in which the inter-BS interference dominates the performance. Consequently, the outage probability remains constant when the spatial density of picocell BSs is high enough to cancel the effect of both biasing and thermal noise. On the hand, the outage probability for the LAC scheme is improved for the same case (i.e., when $\alpha_1 = \alpha_2$), because the proposed scheme mitigates the highest interferer from the picocell network tier and also uses it as a serving transmitter. For the case when α_2 is higher than α_1, the picocell BSs become more isolated from the macrocell BSs which, in turn, reduces the effect of interference and improves the overall outage probability for the LAC and RE schemes. However, the improvement in outage due to the LAC scheme is much higher than that to the RE scheme because of the same reason mentioned in the previous case. Finally, in the case when α_2 is less than α_1, the outage performance deteriorates for the two schemes. However, the

proposed LAC scheme limits the performance loss by using cooperation between the original serving BS and the highest interferer from the other tier to serve the user in CoMP mode.

Figure 2.5 depicts the effect of increasing the cooperation threshold (bias factor) β on the outage performance of each operation mode for the proposed scheme and the RE scheme. Since the outage probability of the offloaded users is added to the outage of the picocell users in the RE scheme, for a fair comparison, in Figure 2.5 I add the outage of CoMP users in the LAC scheme to the picocell users' outage as well (i.e., $q_P\mathcal{O}_P(\tau) + q_C\mathcal{O}_C(\tau)$). In Figure 2.5, from the perspective of macrocell users, as the cooperation threshold (bias factor) increases, both schemes improve the outage performance compared to the Tr scheme (i.e., when $\beta = 0$ dB). This improvement is due to offloading macrocell users with poor SINR conditions to the picocell network tier (in the RE scheme) or to the CoMP transmission mode (in the LAC scheme). Although offloading users improves the outage of the macrocell network tier in the RE scheme, it degrades the outage of the picocell network tier and the overall network as shown in Figure 2.5. This degradation in outage occurs because each offloaded user connects to a picocell BS that does not result in the strongest received power, hence, the user's SINR deteriorates. On the other hand, in the LAC scheme, CoMP users are served by both BSs which boosts the SINR of these users and compensates for the loss incurred in the RE scheme. That is, the LAC scheme provides a better outage for the CoMP users compared to the offloaded users in the RE scheme while maintaining the same macrocell network tier performance.

In Figure 2.6, it can be seen that the overall outage probability of the proposed scheme lies between those of the traditional and the full cooperation schemes. Furthermore, compared to the RE scheme, the proposed scheme significantly improves

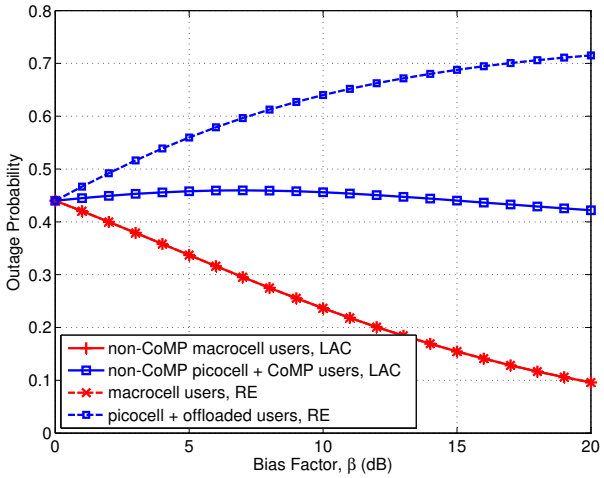

Figure 2.5: LAC vs. Range Expansion: Outage probability vs. the cooperation threshold (bias factor) β where $\lambda_1 = (0.5^2\pi)^{-1}$ BS/km^2, $\lambda_2 = 5(0.5^2\pi)^{-1}$ BS/km^2, $P_1 = 37$ dBm, $P_2 = 20$ dBm, $\alpha_1 = \alpha_2 = 4$, and $\sigma^2 = -104$ dBm.

the overall outage probability of the system. As the cooperation threshold (bias factor) increases, more users are served via cooperation and the performance of the LAC scheme approaches that of the FC scheme. When $\beta \to \infty$, the gap between the two curves results from the outage of the non-CoMP picocell users which is not affected by increasing the bias factor. On the other hand, the gap between the performance of the RE scheme and the Tr scheme increases when the bias factor increases. This is because, a higher β causes more users to be offloaded to the picocell network tier and served with SINR less than 0 dB, hence, the overall outage probability deteriorates. That is, the LAC scheme outperforms both Tr and RE schemes in terms of overall outage probability while approaching the performance of the full cooperation scheme.

2.5.4 Spectral Efficiency

In terms of the overall average achievable rate, it can be seen in Figure 2.7 that the LAC scheme improves the performance of the network compared to the Tr scheme

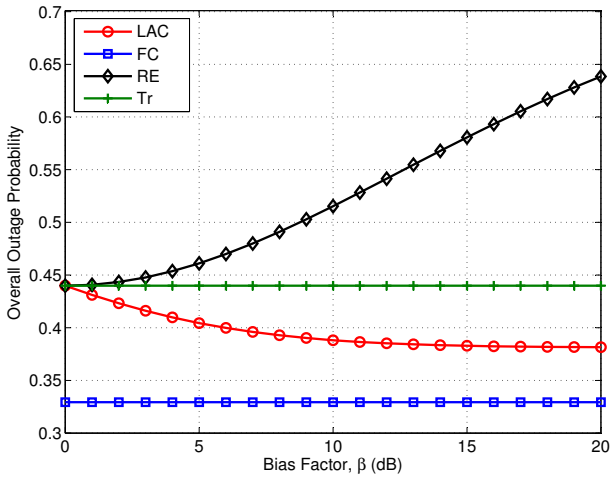

Figure 2.6: LAC vs. Traditional, Range Expansion, and Full Cooperation: Overall outage probability vs. the cooperation threshold (bias factor) β where $\lambda_1 = (0.5^2\pi)^{-1}$ BS/km^2, $\lambda_2 = 5(0.5^2\pi)^{-1}$ BS/km^2, $P_1 = 37$ dBm, $P_2 = 20$ dBm, $\alpha_1 = \alpha_2 = 4$, and $\sigma^2 = -104$ dBm.

as the cooperation threshold increases. This result is consistent with that in Figure 2.5. By using CoMP transmission, the proposed scheme increases the SINR of users who receive high interference from the picocell network tier, by increasing the useful signal power along with decreasing the interference power. On the other hand, as the bias factor increases, the overall average ergodic rate deteriorates with the RE scheme compared to both Tr and LAC schemes. This is also consistent with the results in Figure 2.5 since the offloaded users have lower SINR compared to that they had before the offloading. As expected, the full cooperation scheme offers the highest achievable data rate, however, the data rate offered by the LAC scheme approaches that of the full cooperation scheme when the value of the cooperation threshold is high enough.

In order to show the impact of using the different schemes on the rate of the legacy users, Figure 2.8 compares the performance of the LAC scheme to that of RE scheme in terms of the minimum average ergodic rate the network can provide to a user by

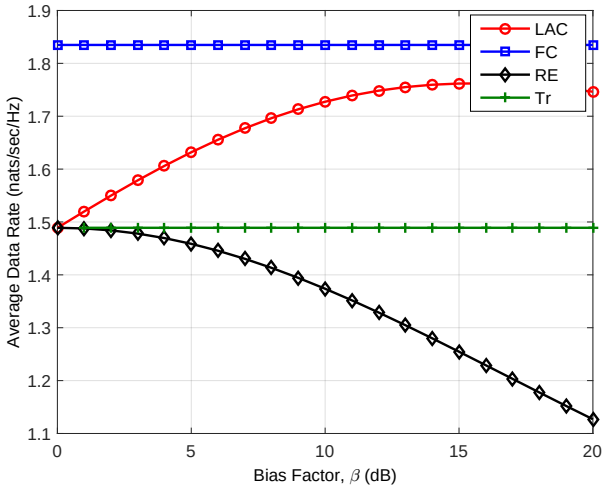

Figure 2.7: LAC vs. Traditional, Range Expansion, and Full Cooperation: Overall average ergodic rate vs. the cooperation threshold (bias factor) β where $\lambda_1 = (0.5^2\pi)^{-1}$ BS/km^2, $\lambda_2 = 5(0.5^2\pi)^{-1}$ BS/km^2, $P_1 = 37$ dBm, $P_2 = 20$ dBm, $\alpha_1 = \alpha_2 = 4$, and $\sigma^2 = -104$ dBm.

any of its tiers. The minimum average user rate offered by a certain BS can be defined as the ratio of the average ergodic rate defined in Section 2.4.3 to the number of users per this BS defined in Table 2.1. For example, the minimum average rate offered by a macrocell BS to its users when adopting the LAC scheme is obtained as

$$\frac{q_M\mathcal{R}_M + q_C\mathcal{R}_C}{q_M + q_C}\frac{\lambda_1}{\lambda_u(q_M + q_C)}$$

where the minimum rate offered by a picocell BS is

$$\frac{q_P\mathcal{R}_P + q_C\mathcal{R}_C}{q_P + q_C}\frac{\lambda_2}{\lambda_u(q_P + q_C)}.$$

Hence, the minimum average rate offered by the network for the LAC scheme can be

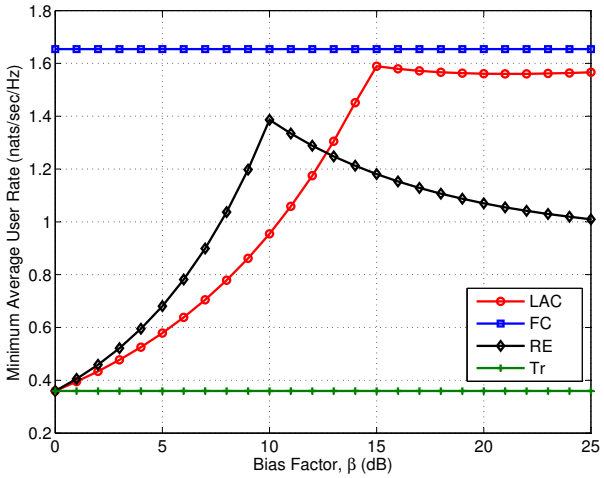

Figure 2.8: LAC vs. Range Expansion: Minimum average user rate for different spatial densities of BSs vs. the cooperation threshold (bias factor) β where $\lambda_1 = (0.5^2\pi)^{-1}$ BS/km^2, $\lambda_2 = 5(0.5^2\pi)^{-1}$ BS/km^2, $\lambda_u = 10(0.5^2\pi)^{-1}$ user/km^2, $P_1 = 37$ dBm, $P_2 = 20$ dBm, $\alpha_1 = \alpha_2 = 4$, and $\sigma^2 = -104$ dBm.

obtained as

$$\min\left\{\frac{q_M\mathcal{R}_M + q_C\mathcal{R}_C}{(q_M+q_C)^2}\frac{\lambda_1}{\lambda_u}, \frac{q_P\mathcal{R}_P + q_C\mathcal{R}_C}{(q_P+q_C)^2}\frac{\lambda_2}{\lambda_u}\right\}. \tag{2.29}$$

Similarly, the minimum average user rate offered by the network for the RE scheme can be obtained as

$$\min\left\{\frac{\mathcal{R}_M}{q_M}\frac{\lambda_1}{\lambda_u}, \frac{\mathcal{R}_P^{\mathrm{RE}}}{q_P+q_C}\frac{\lambda_2}{\lambda_u}\right\}. \tag{2.30}$$

For the Tr scheme, the minimum rate is equal to that of RE scheme when β goes to 0, while for the FC scheme, it is equal to that of LAC when β approaches infinity.

It can be seen in Figure 2.8 that, for the RE scheme, as the bias factor increases, the average user rate offered by the network improves up to a maximum point. After this point, the rate offered by picocell BSs starts to limit the network performance

due to the increase in the number of users per picocell BS, hence, the minimum rate starts to degrade. This effect is less severe in the LAC scheme as the increase in the number of users per picocell BS due to the increase in the cooperation threshold is compensated by the improvement in the overall rate of the CoMP users offered by the network. That is, the minimum average user rate remains almost constant for high bias factor values. It can also be seen that the performance of the proposed scheme approaches the performance of full cooperation scheme when β is high enough. In addition, the minimum rate offered by each of the LAC and RE schemes is better than that of the Tr scheme for all $\beta > 0$.

2.5.5 Average Load per BS

Figure 2.9 shows the impact of increasing the cooperation threshold (bias factor) on the average load per BS for the RE scheme, FC scheme, as well as the LAC scheme. It can be seen that, as the bias factor increases, the RE scheme reduces the number of users per macrocell BS compared to the Tr scheme without biasing (i.e, when $\beta = 0$ dB), by offloading some of the macrocell users to the picocell network tier based on the received powers at these users. On the other hand, the FC scheme increases the number of users per both macrocell BS and picocell BS compared to the Tr scheme in a two-tier cellular network since it serves all users by using cooperation between BSs in the two tiers. Finally, it can be seen that the LAC scheme keeps the same number of users per macrocell BS while increasing the number of users per picocell BS when compared to the Tr scheme. This is due to the fact that the proposed scheme does not actually offload any users to a different tier. Instead, it changes the mode of operation of users with bad SINR conditions which are now served by the original macrocell BS along with the strongest interfering picocell BS.

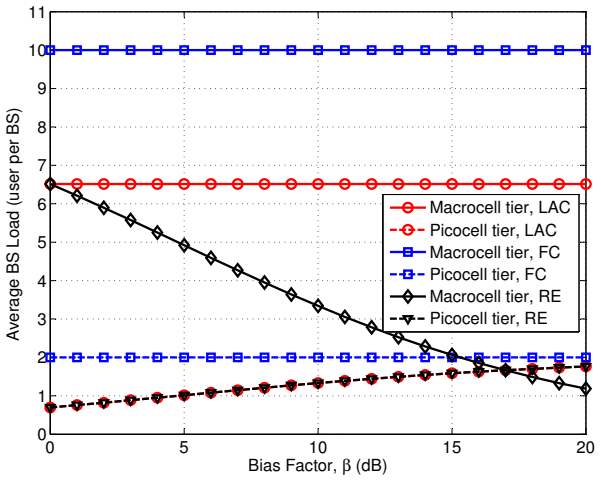

Figure 2.9: LAC vs. Range Expansion and Full Cooperation: Average load per BS vs. the cooperation threshold (bias factor) β where $\lambda_1 = (0.5^2\pi)^{-1}$ BS/km^2, $\lambda_2 = 5(0.5^2\pi)^{-1}$ BS/km^2, $\lambda_u = 10(0.5^2\pi)^{-1}$ user/km^2, $P_1 = 37$ dBm, $P_2 = 20$ dBm, $\alpha_1 = \alpha_2 = 3.5$, and $\sigma^2 = -104$ dBm.

The load per BS can reflect the amount of backhaul data exchange required by each scheme. For example, none of the Tr and RE schemes requires any users' data exchange between BSs over the backhaul links since all users are served by a single BS all the time. On the other hand, among the four schemes, the FC scheme requires the maximum amount of backhaul data exchange since it uses cooperation to serve all users. In the proposed scheme, the amount of backhaul data exchange lies between those of the Tr and RE, and FC schemes.

In order to compare the FC scheme with the proposed scheme, Figure 2.10 shows the joint PDF of the distances of a CoMP user to serving BSs for both schemes. It can be seen in Figure 2.10(a) that the FC scheme serves all users by CoMP transmission regardless of their locations in the network. For the LAC scheme, Figures 2.10(b) and 2.10(c) show the effect of increasing the cooperation threshold on the area of cooperation region. With a higher cooperation threshold β, more users are included in the cooperation regions which, in turn, increases the amount of users'

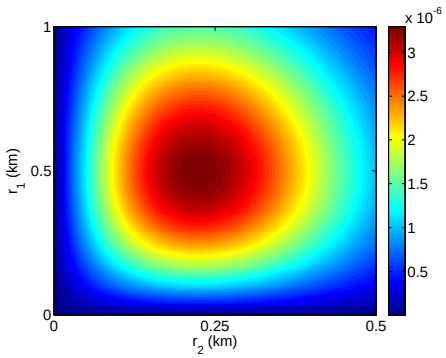

(a) Case I: Full Cooperation scheme, $\alpha_1 = \alpha_2 = 4$

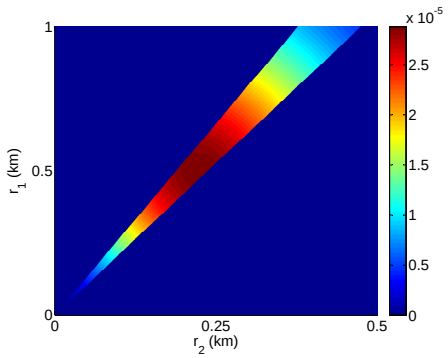

(b) Case II: LAC scheme, $\alpha_1 = \alpha_2 = 4$ and $\beta = 4$ dB

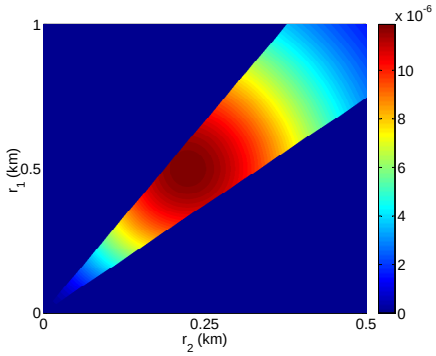

(c) Case III: LAC scheme, $\alpha_1 = \alpha_2 = 4$ and $\beta = 10$ dB

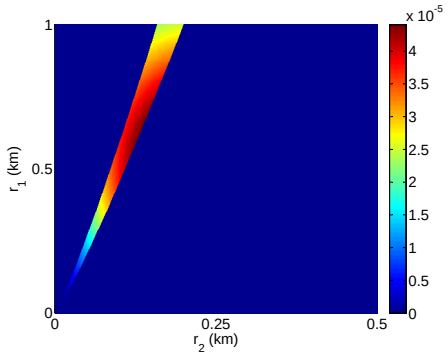

(d) Case IV: LAC scheme, $\alpha_1 = 3.5$, $\alpha_2 = 4$ and $\beta = 4$ dB

Figure 2.10: LAC vs. Full Cooperation: Joint PDF of the distance of a CoMP user to serving BSs where $\lambda_1 = (0.5^2\pi)^{-1}$ BS/km^2, $\lambda_2 = 5(0.5^2\pi)^{-1}$ BS/km^2, and $P_1 = 37$ dBm, $P_2 = 20$ dBm.

data exchange over the backhaul network. Compared to Figure 2.10(a), it can be seen that users with good SINR conditions, who are close to the serving BS and far from the strongest interferer, do not use CoMP transmission to save the resources of the backhaul network. Figure 2.10(d) shows that the effect of cross-tier interference decreases when the path-loss exponent of the picocell network tier is higher than that of the macrocell network tier, which isolates the picocell BSs. That is, CoMP transmission is limited to users who are very close to the picocell BSs and thus the amount of required data exchanges is reduced.

2.6 Chapter Summary

In this chapter, the concept of cross-tier cooperation in two-tier cellular networks has been investigated. I have proposed a novel location-aware cross-tier cooperation scheme that uses downlink CoMP transmission depending on the locations of the users and their nearest macrocell and picocell BSs. Tools from stochastic geometry have been used to analyze the outage probability and average rate for the proposed scheme. The proposed scheme has been compared with three other schemes, namely, Traditional (Tr), Range Expansion (RE), and Full Cooperation (FC) schemes. The comparison has been performed in terms of outage probability, average ergodic rate, as well as load per BS. The results have shown that the proposed LAC scheme outperforms both RE and Tr schemes in terms of outage probability and average ergodic rate. However, this performance gain with the proposed scheme comes at the expense of the overhead due to the exchange of users' data between the two cooperating BSs. In addition, the performance of the proposed scheme approaches that of the FC scheme for sufficiently high cooperation threshold. In this way, the LAC scheme provides a tradeoff between the improved outage probability and the cost of cooperation between BSs in terms of load per BS which reflects the amount of users' data exchange over the backhaul network.

Chapter 3

Cognitive and Energy Harvesting-Based D2D Communication in Multi-Tier Cellular Networks

While cognitive radio enables spectrum-efficient wireless communication, radio frequency (RF) energy harvesting from ambient interference is an enabler for energy-efficient wireless communication. In this chapter, I model and analyze cognitive and energy harvesting-based device-to-device (D2D) communication in multi-channel multi-tier cellular networks. In this case, a macrocell network tier is underlaid with a second network tier of cognitive D2D transmissions. The cognitive D2D transmitters harvest energy from ambient interference and use one of the channels allocated to cellular users (in uplink or downlink), which is referred to as the D2D channel, to communicate with the corresponding receivers. I investigate two spectrum access policies for cellular communication in the uplink or downlink, namely, random spec-

trum access (RSA) policy and prioritized spectrum access (PSA) policy. In RSA, any of the available channels including the channel used by the D2D transmitters can be selected randomly for cellular communication, while in PSA the D2D channel is used only when all of the other channels are occupied. A D2D transmitter can communicate successfully with its receiver only when it harvests enough energy to perform channel inversion toward the receiver, the D2D channel is free, and the SINR at the receiver is above some predefined threshold, otherwise, an outage occurs for the D2D communication. I use tools from stochastic geometry to evaluate the performance of the proposed communication system model with general path-loss exponent in terms of outage probability for D2D and cellular users. Furthermore, using the proposed framework it is shown that: (i) Energy harvesting can be a reliable alternative to power cognitive D2D transmitters while achieving acceptable performance. (ii) Under the same SINR outage requirements as for the non-cognitive case, cognitive channel access improves the outage probability for D2D users for both spectrum access policies. (iii) When compared with the RSA policy, the PSA policy provides a better performance to the D2D users. (iv) Using an uplink channel provides improved performance to the D2D users in dense networks when compared to a downlink channel. (v) For cellular users, the PSA policy provides almost the same outage performance as the RSA policy.

3.1 Introduction

Harvesting energy from non-traditional sources such as ambient interference is emerging as an attractive solution to power low-energy wireless communication devices [31–33]. On the other hand, in order to improve spectrum utilization and mitigate the scarcity of spectrum, innovative solutions such as cognitive radio [52,53] and D2D

technology have been recently proposed to underlay current cellular networks [9].

I consider cognitive D2D communication underlaying a multi-channel cellular network where the D2D transmitters are able to use only the harvested RF energy from the ambient interference that results from the concurrent downlink and uplink transmissions by both macrocell BSs and cellular users. After harvesting sufficient energy, each D2D transmitter performs spectrum sensing to opportunistically access a predefined nonexclusive D2D channel. The term "cognitive D2D communication" is used in the sense that spectrum sensing is performed at each D2D transmitter before transmission to make sure that the channel designated for D2D transmission is not being used for cellular communication in the uplink or downlink. Here, cognition is with respect to the cellular BSs and cellular users only, which is similar to the concept of semi-cognitive spectrum access in [54]. In a multi-channel environment, I consider two different spectrum access policies for cellular communication (in the uplink/downlink to/from BS) to enable the coexistence of the cellular and D2D users. I use a statistical approach based on stochastic geometry [17,21] to model and evaluate the performance of the proposed system in terms of outage probabilities of D2D users as well as cellular users. Note that the outage for D2D users may occur due to

- Insufficient amount of harvested energy.
- Unavailability of the D2D channel.
- SINR at the receiver falls below the required threshold.

For cellular users, the outage occurs due to

- Unavailability of cellular channels.
- Insufficient SINR.

Due to their analytical tractability, I use independent PPPs to model the locations of BSs, cellular users, and D2D users. The results from the analysis helps to understand the impact of network parameters (such as spatial densities of BSs and users, number of channels, carrier/spectrum sensing threshold, and receiver sensitivity) on the performance measures and provide insightful guidelines for system design.

3.1.1 Contributions

The contributions of this chapter are summarized as follows.

- Using tools from stochastic geometry, I provide a tractable analytical framework for statistical analysis of cognitive D2D communication using energy harvested from the ambient interference. For a general path-loss exponent, I derive simple and closed-form expressions for the probability of harvesting sufficient energy, the probability that the channel to be used by D2D users is free, the SINR outage probability for both D2D and cellular users, and the overall outage probability for D2D users. I discuss the different trade-offs in the system and show the effect of varying network parameters such as spectrum sensing threshold, spatial densities of BSs and cellular users, number of available channels, and sensitivity of the receivers on the system performance.

- While D2D users perform spectrum sensing-based transmission and a channel inversion power control, two different spectrum access policies are proposed for cellular communication, namely, random spectrum access (RSA) and prioritized spectrum access (PSA) policies. For each spectrum access policy, I analyze the performance of energy-harvesting D2D communication. I also show how cellular users are affected by the adopted spectrum access policy.

- I consider both cases when D2D transmissions take place in a channel assigned for downlink cellular transmissions or uplink cellular transmissions. I investigate the different scenarios to show when uplink channels are preferable to downlink channels and vice versa. More specifically, I obtain a closed-form expression for the value of spatial density of BSs after which uplink channels should be used to achieve a better performance for D2D communication when compared to using downlink channels.

- I show that provisioning of multiple channels can be used along with cognition by D2D users to protect the cellular transmissions. For the same network parameters and SINR outage requirements, I also show that the overall outage performance of D2D users is always superior with the PSA policy compared to the RSA policy while the performance of the cellular users is almost the same for both spectrum access policies.

3.1.2 Organization

The rest of this chapter is organized as follows. A review of the related work is presented in Section 2.2. The system model is described in Section 3.3. In Section 3.4, the transmission probability of a D2D transmitter (i.e., the probability that the transmitter is able to harvest enough energy for channel inversion toward its intended receiver and the designated channel for transmission is available) is derived for different spectrum access policies for cellular communication. Section 3.5 presents the analysis of the outage probability for D2D users and cellular users. Finally, the numerical results are presented in Section 3.6 before the chapter is summarized in Section 3.7.

3.2 Related Work

In the context of energy harvesting in wireless networks, one way to evaluate the performance of the system under investigation is to use statistical modeling [55–58]. Although statistical modeling gives insights into the long-term performance behavior and helps to select the statistically optimal network parameters, these parameters are not necessarily optimal on a short time-scale. On the other hand, tools from optimization theory can be used to model the network and evaluate the short-term performance to find optimal parameters that maximize certain objective functions [59–61]. However, obtaining the optimal parameters on a short time basis generally increases the computational complexity and puts a burden on the system due to more frequent exchange of information.

In [55], the authors deploy dedicated stations called "power beacons" that radiate out-of-band microwave signals to power all mobile devices. Under an outage constraint, the uplink cellular network performance is evaluated using a statistical model and the region of feasible operation is defined for different setups. In [56], the authors propose a cognitive radio model in which a low-energy secondary transmitter harvests RF energy from transmissions by primary users in its vicinity. Statistical analysis is used to optimally choose network parameters such as power and spatial density of secondary transmitters in order to maximize the spatial throughput while satisfying some outage constraints. In [57], the authors use Ginibre determinantal point process to obtain bounds on the performance of a wireless sensor network with RF energy harvesting. The author in [58] derives the outage probability and the average harvested energy of the simultaneous information and power transfer. The author considers a large-scale network with large number of randomly located transmitter-receiver pairs with and without relaying.

In [59], the authors use dynamic programming to derive the optimal power control policy that minimizes the outage probability. The optimization problem is formulated and solved for block fading channels under energy harvesting constraints such that the transmit power is upper bounded by the amount of energy harvested. In [60], for a point-to-point wireless link, the authors assume that the receiver can either harvest energy from ambient RF signals or decode information at any point of time. For this scenario, the authors use optimization tools to obtain the optimal mode switching point that balances the tradeoff between the amount of harvested energy, data rate, and outage probability. In [61], the authors use fractional programming and dual decomposition to propose a resource allocation algorithm that maximizes the energy efficiency of a downlink single-cell orthogonal frequency division multiple access (OFDMA) network.

In the context of multi-channel cognitive cellular networks, the authors in [52] provide a framework to model such a network in which macrocell BSs are underlaid with cognitive femtocell BSs. For the network under consideration, statistical analysis is used to obtain a long-term optimal spectrum sensing threshold that minimizes the outage probability of the cognitive femtocell BSs. On the other hand, in the context of D2D communication, the authors in [62] use statistical analysis to investigate the effect of distance-based mode selection and power control on the outage performance in the uplink. Another statistical framework is presented in [63] that takes the quality of the links between D2D users and BSs into consideration in the mode selection phase, furthermore, it accounts for the maximum transmit power of users. For performance evaluation of D2D transmissions underlaying a cellular network, the authors in [64–66] consider different scenarios and optimization problems. In [64], the authors propose a greedy algorithm to solve the resource allocation problem where the optimization

problem is formulated as a mixed-integer non-linear program to maximize the sum-rate of both cellular and D2D under SINR constraints. The authors in [65] consider a network scenario in which cellular and D2D users share the same resources. The system aims to maximize the network throughput via mode selection and power control while satisfying spectral efficiency and power constraints. For some special cases, the optimal solution is obtained either in a closed-form or by searching a finite set. In [66], the authors propose a joint resource block allocation and power control scheme to maximize the spectrum utilization while fulfilling some interference constraints and traffic demands of cellular and D2D users, respectively.

3.3 System Model and Assumptions

3.3.1 Network Model

I consider a cellular network in which macrocell BSs are underlaid with randomly located cognitive D2D transmitters. The locations of macrocell BSs are modeled by a homogeneous PPP $\mathbf{\Phi} = \{x_i : i = 1, 2, \dots\}$ of spatial density λ_b where $x_i \in \mathbb{R}^2$ denotes the location of the i-th BS. All BSs are from the same type, i.e., macrocell BSs in this case, and transmit in the downlink with the same power level P_b. Cellular users are spatially distributed in $\mathbb{R}^2$ according to an independent homogeneous PPP $\mathbf{\Psi} = \{u_i : i = 1, 2, \dots\}$ of spatial density λ_u. Each cellular user associates with the closest BS, i.e., the BS from which she receives the strongest average signal. Cognitive D2D transmitters are also modeled by an independent two-dimensional PPP $\mathbf{\Xi} = \{y_i : i = 1, 2, \dots\}$ with spatial density λ_d. A D2D communication link is established only when the intended receiver is within a disc of radius $d_\circ$ and centered

around the D2D transmitter[1]. For the reliability of communication links, all users (i.e., D2D transmitters and cellular users) use channel inversion power control to adjust their transmit power by inverting the path-loss to insure that the average received signal power at the intended receiver (i.e., D2D receivers and BSs) is equal to its sensitivity. Here, I use P_u and P_d to denote the transmit power of an uplink cellular user and a D2D transmitter, respectively. It is assumed that all the D2D receivers have the same sensitivity ρ_d and all the BSs have a sensitivity of ρ_b. Saturation condition is assumed where each transmitter (i.e., BS in downlink, cellular user in uplink, or D2D transmitter) has at least one packet ready for transmission at the beginning of each time slot in a time-slotted transmission scenario.

3.3.2 Channel Model

The total available bandwidth is divided into a set of orthogonal channels $\mathcal{S} = \{s_1, s_2, \ldots, s_{|\mathcal{S}|}\}$ where $|\cdot|$ denotes the set cardinality. Furthermore, the set of channels $\mathcal{S}$ is partitioned into two disjoint subsets of channels $\mathcal{S}^{\mathrm{D}}$ and $\mathcal{S}^{\mathrm{U}}$ for downlink and uplink transmissions, respectively. While a cellular user can be served (in downlink or uplink) over any channel $s_i \in \mathcal{S}$ depending on the channel availability at the serving BS, all D2D transmissions take place on the same channel $s_d \in \mathcal{S}$, cf. Figure 3.1. Note that channel s_d is not exclusive for D2D transmissions and can be used for cellular communication depending on the adopted spectrum access policy (i.e., RSA or PSA). Note also that s_d can be either an uplink channel or a downlink channel used for cellular communication. In this work, I consider both cases when the D2D transmissions can take place either in one of the uplink channels or one of the down-

[1]Since the problem of mode selection is not within the scope of this work, I assume that each D2D transmitter has an intended receiver within a distance $d_\circ$ with probability 1. For the mode selection in D2D Poisson networks, refer to [62, 63].

link channels. At any BS, each associated cellular user is served by only one channel at most. In addition, there is no intra-cell interference assuming that each BS serves no more than one user in each channel.

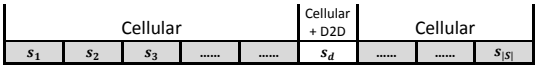

Figure 3.1: Spectrum allocation for cellular and D2D transmissions.

The power of the signal transmitted by a BS or a cellular user is assumed to decay at a rate of $r^{-\alpha}$ where α is the path-loss exponent and r is the propagation distance. On the other hand, the decay of the power transmitted by a D2D transmitter occurs at a rate of $r^{-\beta}$ where β is the path-loss exponent[2]. Rayleigh fading is used to model small-scale fading over each channel where independence between channels is assumed. Hence, under the assumption that the channel gains are i.i.d., the power gain from a transmitter (i.e., BS, cellular user, or D2D transmitter) located at x toward a generic point at y on a channel s is denoted by $h_s(x, y) \sim \text{Exp}(1)$.

3.3.3 Energy Harvesting Model

All D2D transmitters are powered by energy harvested from the ambient interference caused by the simultaneous cellular transmissions in the network (i.e., downlink and uplink transmissions). It is assumed that each D2D transmitter is equipped with an energy harvesting circuit that harvests RF power from all channels including both downlink and uplink channels. Therefore, the total power available for harvesting by a D2D transmitter located at a generic location $y \in \mathbb{R}^2$ can be expressed as

$$P_{\text{H}}(y) = a \sum_{s \in \mathcal{S}^{\text{D}}} \sum_{x \in \tilde{\mathbf{\Phi}}(s)} P_b h_s(x, y) \|x - y\|^{-\alpha} + a \sum_{s \in \mathcal{S}^{\text{U}}} \sum_{u \in \tilde{\mathbf{\Psi}}(s)} P_u h_s(u, y) \|u - y\|^{-\alpha} \quad (3.1)$$

[2]The channel model can be extended by incorporating multi-slope path-loss models as in [67].

where the first term represents the amount of RF power harvested from the concurrent downlink cellular transmissions and the second term is for the RF power harvested from the concurrent uplink cellular transmissions. It is worth mentioning that the amount of power received from other concurrent D2D transmissions at the harvesting unit is not considered in P_{H}. In (3.1), $\tilde{\mathbf{\Phi}}(s)$ is a PPP with spatial density $q_c\lambda_b$ that represents the set of BSs using channel $s \in \mathcal{S}^{\mathrm{D}}$ where q_c is the probability that a BS uses this channel[3]. $\tilde{\mathbf{\Psi}}(s)$ is a point process with spatial density $q_c\lambda_b$ that represents the set of users using channel $s \in \mathcal{S}^{\mathrm{U}}$. Note that, unlike $\tilde{\mathbf{\Phi}}(s)$, $\tilde{\mathbf{\Psi}}(s)$ is not a PPP due to the correlation among uplink cellular users. $0 < a \leq 1$ is the efficiency of the conversion from RF to DC power, and $\|\cdot\|$ denotes the Euclidean distance.

It is worth noting that a D2D transmitter may not harvest enough energy in one time slot to transmit with sufficient power since the power available for harvesting varies depending on the location of the D2D transmitter and the network statistics such as the channel power gains. Therefore, with a time-slotted "harvest-then-transmit" strategy, it is assumed that the RF energy harvesting and DC conversion circuits of a D2D transmitter are activated only when the available power in the time-slot is at least equal to the amount of power needed to invert the channel to its intended receiver. There is no energy storage assumed where a D2D transmitter can save the extra harvested energy for the next time slot.

3.3.4 Spectrum Sensing Model for D2D Transmission

All D2D transmitters are assumed to be cognitive where each transmitter senses the state of the channel s_d at the beginning of each time slot before it decides whether or not to use the channel for transmission. In this work, the main purpose of spectrum

[3] q_c, the spectrum access probability of a BS, will be discussed in detail later in Section 3.4.

sensing is to avoid the interference that results from nearby cellular transmissions on channel s_d. That is, the D2D transmitter does not use the channel s_d if the received interference from any neighboring transmitter (i.e., BS in the downlink or cellular user in the uplink) on this channel is higher than a predefined sensing threshold ζ, otherwise, the channel is available to be used by the D2D transmitter. Note that increasing the sensing threshold increases the probability to access the channel s_d while increasing the aggregate interference at the same time. On the other hand, decreasing the sensing threshold provides more protection to the D2D transmission by decreasing the aggregate interference, however, it reduces the chance to access the channel s_d. In other words, cognition provides a protection region around each D2D transmitter in which that D2D transmitter cannot use the channel s_d if there is at least one active transmitter using this channel inside this region.

In general, the protection region $\mathcal{B}_y(\zeta) \subset \mathbb{R}^2$ around a generic D2D transmitter located at y follows a random shape. For example, if the D2D transmission takes place in a downlink channel s_d, the protection region can be defined as

$$\begin{aligned}\mathcal{B}_y(\zeta) &= \left\{x \in \mathbb{R}^2 : P_b h_{s_d}(x,y)\|x-y\|^{-\alpha} > \zeta\right\} \\ &= \left\{x \in \mathbb{R}^2 : \|x-y\| < r_P, r_P = \left(\frac{P_b h_{s_d}(x,y)}{\zeta}\right)^{\frac{1}{\alpha}}\right\} \end{aligned} \tag{3.2}$$

where r_P represents the random radius of the protection region. On the other hand, if the D2D transmission takes place in an uplink channel s_d, the radius of the protection region is defined as

$$r_P = \left(\frac{P_u h_{s_d}(u,y)}{\zeta}\right)^{\frac{1}{\alpha}} \tag{3.3}$$

where P_u is the transmit power of the cellular user. Note that, unlike P_b, P_u is a

random variable due to the distance-dependent uplink power control scheme used by the cellular users.

On average, the protection region can be approximated by a disc $\mathcal{B}_y(\bar{r}_P) \subset \mathbb{R}^2$ centered around the D2D transmitter with a radius $\bar{r}_P = \mathbb{E}_{P,h}[r_P]$. That is, in the downlink scenario, the radius is defined such that

$$\bar{r}_P = \left(\frac{P_b}{\zeta}\right)^{\frac{1}{\alpha}} \zeta\left(\frac{\alpha+1}{\alpha}\right), \quad \text{for } s_d \in \mathcal{S}^{\mathrm{D}} \tag{3.4}$$

where $\mathbb{E}_h\left[h_{s_d}^m(x,y)\right] = \zeta(1+m)$ for any $m \in \mathbb{R}_+$ is used to derive (3.4) and $\zeta(z) = \int_0^\infty t^{z-1}e^{-t}\,\mathrm{d}t$ is the gamma function. Similarly, in the uplink scenario, $\bar{r}_P$ can be expressed as

$$\begin{aligned}\bar{r}_P &= \mathbb{E}_P\left[\left(\frac{P_u}{\zeta}\right)^{\frac{1}{\alpha}}\right]\zeta\left(\frac{\alpha+1}{\alpha}\right)\\ &= \frac{1}{2\sqrt{\lambda_b}}\left(\frac{\rho_b}{\zeta}\right)^{\frac{1}{\alpha}}\zeta\left(\frac{\alpha+1}{\alpha}\right), \quad \text{for } s_d \in \mathcal{S}^{\mathrm{U}}\end{aligned} \tag{3.5}$$

where (3.5) follows by using the $\frac{1}{\alpha}$-th moment of the transmit power of a cellular user, i.e., $\mathbb{E}\left[P_u^{\frac{1}{\alpha}}\right] = \frac{\rho_b^{\frac{1}{\alpha}}}{2\sqrt{\lambda_b}}$ when using channel inversion uplink power control as will be derived shown in Chapter 4.

Without loss of generality, Figure 3.2 shows a realization of a cellular network whose macrocell BSs are underlaid with D2D transmitters. Note that not every D2D transmitter in Figure 3.2 can use the D2D channel since it depends on the allocation of channels to the cellular transmitters, which are located in the protection region of the D2D transmitter.

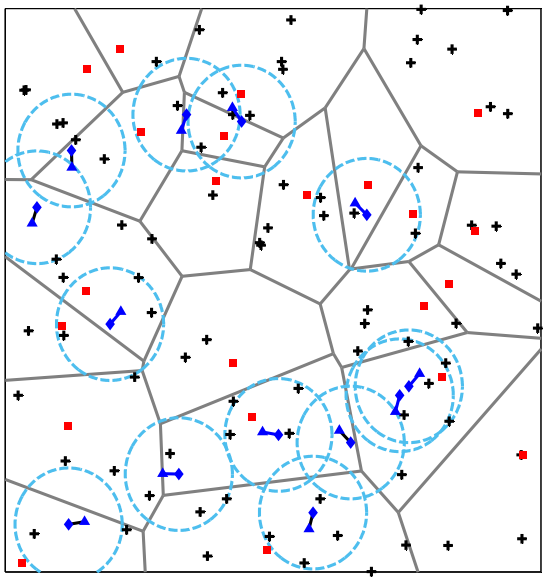

Figure 3.2: A realization of the described network model where red squares represent the BSs, crosses represent the cellular users, and blue lines represent the potential D2D links between the D2D transmitters (blue diamonds) and D2D receivers (blue triangles). Each D2D transmitter is surrounded by a protection region $\mathcal{B}(\bar{r}_P)$ (dashed circles) with radius $\bar{r}_P$. The spatial densities are $\lambda_u = 4\lambda_b$ and $\lambda_d = \lambda_b$.

3.3.5 Spectrum Access Model for Cellular Transmissions

I consider two spectrum access policies, namely, random spectrum access (RSA) and prioritized spectrum access (PSA) policies, that define how the spectrum is assigned for downlink and uplink transmissions to serve the cellular users. In RSA, in each cell, any channel $s_i \in \mathcal{S}$ (including channel s_d which is used for D2D transmission) can be independently and randomly assigned with the same probability to serve one of the cellular users. On the other hand, in PSA, any channel $s_i \in \mathcal{S} \setminus \{s_d\}$ can be independently and randomly assigned to a cellular user as long as the number of cellular users is less than the number of available channels $|\mathcal{S}|$. When the number of cellular users is higher than $|\mathcal{S}| - 1$, only then, s_d will be assigned to a cellular user.

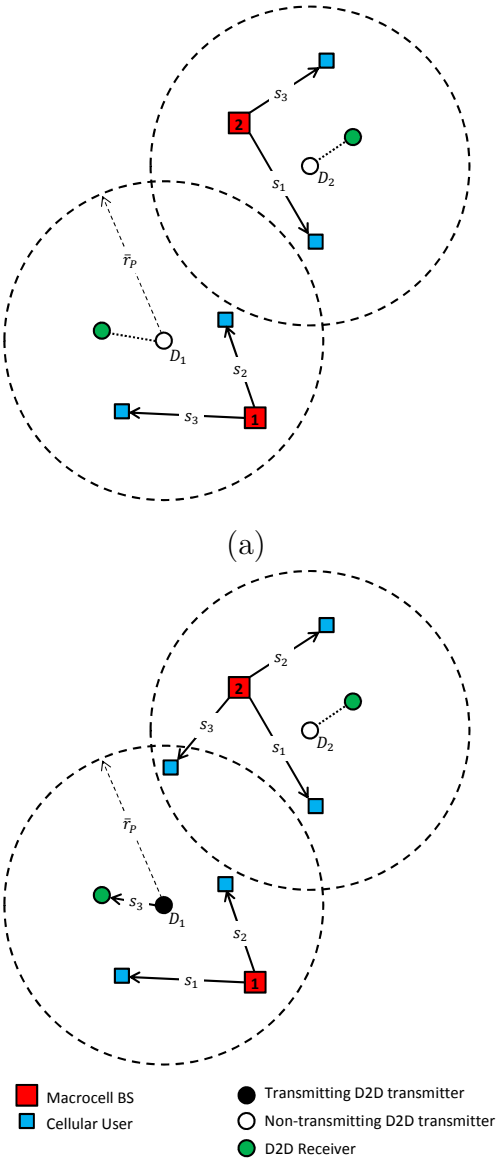

Figure 3.3: Spectrum access policies: (a) RSA (b) PSA, where the network consists of 2 BSs and 2 D2D transmitters, i.e., D_1 and D_2, $\mathcal{S} = \{s_1, s_2, s_3\}$ and $s_d = s_3$.

To illustrate, Figure 3.3 shows a realization of RSA and PSA policies, respectively, where the number of available channels in the network is 3 and channel s_3 is shared by both cellular and D2D transmissions. For the RSA policy in Figure 3.3(a), although each BS has only two cellular users, both of D2D transmitters are unable to use

channel s_3 since each of them has at least one BS in its protection region that uses s_3 to serve one of its users. That is, since there is no restriction on any BS to use any channel regardless of the number of its associated users, s_3 may be used by both BSs. This prevents both D2D transmitters from using channel s_2. For the PSA policy in Figure 3.3(b), it can be seen that the D2D transmitter D_1 uses s_3 for transmission because the only BS in its protection region, i.e., BS 1, does not use s_3 since it has only two cellular users (i.e., less than $|\mathcal{S}|$). On the other hand, D_2 cannot transmit on channel s_3 because BS 2, that lies in its protection region, has to use all the available channels to serve its three users. Obviously, when compared to the RSA policy, PSA policy increases the probability that a D2D transmitter is able to access the D2D channel s_d. Note that, in the worst case, when all BSs have more users than the available channels, both access policies have the same performance.

3.3.6 Methodology of Analysis

Based on the system model described above, I aim at quantifying the performance of both D2D and cellular communications in terms of transmission probability for D2D users (i.e., the probability that there is a channel available for transmission and the amount of harvested energy is sufficient for D2D transmission) and SINR outage probability of both D2D and cellular users. The performance metrics are obtained for a test user located at the origin $(0, 0) \in \mathbb{R}^2$, therefore, the notation for the test user's location will be dropped. According to Slivnyak's Theorem [17], these results should be then valid for any generic user. I derive the spectrum access probabilities for the cellular transmissions and a generic D2D transmitter for both RSA and PSA policies. Then, the PDF of the interference power available for energy harvesting is derived to evaluate the probability that a D2D transmitter can harvest sufficient energy for

transmission. Based on the obtained probabilities, the SINR outage probability is quantified for both cellular and D2D users.

Note that there is no restriction on any BS to independently adopt either of the spectrum access policies. The spatial density of BSs using each policy can be easily obtained by using the thinning property of a PPP [28], however, I consider the case when all BSs adopt the same spectrum access policy.

3.4 Spectrum Access Probabilities for Cellular Communication and Transmission Probabilities for D2D Users

3.4.1 Spectrum Access Probabilities for Cellular Communication

For a cellular user, a connection (i.e., downlink or uplink connection) can only be established when a channel $s_i \in \mathcal{S}$ is available. Therefore, I define q_f as the probability that a BS has a free channel to assign to one of its associated users for uplink or downlink transmission.

Based on the spectrum access policies defined in Section 3.3.5, I derive the availability of any channel $s_i \in \mathcal{S}$ for cellular communication. Firstly, let N_u denote the number of users associated to a BS where the association policy is based on the nearest BS. According to [52, Appendix A], the probability mass function (PMF) of the number of users served by a generic BS is obtained as

$$\mathbb{P}\{N_u = n\} = \zeta \, \frac{\zeta(n+b)}{\zeta(n+1)} \frac{(\mathbb{E}[N_u])^n}{(b+\mathbb{E}[N_u])^{n+b}} \tag{3.6}$$

where $\zeta = \frac{b^b}{\zeta(b)}$ is a constant and $\mathbb{E}[N_u] = \frac{\lambda_u}{\lambda_b}$ is the average number of cellular users per BS. This expression is derived by approximating the area of a Voronoi cell

by a gamma-distributed random variable with a shape parameter $b = 3.575$ and a scale parameter $\frac{1}{b\lambda_b}$. Note that this expression is valid only when the cellular users are assumed to be spatially distributed according to an independent PPP and their associations to the BSs are based on the maximum average received signal power, i.e., each user associates with her nearest BS.

Note that all BSs in the cellular network share the same set of channels $\mathcal{S}$. While the number of channels assigned by each BS depends only on the number of its associated users N_u, the subset of channels used by each BS varies according to the adopted spectrum access policy. That is, the number of channels used by a BS for cellular communication is $\min\{N_u, |\mathcal{S}|\}$ and the probability that there is a free channel to serve a cellular user does not depend on the adopted spectrum access policy. Thus, (3.6) is used to derive the probability q_f that a cellular user finds a free channel available when it associates with a generic BS.

Lemma 3.1. The probability that a cellular user is assigned a channel by her serving BS is

$$q_f = 1 - \sum_{n=|\mathcal{S}|+1}^{\infty} \frac{n - |\mathcal{S}|}{n} \mathbb{P}\{N_u = n\} \tag{3.7}$$

where $\mathbb{P}\{N_u = n\}$ is given by (3.6).

Proof. See **Appendix B.1.1**. □

Intuitively, **Lemma 3.1** shows that the probability that a BS is able to serve more cellular users increases with increasing number of channels $|\mathcal{S}|$, increasing the spatial densities of BSs λ_b, or decreasing spatial density of cellular users λ_u.

Note that the expression in (3.7) can be used for both RSA and PSA policies. To illustrate the impact of the adopted spectrum policy on the subset of the channels

used for cellular communication, I define q_c as the probability of a generic BS to assign a specific channel $s_i \in \mathcal{S} \setminus \{s_d\}$ to serve one of its associated users. I also define q_d as the probability that a generic BS assigns the D2D channel s_d to serve one of its associated users.

3.4.1.1 Spectrum access probabilities for the RSA policy

Since any BS randomly and independently assigns any channel $s_i \in \mathcal{S}$ with the same probability, the spectrum access probabilities q_c^{RSA} and q_d^{RSA} can be expressed as in the following lemma.

Lemma 3.2. For the RSA policy, the probability that a BS uses a generic channel $s_i \in \mathcal{S}$ to serve one of its associated cellular users is given by

$$q_c^{\text{RSA}} = 1 - \sum_{n=0}^{|\mathcal{S}|-1} \frac{|\mathcal{S}| - n}{|\mathcal{S}|} \mathbb{P}\{N_u = n\} \tag{3.8}$$

where $q_d^{\text{RSA}} = q_c^{\text{RSA}}$ and $\mathbb{P}\{N_u = n\}$ is given by (3.6).

Proof. See **Appendix B.1.2**. □

3.4.1.2 Spectrum access probabilities for the PSA policy

With PSA, since a BS uses s_d only when it runs out of the rest of the available channels, the probability of using a channel $s_i \in \mathcal{S} \setminus \{s_d\}$ by a generic BS is different from that of using s_d, i.e., $q_c^{\text{PSA}} \neq q_d^{\text{PSA}}$. The expressions for q_c^{PSA} and q_d^{PSA} are presented in the following lemma.

Lemma 3.3. For the PSA policy, the probability that a BS uses a generic channel

$s_i \in \mathcal{S} \setminus \{s_d\}$ to serve one of its associated cellular users is given by

$$q_c^{\text{PSA}} = 1 - \sum_{n=0}^{|\mathcal{S}|-1} \frac{|\mathcal{S}| - n - 1}{|\mathcal{S}| - 1} \mathbb{P}\{N_u = n\} \tag{3.9}$$

while the probability that a BS has to use s_d to serve one of its associated cellular users is given by

$$q_d^{\text{PSA}} = 1 - \sum_{n=0}^{|\mathcal{S}|-1} \mathbb{P}\{N_u = n\} \tag{3.10}$$

where $\mathbb{P}\{N_u = n\}$ is given by (3.6).

Proof. See **Appendix B.1.3**. □

Figure 3.4 compares the access probabilities q_c and q_d for both RSA and PSA presented in **Lemma 3.2** and **Lemma 3.3**. It can be seen that PSA reduces the access probability of s_d compared to RSA where this improvement is proportional to the number of available channels $|\mathcal{S}|$. It can also be seen that the increase in the access probability of any channel other than s_d is very small since the additional probability of not using s_d is distributed evenly across all the $|\mathcal{S}| - 1$ channels. This means that channels other than s_d become slightly more congested when adopting the PSA policy while the D2D channel s_d is less congested (compared to the RSA policy) to protect the D2D transmissions. The decrease in the access probability of s_d is

$$q_d^{\text{RSA}} - q_d^{\text{PSA}} = \sum_{n=0}^{|\mathcal{S}|-1} \frac{n}{|\mathcal{S}|} \mathbb{P}\{N_u = n\}. \tag{3.11}$$

As stated earlier, this reduction in the access probability of s_d comes at the expense of congesting other channels in $\mathcal{S} \setminus \{s_d\}$. The increase in the access probability of a

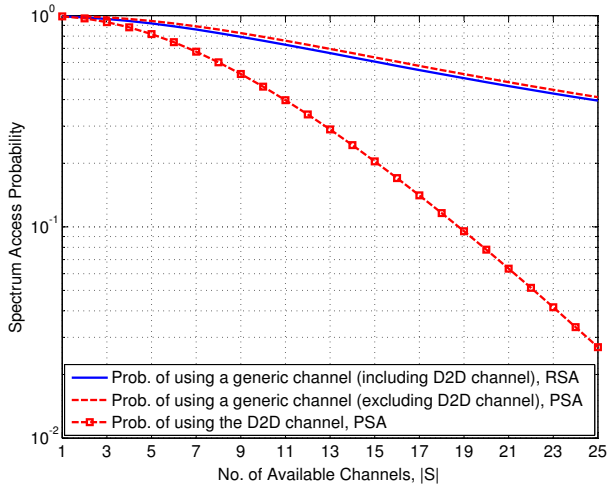

Figure 3.4: Spectrum access probabilities (q_c and q_d) of a generic BS for RSA and PSA policies where $\lambda_u = 10\lambda_b$.

channel $s_i \in \mathcal{S} \setminus \{s_d\}$ is

$$q_c^{\text{PSA}} - q_c^{\text{RSA}} = \frac{q_d^{\text{RSA}} - q_d^{\text{PSA}}}{|\mathcal{S}| - 1} \tag{3.12}$$

which clearly shows that this increase is divided by $|\mathcal{S}| - 1$ across all channels other than s_d.

3.4.2 Transmission Probability for D2D Transmitters

As described above, a D2D transmitter can access channel s_d only when it has not been assigned to any user by any of the BSs in the protection region defined in (3.2) (when s_d is a downlink channel) or (3.3) (when s_d is an uplink channel). In other words, the probability that a D2D transmitter is able to use channel s_d is equal to the probability that the number of BSs, which use this channel in the protection region of this D2D transmitter, is zero. Let p_f denote this probability. The D2D transmitter also needs to harvest sufficient energy to perform channel inversion, the probability

of which is denoted by p_s. Hence, the transmission probability of a D2D transmitter can be defined as

$$p_t = p_s p_f. \tag{3.13}$$

3.4.2.1 Calculation of p_f

The expression for p_f is provided in the following lemma.

Lemma 3.4. For a generic D2D transmitter, the probability that the D2D channel (i.e., s_d) is free is given by

$$p_f = \exp[-\theta q_d] \tag{3.14}$$

where

$$\theta = \begin{cases} \pi\lambda_b \left(\frac{P_b}{\zeta}\right)^{\frac{2}{\alpha}} \zeta\left(\frac{\alpha+2}{\alpha}\right), & \text{for } s_d \in \mathcal{S}^{\mathrm{D}} \\ \left(\frac{\rho_b}{\zeta}\right)^{\frac{2}{\alpha}} \zeta\left(\frac{\alpha+2}{\alpha}\right), & \text{for } s_d \in \mathcal{S}^{\mathrm{U}}. \end{cases} \tag{3.15}$$

Here, q_d is the probability that the D2D channel is used by a generic BS for cellular communication, which is given by (3.8) and (3.10) for the RSA and PSA policies, respectively.

Proof. See **Appendix B.2**. □

3.4.2.2 Calculation of p_s

Although each D2D transmitter has an intended receiver within a circle with a radius $d_\circ$, I consider the worst-case scenario where the receiver is at the boundary of the circle (i.e., at a distance $d_\circ$). Note that this assumption provides an upper bound

on the amount of transmit power required to perform channel inversion uplink power control, hence, it provides a lower bound on the probability of harvesting sufficient energy. Relaxing this assumption complicates the derived expressions without adding more insights [68].

For a D2D transmitter with an intended receiver at a distance $d_\circ$, the minimum required transmit power that results in a received signal of ρ_d at the intended receiver by channel inversion is $P_d = \rho_d d_\circ^\beta$. Let us define the probability p_s that a D2D transmitter harvests sufficient energy to perform channel inversion as follows

$$p_s = \mathbb{P}\left[P_{\mathrm{H}}(y) > P_d\right], \tag{3.16}$$

where $P_{\mathrm{H}}(y)$ is defined in (3.1). The following lemma provides an expression for p_s for a general path-loss exponent α.

Lemma 3.5. The probability that a typical D2D transmitter harvests sufficient energy for transmission is

$$p_s = \frac{\alpha}{2\pi}\int_0^\infty \frac{1}{u}\exp\left[-\rho_d d_\circ^\beta \left(\frac{u}{\kappa_3}\right)^{\frac{\alpha}{2}}\right] \times \exp\left[-u\cos\left(\frac{2\pi}{\alpha}\right)\right]\sin\left(u\sin\left(\frac{2\pi}{\alpha}\right)\right)\,\mathrm{d}u \tag{3.17}$$

where $\kappa_3 = \kappa_1 + \kappa_2$ and

$$\kappa_1 = \frac{2\pi q_c^{\mathrm{D}}\lambda_b (aP_b)^{\frac{2}{\alpha}}\zeta\left(\frac{\alpha-2}{\alpha}\right)}{\alpha}\sum_{k=1}^{|\mathcal{S}^{\mathrm{D}}|}\frac{\zeta\left(k-\frac{\alpha-2}{\alpha}\right)}{(k-1)!}, \tag{3.18}$$

$$\kappa_2 = \frac{2\pi q_c^{\mathrm{U}}|\mathcal{S}^{\mathrm{U}}|(a\rho_b)^{\frac{2}{\alpha}}}{\alpha\sin\left(\frac{2\pi}{\alpha}\right)}. \tag{3.19}$$

Here, q_c^{D} and q_c^{U} are the access probabilities corresponding to a channel $c \in \mathcal{S}^{\mathrm{D}}$ and a channel $c \in \mathcal{S}^{\mathrm{U}}$, respectively. They are obtained based on (3.8) by using $|\mathcal{S}^{\mathrm{D}}|$ and $|\mathcal{S}^{\mathrm{U}}|$, respectively.

Proof. See **Appendix B.3**. □

Furthermore, in the following corollary I show that the probability of harvesting sufficient energy p_s can be presented in a closed-form expression in the special case when $\alpha = 4$.

Corollary 3.1. The probability that a typical D2D transmitter harvests sufficient energy for transmission when $\alpha = 4$ is

$$p_s = \mathrm{erf}\left(\frac{\kappa_3}{2\sqrt{\rho_d d_\circ^\beta}}\right) \tag{3.20}$$

where $\mathrm{erf}(z) = \frac{2}{\sqrt{\pi}} \int_0^z e^{-t^2}\, \mathrm{d}t$ is the error function and κ_3 can be reduced as

$$\kappa_3 = \frac{1}{2}\pi^2 q_c^{\mathrm{D}} \lambda_b \sqrt{aP_b} \sum_{k=0}^{|\mathcal{S}^{\mathrm{D}}|-1} \frac{1}{4^k}\binom{2k}{k} + \frac{1}{2}\pi q_c^{\mathrm{U}} |\mathcal{S}^{\mathrm{U}}| \sqrt{a\rho_b}. \tag{3.21}$$

Proof. When $\alpha = 4$, the CDF of aggregate received interference follows a Lévy distribution with a location parameter 0 and a scaling parameter $\frac{\kappa_3^2}{2}$. Hence, $F_{P_{\mathrm{H}}}(x) = \mathrm{erfc}(\frac{\kappa_3}{2\sqrt{x}})$ where $\mathrm{erfc}(z) = 1 - \mathrm{erf}(z)$ is the complementary error function. □

Remark: Note that: (i) From (3.17) and (3.20), it can be seen that p_s is an increasing function of κ_i for $i = \{1, 2, 3\}$. (ii) All q_cs are decreasing functions of the number of channels $|\mathcal{S}|$. (iii) The summations in (3.18) and (3.21) are increasing

functions of the number of channels. Thus, it can be easily proven that κ_is are discrete concave functions and there exists an optimal value of $|\mathcal{S}|$ that maximizes both κ_3 and p_s. Note also that, increasing the number of available channels to a very large value does not necessarily improve p_s since not all channels will be used by each BS and p_s becomes limited by the ratio of λ_b and λ_u. This can be seen in (3.19) by noting that $\lim_{|\mathcal{S}|\to\infty} q_c|\mathcal{S}| = \frac{\lambda_u}{\lambda_b}$.

3.5 Analysis of SINR Outage Probability

In this section, I characterize the SINR outage probability for both cellular and D2D receivers. A receiver is considered in outage if the SINR falls below a given threshold τ. Note that τ can be chosen based on users' QoS requirements.

3.5.1 Outage Probability for a D2D Receiver

For the analysis of SINR outage probability, let us consider a typical D2D receiver at the origin $(0,0) \in \mathbb{R}^2$ while the results hold for any generic D2D receiver. In addition, the SINR outage probability is derived given that the corresponding D2D transmitter has sufficient energy to invert the channel and the D2D channel s_d is not used within its protection region. Each D2D receiver suffers from two sources of interference, i.e., cellular network and D2D network. For the cellular network, the aggregate interference results from all macrocell BSs (if s_d is a downlink channel) or all cellular users (if s_d is an uplink channel) that use channel s_d. Hence, I define a homogenous PPP $\tilde{\mathbf{\Phi}}(s_d)$ with spatial density $q_d\lambda_b$ that represents the set of BSs that use channel s_d and another PPP $\tilde{\mathbf{\Psi}}(s_d)$ with spatial density $q_d\lambda_b$ that represents the set of users who use channel s_d where q_d is defined in (3.8) and (3.10), respectively, for the RSA and PSA policies. For the D2D network, the aggregate interference results only from other

D2D transmitters that have sufficient energy to invert the channel to their intended receivers and can transmit on s_d. Hence, the interfering D2D transmitters do not constitute a homogeneous point process anymore and analytical characterization of interference is not possible[4]. Therefore, for analytical tractability, correlation among the locations of the interfering D2D transmitters is ignored and the resulting point process is approximated by a homogenous PPP $\tilde{\mathbf{\Xi}}$ with the same spatial density $p_t\lambda_d$ where $p_t = p_s p_f$. This approximation will be validated in Section 3.6.

For a typical D2D receiver, the SINR can be written as

$$\mathrm{SINR}_D = \frac{\rho_d h(y_\circ, 0)}{\mathcal{I}_C + \mathcal{I}_D + \sigma^2} \tag{3.22}$$

where

$$\begin{aligned} \mathcal{I}_C &= \sum_{x \in \tilde{\mathbf{\Phi}}(s_d)} P h(x,0) \|x\|^{-\alpha} \\ \mathcal{I}_D &= \sum_{y \in \tilde{\mathbf{\Xi}} \setminus \{y_\circ\}} P_d h(y,0) \|y\|^{-\beta} \end{aligned} \tag{3.23}$$

where $y_\circ$ is the corresponding D2D transmitter at a distance $d_\circ$, $h(y_\circ, 0)$ is the small-scale fading coefficient between the typical D2D receiver at $(0,0)$ and its D2D transmitter, and σ^2 is the variance of the additive noise at the receiver where no specific noise distribution is assumed. $\mathcal{I}_C$ and $\mathcal{I}_D$ denote the aggregate interference on channel s_d resulting from the cellular network (downlink or uplink) and other D2D transmitters, respectively. $P = P_b$ when $s_d \in \mathcal{S}^{\mathrm{D}}$ and $P = P_u$ when $s_d \in \mathcal{S}^{\mathrm{U}}$. $h(x,0)$ and $h(y,0)$ are fading coefficients of interference channels.

[4]This point process is called "point hole process" since the active D2D transmitters cannot be at a distance less than r_p to a cellular transmitter that uses channel s_d. The analysis of such a point process is intractable due to unknown probability generating functional [69].

Using the instantaneous SINR in (3.22), I can obtain the SINR outage probability $\mathcal{O}_D(\tau)$ for a typical D2D receiver for both cases when s_d is either a downlink channel or an uplink channel. Recall that the outage probability is defined as the probability that the SINR at the receiver is less than a predefined threshold τ, i.e.,

$$\mathcal{O}_D(\tau) = \mathbb{P}\left[\mathrm{SINR}_D \leq \tau\right].$$

The SINR outage probability is obtained in the following theorem.

Theorem 3.1. The SINR outage probability for a typical D2D receiver is given by

$$\mathcal{O}_D(\tau) = 1 - \exp\left[-\mathcal{K}_1\right]$$

where

$$\mathcal{K}_1 = \frac{\tau\sigma^2}{\rho_d} + \frac{2\pi^2 d_{\circ}^2 p_s p_f \lambda_d}{\beta \sin\left(\frac{2\pi}{\beta}\right)} \tau^{\frac{2}{\beta}} + \frac{2\pi q_d \lambda_b}{\alpha - 2} \mathcal{G}\left[\left(\frac{\rho_d}{\zeta\tau}\right)^{\frac{1}{\alpha}} \zeta\left(\frac{\alpha+1}{\alpha}\right), \alpha\right] \left(\frac{\bar{P}}{\rho_d}\tau\right)^{\frac{2}{\alpha}} \tag{3.24}$$

such that

$$\bar{P} = \begin{cases} P_b, & \text{for } s_d \in \mathcal{S}^{\mathrm{D}} \\ \dfrac{\rho_b}{(\pi\lambda_b)^{\frac{\alpha}{2}}}, & \text{for } s_d \in \mathcal{S}^{\mathrm{U}} \end{cases} \tag{3.25}$$

where $\mathcal{G}[y, \alpha] = y^{2-\alpha}\, {}_2F_1\left[1, \frac{\alpha-2}{\alpha}; \frac{2\alpha-2}{\alpha}; -y^{-\alpha}\right]$ and ${}_2F_1\left[a, b; c; x\right]$ is Gauss Hypergeometric function.

Proof. See **Appendix B.4**. □

Combining the results in **Theorem 3.1** and **Lemma 3.4**, I can obtain the reference value of λ_b (as given in the lemma below) that can be used to decide whether to

use a downlink channel or an uplink channel for D2D transmissions.

Lemma 3.6. The spatial density of BSs beyond which using an uplink channel is more beneficial for cognitive D2D communication compared to using a downlink channel is given by

$$\lambda_b^{\text{ref}} = \frac{1}{\pi}\left(\frac{\rho_b}{P_b}\right)^{\frac{2}{\alpha}}. \tag{3.26}$$

Proof. From (3.15) and (3.25), at λ_b^{ref}, θ, and $\bar{P}$ are the same for both downlink and uplink cases. Increasing λ_b beyond this value increases θ for the downlink case and reduces $\mathcal{K}_1$ for the uplink case, and vice versa. This improves the overall performance of D2D communication (i.e., higher p_f and lower SINR outage) when s_d is an uplink channel compared to the case when s_d in a downlink channel. □

Now, the overall outage probability for a generic D2D receiver can be obtained as

$$\mathcal{O}_D^{\text{tot}}(\tau) = 1 - p_t + p_t\mathcal{O}_D(\tau) \tag{3.27}$$

where this overall outage includes all the three possible events that cause outage, i.e., the event of not harvesting sufficient energy, the event of not finding the channel s_d to be free, and the event of receiving an insufficient level of SINR.

3.5.2 Outage Probability for a Cellular User

Since each cellular user associates with the closest BS, Let $x_\circ$ denote the BS to which a cellular user located at u is associated where it can be defined as follows

$$x_\circ = \arg\max_{x \in \mathbf{\Phi}} \left\{ \|x - u\|^{-\alpha} \right\}. \tag{3.28}$$

Note that this association policy ensures that a generic cellular user is closer to its serving BS than any interfering BS in the downlink. This is not true for a generic BS in the uplink network. Hence, the received SINR at a typical cellular user (in downlink) or a macrocell BS (in uplink) on a generic channel $s \in \mathcal{S}$ can be written as

$$\mathrm{SINR}_C(s) = \begin{cases} \dfrac{P_b h(x_\circ, 0) \|x_\circ\|^{-\alpha}}{\mathcal{I}_C^{\mathrm{D}}(s) + \mathcal{I}_D \cdot \mathbf{1}_{c=s_d} + \sigma^2}, & \text{for } s \in \mathcal{S}^{\mathrm{D}} \\ \dfrac{\rho_b h(x_\circ, 0)}{\mathcal{I}_C^{\mathrm{U}}(s) + \mathcal{I}_D \cdot \mathbf{1}_{c=s_d} + \sigma^2}, & \text{for } s \in \mathcal{S}^{\mathrm{U}} \end{cases} \tag{3.29}$$

where $x_\circ$ is the serving BS and $\mathbf{1}_A$ is the indicator function that equals 1 only when A is true and 0 otherwise.

For the interference in the downlink network, $\tilde{\mathbf{\Phi}}(s)$ represents a point process of BSs using channel c, which has an spatial density of $q_c\lambda_b$ for $c \in \mathcal{S}^{\mathrm{D}} \setminus \{s_d\}$ and $q_d\lambda_b$ for $c = s_d$. For the uplink transmissions, $\tilde{\mathbf{\Psi}}(s)$ represents a point process of users using channel c, which has a spatial density of $q_c\lambda_b$ for $c \in \mathcal{S}^{\mathrm{U}} \setminus \{s_d\}$ and $q_d\lambda_b$ for $c = s_d$. It is worth mentioning that the SINR outage probability $\mathcal{O}_C(\tau)$ for a typical cellular user depends on the adopted spectrum access probability for cellular communication since the SINR depends on channel c. Using the instantaneous SINR, I can obtain the SINR outage probability $\mathcal{O}_C(\tau, c)$ for a typical cellular user on channel c as

$$\mathcal{O}_C(\tau, c) = \mathbb{E}_x \left[\mathbb{P} \left[\mathrm{SINR}_C(s) \leq \tau \right] \right]. \tag{3.30}$$

The overall SINR outage probability is obtained in the following theorem.

Theorem 3.2. For an interference-limited cellular network with $\alpha = \beta$, the SINR outage probability for a typical cellular user on channel c is given by

$$\mathcal{O}_C(\tau, c) = \begin{cases} 1 - \dfrac{\pi\lambda_b}{\pi\lambda_b(1+\mathcal{K}_2) + \left(\frac{\rho_d}{P_b}\right)^{\frac{2}{\beta}} \mathcal{K}_3}, & \text{for } s \in \mathcal{S}^{\mathrm{D}} \\ 1 - \exp\left[-\left(\mathcal{K}_2 + \left(\dfrac{\rho_d}{\rho_b}\right)^{\frac{2}{\beta}} \mathcal{K}_3\right)\right], & \text{for } s \in \mathcal{S}^{\mathrm{U}} \end{cases} \tag{3.31}$$

where

$$\mathcal{K}_2 = \frac{2\hat{q}}{\alpha - 2} \mathcal{G}\left[\left(\frac{1}{\tau}\right)^{\frac{1}{\alpha}}, \alpha\right] \tau^{\frac{2}{\alpha}} \tag{3.32}$$

$$\mathcal{K}_3 = \frac{2\pi^2 p_s p_f \lambda_d d_\circ^2}{\beta \sin\left(\frac{2\pi}{\beta}\right)} \tau^{\frac{2}{\beta}} \cdot \mathbf{1}_{c=s_d} \tag{3.33}$$

and

$$\hat{q} = \begin{cases} q_c, & \text{for } c \in \mathcal{S} \setminus \{s_d\} \\ q_d, & \text{for } c = s_d \end{cases} \tag{3.34}$$

in which q_c and q_d are given for both RSA and PSA policies in (3.8)-(3.10).

Proof. See **Appendix B.5**. □

To average the SINR outage probability over all channels, by using the law of total probability, the average SINR outage probability $\mathcal{O}_C^{\mathrm{avg}}(\tau)$ can be obtained. Note that the probability of a user to be served on a certain channel can be obtained in the same manner as q_c and q_d. Note also that, for RSA, the SINR outage probabilities corresponding to all channels are the same. To obtain the overall outage probability

for a cellular user $\mathcal{O}_C^{\text{tot}}(\tau)$, the probability that a BS has at least one free channel for each of its associated users, i.e., q_f, should be incorporated as defined in (3.7).

3.6 Numerical Results and Discussion

3.6.1 Performance Metrics and System Parameters

I use the obtained closed-form expressions to evaluate system performance in different scenarios for both access policies (i.e., RSA and PSA) and both cases when s_d is a downlink channel or an uplink channel. Hence, I have four possible scenarios as follows

1. Downlink-RSA.
2. Downlink-PSA.
3. Uplink-RSA.
4. Uplink-PSA.

The performance metrics for D2D users include

- The probability of harvesting sufficient energy (p_s).
- Channel access probability for a D2D user (p_f).
- Transmission probability for a D2D user (p_t).
- SINR outage probability ($\mathcal{O}_D(\tau)$).
- Overall outage probability ($\mathcal{O}_D^{\text{tot}}(\tau)$).

To show the effect of the proposed spectrum policies on the performance of cellular users, the following performance metrics are also included

- Channel access probability (q_f).
- SINR outage probability ($\mathcal{O}_C^{\text{avg}}(\tau)$).

Moreover, Monte Carlo simulations are used to validate the PPP assumptions used in deriving all the expressions.

For numerical evaluation, unless otherwise stated, the transmit power of a macrocell BS is assumed to be 37 dBm while the thermal noise power σ^2 is -104 dBm. The receiver sensitivity of macrocell BSs ρ_b is -70 dBm. The spatial densities of macrocell BSs, cellular users, and D2D transmitters are $\lambda_b = 1$ BS/km^2, $\lambda_u = 10\lambda_b$ user/km^2, and $\lambda_d = 20$ user/km^2, respectively. i.i.d Rayleigh fading with unit variance is considered for all links. The path-loss exponent for the cellular propagation is $\alpha = 4$ and that for D2D transmission is $\beta = 3$. The total number of channels is $|\mathcal{S}| = 10$ channels. The reference distance $d_\circ$ is set to 10 m, power conversion efficiency a is set to 1, and for the evaluation of outage probability, the threshold τ is set to 0 dB. It is worth mentioning that the effect of RF-to-DC conversion inefficiency (i.e., when $a < 1$) is equivalent to increasing the receiver's sensitivity by a factor of a^{-1}. That is, varying a only scales the resulting figures when plotted against ρ_d. Simulation parameters are summarized in Table 3.1.

3.6.2 Validation of Analysis

The proposed analytical framework is validated against Monte Carlo simulations. A simulation area of 20 km $\times$20 km is chosen in order to guarantee a negligible matching error and boundary effects. The simulations are carried out by using MATLAB and the results are averaged over 10,000 iterations. To validate the derived expressions, none of the PPP assumptions made during the analytical derivations are retained during the simulation where all user selection and scheduling are performed by the

Table 3.1: Simulation Parameters

Parameter	**Value**
Transmit powers of BSs	37 dBm
Receiver sensitivity of BSs	-70 dBm
Spatial density of BSs	1 BS/km^2
Spatial density of cellular users	10 user/km^2
Spatial density of D2D users	20 user/km^2
No. of channels	10
Reference distance	10 m
SINR threshold	1
path-loss exponent of cellular links	4
path-loss exponent of D2D links	3

simulator. In the following figures, the simulation results are represented by curves with black cross markers, i.e., "+". As can be seen in Figures 3.5-3.10, the analytical results of all derived performance metrics match exactly with the simulation results for several ranges of network parameters. This reflects the accuracy of the expressions derived above.

3.6.3 Transmission Probability for a D2D Transmitter

Figure 3.5 shows the effect of varying the spatial density of macrocell BSs on the transmission probability for the four different scenarios. Figure 3.6 elaborates more on this effect for one of these scenarios (i.e., Downlink-PSA) and the same explanations hold for the all other scenarios. From **Lemma 3.4**, it can be seen that increasing λ_b has two effects on the probability that the D2D channel is free (p_f). The first effect is captured in the term θ which reflects the increase in the number of BSs inside the protection region of the D2D transmitter. The second effect is the reduction in access probability of D2D channel s_d by the macrocell BSs where this effect is included in the term q_d. Note that the first effect is independent of the spectrum access policy

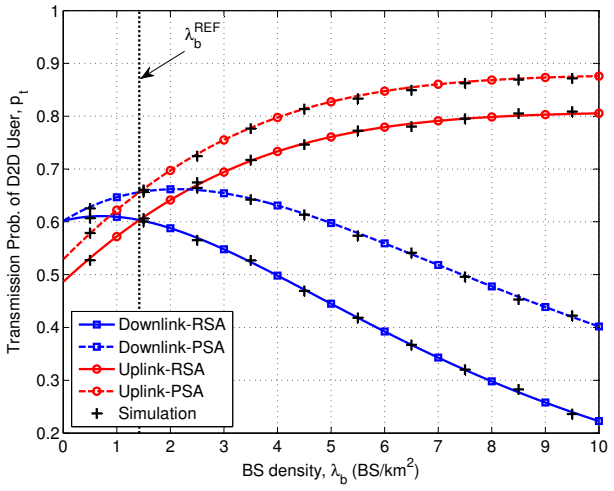

Figure 3.5: Transmission probability p_t for a generic D2D transmitter vs. the spatial density of BSs when s_d is a downlink or an uplink channel. The network parameters are $\rho_d = -80$ dBm, $d_\circ = 10$ m, $\zeta = -60$ dBm, and $\lambda_u = 10\lambda_b$. The results are shown for both RSA and PSA policies.

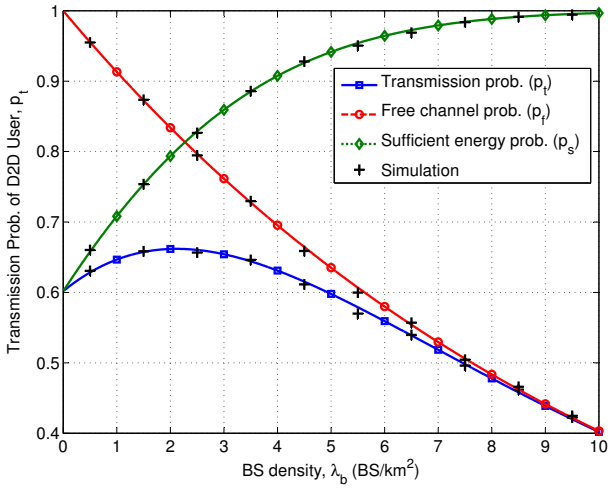

Figure 3.6: Transmission probability p_t for a generic D2D transmitter vs. the spatial density of BSs when s_d is a downlink channel and PSA policy is used. The network parameters are $\rho_d = -80$ dBm, $d_\circ = 10$ m, $\zeta = -60$ dBm, and $\lambda_u = 10\lambda_b$.

and depends on whether s_d is a downlink or an uplink channel. On the other hand, q_d is a function of the adopted spectrum access policy and independent of s_d. Regarding q_d, since the average number of cellular users per BS (i.e., $\mathbb{E}[N_u] = \frac{\lambda_u}{\lambda_b}$) is fixed, it

becomes independent of λ_b as can be noticed in (3.8), (3.10), and (3.6). On the other hand, since the transmit power of BSs is constant, θ becomes an increasing function of λ_b when s_d is a downlink channel. When s_d is an uplink channel, since cellular users use channel inversion power control and the average transmit power is a decreasing function of λ_b, the overall effect makes θ independent of λ_b in this case as can be seen in (3.15).

When s_d is a downlink channel, it can be concluded that the effect of increasing λ_b is always dominated by the increase in θ (as shown in Figure 3.6 for Downlink-PSA). As a result, p_f decreases. On the other hand, for the uplink case, it can be concluded that p_f is constant since both θ and q_d are independent of λ_b. Furthermore, from **Lemma 3.5**, the probability that a D2D transmitter harvests sufficient energy (p_s) is an increasing function of λ_b as also shown in Figure 3.6. That is, increasing the number of BSs allows the network to schedule more users at the same time slot which in turn increases the number of concurrent cellular transmissions that the D2D transmitters can harvest from.

Overall, it can be seen in Figures 3.5 and 3.6 that λ_b balances the trade-off between p_f and p_s. For instance, it is not helpful to have a very high probability of finding the D2D channel free by decreasing the spatial density of BSs while having a very low chance to harvest sufficient energy, and vice versa. For the downlink scenario, it can be seen that as λ_b increases, the transmission probability of a D2D transmitter increases up to a maximum value, then it starts to decrease. The behavior can be explained as follows. For networks with low spatial density of BSs, the effect of harvesting sufficient energy dominates the transmission probability and improves it despite the degradation in p_f. However, as λ_b increases, the probability of harvesting sufficient energy p_s saturates and the effect of the degradation in p_f starts to dominate the D2D

transmission probability. Hence, the transmission probability starts to decrease. For the uplink scenario, since p_f is constant, the overall performance simply follows the same trend of p_s as shown in Figure 3.5. Furthermore, this figure shows that the PSA policy always outperforms the RSA policy for any value of λ_b. This result is intuitive since the PSA policy offers a better performance in terms of p_f by avoiding the use of s_d as much as possible when compared to RSA as explained earlier in Section 3.3.

It is also observed that the using an uplink channel for D2D communication is more beneficial than using a downlink channel. This is due to the difference in transmit powers of the BSs in downlink and the cellular users in uplink. This means that, under the same sensing threshold, the D2D transmitter needs to avoid less amount of interference when using an uplink channel when compared to a downlink channel, which increases p_f. Note that, from **Lemma 3.6**, $\lambda_b^{\text{ref}} = 1.42$ BS/km^2 in this case which coincides with the results presented in Figure 3.5.

3.6.4 Outage Probability for D2D users

I now discuss the SINR outage probability as well as the overall outage probability for D2D users and show the effect of different network parameters (e.g., λ_b, ζ, $|\mathcal{S}|$) on these important performance metrics.

Figure 3.7 depicts the SINR outage probability for D2D users as a function of the spectrum sensing threshold for the different scenarios. As stated in **Theorem 3.1**, for all scenarios, decreasing ζ improves the performance of the SINR outage probability by offering more protection for the D2D transmissions. This result highlights the importance of carefully choosing the spectrum sensing threshold after considering its effect on both transmission probability and SINR outage probability. In Figure 3.7, it can also be seen that the PSA policy offers a better coverage probability compared

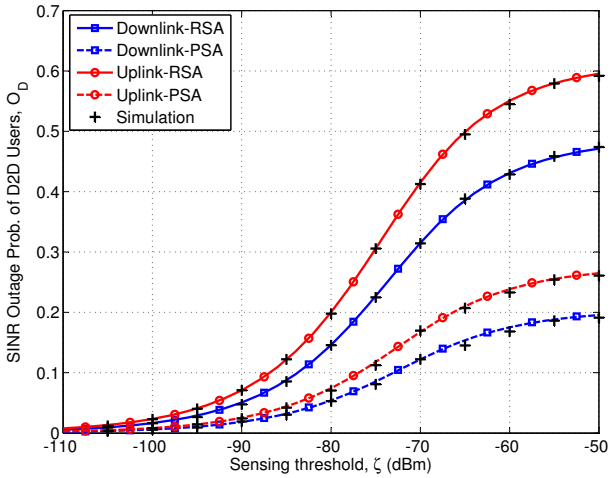

Figure 3.7: SINR outage probability $\mathcal{O}_D(\tau)$ for D2D transmissions vs. spectrum sensing threshold (in dBm) when s_d is a downlink or an uplink channel. The network parameters are $|\mathcal{S}| = 15$ channels, $\rho_d = -70$ dBm, and $d_\circ = 10$ m. The results are shown for both RSA and PSA policies.

to the RSA policy for all values of ζ irrespective of whether s_d is a downlink or an uplink channel. For example, when $\zeta = -60$ dBm, the outage reduces from 43% to 17% dBm when s_d is a downlink channel and from 55% to 24% dBm when s_d is an uplink channel. The PSA policy reduces the probability of cellular users to access the D2D channel, hence, it reduces the number of active interferers on this channel, and consequently, improves the SINR. In order to compare the downlink and uplink channel cases for s_d, recall Figure 3.5 in which it can see that for the chosen simulation parameters (i.e., $\lambda_b = 1$ BS/km^2), the transmission probabilities of the cellular transmitters for the uplink channel case are higher than those for the downlink channel case (since $\lambda_b^{\text{ref}} = 1.42$ BS/km^2 from **Lemma 3.6**). Hence, when s_d is an uplink channel, the spatial density of interferers is higher and the SINR outage is higher when compared to the case when s_d is a downlink channel, cf. Figure 3.7. Note that, if λ_b increases beyond λ_b^{ref}, the uplink case will outperform the downlink case. This is for the same reason as that for Figure 3.5. That is, as

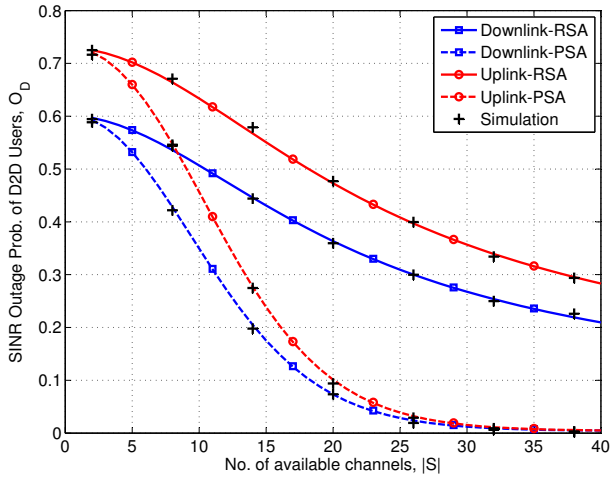

Figure 3.8: SINR outage probability $\mathcal{O}_D(\tau)$ for D2D transmissions vs. the number of available channels when s_d is a downlink or an uplink channel. The network parameters are $\rho_d = -70$ dBm, $d_\circ = 10$ m, and $\zeta = -60$ dBm. The results are shown for both RSA and PSA policies.

λ_b increases, the transmit power of cellular users decreases, and consequently, the aggregate interference decreases when compared to the downlink case in which the transmit power is fixed.

Figure 3.8 shows the effect of varying the number of available channels (i.e., downlink or uplink) on the SINR outage probability of D2D users for different scenarios. It can be seen that increasing $|\mathcal{S}|$ can improve the performance of both spectrum access policies and both uplink and downlink channel cases for s_d. Note that the PSA policy outperforms the RSA policy where it can achieve very low SINR outage probability for a relatively small number of channels. For example, in an uplink channel scenario, using only 11 channels provides an outage probability of less than 0.3 for the PSA policy. On the other hand, for the RSA policy, at least 25 channels are required to achieve similar outage performance.

Figure 3.9 shows variations in the overall outage probability for D2D users (as given in (3.27)) with the sensitivity of the D2D receiver (ρ_d) for all scenarios (or

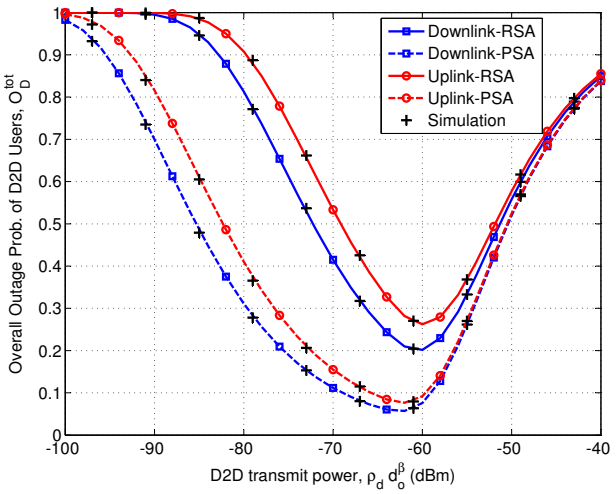

Figure 3.9: Overall outage probability $\mathcal{O}_D^{\text{tot}}(\tau)$ for D2D transmissions vs. the receiver sensitivity (in dBm) when s_d is a downlink and an uplink channel. The network parameters are $\lambda_u = 5\lambda_b$, $\zeta = -60$ dBm and $|\mathcal{S}| = 10$ channels. The results are shown for both RSA and PSA policies.

equivalently, the transmit power of a D2D user when $d_\circ$ is fixed). I observe that there is an optimal value of ρ_d which minimizes the overall outage probability. Starting from the optimal point, when ρ_d decreases, p_s approaches 1, however, the SINR decreases due to the reduction in the power of the received useful signal compared to the aggregate interference. Therefore, the SINR outage probability ($\mathcal{O}_D(\tau)$) dominates and the overall outage probability increases. When ρ_d increases from the optimal point, the SINR outage improves, however, p_s decreases. In this case p_s dominates the performance and the overall outage probability increases. The same observations can be made when comparing the different scenarios as in Figures 3.5-3.8.

3.6.5 Outage Probability for Cellular Users

In order to show the effect of cognition and D2D channel selection on the performance of cellular users, Figure 3.10 shows the average SINR outage probability in presence

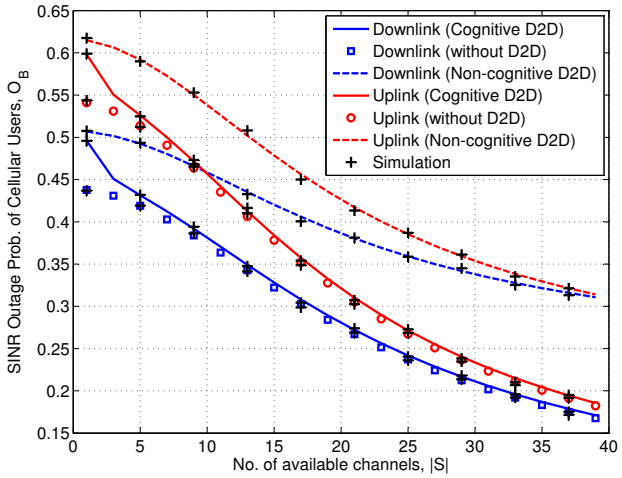

Figure 3.10: Average SINR outage probability $\mathcal{O}_C^{\text{avg}}(\tau)$ for cellular transmissions vs. the number of available channels when s_d is a downlink or an uplink channel. The network parameters are $\rho_d = -60$ dBm, $\beta = 4$, $d_\circ = 15$ m, and $\zeta = -60$ dBm. The results are shown for the RSA policy.

of D2D communication with and without cognition. Note that $\mathcal{O}_C^{\text{avg}}(\tau)$ is averaged over all channels. In this comparison, I consider the performance of the case without D2D transmission as the reference scenario. In addition, I consider a worst-case scenario when all D2D transmitters have sufficient energy to perform channel inversion power control, i.e., $p_s = 1$. It can be seen that D2D communication without cognition degrades the SINR outage probability. From a cellular user's perspective, this is expected as new interferers (i.e., D2D transmitters) are added to the system. With cognitive D2D transmission, the interference caused to the cellular users can be mitigated. Note that, cognitive D2D transmissions protect the cellular transmissions by controlling the spatial density of active D2D transmitters. Note also that the same results and observations in Figure 3.10 hold for the PSA policy with a very slight difference in the performance as can be noticed from (3.11) and (3.12).

3.7 Chapter Summary

I have presented a novel model for cognitive D2D communication using RF energy harvesting from the ambient interference in a multi-channel downlink-uplink cellular network. For coexistence of the underlaying D2D transmissions in downlink and uplink channels, I have proposed two different spectrum access policies for the cellular network, namely, random and prioritized access policies. I have used stochastic geometry to provide a complete framework to model, analyze, and evaluate the performance of the proposed system in terms of transmission probability and SINR outage probabilities for D2D and cellular users. Under the same network setup, the prioritized spectrum access method is shown to outperform the random spectrum access method for all considered performance metrics for the D2D users. Furthermore, for the cellular users, the effect of the prioritized spectrum access policy adopted by the BSs has been observed to be negligible compared to the random access policy. In addition, I have shown that, while uplink channels are preferable to downlink channels for D2D transmissions in dense cellular networks, downlink channels provide better performance in cellular networks with low spatial density of BSs. I have also illustrated that by carefully tuning the network design parameters, energy harvesting can be used along with cognitive D2D transmission to provide an acceptable quality of service performance of D2D communication without significantly affecting the performance of cellular communication.

Chapter 4

Ambient RF Energy Harvesting in Multi-Tier Uplink Cellular Networks

In this chapter, I use stochastic geometry to develop a comprehensive modeling framework for multi-tier uplink cellular networks with RF energy harvesting from the concurrent cellular transmissions. In the considered system model, channel inversion power control is used and cellular users are equipped with energy storage units. I also use tools from queueing theory, namely, Markov chain analysis, to model the level of stored energy in each user's battery. A successful transmission is assumed only when the amount of energy stored in a user's battery is sufficient to perform channel inversion with a received signal-to-interference ratio (SIR) above a predefined threshold. The performance of the proposed system model is evaluated in terms of the transmission probability, the SIR coverage probability, and the overall success probability. I use a PPP-based network model to derive simple expressions for these performance metrics in order to obtain insights for network design and optimization.

I show the effect of varying different network parameters such as the spatial density of BSs and the receiver sensitivity. In addition, I discuss several special cases and provide guidelines on the extensions of the proposed framework. In addition, the gain of using RF energy harvesting is shown to be highly improved by a proper choice of the network design parameters.

4.1 Introduction

Energy harvesting (also referred to as energy scavenging) has recently attracted significant attention as a mean of exploiting the free-flowing ambient radio frequency (RF) energy and converting it into useful DC power to power up devices such as cell phones. RF energy sources include TV towers, radio networks, Wi-Fi networks, and cellular BSs. This technology is becoming feasible thanks to the technological advances in the electronics industry [31–33]. On the other hand, multi-tier cellular wireless networks are being developed to support higher data rates to satisfy the increasing user demand for broadband wireless services. In multi-tier cellular networks, macrocell network tier is overlaid by different classes of smaller and lower-power BSs such as femtocells and picocells [50, 70, 71].

In this chapter, I consider a K-tier uplink cellular network where cellular users harvest RF energy from the concurrent downlink transmissions from all network tiers. Then, each user stores the harvested energy into an attached battery until the the energy is sufficient to perform channel inversion power control. In order to evaluate the performance of this network, I propose a comprehensive framework using a stochastic geometry-based approach to capture the network randomness [17, 21, 28]. Furthermore, I use Markov chain modeling to take the battery dynamics into account. The performance of the proposed system is quantified in terms of SIR coverage probability,

transmission probability, and success probability. Note that, a successful transmission happens only when a user has sufficient energy in her battery and the level of the SIR at the receiver is higher than some predefined threshold.

4.1.1 Contributions

The contributions of this chapter are summarized as follows.

- Using tools from stochastic geometry, I provide a tractable analytical framework for statistical analysis of energy harvesting from ambient RF interference in multi-tier uplink cellular networks. I derive simple and closed-form expressions for the probability density functions (PDFs) and cumulative distribution functions (CDFs) of the transmit power and the harvested energy. Under channel inversion power control, I derive a closed-form expression for the SIR coverage probability for cellular users.

- I use a discretization technique to approximate the battery level after storing the harvested energy which enables us to use Markov chain modeling to capture the battery dynamics. Using the steady-state probability analysis, I derive simple expressions for the probability of having sufficient energy stored in the battery for transmission using channel inversion power control (which is referred to as transmission probability). Then, I obtain the overall probability of successful transmission.

- I show how the proposed framework can be extended to different special cases and models in the literature. In addition, I highlight different tradeoffs in the system and show the effect of varying network parameters such as patial densities of BSs and sensitivity of the receivers on the system performance.

- Via numerical results, I show the feasibility of energy harvesting to power up cellular devices while providing an acceptable performance for uplink transmissions in cellular networks. Also, I illustrate the effect of different network design parameters on the performance metrics.

4.1.2 Organization

The rest of this chapter is organized as follows. A review of the related work is presented in Section 4.2. The system model and the assumptions are described in Section 4.3. In Section 4.4, the transmission probability of a typical user (i.e., the probability that the user has stored enough energy to perform channel inversion toward her serving BS) is derived. Extensions of the proposed analytical model to several other energy harvesting and uplink transmission scenarios are discussed in Section 4.5. Section 4.6 presents the analysis of the coverage probability. Finally, the numerical results and discussion are presented in Section 4.7 before the chapter is summarized in Section 4.8.

4.2 Related Work

In the context of RF energy harvesting, the authors in [57] investigate a wireless sensor network where all the sensor nodes are powered by energy harvesting and assumed to be battery-free. For performance evaluation, Ginibre determinantal point process is used to model the network and provide some bounds on the outage probability and the achievable data rate using the expected amount of harvested energy under a bounded path-loss model. In [55], the authors propose to use dedicated power beacons to radiate RF energy that can be harvested by the cellular users. The authors consider an uplink network where no power control is assumed and all the users transmit

with a fixed power. PPP is used to model the network and obtain the feasibility regions of the network parameters under a set of outage and power constraints for different setups. Although the users are equipped with batteries, the dynamics of the energy stored are not considered in this work. To capture this, the author in [72] uses the random-walk theory with a uniform energy arrival rate to maximize the spatial throughput of an ad hoc network.

In [56], the authors consider a network with cognitive sensor nodes that harvest RF energy from transmissions by primary users in their vicinity. The nodes are assumed to be equipped with a limited battery that can store only the amount of energy required for one transmission at a fixed power level. Under some outage constraints, the authors use PPP analysis to optimize the network parameters and maximize the spatial throughput. In [61], the authors consider the problem of resource allocation in OFDMA-based networks with simultaneous wireless information and power transfer. An optimization problem is formulated to maximize the energy efficiency and solved by means of fractional programming and dual decomposition. To minimize the outage probability in a point-to-point wireless link, the authors in [59] use dynamic programming to derive the optimal power control policy under energy harvesting constraints where the transmit power is upper bounded by the amount of energy harvested. The effect of both flexible cell association and energy harvesting on uplink networks where no energy storage is assumed at the cellular users will be studied in Chapter 5. A more general survey on RF energy harvesting in cellular networks can be found in [73].

In the context of statistical modeling of multi-tier cellular networks, the authors in [20,42] present a general framework for the performance evaluation of K-tier downlink cellular networks. In this model, the locations of BSs in each tier are modeled according to independent PPPs where each network tier differs in the transmit power,

propagation environment, and spatial density. Using the PPP assumption, closed-form expressions are derived for the the outage probability and ergodic data rate. For uplink cellular networks, the authors in [74] consider a single-tier uplink network with fractional power control. A PPP is used to model the locations of the users where each user is assumed to have exactly one BS in her vicinity. Furthermore, the authors in [75] consider the uplink cellular networks with multi-tier deployment. Using stochastic geometry analysis, a general framework is developed for modeling and performance evaluation of the uplink network with truncated channel inversion power control.

4.3 System Model and Assumptions

4.3.1 Multi-Tier Cellular Network Model

I consider a wireless cellular network composed of K independent network tiers of BSs that differ in spatial densities, receiver sensitivity, and transmit powers. It is assumed that the BSs belonging to tier k are spatially distributed according to an independent PPP $\mathbf{\Phi}_k = \{x_i : i = 1, 2, \dots\} \in \mathbb{R}^2$ with spatial density λ_k (BS/km^2) where x_i denotes the location of the i-th BS. In addition, BSs belonging to the same tier k have the same receiver sensitivity ρ_k (Watt) and transmit power P_k (Watt). Users are also modeled by an independent two-dimensional PPP $\Psi = \{y_i : i = 1, 2, \dots\}$ with spatial density λ_u. For the reliability of the uplink transmissions, users use channel inversion power control to adjust their transmission powers such that the average received power by the serving BS is equal to its receiver sensitivity. It is assumed that different users in a cell are served by using orthogonal resources (i.e., different time slots and/or channels) and hence there is no intra-cell interference. In addition,

I consider a universal frequency reuse scenario in which all BSs can use the same channel. Without loss of generality, the following analysis focuses on a typical user located at the origin $(0, 0)$. Saturation condition is assumed in which all network elements (users and BSs) always have data to transmit.

4.3.2 Channel Model and Cell Association

Channels are assumed to be symmetric where the power of a signal transmitted by any network node (BS or user) is subject to a distance-dependent path-loss with a rate of $r^{-\alpha}$ where $\alpha > 2$ is the path-loss exponent and r is the propagation distance. In addition, all transmissions experience independent Rayleigh fading and the channel power gains are modeled by independent exponential random variables $h(x, y)$ with unit mean where x and y are the location of the transmitter and any location in the network, respectively, i.e., $h(x, y) \sim \text{Exp}(1)$. It is assumed that the downlink and uplink transmissions are separated from each other in time (e.g., time division duplex (TTD)) or frequency (e.g. frequency division duplex (FDD)) such that there is no interference between them. Channel coherence time is assumed to be greater than or equal to the frame duration.

In the uplink, each user is associated with the BS that offers the best average channel gain, i.e., lowest path-loss. Furthermore, all BSs are assumed to employ an open access policy in which any user can associate with any BS from any network tier. In other words, each user is served in the uplink by the nearest BS. For example, for a user located at $y \in \mathbb{R}^2$, let $x_\circ$ denote the serving BS with the best channel gain, hence,

$$x_\circ = \underset{x \in \cup_{k=1}^{K} \mathbf{\Phi}_k}{\arg\max} \{\|x - y\|^{-\alpha}\} \tag{4.1}$$

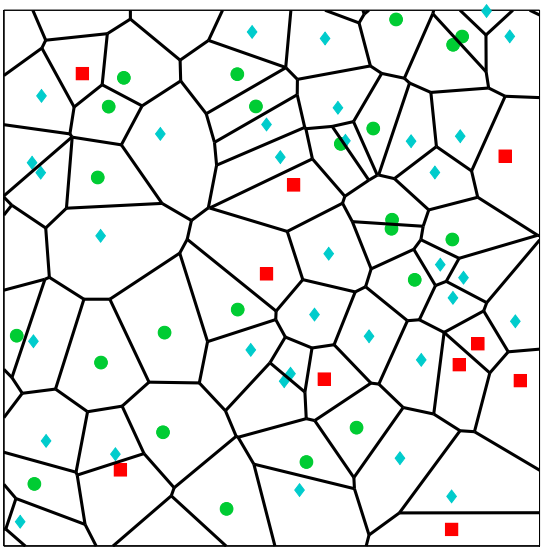

Figure 4.1: A multi-tier cellular network in an area of 3km $\times$ 3km, where $K = 3$. A macrocell network tier (squares) with spatial density $0.5(0.5^2\pi)^{-1}$ BS/km^2 is overlaid with lower-power and 3 times denser picocells (circles) and 5 times denser femtocells (diamonds). Solid lines show the coverage area of each BS for the uplink association criterion defined in (4.1).

where $\|\cdot\|$ is the Euclidean distance. Without loss of generality, Figure 4.1 shows a realization of a 3-tier cellular network with a macrocell network tier deployed as tier 1, and overlaid with a denser and lower power femtocell and picocell network tiers as tiers 2 and 3, respectively.

4.3.3 Energy Harvesting and Battery Model

It is assumed that mobile users rely only on energy harvested from the ambient RF energy sources to power up their devices for uplink transmissions. In this system model, RF energy sources are BSs where users harvest energy from concurrent downlink transmissions from all BSs. Each user device is equipped with an energy harvesting module to convert the RF power into useful DC power with RF-to-DC conversion efficiency $a \leq 1$. Similar to (3.1), the total power harvested by a generic

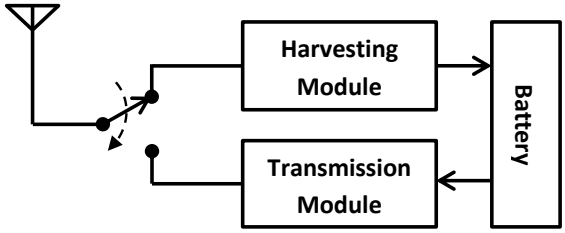

Figure 4.2: Model for an energy harvesting user device which consists of a single antenna, an energy harvesting module, an energy storage unit, and a transmission module.

user located at $(0,0) \in \mathbb{R}^2$ at any time slot is given by

$$P_{\mathrm{H}} = a \sum_{k=1}^{K} \sum_{x \in \Psi_k} P_k h(x,0) \|x\|^{-\alpha}. \tag{4.2}$$

In addition, each user device is assumed to be equipped with a power storage unit (i.e., battery) with storage capacity[1] B (Watt). As shown in Figure 4.2, it is assumed that all users have a single antenna configuration in which both energy harvesting and transmission modules share the same antenna. In other words, users are unable to harvest energy and transmit data at the same time slot. Thus, the users adopt a time-slotted "harvest-then-transmit" strategy. In this strategy, a user device starts to harvest energy from the downlink transmissions and stores this energy in its battery. Upon having a sufficient amount of energy to perform channel inversion power control, a user transmits to her serving BS. That is, the user device checks the battery level at the beginning of each time slot and transmits only when it is sufficient to perform channel inversion, otherwise, it harvests and stores more energy.

Note that P_{H} as defined in (4.2) is an implicit function of the time since fading coefficients are random and assumed to vary over time. That is, the number of time

[1]Note that the terms "power" and "energy" can be used interchangeably in the context of time-slotted transmissions.

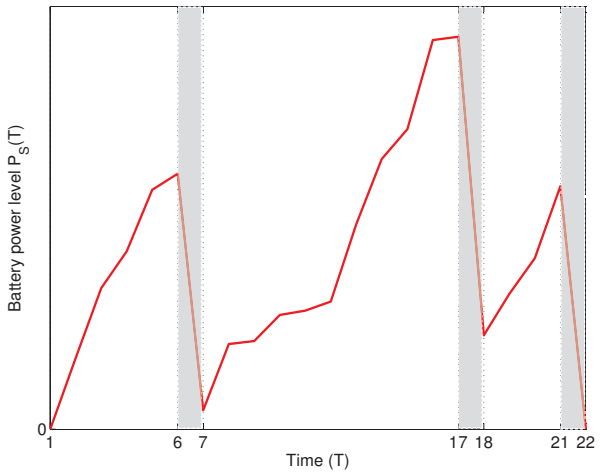

Figure 4.3: Total amount of power stored in a user equipment's battery vs. time. Gray areas represent time slots when the user is transmitting.

slots used by each mobile device for harvesting energy before data transmission is not the same for each transmission. In general, the number of time slots used for energy harvesting is random and differs from a user to another and from transmission to another even for the same user. Hence, the total amount of the power $P_{\mathrm{S}}(T)$ stored in a user equipment's battery after T time slots can be given by

$$P_{\mathrm{S}}(T) = P_{\mathrm{S}}(t_{\circ}) + \sum_{t=t_{\circ}+1}^{t_{\circ}+T} P_{\mathrm{H}} \tag{4.3}$$

where $t_{\circ}$ is the time slot of the last transmission.

Figure 4.3 shows an example of the battery level as a function of time to illustrate the behavior of the user based on the energy harvesting model described above. The following three main remarks can be be made on this figure.

1. The number of time slots required for harvesting sufficient energy is random, e.g., it is 5 time slots for the first transmission, 10 time slots for the second transmission, and only 3 time slots for the third transmission.

2. Due to network randomness, the amount of harvested energy is not the same in every time slot even though $P_{\mathrm{S}}(T)$ is shown for a single user.

3. The amount of transmit power required for channel inversion is a function of time as can be seen in slots 6, 17, and 21.

4.3.4 Methodology of Analysis

Based on the system model described above, I aim at quantifying the performance of a generic user at the origin in terms of transmission probability (i.e., the probability that the amount of energy stored in the user device's battery is sufficient to perform channel inversion power control) and coverage probability (i.e., the probability that the received SIR is above a predefined threshold). Note that the coverage probability is introduced as a performance metric because the channel inversion power control may not guarantee a successful transmission (i.e., the required SIR may not be achieved at the BS). I first derive the distribution of both power harvested per time slot and required amount of transmission power for the typical user. Then, I use these distributions and use an approximation technique to obtain the transmission probability using Markov chain modeling. Next, I present some special cases and discuss some extension techniques in order to use the proposed framework in different scenarios. Finally, the SIR coverage probability is quantified for the typical user.

4.4 Analysis of Uplink Transmission Probability

Transmission probability η_k is defined as the probability of a user associated with tier k to have sufficient amount of energy stored in her device's battery to be able to perform channel inversion toward her serving BS. That is, the energy harvested by

this user device exceeds the amount of transmit power required to have a received power equal to or larger than the serving BS's receiver sensitivity. In this section, I derive the distributions of the harvested power and the transmission power for a typical user. Then, I obtain the transmission probability.

4.4.1 Analysis of Harvested Power

I use (4.2) to derive the CDF of the harvested power at a certain time slot by a typical user located at the origin and this result can be generalized for any generic user. The following lemma provides an expression for $F_{P_{\mathrm{H}}}(t)$ which is defined as

$$F_{P_{\mathrm{H}}}(t) = \mathbb{P}\left[P_{\mathrm{H}} \leq t\right], \quad t \geq 0. \tag{4.4}$$

Lemma 4.1. The distribution of the amount of harvest energy by a typical user is given by

$$F_{P_{\mathrm{H}}}(t) = 1 - \int_0^{\infty} \frac{1}{\pi u} \exp\left[-ut\right] \times \exp\left[-\frac{2\pi^2 \xi a^{\frac{2}{\alpha}}}{\alpha \tan\left(\frac{2\pi}{\alpha}\right)} u^{\frac{2}{\alpha}}\right] \sin\left(\frac{2\pi^2 \xi a^{\frac{2}{\alpha}}}{\alpha} u^{\frac{2}{\alpha}}\right) \mathrm{d}u \tag{4.5}$$

where

$$\xi = \sum_{k=1}^{K} \lambda_k P_k^{\frac{2}{\alpha}}. \tag{4.6}$$

Proof. See **Appendix C.1**. □

Note that, the expression in (4.5) cannot be obtained in a closed-form for a general path-loss exponent, however, it can be easily evaluated numerically. Furthermore, a closed-form for the integral in (4.5) exists when $\alpha = 4$. In this case, the CDF of

the aggregate amount of energy harvested by a typical user in one time slot can be obtained as

$$F_{P_{\mathrm{H}}}(t) = \mathrm{erfc}\left(\frac{\pi^2 \xi}{4}\sqrt{\frac{a}{t}}\right), \quad t \geq 0 \tag{4.7}$$

and its corresponding PDF is given by

$$f_{P_{\mathrm{H}}}(t) = \left(\frac{\pi}{2}\right)^2 \xi \sqrt{\frac{a}{\pi t^3}} \exp\left[-\left(\frac{\pi}{2}\right)^4 \frac{a\xi^2}{t}\right], \quad t \geq 0 \tag{4.8}$$

where $\mathrm{erfc}(z) = \frac{2}{\sqrt{\pi}} \int_z^\infty e^{-t^2}\, \mathrm{d}t$ is the complementary error function.

Note that the PDF in (4.8) takes the form of a Lévy distribution with a zero-location parameter and a scale parameter of $\frac{\pi^4 a \xi^2}{8}$. By intuition, it can be seen from (4.7) that the amount of energy harvested is directly proportional to both spatial density and transmit power of BSs. Figure 4.4 validates the analytical result for $F_{P_{\mathrm{H}}}(t)$ as it can be seen that the gap between the results obtained using (4.5) and those obtained from simulations is tight for different values of the path-loss exponent.

4.4.2 Analysis of Uplink Transmission Power

Based on the system model described above, users served by a BS from the k-th tier are assumed to perform channel inversion power control in order to satisfy a power level requirement ρ_k at the serving BS. Thus, I define the required amount of transmit power of a user when it associates with a BS from the k-th tier as

$$\gamma_k = \rho_k R^\alpha \tag{4.9}$$

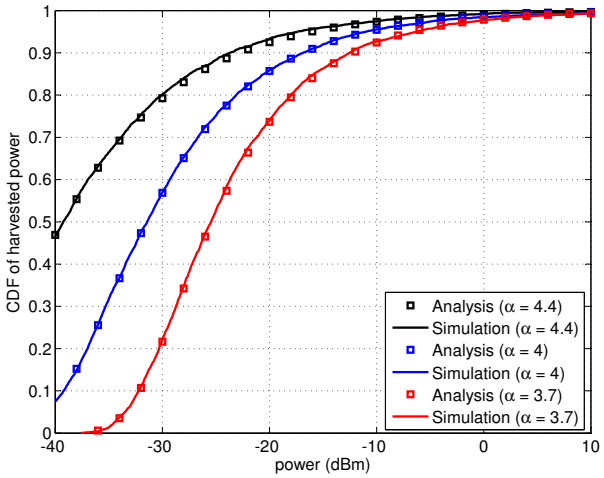

Figure 4.4: CDF of the amount of power harvested per time slot (simulation vs. analysis) for different values of the path-loss exponent α. Simulation parameters: $P_1 = 53$ dBm, $P_2 = 33$ dBm, and $P_3 = 23$ dBm, $\lambda_1 = 5(0.5^2\pi)^{-1}$ BS/km^2, $\lambda_2 = 5\lambda_1$, and $\lambda_3 = 10\lambda_1$, and $a = 1$.

where R is the distance to the serving BS from tier k. Here, I use γ_k to denote the instantaneous transmit power of a user transmitting to a BS from the k-th tier where Γ_k is the corresponding random variable. Based on the association criterion defined in (4.1), using the superposition property of PPPs and the null probability, the PDF of R can be obtained as follows

$$f_R(r) = 2\pi\Lambda r \exp\left[-\pi\Lambda r^2\right], \quad r \geq 0 \tag{4.10}$$

where

$$\Lambda = \sum_{k=1}^{K} \lambda_k. \tag{4.11}$$

Now, (4.9) and (4.10) can be used to derive the distribution of the amount of transmit power required by a typical user when it associates with the k-th tier as

presented in the following lemma.

Lemma 4.2. The CDF of the transmit power of a generic user associated with tier k to achieve a received power of ρ_k at her serving BS is given by

$$F_{\Gamma_k}(t) = 1 - \exp\left[-\pi\Lambda\left(\frac{t}{\rho_k}\right)^{\frac{2}{\alpha}}\right], \quad t \geq 0 \tag{4.12}$$

while its PDF is given by

$$f_{\Gamma_k}(t) = \frac{2\pi\Lambda}{\alpha\rho_k}\left(\frac{t}{\rho_k}\right)^{\frac{2}{\alpha}-1}\exp\left[-\pi\Lambda\left(\frac{t}{\rho_k}\right)^{\frac{2}{\alpha}}\right] \tag{4.13}$$

and its $\frac{2}{\alpha}$-moment is

$$\mathbb{E}\left[\Gamma_k^{\frac{2}{\alpha}}\right] = \frac{\rho_k^{\frac{2}{\alpha}}}{\pi\Lambda} \tag{4.14}$$

where Λ is given by (4.11).

Proof. See **Appendix C.2**. □

Figure 4.5 validates the CDF of the required transmission power (i.e., $F_{\Gamma_k}(t)$) derived above by comparing it with the one obtained by using simulation. It can be seen that the CDF obtained from analysis and simulation coincide in the different scenarios.

4.4.3 Transmission Probability

As defined above, the transmission probability of a user associated with the k-th tier can be expressed as

$$\eta_k = \mathbb{P}[P_{\mathrm{S}}(T) > \gamma_k] \tag{4.15}$$

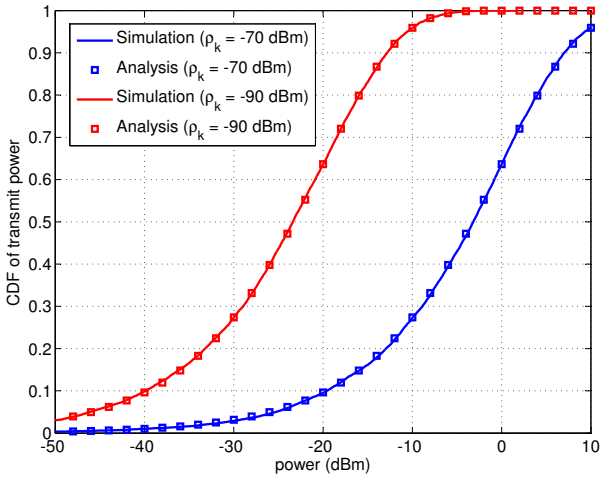

Figure 4.5: CDF of the required transmission power (simulation vs. analysis) for different values of the receiver sensitivity ρ_k. Simulation parameters: $\lambda_1 = 5(0.5^2\pi)^{-1}$ BS/km^2, $\lambda_2 = 5\lambda_1$, and $\lambda_3 = 10\lambda_1$, and $\alpha = 4$.

where $P_{\mathrm{S}}(\mathrm{T})$ is the amount of stored power defined in (4.3). The time-varying nature of link quality between BSs and the tagged user directly affects the amount of harvested energy in each time slot. Consequently, it affects the number of time slots $T_\circ$ required to charge the battery with sufficient power (energy) to perform channel inversion (i.e., γ_k). Hence, $T_\circ$ is a random variable that represents the number of time slots required to harvest energy before each transmission and depends on both the required amount of transmit power and the amount of energy harvested since the last transmission.

Note also that the state (or level) of the battery is a continuous random variable which is equivalent to the difference between the summation of random number of Lévy-distributed random variables given in (4.8) and one random variable given in (4.13). Hence, the level of the battery can be modeled as a simple (discrete-time) one-dimensional random walk on $\mathbb{R}_+$. Unfortunately, using the random walk theory and the boundary crossing probability complicates the analysis. Furthermore, it is

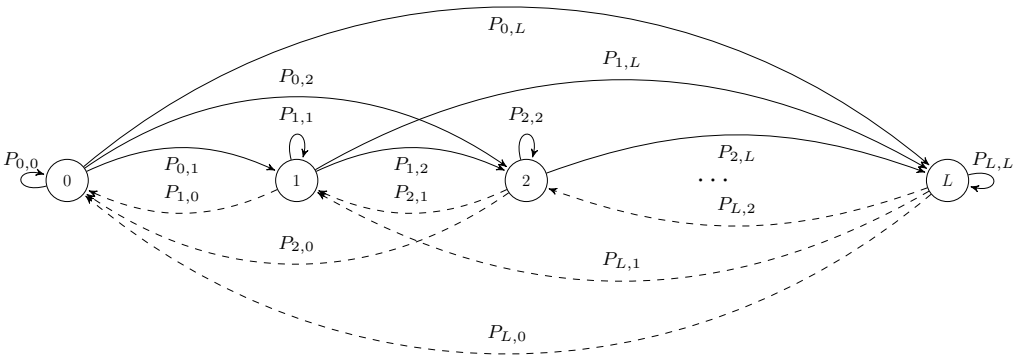

Figure 4.6: Markov chain model of the battery state with $L+1$ discrete levels.

not possible to obtain closed-form expressions in this case for the distributions in (4.8) and (4.13). Therefore, I propose a different method to obtain the boundary crossing probability in (4.15) by approximate the process to a discrete random walk that can be modeled by a finite state Markov chain. In other words, I discretize the states of the battery into a finite number of levels so that the state space $\mathcal{S}$ can be described as a finite set. Note that the this stochastic process shows the Markov property such that the battery state at a given time slot depends only on the level at the previous time slot, i.e.,

$$\mathbb{P}[P_{\mathrm{S}}(T) > s_T | \mathbb{P}[P_{\mathrm{S}}(T-1) > s_{T-1}] = \mathbb{P}[P_{\mathrm{S}}(T) > s_T | \mathbb{P}[P_{\mathrm{S}}(T-1) > s_{T-1}, \ldots, \mathbb{P}[P_{\mathrm{S}}(T-T_\circ) > s_{T-T_\circ}]. \tag{4.16}$$

Note also that the accuracy of the approximation depends on the number of levels. Therefore, I define w and L as the resolution (or step size) of the approximation and the total number of levels, respectively, i.e., $B = Lw$.

In order to discretize the random walk, I define two probabilities p_i and q_i. On one hand, p_i is the probability that the amount of power harvested by a user in a

certain time slot is between iw and $(i+1)w$ Watt, i.e.,

$$p_i = \mathbb{P}[iw \leq P_{\mathrm{H}} < (i+1)w], \quad i = \{0, 1, 2, \ldots, L-1\}$$

and $p_L = \mathbb{P}[P_{\mathrm{H}} \geq B = Lw]$. On the other hand, q_i is the probability that the amount of transmit power required by a user in a certain time slot is between $(i-1)w$ and iw Watt, i.e.,

$$q_i = \mathbb{P}[(i-1)w < \gamma_k \leq iw], \quad i = \{1, 2, 3, \ldots, L\}.$$

Hence, p_i and q_i can be expressed as

$$p_i = F_{P_{\mathrm{H}}}\left((i+1)w\right) - F_{P_{\mathrm{H}}}(iw) \tag{4.17}$$

and

$$q_i = F_{\Gamma_k}(iw) - F_{\Gamma_k}\left((i-1)w\right) \tag{4.18}$$

where $F_{P_{\mathrm{H}}}(t)$ and $F_{\Gamma_k}(t)$ are given in (4.5) and (4.12), respectively.

That is, I round the amount of harvested power down to the nearest level while rounding the required amount of transmit power up to the nearest level. Using p_i and q_i along with the harvest-then-transmit policy discussed above, the state diagram of the Markov chain can be constructed as in Figure 4.6 and the transition probability matrix $\mathbf{P}$ can be expressed as in (4.19), where $P_{i,j}$ is the one-step transition probability from state i to state j. Note that in this model the battery has a total of $L+1$ distinct states (power levels) such that the l-th state denotes a battery level of lw Watt, i.e.,

$\mathcal{S} = \{0, 1, 2, \ldots, L\}$.

$$\mathbf{P} = [P_{i,j}] = \tag{4.19}$$

$$\begin{bmatrix}
p_0 & p_1 & p_2 & p_3 & \cdots & p_{L-1} & p_L \\
q_1 & p_0(1-q_1) & p_1(1-q_1) & p_2(1-q_1) & \ldots & p_{L-2}(1-q_1) & (p_{L-1}+p_L)(1-q_1) \\
q_2 & q_1 & p_0(1-q_1-q_2) & p_1(1-q_1-q_2) & \ldots & p_{L-3}(1-q_1-q_2) & (p_{L-2}+p_{L-1}+p_L)(1-q_1-q_2) \\
\vdots & \vdots & \vdots & \vdots & \ddots & \vdots & \vdots \\
q_L & q_{L-1} & q_{L-2} & q_{L-3} & \cdots & q_1 & 1-q_1-q_2-\cdots-q_L
\end{bmatrix}$$

Note that the transition from a higher state to a lower state (dashed edges) in Figure 4.6 indicates that the user is transmitting data and the amount of energy stored in the battery is sufficient to perform channel inversion. On the other hand, the transition from one state to a higher state or staying at the same state (solid edges) indicates that the user is harvesting energy where the amount of energy stored in the battery is not sufficient for data transmission.

In order to perform the steady-state analysis, I define $\mathbf{v} = [v_0 \ v_1 \ \ldots \ v_L]$ as the steady-state probability vector (or the stationary distribution) where v_l is the probability of the Markov chain to be in state l and

$$\sum_{l=0}^{L} v_l = 1.$$

Hence,

$$\mathbf{v} = \mathbf{vP}, \tag{4.20}$$

$$1 = \mathbf{v1} \tag{4.21}$$

where $\mathbf{1} = [1 \ 1 \ \ldots \ 1]^T$ is an all-ones column vector of length $L+1$.

In order to obtain v_l, the system of linear equations in (4.20) and (4.21) needs

Table 4.1: Sheskin algorithm to obtain the steady-state probability vector in (4.20) and (4.21)

Sheskin Algorithm

Initialization: $\mathbf{P}'_n = \mathbf{P}$, $k_0 = 1$

for $n = 1$ **to** L

$$P'_{i,L-n} \leftarrow \frac{P'_{i,L-n}}{1 - P'_{L-n,L-n}}, \quad 0 \leq i < L - n$$

$$P'_{i,j} \leftarrow P'_{i,j} + P'_{i,L-n} P'_{L-n,j}, \quad 0 \leq i, j < L - n$$

save last column of $\mathbf{P}'_n$

end

for $n = 1$ **to** L

$$k_n = \sum_{i=0}^{n-1} P'_{i,n} k_i$$

end

$$v_i = \frac{k_i}{\sum_{j=0}^{L} k_i}, \quad 0 \leq i \leq L.$$

to be solved. Note that $\mathbf{P}$ is a $(L+1) \times (L+1)$ transition probability matrix, the rank of $\mathbf{P}$ is L, and $\sum_{j=0}^{L} P_{ij} = 1$. In order to reduce the solution complexity, I use Sheskin algorithm to obtain the steady-state probabilities while avoiding matrix inversion and multiplication [76]. In this algorithm, the steady-state probabilities are obtained recursively where the size of the matrix is reduced iteratively by using only additions and multiplications of some of the matrix elements. Then, the vector $\mathbf{v}$ is calculated using the reduced matrix and some saved values from each iteration. The algorithm is summarized in Table 4.1 and more details can be found in [76].

Using the fact that the user device is transmitting when it transits to a lower

state in the Markov chain model (i.e., the lower triangle of the transition matrix $\mathbf{P}$), transmission probability η_k can be obtained using the definition in (4.15) and the steady-state vector obtained. That is, for a user served by a BS belonging to the k-th tier, the probability that the amount of energy stored in the battery is sufficient to perform channel inversion uplink power control at the beginning of a certain time slot is given by

$$\begin{aligned}\eta_k &= \sum_{i=1}^{L} v_i \sum_{j=1}^{i} q_j \\ &= 1 - \sum_{i=1}^{L} v_i \exp\left[-\pi\Lambda\left(\frac{iw}{\rho_k}\right)^{\frac{2}{\alpha}}\right] \end{aligned} \tag{4.22}$$

where (4.22) follows the definition of q_i.

In order to show the accuracy of the proposed approximation, Figure 4.7 demonstrates the effect of varying the number of levels L (i.e., number of battery states) on the accuracy of the obtained transmit probability η_k. Note that the accuracy of the approximation is compared against the transmission probability obtained by simulation with continuous state space. As expected, increasing L improves the accuracy of the solution. However, note that L controls the tradeoff between the accuracy of the calculation and the complexity of obtaining the solution for (4.20). For example, the computational complexity of solving (4.20) for v_i is of $\mathcal{O}(L!)$. Although using other algorithms such as Sheskin approach yields a much less complexity of $\mathcal{O}(\frac{2}{3}L^3)$, it is still computationally huge for large L. Thus, the size of the state space should be chosen wisely to balance this tradeoff.

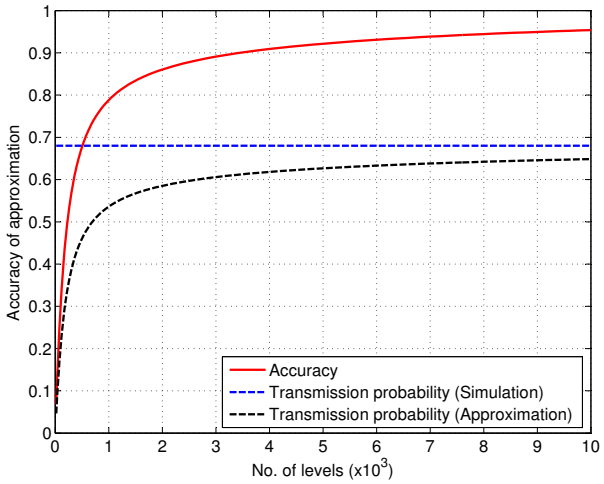

Figure 4.7: Accuracy of proposed approximation of Markov chain, and the transmission probability η_k (obtained from both simulation and analysis) under varying number of battery levels used for the Markov chain approximation. Simulation parameters: $P_1 = 53$ dBm, $P_2 = 33$ dBm, and $P_3 = 23$ dBm, $\lambda_1 = 5(0.5^2\pi)^{-1}$ BS/km^2, $\lambda_2 = 5\lambda_1$, and $\lambda_3 = 10\lambda_1$, $\rho_k = -80$ dBm, $a = 1$, and $\alpha = 4$.

4.5 Extensions and Special Cases

In this section, I use the results presented so far in order to make some important remarks and extend the proposed framework. The main remarks, extensions, and special cases can be summarized as follows.

- As a generalization for the used transmission model, I can adopt a more general harvest-then-transmit strategy in which the user harvests energy for N consecutive time slots instead of only one then checks if the battery has sufficient energy to perform channel inversion power control. Then, the user transmits if the energy is sufficient, otherwise, she harvests for more N time slots, and so on. The same results can still be used except that p_i should be modified as

follows

$$p_i = \text{erfc}\left(\frac{\pi^2 N\xi}{4}\sqrt{\frac{a}{(i+1)w}}\right) - \text{erfc}\left(\frac{\pi^2 N\xi}{4}\sqrt{\frac{a}{iw}}\right) \tag{4.23}$$

where (4.23) follows because the summation of N identical Lévy-distributed random variables with location parameter of zero is also Lévy-distributed with location parameter of zero and the scaling parameter is multiplied by N.

- In the considered system model, a simple power consumption model that only considers the required RF transmit power (i.e., γ_k) is used. However, in practice, a better model should be used to account for other power dissipation in the user device such as the processing power and the inefficiency of RF amplifiers. For example, the following power consumption model can be used

$$\gamma_k^{\text{tot}} = b\gamma_k + P_{\text{proc}} \tag{4.24}$$

where γ_k^{tot} is the total power consumption in the user device, P_{proc} is a constant that includes all the processing power, and $b \geq 1$ is the inefficiency of RF power amplifier. The effect of using this power consumption model can be captured in (4.12) and the CDF of the total power consumption can be obtained as follows

$$\mathbb{P}\left[\gamma_k^{\text{tot}} \leq t\right] = \begin{cases} 0, & t < P_{\text{proc}} \\ 1 - \exp\left[-\pi\Lambda\left(\frac{t - P_{\text{proc}}}{b\rho_k}\right)^{\frac{2}{\alpha}}\right], & t \geq P_{\text{proc}} \end{cases}. \tag{4.25}$$

Thus, q_i needs to be updated accordingly. By defining some integer constant

$c_1 = \left\lceil \frac{P_{\text{proc}}}{w} \right\rceil$, q_i can be expressed as follows

$$q_i = \begin{cases} 0, & i < c_1 \\ F_{\Gamma_k}\left(\frac{(i-c_1)w}{b}\right) - F_{\Gamma_k}\left(\frac{(i-c_1-1)w}{b}\right), & i \geq c_1 \end{cases} \tag{4.26}$$

where $\lceil x \rceil$ denotes the smallest integer not less than x.

- Although the analysis is performed for transmission with channel inversion power control, the results could be suited for other transmission schemes. For example, assume that the user has an intended receiver at a fixed distance, e.g., device-to-device communication and wireless sensor networks. In this case, the user will transmit with a fixed level of power and consume a total power of Γ that includes the processing power. Let us define an integer constant $c_2 = \left\lceil \frac{\Gamma}{w} \right\rceil$. That is, the user transmits the next data packet if and only if the battery is at state $l \geq c_2$, and the battery level will go back to the $(l - c_2)$-th level after transmission. Hence, the entries of the transition matrix $\mathbf{P}$ in (4.19) vary according to the following definition of q_i

$$q_i = \begin{cases} 1, & i = c_2 \\ 0, & i \neq c_2 \end{cases} \tag{4.27}$$

and the transmission probability is given by

$$\eta_k = 1 - \sum_{i=0}^{c_2-1} v_i. \tag{4.28}$$

It is worth mentioning that this assumption with fixed power transmission has been used in the literature such as in [55, 56, 72].

- This system model can also be extended for scenarios in which each user harvests RF energy from a dedicated (fixed) power source(s). That is, assume that a user harvests energy from a source at a fixed distance R_h with transmit power P_h, the amount of harvested power P_{H} will be constant and equal to $aP_hR_h^{-\alpha}$. In other cases, e.g., as [56], P_{H} may also be used as a lower bound on the amount of energy harvested where a user can harvest energy only when she is inside a disk with radius R_h centered at the the energy source. Another scenario is to assume that the amount of energy harvested in a cellular network is equal to the mean of P_{H}. That is, under the assumption of a bounded path-loss model (e.g., $\min(1, \|x\|^{-\alpha})$), the expected value of P_{H} in (4.2) can be derived as in [28, Chapter 3] as follows[2]

$$\mathbb{E}[P_{\mathrm{H}}] = a \sum_{k=1}^{K} \frac{\pi \alpha P_k \lambda_k}{\alpha - 2}. \tag{4.29}$$

  Note that this assumption is used in [55, 56]. Now, in order to use the proposed framework under this assumption, let us define an integer constant $c_3 = \left\lceil \frac{aP_hR_h^{-\alpha}}{w} \right\rceil$ such that the battery level goes c_3 levels up for each energy harvesting time slot. In this case, p_i can be expressed as follows

$$p_i = \begin{cases} 1, & i = c_3 \\ 0, & i \neq c_3 \end{cases}. \tag{4.30}$$

- An interesting case is when the battery goes back to state 0 after each transmission (i.e., each user uses all stored energy for transmission once harvesting

[2]For the unbounded path-loss model $\|x\|^{-\alpha}$, the average received power in (4.2) becomes infinite due to the singularity at $x = (0, 0)$. This also can be seen in (4.8) since the Lévy distribution exhibits a heavy tail behavior.

sufficient energy). In this case, the transition matrix can be rewritten as follows

$$\mathbf{P} = \tag{4.31}$$

$$\begin{bmatrix} p_0 & p_1 & p_2 & p_3 & \dots & p_L \\ q_1 & p_0(1-q_1) & p_1(1-q_1) & p_2(1-q_1) & \dots & (p_{L-1}+p_L)(1-q_1) \\ q_1+q_2 & 0 & p_0(1-q_1-q_2) & p_1(1-q_1-q_2) & \dots & (p_{L-2}+p_{L-1}+p_L)(1-q_1-q_2) \\ \vdots & \vdots & \vdots & \vdots & \ddots & \vdots \\ q_1+q_2+\cdots+q_L & 0 & 0 & 0 & \dots & 1-q_1-q_2-\cdots-q_L \end{bmatrix}.$$

Furthermore, a closed-form expression for the transmission probability can be obtained. The unnormalized steady-state probabilities k_i (cf. Table 4.1) for this case can be expressed as follows

$$k_i = \begin{cases} 1, & i = 0 \\ \dfrac{\sum_{j=0}^{i-1} p_{i-j} \exp\left[-\pi\Lambda\left(\frac{jw}{\rho_k}\right)^{\frac{2}{\alpha}}\right] k_j}{1 - p_0 \exp\left[-\pi\Lambda\left(\frac{iw}{\rho_k}\right)^{\frac{2}{\alpha}}\right]}, & 1 \le i < L \\ \dfrac{\sum_{j=0}^{L-1} p_{L-j} \exp\left[-\pi\Lambda\left(\frac{jw}{\rho_k}\right)^{\frac{2}{\alpha}}\right] k_j}{1 - \exp\left[-\pi\Lambda\left(\frac{B}{\rho_k}\right)^{\frac{2}{\alpha}}\right]}, & i = L \end{cases}. \tag{4.32}$$

Then, v_i can be obtained by normalizing the values of k_i and the transmission probability can be calculated by using (4.22). Note that (4.20) can be solved by using direct substitution, and therefore, the computational complexity in this case is much lower than the general Sheskin algorithm in Table 4.1.

- Another special case that has been used in the literature is when the user does not have a battery and transmits with all the energy harvested each time slot as

in [57]. In this case, the battery goes back to the 0 state after each transmission. This assumption can be captured in the proposed framework by updating the following entries of the $\mathbf{P}$ matrix in (4.19)

$$\begin{cases} P_{i,j} = 0, \text{ for } i = j, \text{ and } i > j \text{ and } j \geq 1 \\ P_{i,j} = \exp\left[-\pi\Lambda\left(\frac{iw}{\rho_k}\right)^{\frac{2}{\alpha}}\right], \text{ for } i \geq 1 \text{ and } j = 1 \end{cases}. \tag{4.33}$$

This case can be of a particular interest from the computational point of view since the resulting matrix is lower triangular and (4.20)-(4.21) can be solved efficiently using forward substitution with low complexity.

4.6 Analysis of SIR Coverage Probability

The uplink SIR coverage probability of the k-th tier is defined as the probability that the received SIR at a BS in this tier is higher than a predefined threshold τ_k. Note that I assume the network to be operating in an interference-limited environment, i.e., no additive noise. Thus, the SIR coverage probability offered by the k-th tier can be mathematically defined as

$$\mathcal{C}_k(\tau_k) = \mathbb{P}\left[\mathrm{SIR}_k > \tau_k\right] \tag{4.34}$$

where SIR_k is the SIR received at a typical BS belonging to the k-th tier.

Based on the association criterion defined in (4.1), SIR_k used in (4.34) can be defined for a typical BS located at the origin as

$$\mathrm{SIR}_k = \frac{\rho_k h(u_\circ, 0)}{\sum\limits_{j=1}^{K} \sum\limits_{u \in \tilde{\mathbf{\Phi}}_j \setminus \{u_\circ\}} \gamma_j h(u,0) \|u_i\|^{-\alpha}} \tag{4.35}$$

where $h(u,0)$ is the small-scale fading coefficients between the typical BS and a user located at u and $u_\circ$ is the user served by the typical BS. $\tilde{\mathbf{\Psi}}_k$ is a point process with density $\eta_k\lambda_k$ that represents the set of active users at a certain time slot, where "active users" refer to users who have sufficient energy stored in the battery and ready for transmission. Note that, in general, $\tilde{\mathbf{\Psi}}_k$ is not a PPP, however, for analytical tractability, I assume that the active users at a certain time slot constitute a PPP. This assumption has been used and validated in the literature, e.g., in [74, 75].

Using the instantaneous SIR_k given in (4.35) and the definition in (4.34), I obtain the coverage probability of the uplink transmission for a user served by a typical BS belonging to the k-th tier and located at the origin as presented in the following theorem where the statistics of the network can be generalized to a generic user.

Theorem 4.1. The coverage probability offered by the k-th tier in an uplink cellular network for a generic user is given by

$$\mathcal{C}_k(\tau_k) = \exp\left[-\frac{2}{\Lambda}\sum_{j=1}^{K}\eta_j\lambda_j\left(\tau_k\frac{\rho_j}{\rho_k}\right)^{\frac{2}{\alpha}}\mathcal{F}\left[\left(\frac{1}{\tau_k}\frac{\rho_k}{\rho_j}\right)^{\frac{1}{\alpha}},\alpha\right]\right] \tag{4.36}$$

where Λ is given by (4.11) and $\mathcal{F}[y,\alpha] = \int_y^\infty \frac{u}{1+u^\alpha}\,\mathrm{d}u$.

Proof. See **Appendix C.3**. □

Note that the integration in $\mathcal{F}[y,\alpha]$ can be evaluated numerically. It reduces to simple closed-form expressions for some special values of α as presented in **Appendix A.3**. Note also that, using (4.35) and the law of total probability, the average uplink SIR coverage probability $\mathcal{C}(\tau_k)$ of the overall system is obtained as

$$\mathcal{C}(\tau_1,\tau_2,\ldots,\tau_K) = \frac{1}{\Lambda}\sum_{k=1}^{K}\lambda_k\mathcal{C}_k(\tau_k) \tag{4.37}$$

where $\frac{\lambda_k}{\Lambda}$ represents the probability of a user to associate with the k-th tier. This result is consistent with the work on uplink (when $\eta_j = 1$) presented in [75, Theorem 3] for the case when $P_u = \infty$.

Now, I introduce a special case for a single-tier uplink network to highlight the consistency between the proposed model and previous results in the literature.

Corollary 4.1. (*Single-tier Uplink Network,* $\alpha = 4$) In the special case of an interference-limited single-tier uplink network, the overall coverage probability is given by

$$\mathcal{C} = \exp\left[-\eta\sqrt{\tau}\arctan\left(\sqrt{\tau}\right)\right]. \tag{4.38}$$

This result shows that, for single-tier uplink cellular networks, the coverage probability is independent of the the spatial density of BSs, receiver sensitivity, and transmit power when $\eta = 1$. The same conclusion can be found in previous work on uplink and downlink (when $\eta = 1$) [19, 34, 42, 74, 75].

4.7 Numerical Results and Discussion

4.7.1 Performance Metrics and System Parameters

As mentioned before, a user can establish a successful communication link with her serving BS under two conditions:

1. The amount of energy stored in the battery of this user is greater than the required amount of transmit power to perform channel inversion toward the corresponding BS. The probability that this condition holds true (i.e., transmission probability η_k) has been discussed in Section 4.4 and derived using

Markov chain modeling as expressed in (4.22).

2. The level of the received SIR at the serving BS is greater than a predefined threshold (i.e., τ) in order to guarantee an acceptable quality of service. The probability of this event is referred to as the coverage probability and discussed in Section 4.6 where a closed-form expression has been obtained in (4.36).

Therefore, I define the success probability as the probability that both of the aforementioned conditions are satisfied. That is,

$$\text{success probability} = \eta_k \times \mathcal{C}_k(\tau_k). \tag{4.39}$$

In this section, I present typical performance results obtained from the proposed framework for K-tier cellular uplink networks with energy harvesting. I focus on the tradeoffs between the different metrics such as the transmission probability (η_k), SIR coverage probability ($\mathcal{C}_k(\tau_k)$), and success probability of a user associated with the k-th tier. In addition, I show how different network setups (e.g., the spatial density of BSs, the sensitivity of the BSs' receivers, etc.) affect the performance metrics.

The network scenario under consideration is composed of 3 different tiers of BSs. In this system, tiers 1, 2, and 3 denote the macrocell tier, picocell tier, and femtocell tier, respectively. Unless otherwise stated, the transmit powers of BSs are assumed to be $P_1 = 53$ dBm, $P_2 = 33$ dBm, and $P_3 = 23$ dBm while the thermal noise is ignored (i.e., interference-limited scenario). Spatial densities of the network tiers are $\lambda_1 = 5(0.5^2\pi)^{-1}$ BS/km^2, $\lambda_2 = 5\lambda_1$, and $\lambda_3 = 10\lambda_1$. An independent and identically distributed Rayleigh fading with unit mean is considered for all links and the path-loss exponent is $\alpha = 4$. The battery capacity is assumed to be 27 dBm and the number of levels used for approximating the battery state by a Markov chain is 5×10^3 which

Table 4.2: Simulation Parameters

Parameter	**Value**
Transmit powers of BSs	53, 33, 23 dBm
Spatial densities of BSs ($\times(0.5^2\pi)^{-1}$)	1, 5, 10 BS/km^2
Battery capacity	27 dBm
No. of battery levels	5×10^3
SIR threshold	1
path-loss exponent	4

provides accuracy level of more than 95% as has been shown in Figure 4.7. The power conversion efficiency a is set to 1 and the SIR threshold τ_k is set to 1 (i.e., 0 dB) for all network tiers. The effect of RF-to-DC conversion inefficiency (i.e., when $a < 1$) is equivalent to increasing the receiver's sensitivity by a factor of a^{-1}. That is, varying a only scales the resulting figures when plotted against ρ_k. Simulation parameters are summarized in Table 4.2. Note also that, all expressions are exact while all the approximations have been validated in Figures 4.4, 4.5, and 4.7. In addition, the assumption that the active users are modeled by a PPP is validated by simulation in [74, 75].

4.7.2 Success Probability

Figure 4.8 illustrates the effect of varying the spatial density of BSs λ_k on the transmission probability, coverage probability, and success probability. It is worth mentioning that increasing the spatial density of BSs results in three different consequences;

1. It reduces the distance between the user and her serving BS which in turn lowers the required transmission power, (cf. (4.9)-(4.13)).

2. It increases the amount of harvested energy due to both reduction in distance and increase in the number of available power sources (i.e., BSs), (cf. (4.7),

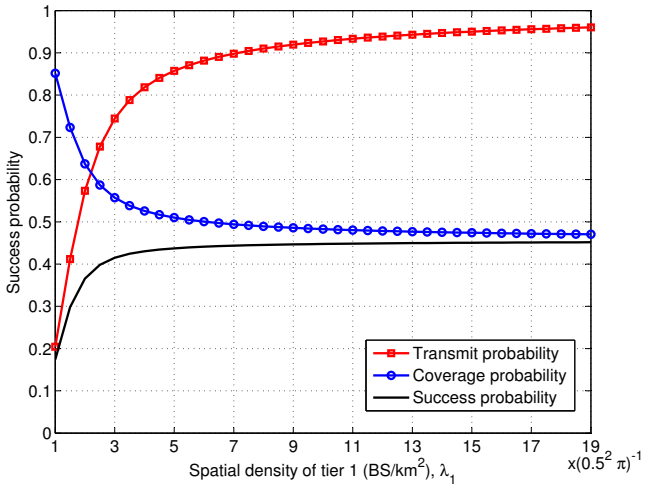

Figure 4.8: Transmission probability, coverage probability, and success probability of a macrocell user vs. spatial density of BSs. Simulation parameters: $K = 3$, $\lambda_2 = 5\lambda_1$ and $\lambda_3 = 10\lambda_1$, and $\rho_1 = \rho_2 = \rho_3 = -90$ dBm.

(4.8)).

3. On the other hand, the users experience higher interference due to the increase in the density of the transmitters (i.e., density of the point process $\tilde{\mathbf{\Psi}}_k$ which is equal to $\eta_k\lambda_k$). In addition, the interferers become closer. This increase in the interference degrades the SIR level at the receiving BS since the useful signal level is always constant (i.e., ρ_k), (cf. (4.35), (4.36)).

Consequently, as can be seen in Figure 4.8, while the coverage probability $\mathcal{C}_k(\tau_k)$ starts to fall with increasing λ_k, the transmission probability η_k improves. However, for low-density of BSs, it can also be seen that the improvement in η_k dominates the deterioration of $\mathcal{C}_k(\tau_k)$ and the overall success probability increases. This happens up to some point after which deploying more BSs does not have a significant effect on the overall performance where both $\mathcal{C}_k(\tau_k)$ and η_k become almost constants. This behavior can be explained as follows. When the spatial density of BSs becomes very high, the expected amount of transmit power becomes very low (cf. the first moment

of γ_k in (4.14)) whereas the energy available for harvesting becomes very high. Combining both effects, the transmission probability η_k approaches 1. Furthermore, when $\eta_k \to 1$, the coverage probability $\mathcal{C}_k(\tau_k)$ becomes independent of λ_k and approaches a constant level (cf. (4.36)).

On the other hand, Figure 4.9 shows the effect of varying ρ_k on the system performance under the same network configuration. Intuitively, decreasing the sensitivity of the receiver (i.e., increasing ρ_k) increases the required transmission power in order to perform channel inversion (cf. (4.9)). This, in turn, increases both the level of useful signal and interference power received at the BS. Hence, as shown in Figure 4.9, while the coverage probability $\mathcal{C}_k(\tau_k)$ improves with increasing ρ_k (cf. (4.36)), the transmission probability η_k deteriorates (cf. (4.7)-(4.13)). Regarding the overall performance, it can be seen that there exists an optimal value of ρ_k that maximizes the success probability and divides the performance into two regimes. That is, as ρ_k increases, the success probability of a user increases up to a maximum value, then it starts to decrease. The behavior of the system in this case can be explained as follows. When ρ_k is very low (the left side of the optimal point), although the user can achieve a high transmission probability, the coverage probability is almost 0. As ρ_k increases, η_k stays almost the same while the SIR coverage improves and this increase in $\mathcal{C}_k(\tau_k)$ dominates the success probability. This happens until achieving the maximum success probability. After this point, as ρ_k increases (the right side of the optimal point), η_k starts to fall and the SIR coverage probability becomes almost constant. Hence, the overall success probability starts to decrease.

It has been shown in Figure 4.8 that increasing the spatial density of the network will not be beneficial to the success probability after some point under the same network configuration. However, Figure 4.9 has shown that optimizing ρ_k can maximize

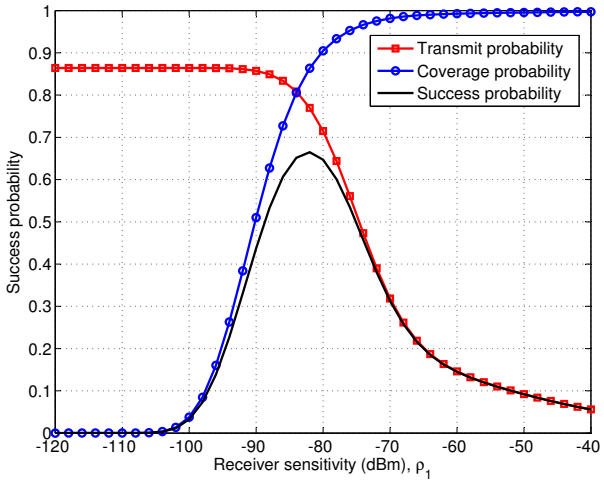

Figure 4.9: Transmission probability, coverage probability, and success probability of a macrocell user vs. BSs' receiver sensitivity. Simulation parameters: $K = 3$, and $\rho_2 = \rho_3 = -90$ dBm.

the system performance in terms of success probability. Therefore, in Figure 4.10 I show how to exploit the deployment of more BSs in order to improve the overall performance of the network. Compared to Figure 4.8, Figure 4.10 shows the maximum achievable success probability when increasing the spatial density of the BSs and optimizing the sensitivity of the BS receiver accordingly. For example, a network with spatial density of $\lambda_1 = 10 \times (0.5^2\pi)^{-1}$ BS/km^2 can achieve a 82% success probability when optimizing ρ_k (i.e., -77 dBm) compared to only a 45% success probability with the same density of BSs and -90 dBm sensitivity as shown in Figure 4.8.

4.7.3 Feasibility Regions for Network Parameters

Figure 4.11 shows the feasibility region of the network parameters under a transmission probability constraint. The feasibility region $\mathcal{A}$ is defined as

$$\mathcal{A} = \{(\lambda_k, \rho_k) \in \mathbb{R}_+^2 \mid \eta_k \geq \theta\} \tag{4.40}$$

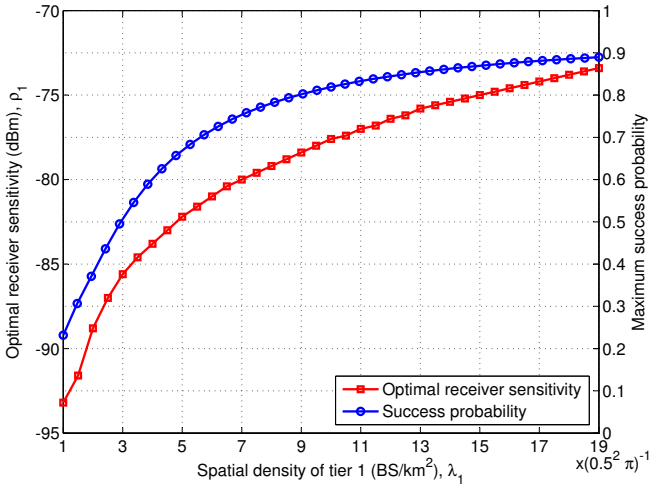

Figure 4.10: Maximum success probability and the optimal receiver sensitivity vs. spatial density of BSs. Simulation parameters: $K = 3$, $\lambda_2 = 5\lambda_1$ and $\lambda_3 = 10\lambda_1$, and $\rho_2 = \rho_3 = -90$ dBm.

where θ is the target transmission probability. Note that the solid lines represent the boundary of each feasibility region with different θ. These graphs are very important and insightful for the network design and optimization phases. That is, for a given receiver sensitivity ρ_k, the minimum required spatial density λ_k that satisfies the transmission probability constraint θ can be obtained on the corresponding solid line. In addition, increasing the receiver sensitivity is not necessary after satisfying the required constraint from the cost efficiency point of view. For example, for $\lambda_1 = 5 \times (0.5^2\pi)^{-1}$ BS/km^2, it can be seen that deploying more sensitive receivers (e.g., receiver sensitivity changes from -74 dBm to -84 dBm) at the BS can increase the transmission probability by a factor of 4 (i.e., from 20% to 80%). It can also be seen that decreasing the sensitivity threshold of the receivers beyond this point (i.e., less than -84 dBm) is not necessary. In fact, the receiver's sensitivity threshold should not be decreased after meeting the transmission probability constraint because doing so will also degrade the SIR coverage probability (cf. Figure 4.9 and (4.36)).

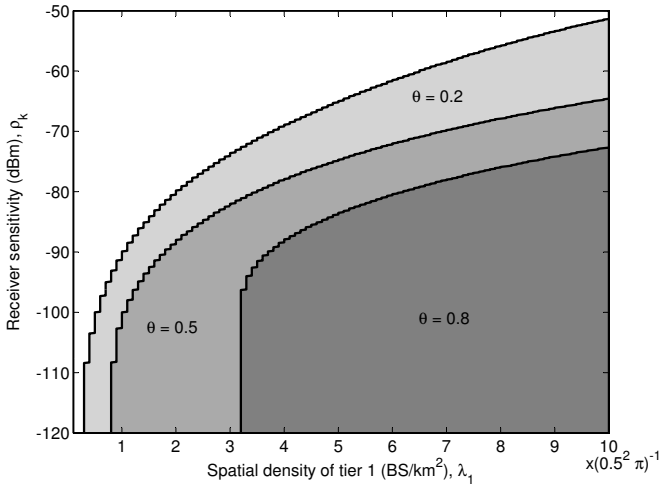

Figure 4.11: Feasibility region of the two network parameters λ_k and ρ_k for different transmission probability constraints. Simulation parameters: $K = 3$, $\lambda_2 = 5\lambda_1$ and $\lambda_3 = 10\lambda_1$, and $\rho_1 = \rho_2 = \rho_3 = \rho_k$.

Figure 4.12 shows the feasibility region of the network parameters under some SIR coverage probability constraint. In this case, the feasibility region $\mathcal{B}$ is defined as

$$\mathcal{B} = \{(\lambda_k, \rho_k) \in \mathbb{R}_+^2 \mid \mathcal{C}_k(\tau_k) \geq \beta\} \tag{4.41}$$

where β is the target SIR coverage probability. It can be seen that the coverage probability exhibits an opposite behavior compared to the transmission probability as shown in Figures 4.9 and 4.11. That is, for the same receiver sensitivity, increasing the spatial density of the BSs degrades the coverage probability. In addition, for the same spatial density, increasing the receiver sensitivity threshold improves the coverage probability. This behavior of the network, shown in Figures 4.9 and 4.11, highlights the tradeoff between these two performance metrics. In addition, it gives design guidelines and shows the importance of selecting the proper values of the network parameters.

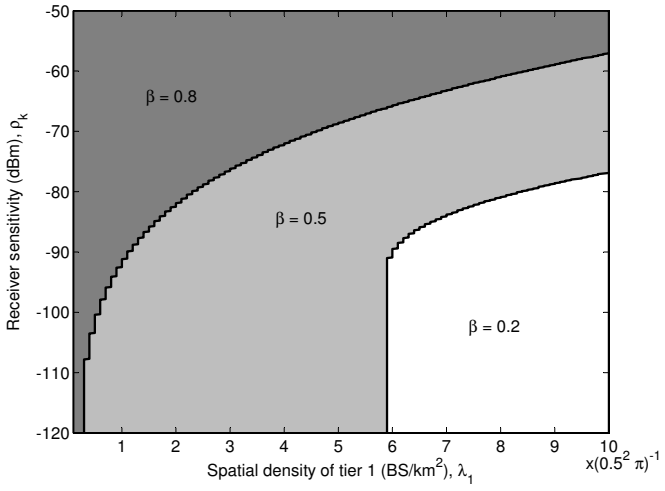

Figure 4.12: Feasibility region of the two network parameters λ_k and ρ_k for different SIR coverage probability constraints. Simulation parameters: $K = 3$, $\lambda_2 = 5\lambda_1$ and $\lambda_3 = 10\lambda_1$, and $\rho_1 = \rho_2 = \rho_3 = \rho_k$.

4.8 Chapter Summary

I have used stochastic geometry to develop a novel framework to model, analyze, and evaluate the performance of RF energy harvesting in multi-tier uplink cellular networks. A Markov chain model for the battery dynamics of each user has been presented. I have obtained simple expressions for the SIR coverage probability, transmission probability, and success probability. Furthermore, I have presented some guidelines to design energy harvesting-based multi-tier cellular networks and optimize their performance. The numerical results based on the analysis show that RF energy harvesting can be a viable technology to power cellular devices. In an energy harvesting environment, the performance of cellular users in the uplink can be optimized by carefully tuning the network design parameters such as receiver sensitivity at the BSs and spatial densities of the BSs.

Chapter 5

Ambient RF Energy Harvesting in Multi-Tier Uplink Cellular Networks with Flexible Cell Association

In this chapter, model and analyze a multi-tier-tier uplink cellular network with flexible cell association where all transmissions are powered by energy harvesting from ambient interference. Similar to the system model presented in Chapter 4, each user transmits data to her corresponding BS only when the amount of energy harvested is sufficient to perform channel inversion towards the serving BS. Furthermore, the data transmitted can be successfully decoded only when the SINR at the receiver is above a predefined threshold. Different from the system in Chapter 4, I adopt flexible cell association in which users do not necessarily associate with the nearest BS for any reason such as the load per BS [42]. That is, each network tier has a specific bias factor that is added to the decision criterion of the association. I use

statistical modeling based on stochastic geometry to capture the randomness of the network topology, e.g., channels gain and locations of BSs and users locations. In particular, for analytical tractability, I use independent PPPs to model the locations of BSs and users. I evaluate the performance of the system model in terms of SINR coverage probability, transmission probability, and success probability. I show the effect of varying different parameters of the network such as receiver sensitivity and bias factors on the performance metrics.

5.1 Contributions and Organization

The contributions of this chapter are summarized as follows.

- Using stochastic geometry, I provide a tractable analytical framework to model and analyze the performance of energy harvesting in multi-tier uplink cellular networks with flexible cell association. Furthermore, I consider a practical system model in which users perform power control in order to mitigate the near-far problem.

- I show that energy harvesting can provide an acceptable performance for uplink transmissions in cellular networks especially for users with short-range communication links. Furthermore, I show that adjusting network parameters increases the achievable gain by balancing the trade-off between the probability of harvesting sufficient power and the probability of transmitting with acceptable power level to satisfy a certain SINR threshold at the receiver.

The rest of this chapter is organized as follows. The system model and the assumptions are described in Section 5.2. In Section 5.3, the transmission probability

of a typical user (i.e., the probability that the user has stored enough energy to perform channel inversion toward her serving BS) is derived. Section 5.4 presents the analysis of the coverage probability. Finally, the numerical results and discussion are presented in Section 5.5 before the chapter is summarized in Section 5.6.

5.2 System Model and Assumptions

5.2.1 Multi-Tier Cellular Network Model

I consider a K-tier cellular network where the locations of BSs belonging to tier k are modeled by an independent PPP $\mathbf{\Phi}_k = \{x_i : i = 1, 2, \dots\}$ with spatial density λ_k where $x_i \in \mathbb{R}^2$ denotes the location of the i-th BS. BSs belonging to the same tier k have the same receiver sensitivity ρ_k and transmit power P_k. The complete set of users is also modeled by an independent PPP $\mathbf{\Psi} = \{y_i : i = 1, 2, \dots\}$ with spatial density λ_u. In the uplink, each user performs channel inversion to adjust her transmit power to ensure that the average received power at the serving BS is equal to its receiver sensitivity. Orthogonal channel access is assumed to avoid intra-cell interference.

5.2.2 Channel Model and Cell Association

The network is assumed to operate in the TDD mode such that the downlink and uplink transmissions are separated from each other in time. That is, there is no interference between the downlink network and the uplink network even though both networks use the same set of channels. The power of the signal transmitted on any channel decays at a rate of $r^{-\alpha}$ where $\alpha = 4$ is the path-loss exponent and r is the propagation distance. In addition, the power envelope of each channel is modeled

by an independent exponential random variable with unit mean, i.e., Rayleigh fading assumption. Channel coherence time is assumed to be greater than the frame duration.

In the uplink, flexible cell association is used such that association with BSs belonging to the same tier is biased with a positive bias factor β_k . That is, each user is assumed to be served in the uplink by the BS that offers the best biased average channel gain (i.e., average channel gain plus bias factor). For example, the bias factors can be chosen according to the receiver sensitivity of each tier in order to make users biased to associate with the tier that requires lowest transmit power. Another scenario is when $\beta_k = P_k$ in which each users is served by the same BS in both downlink and uplink.

For a user located at $y \in \mathbb{R}^2$, let x_k and $x_\circ$ denote the BS with the best biased channel gain from the k-th tier and the serving BS, respectively. Hence, the flexible cell association criterion is described as

$$x_k = \arg\max_{x \in \mathbf{\Phi}_k} \{\beta_k \|x - y\|^{-\alpha}\} \tag{5.1}$$

$$x_\circ = \arg\max_{x \in \{x_k : k=1,2,\ldots,K\}} \{\beta_k \|x - y\|^{-\alpha}\} \tag{5.2}$$

where $\|\cdot\|$ is the Euclidean distance. Without loss of generality, Figure 5.1 shows a realization of a downlink-uplink cellular network with three different tiers, e.g., a macrocell network tier, a picocell network tier, and a femtocell network tier.

5.2.3 Energy Harvesting Model

Each user is equipped with an energy harvesting unit that converts the ambient RF power received from the interference caused by the downlink cellular transmissions

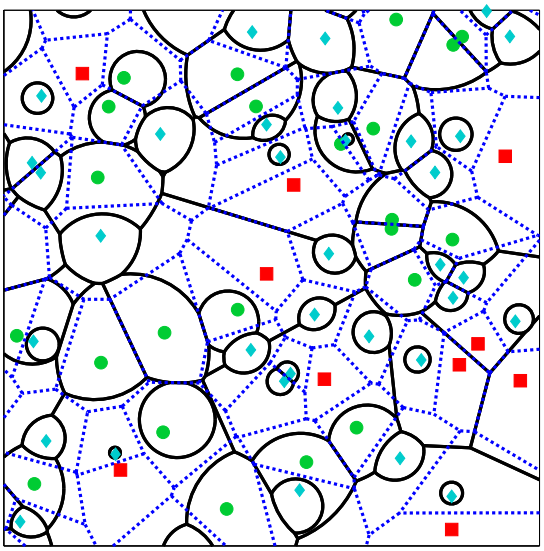

Figure 5.1: A 3-tier cellular network with flexible cell association. A macrocell network tier (squares) is overlaid with lower-power and 3 times denser picocells (circles) and 5 times denser femtocells (diamonds). Solid lines show the coverage area of each BS for biased uplink association criterion defined in (5.2) where $\beta_1 = 5$, $\beta_2 = 2$, and $\beta_3 = 1$. Dashed lines show the coverage area for uplink when association is unbiased, i.e., $\beta_k = 1, k \in \{1, 2, 3\}$.

into useful DC power. Hence, the total power received at the harvesting unit of a user located at y is given by

$$P_{\mathrm{H}}(y) = a \sum_{k=1}^{K} \sum_{x \in \Phi_k} P_k h(x, y) \|x - y\|^{-\alpha} \tag{5.3}$$

where $h(x, y)$ is the small-scale fading and $a \leq 1$ is the RF-to-DC power conversion efficiency.

Based on the TDD operation, users are assumed to adopt a time-slotted "harvest-then-transmit" strategy in which a user transmits only when the power harvested in one time slot (i.e., the downlink time slot) is sufficient to perform channel inversion power control (i.e., in the uplink time slot). There is no energy storage assumed such that no user can save the extra harvested energy for the next time slot.

5.3 Analysis of Uplink Transmission Probability

As mentioned earlier, for a user to be able to make an uplink transmission, the energy harvested by this user should be sufficient to perform channel inversion towards the serving BS. Hence, I define η_k as the probability of transmission by a user in the k-th tier after harvesting sufficient energy. To derive the transmission probability, both PDFs of transmit power and harvested energy are required.

5.3.1 Analysis of Harvested Power

For the PDF of the power received at the energy harvesting module of a generic user, I use the expression derived earlier in (4.8) for the special case when $\alpha = 4$. That is,

$$f_{P_{\mathrm{H}}}(t) = \left(\frac{\pi}{2}\right)^2 \xi \sqrt{\frac{a}{\pi t^3}} \exp\left[-\left(\frac{\pi}{2}\right)^4 \frac{a\xi^2}{t}\right], \quad t \geq 0 \tag{5.4}$$

where

$$\xi = \sum_{k=1}^{K} \lambda_k P_k^{\frac{2}{\alpha}}. \tag{5.5}$$

Although (5.4) is for the special case when $\alpha = 4$. However, α does not need to be 4 for the rest of the analysis, for example when $\alpha < 4$, this expression provides a pessimistic bound on the amount of harvested power and vice versa.

5.3.2 Analysis of Uplink Transmission Power

Similar to Section 4.4.2, I define the transmit power of a user when it associates with a BS from the k-th tier at a distance R_k as,

$$\gamma_k = \rho_k R_k^{\alpha}. \tag{5.6}$$

Hence, I firstly need to derive the PDF of the distance R_k in order to derive the PDF of the transmit power. Conditioned on the event of a generic user to be served by a BS belonging to the k-th tier, the following lemma presents the PDF of the distance between this user and her serving BS.

Lemma 5.1. The PDF of the distance between a generic user associated with tier k and her serving BS is

$$f_{R_k}(r) = 2\pi\Lambda_k r \exp\left[-\pi\Lambda_k r^2\right] \tag{5.7}$$

where

$$\Lambda_k = \beta_k^{-\frac{2}{\alpha}} \sum_{j=1}^{K} \lambda_j \beta_j^{\frac{2}{\alpha}}. \tag{5.8}$$

Proof. See **Appendix D.1**. □

Unlike the expression in (4.10), the PDF of the distance distribution to the serving BS in (5.7) differs is not the same for all tiers due to the biased cell association. Using **Lemma 5.1** and (5.6) I derive the PDF of a generic user's transmit power when it associates with the k-th tier as stated in the following lemma where the proof is similar to **Appendix C.2**.

Lemma 5.2. The CDF of the transmit power of a generic user associated with tier k to achieve a received power of ρ_k at her serving BS is given by

$$F_{\Gamma_k}(t) = 1 - \exp\left[-\pi\Lambda_k \left(\frac{t}{\rho_k}\right)^{\frac{2}{\alpha}}\right], \quad t \geq 0 \tag{5.9}$$

while its PDF is given by

$$f_{\Gamma_k}(t) = \frac{2\pi\Lambda_k}{\alpha\rho_k}\left(\frac{t}{\rho_k}\right)^{\frac{2}{\alpha}-1} \exp\left[-\pi\Lambda_k \left(\frac{t}{\rho_k}\right)^{\frac{2}{\alpha}}\right] \tag{5.10}$$

and its $\frac{2}{\alpha}$-moment is

$$\mathbb{E}\left[\Gamma_k^{\frac{2}{\alpha}}\right] = \frac{\rho_k^{\frac{2}{\alpha}}}{\pi\Lambda_k} \tag{5.11}$$

where Λ_k is given by (5.8).

Note that, the expressions in **Lemma 5.2** reduce to that in **Lemma 5.2** when the bias factor β_k is set to 1 for all network tiers. Furthermore, for the unbiased cell association (i.e., $\beta_k = 1$) and when all BSs have the same receiver sensitivity, the transmit power of any user is independent of which tier the user is associated with. That is because the association in this case is made to the nearest BS regardless of its tier.

5.3.3 Transmission Probability

As described above, the transmission probability of a user associated with the k-th tier can be defined as

$$\eta_k = \mathbb{P}[P_{\mathrm{H}}(y) > \gamma_k] \tag{5.12}$$

and the following theorem provides a closed-form expression for this probability.

Theorem 5.1. For a user served by a BS belonging to the k-th tier, the probability that this user harvests sufficient energy to perform channel inversion towards her serving BS is given by

$$\eta_k = 1 - \frac{1}{\pi} G_{0,3}^{3,0}\Big(\Big(\frac{\pi}{2}\Big)^6 \frac{a\xi^2\Lambda_k^2}{\rho_k}\Big| \, 0, \frac{1}{2}, \frac{1}{2}\Big) \tag{5.13}$$

where ξ and Λ_k are given by (5.5) and (5.8), respectively, and $G_{0,3}^{3,0}(x|a_1, a_2, a_3)$ denotes the Meijer G-function.

Proof. See **Appendix D.2**. □

Note that the function $G_{0,3}^{3,0}(x|0, \frac{1}{2}, \frac{1}{2})$ in (5.13) is a decreasing function of x, furthermore, it can be calculated numerically by many computer algebra systems, e.g., MuPAD, MATLAB, Maple, and Mathematica. Also note that, for the unbiased cell association (i.e., $\beta_k = 1$), the transmission probability is independent of which tier the user is associated with when all BSs have the same receiver sensitivity.

5.4 Analysis of SIR Coverage Probability

Based on the association criterion defined in (5.2) for the uplink and similar to 4.35, the SINR received at a typical BS belonging to the k-th tier and located at $(0, 0) \in \mathbb{R}^2$ can be written as

$$\mathrm{SINR}_k = \frac{\rho_k h(u_\circ, 0)}{\sum\limits_{j=1}^{K} \sum\limits_{u \in \tilde{\mathbf{\Psi}}_j \setminus \{u_\circ\}} \gamma_j h(u, 0) \|u\|^{-\alpha} + \sigma^2} \tag{5.14}$$

where σ^2 is the variance of the additive noise at the BS where no specific distribution is assumed. $u_\circ$ and $\tilde{\mathbf{\Psi}}_k$ are defined in (5.2).

Using (5.14), uplink SINR coverage probability of the overall system can be obtained. Let $\mathcal{C}_k(\tau_k)$ denote the SINR coverage probability offered by the k-th tier to the users associated with this tier. Here, uplink SINR coverage probability of the k-th tier is defined similar to (4.34). Therefore, using the law of total probability, the overall SINR coverage probability is obtained as

$$\mathcal{C} = \sum_{k=1}^{K} \frac{\lambda_k}{\Lambda_k} \mathcal{C}_k(\tau_k) \tag{5.15}$$

where $\dfrac{\lambda_k}{\Lambda_k}$ represents the probability of a user to associate with the k-th tier and Λ_k is given by (5.8).

In the following theorem, I obtain the coverage probability of the uplink transmission for a user served by a typical BS belonging to the k-th tier and located at the origin where the statistics of the network can be generalized to a generic user. The proof is similar to **Appendix C.3**, thus, is not presented here. The main difference is in the distance z to the closest interfere (cf. (C.10)). That is, due to using channel inversion power control, it is known for sure that the closest interferer to a BS belonging to the k-th tier from the j-th tier is at least at a distance of

$$z > \left(\frac{\beta_k}{\beta_j} \frac{\gamma_j}{\rho_j} \right)^{\frac{1}{\alpha}}. \tag{5.16}$$

Theorem 5.2. The coverage probability offered by the k-th tier in an uplink cellular

network for a generic user is given by

$$\mathcal{C}_k(\tau_k) = \exp\left[-\frac{\tau_k}{\rho_k}\sigma^2 - 2\sum_{j=1}^{K}\frac{\eta_j\lambda_j}{\Lambda_j}\left(\tau_k\frac{\rho_j}{\rho_k}\right)^{\frac{2}{\alpha}}\mathcal{F}\left[\left(\frac{1}{\tau_k}\frac{\beta_k}{\beta_j}\frac{\rho_k}{\rho_j}\right)^{\frac{1}{\alpha}},\alpha\right]\right]. \tag{5.17}$$

where Λ_j is given by (5.8) and $\mathcal{F}[y,\alpha] = \int_y^\infty \frac{u}{1+u^\alpha}\,\mathrm{d}u$.

Now, I introduce a special case for a multi-tier uplink network with best uplink channel association (i.e., unbiased cell association). In this case, for the uplink, the serving BS is simply the closest BS since all tiers have the same propagation path-loss exponent.

Corollary 5.1. (*Unbiased uplink association,* $\sigma^2 = 0$) In the special case when a user associates to the nearest BS in the uplink, the coverage probability of the k-th tier in an interference-limited multi-tier network is given by

$$\mathcal{C}_k(\tau_k) = \exp\left[-2\sum_{j=1}^{K}\frac{\eta_j\lambda_j}{\Lambda}\left(\tau_k\frac{\rho_j}{\rho_k}\right)^{\frac{2}{\alpha}}\mathcal{F}\left[\left(\frac{1}{\tau_k}\frac{\rho_k}{\rho_j}\right)^{\frac{1}{\alpha}},\alpha\right]\right] \tag{5.18}$$

where $\Lambda = \sum_{j=1}^{K}\lambda_j$.

Proof. The expression follows from (5.17) by setting β_k to 1 and $\sigma^2 = 0$. □

This result is consistent with **Theorem 4.1** presented in Chapter 4.

5.5 Numerical Results and Discussion

5.5.1 Performance Metrics and System Parameters

In this section, I evaluate the performance of the proposed system with energy harvesting and flexible cell association in terms of transmission probability (η_k), SINR coverage probability ($\mathcal{C}_k(\tau_k)$), and success probability (i.e., $\eta_k - \eta_k(1-\mathcal{C}_k(\tau_k)) = \eta_k\mathcal{C}_k(\tau_k)$)

Table 5.1: Simulation Parameters

Parameter	**Value**
Transmit powers of BSs	53, 33, 23 dBm
Spatial densities of BSs ($\times(0.5^2\pi)^{-1}$)	5, 25, 50 BS/km^2
SIR threshold	0.5
path-loss exponent	3.3

for a user associated with the k-th tier. I consider a 3-tier network scenario with macrocell, picocell, and femtocell BSs as tier 1, tier 2, and tier 3, respectively. For numerical evaluation, unless otherwise stated, the transmit powers of BSs are assumed to be $P_1 = 53$ dBm, $P_2 = 33$ dBm, and $P_3 = 23$ dBm while the thermal noise power σ^2 is -104 dBm. The spatial densities of BSs are $\lambda_1 = 5(0.5^2\pi)^{-1}$ BS/km^2, $\lambda_2 = 5\lambda_1$, and $\lambda_3 = 10\lambda_1$. Independent and identically exponential power envelope with unit mean is considered for all links and the path-loss exponent is $\alpha = 3.3$. Power conversion efficiency a is set to 1 and the SINR threshold τ_k is set to 0.5 for all network tiers. Simulation parameters are summarized in Table 5.1.

5.5.2 Coverage Probability

Figure 5.2 shows the effect of the bias factors as well as the SINR threshold on the performance of users associated to different tiers. Since the transmission probability in (5.13) is independent of τ_k, the behavior of both coverage probability and success probability is identical. It can be seen that the success probability decreases with τ_k due to the reduction in the SINR coverage probability in (5.17) where η_k is independent of τ_k. It can also be seen that in the unbiased case (i.e., $\beta = 0$ dB), the performance of all users is the same since each user associates with the nearest BS regardless of its tier. In the flexible cell association case, it can be noticed that when a bias factor is added to one tier, the performance of this tier degrades while the

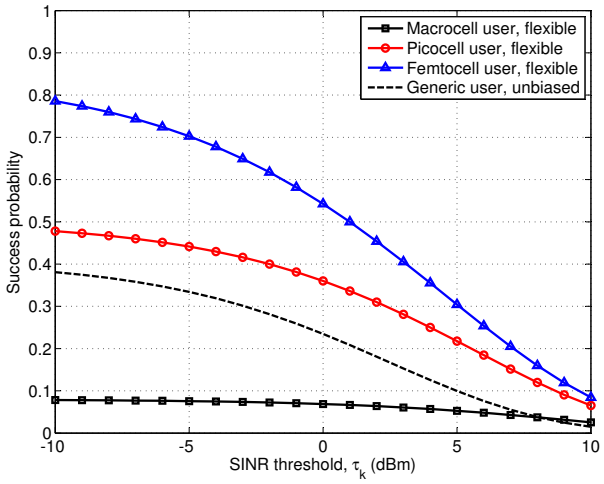

Figure 5.2: Overall coverage probability of a user associated with the k-th tier vs. SINR threshold for the unbiased and flexible cell association. For the flexible cell association, the bias factors are set such that $\beta_k = P_k$, and $\rho_k = -90$ dBm for $k = 1, 2, 3$.

coverage of smaller cells improves. For example, in this case $\beta_1 > \beta_2 > \beta_3$ which means that more users are served by the macrocell network tier and less users are served by the femtocell network tier compared to the unbiased case. This increases the transmission probability of the femtocell users as the femtocell BSs only serve the nearby users and the far users are offloaded to other tiers, hence, less transmit power γ_k is required by the femtocell users. On the other hand, macrocell users suffer from performance degradation as more transmit power is required to invert the channel toward the corresponding BS.

5.5.3 Transmission Probability

To show the effect of the bias factor β_k on the transmission probability in (5.13), Figure 5.3 compares different cases of flexible cell association by varying β_k. Compared to the unbiased case (i.e., $\beta = 0$ dB), it can be seen that biasing the association

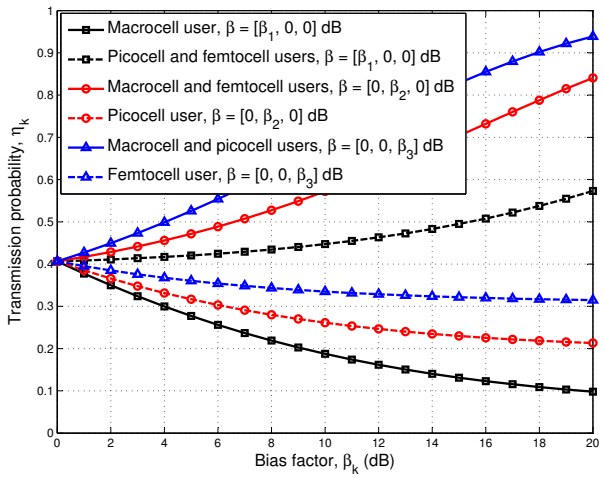

Figure 5.3: Transmission probability of a user associated with the k-th tier vs. the bias factors (for $\rho_1 = \rho_2 = \rho_3 = -90$ dB).

to a certain tier degrades the transmission probability of this tier while improving that of other tiers. However, it can be seen that the degradation is less severe for denser tiers because the number of users added to this tier is divided on all BSs. For the same reason, the improvement in the transmission probability of femtocell and picocell users is higher compared to the macrocell users.

On the other, Figure 5.4 shows the relation between the receiver sensitivity of BSs and the transmission probability where all BSs are assumed to have the same ρ_k. It can be seen that a higher transmission probability for small cell users (i.e., picocell and femtocell users) can be achieved for the same ρ_k by adding a bias factor to the macrocell association. In addition, it can be also seen that the lower ρ_k, the better is the performance for both unbiased and biased association.

5.5.4 Success Probability

Figure 5.5 sums up all the trade-offs presented so far. It shows the behavior of the performance of femtocell users in response to varying the receiver sensitivity ρ_3 of

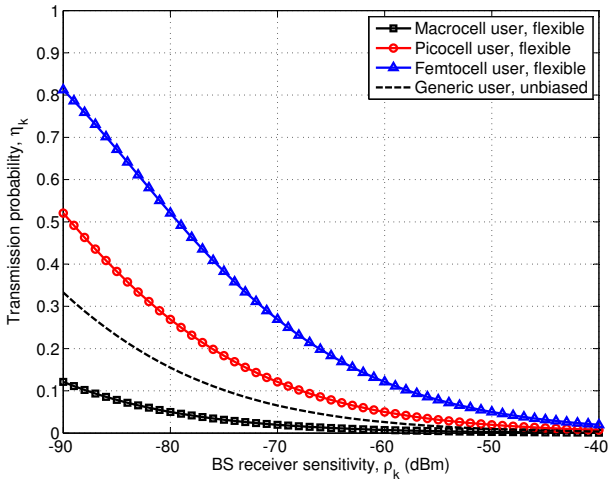

Figure 5.4: Transmission probability of a user associated with the k-th tier vs. BS receiver sensitivity for the unbiased and flexible cell association. For the flexible cell association, the bias factors are set such that $\beta_k = P_k$.

femtocell BSs and the bias factor β_k. The performance is shown in terms of the SINR coverage probability (i.e., $\mathcal{C}_3(\tau_3)$), transmission probability (i.e., η_3), as well as the success probability (i.e., $\eta_3\mathcal{C}_3(\tau_3)$). From this figure, the following observations can be made.

- For both cases (i.e., unbiased and flexible cell association), there exists an optimal value of ρ_k that maximizes the success probability. That is, as ρ_3 increases, the success probability of femtocell users increases up to a maximum value, then it starts to decrease. This behavior can be explained as follows. When the femtocell BS's receiver is more sensitive (i.e., low ρ_3), the femtocell user can achieve high transmission probability (curves with circles), however, the SINR coverage becomes very low, e.g. when $\rho_3 = -110$ dBm. However, as ρ_3 increases, the probability of sufficient power η_3 starts to fall (curves with circles) and the improvement in the SINR coverage (curves with squares) starts to dominate the success probability. Hence, the success probability starts to in-

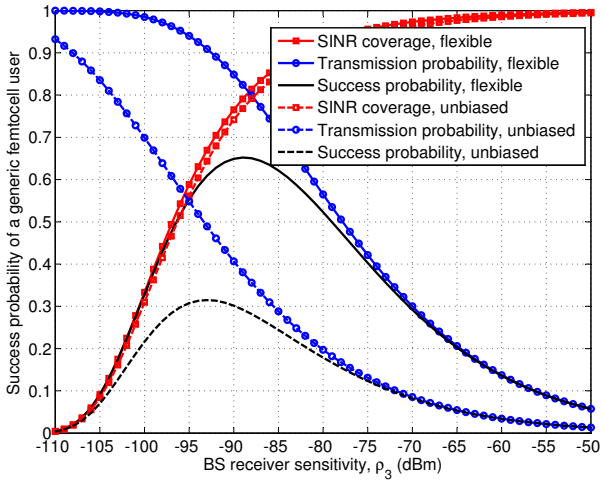

Figure 5.5: Success probability of a generic femtocell user vs. receiver sensitivity of BSs for the unbiased and flexible cell association. For the flexible cell association, the bias factors are set such that $\beta_k = P_k$ (for $\rho_1 = \rho_2 = -90$).

crease. After some value of ρ_3, the decrease of η_3 starts to have more influence on the success probability compared to the SINR coverage probability, hence, the success probability starts to decrease.

- With the flexible (biased) cell association, the success probability of small cell users can be highly improved compared to the unbiased cell association when $\beta_k = 1$. This improvement is introduced by decreasing the distance between a small cell user and her serving BS. This increases the probability of the user to harvest sufficient power to perform channel inversion toward her serving BS (i.e., η_k).

Note that all the results in Figures 5.2-5.5 are under the assumption that all users only depend on harvesting energy from the ambient RF interference as a power source. That is, the degradation in the macrocell users' performance is mainly caused by the degradation in the transmission probability. So, if energy harvesting is considered only for users with short-range communication links such as femtocell users, the same

improvement of performance will be still attainable without performance degradation of macrocell users. Furthermore, same results can be achieved by considering the case when users are powered by a fixed source such as batteries besides harvesting energy.

5.6 Chapter Summary

I have used stochastic geometry to present a novel framework to model, analyze, and evaluate the performance of flexible cell association and RF energy harvesting in multi-tier uplink cellular network. I have shown that energy harvesting can be a reliable source to power cellular users especially those with short-range transmissions such as femtocell users. Furthermore, I have shown how to balance the different trade-offs of the overall performance by varying the network design parameters such as BSs receiver sensitivity and bias factors.

Chapter 6

Cell Association in Multi-Tier Full-Duplex Cellular Networks

In this chapter, I address the problem of cell association in multi-tier in-band full-duplex (FD) networks. Specifically, I consider the case of decoupled cell association (DCA) in which users are not necessarily served by the same BS for uplink and downlink transmissions. Instead, users can simultaneously associate to different BSs based on two independent weighted path-loss (flexible) cell association criteria for the uplink and downlink. I use stochastic geometry to develop a comprehensive modeling framework for the proposed system model where BSs and users are spatially distributed according to independent point processes. I derive closed-form expressions for the mean transmission rates in FD, half-duplex (HD) downlink, and HD uplink networks as well as the mean transmission rate of legacy nodes with only HD capabilities in a multi-tier FD network. I also formulate and solve an optimization problem that aims at maximizing the mean rate of the FD network by jointly optimizing the uplink and downlink cell association criteria. I show the effect of varying different network parameters such as the spatial density of BSs, receiver sensitivity, and weighting (bias)

factors. Furthermore, I investigate the effect of imperfect self-interference cancellation (SIC) and show that it is more severe at uplink, where there exist minimum required SIC capabilities for BSs and users for which FD networks are preferable to HD networks; otherwise, HD networks are preferable. In addition, I discuss several special cases and provide guidelines on the possible extensions of the proposed framework. Finally, I show that DCA outperforms coupled cell association (CCA) in which users associate to the same BS for both uplink and downlink transmissions.

6.1 Introduction

In-band FD communication has been proposed to improve the spectral efficiency of modern cellular networks. In FD transmissions, a network element (e.g., a BS or a user device) transmits and receives information simultaneously in the same frequency band [12]. In contrast, in HD transmissions, a time-frequency resource block is only used for either transmission or reception. Unfortunately, FD communication introduces extra interference between uplink and downlink networks which affects the network performance gains especially for uplink transmissions. The performance of FD networks is also limited by the capability of users and BSs to cancel self-interference (SI), which is caused by the transmitter to its collocated receiver. Fortunately, this technology is becoming feasible thanks to the recent advancements in antenna and digital baseband technologies where SI can be reduced close to the level of noise floor in low-power devices [15].

In this chapter, I focus on the cell association problem in multi-tier cellular networks (i.e., networks that consist of different classes of BSs) that support in-band FD communication. I consider the general case when a cellular user can be simultaneously served by two different BSs for the uplink and downlink data transmission (referred

to as decoupled cell association) [77]. In addition, I aim at optimizing cell association criteria in order to maximize the mean transmission rate offered by FD networks. In order to evaluate and optimize the system performance, I use a statistical approach based on stochastic geometry to capture the network randomness [17,28]. Specifically, in order to derive closed-form expressions for the mean rate in a generic link in the network, due to their analytical tractability, I use independent PPPs to model the locations of BSs [21]. The results from the analysis enable us to optimize cell association to maximize the mean rate utility and to understand the impact of network parameters (such as spatial density of BSs, power control, weighting factors, and SI) on the performance to provide insightful guidelines for system design. I also show that DCA is superior to cell association criteria in which users associate to only one BS for both uplink and downlink transmissions (referred to as coupled cell association). Furthermore, I show that FD networks can outperform HD networks in terms of mean rate for sufficiently high SIC capabilities of BSs and users.

6.1.1 Contributions

The contributions of this chapter are summarized as follows.

- Using tools from stochastic geometry, I provide a tractable framework to analyze the performance of multi-tier FD networks with DCA. I derive closed-form expressions for the association probability, the mean interference received at users and BSs under weighted path-loss cell association. In addition, I derive the mean rate coverage offered by an FD network.
- I investigate the effect of FD transmissions on legacy HD terminals that do not support FD communication and I provide closed-form expressions for mean rate coverage.

- I formulate an optimization problem to maximize the mean rate of FD networks. By jointly optimizing both uplink and downlink cell association to maximize the mean rate, I also show that DCA is superior to CCA in FD networks.

- I show how the proposed framework can be extended to different models in the literature such as traditional HD uplink and HD downlink networks. In addition, I highlight different tradeoffs in the network and show the effect of varying network parameters such as densities of BSs, power control parameters, and cell association weighting factors on network performance.

- I investigate the effect of SI on the performance of an FD network and show that FD mode of operation is preferable to HD mode only if the SIC capabilities of users and BSs are sufficient to mitigate SI. Furthermore, I show that the effect of imperfect SIC is more severe at uplink.

- Via Monte Carlo simulation, I validate the analytical results. Also, through numerical results I show the feasibility of FD communication to increase the mean transmission rate of cellular networks.

6.1.2 Organization

The rest of the chapter is organized as follows. A review of the related work is presented in Section 6.2. System model and assumptions are described in Section 6.3. In Section 6.4, both joint distance distributions and cell association probabilities are derived for a typical user. Section 6.5 presents the analysis for FD interference as well as mean rate of uplink, downlink, and FD transmissions. An optimization problem is formulated in Section 6.6 to maximize the mean rate of FD transmission. Finally, the numerical results and discussion are presented in Section 6.7 before the chapter

is summarized in Section 6.8.

6.2 Related Work

In the context of decoupled cell association (DCA) in multi-tier cellular networks, the authors in [78, 79] propose a framework for performance evaluation of multi-tier HD uplink and downlink cellular networks. In this model, the locations of BSs in each tier are modeled by independent PPPs where each network tier differs in the transmit power and spatial density. Using PPP assumption and weighted path-loss cell association, [78] derives expressions for the rate coverage in HD uplink and downlink networks as well as the joint uplink-downlink rate coverage. On the other hand, closed-form expressions for the mean logarithm of the transmission rate and spectrum for both uplink and downlink transmissions are derived in [79]. Furthermore, utility maximization problems are solved to optimize both cell association and spectrum partitioning. The authors in [80] use stochastic geometry to derive the achievable capacity in an HD network with DCA where a real-world simulation tool (Atoll) is used to verify the accuracy of the expressions. In [81], the DCA problem is formulated as a matching game in which users and BSs in a two-tier FD cellular network rank one another based on some preference metric, which is a function of the achievable SINR, in order to maximize the total throughput.

The authors in [82–86] evaluate the performance of FD networks using statistical modeling. In [82], a hybrid ad hoc network is considered in which nodes with HD or FD capabilities are randomly deployed. For an ALOHA MAC protocol, it shows that FD networks achieve a $0 - 30\%$ higher throughput, compared to HD networks, for practical values of path-loss exponent. It also considers the effect of imperfect SIC and shows how it affects the relative performance of FD and HD transmissions.

The authors in [83] present the effect of transmission duration, SIC, and ratio of HD-to-FD nodes on the performance of ad hoc networks with asynchronous ALOHA MAC protocol. The paper also highlights different optimal operating regions in which FD networks outperform HD networks. In [84], the authors propose a system design that controls the partial overlap between uplink and downlink channels in order to maximize the overall rate of FD cellular networks. The paper compares the performances of two realizations for FD networks: a two-node topology (2NT) with FD users and BSs and a three-node topology (3NT) with FD BSs and HD users. It shows that 3NT achieves performance comparable to that of 2NT, which paves the road to harvest the gains of FD transmissions with HD user terminals. In [85], a hybrid multi-tier FD cellular network is considered in which BSs operate either in FD mode or HD downlink mode. PPP assumption is used to derive expressions for the successful transmission probability and network throughput. The authors in [86] consider a single-cell scenario to derive the outage probability and achievable sum rate under a 3NT considering the effect of SI. It is worth mentioning that nodes (i.e., users or BSs) in [82–86] use CCA to solve the association problem in FD networks.

Although statistical modeling can be used for long-term performance evaluation of FD networks, it does not necessarily provide sufficient insights on short-term network performance. Therefore, tools from optimization theory can be used to evaluate the short-term performance of networks and to find optimal parameters that maximize certain objective functions [87–90]. For example, [87] proposes a joint resource management scheme to mitigate the effect of imperfect SIC in an OFDMA-based two-tier FD cellular network. This is achieved by jointly assigning users and transmit power for each resource block in both uplink and downlink transmission based on the level of SI to maximize a total utility sum of the network. The authors in [88] propose an

iterative algorithm to jointly perform subcarrier assignment and power allocation in order to maximize the sum-rate performance in a single-cell FD network. In [89], the authors propose a joint uplink-downlink user scheduling and power allocation algorithm to maximize the system throughput by investigating the feasibility conditions of FD operation with 3NT. The authors in [90] propose two distributed power control and interference management methods to manage interference in FD networks with 3NT. The proposed MAC protocol with transmit power optimization is shown to outperform its HD counterpart in terms of total throughput.

6.3 System Model and Assumptions

6.3.1 Multi-Tier Network Model

In this chapter, a cellular network that consists of K tiers of BSs is considered. I use an independent homogeneous PPP $\mathbf{\Phi}_k = \{x_{i,k} : i = 1, 2, \dots\}$ with spatial density λ_k to model locations of BSs belonging to the k-th tier where $1 \leq k \leq K$ and $x_{i,k} \in \mathbb{R}^2$ denotes the location of the i-th BS in that tier. For all BSs in k-th tier, transmit power is fixed and equal to P_k. Locations of users are modeled in $\mathbb{R}^2$ according to an arbitrary independent point process $\mathbf{\Psi}$. Saturation condition is assumed where each transmitter (i.e., a BS or a user) sends data packets at the beginning of each time slot in a time-slotted transmission scenario.

6.3.2 Channel Model

I assume a co-channel deployment where the wireless channels are subject to both large-scale (i.e., path-loss) and small-scale fading. Let $\|x - y\|$ be the propagation distance between a generic transmitter (i.e., a BS or a user) located at x and a receiver

located at y. The path-loss of this link is defined as $L(x,y) = \bar{G}\|x-y\|^{\bar{\alpha}}$, where $\bar{\alpha} > 2$ is the path-loss exponent and $\bar{G} > 0$ is a constant gain. I assume different path-loss exponents and gains for different communication links [91]. That is, $\bar{\alpha} = \alpha$ and $\bar{G} = G$ for BS-user links, $\bar{\alpha} = \alpha_b$ and $\bar{G} = G_b$ for BS-BS links, and $\bar{\alpha} = \alpha_u$ and $\bar{G} = G_u$ for user-user links.

In addition to the distance-dependent path-loss, the small-scale fading component of a channel is modeled by Rayleigh fading with unit average power where different links are assumed to be i.i.d.. Hence, the power gain of all channels is exponentially-distributed and denoted by $h(x,y) \sim \text{Exp}(1)$. Channel coherence time is greater than or equal to the frame duration. SI channel is modeled by Nakagami-m fading with parameters (m_{b_k}, σ_{b_k}) and (m_u, σ_u) for BSs from k-th tier and users, respectively. Hence, the power gain of SI channel follows a Gamma distribution and denoted by $h_b \sim \text{Gamma}(m_{b_k}, \frac{\sigma_{b_k}}{m_{b_k}})$ for BSs and $h_u \sim \text{Gamma}(m_u, \frac{\sigma_u}{m_u})$ for users, where $\frac{1}{\sigma_{b_k}}$ and $\frac{1}{\sigma_u}$ are SIC capabilities of BSs and users, respectively. There is no intra-cell interference between uplink (downlink) transmissions where different users in a cell are served in uplink (downlink) using orthogonal time-frequency resources (e.g. OFDMA). Hence, there are only one active user in uplink and one active user in downlink per BS at a certain time slot and channel.

6.3.3 Power Control Model

The users adopt fractional channel inversion power control where a user at x adjusts her transmit power to $\rho_k(G\|x-y\|^{\alpha})^{\epsilon}$ to compensate for the large-scale fading such that the average received signal power at the serving BS at y is equal to $\rho_k(G\|x-y\|^{\alpha})^{-(1-\epsilon)}$. Note that $0 \leq \epsilon \leq 1$ is the power control factor and ρ_k is the open loop power spectral density (or receiver sensitivity). Here, I use γ_k to denote the

instantaneous transmit power of a user transmitting to a BS belonging to the k-th tier where Γ_k is the corresponding random variable. Users have a limited transmit power budget of $P_{\max}$, where users who are unable to perform channel inversion transmit with maximum power. Other power control mechanisms such as interference-aware power control [92] and SI-aware power control [93] can also be adopted.

6.3.4 Mode of Operation and Cell Association

Besides FD links in which a user simultaneously transmits and receives data in the same channel, I also consider network tiers in which users and BSs do not support FD transmissions (i.e., HD users and HD BSs). That is, I also evaluate the performance of the network when (i) there is a typical HD user who can *only receive downlink transmission* from one BS in a channel during a transmission interval, and (ii) there is a network tier of HD BSs each of which can *only receive uplink transmission* in a channel from one user during a transmission interval. A communication link is referred to as a *legacy uplink* when the user-BS channel carries data only from the user to the serving HD BS. On the other hand, when the user-BS channel carries data only from the BS to the HD user being served, the link is referred to as a *legacy downlink*. Furthermore, I consider the 3NT model, where the network consists of FD BSs each of which serves two HD users: one HD user in downlink and one HD user in uplink. The aforementioned scenarios will be discussed in details in Sections 6.5 and 6.7.

In this work, for users with FD capabilities, I consider the case where cell association in the uplink is decoupled from that of the downlink. Hence, an FD user is *not necessarily* served by the same BS in both uplink and downlink. That is, a user may simultaneously receive data from one BS and transmit data to another in the

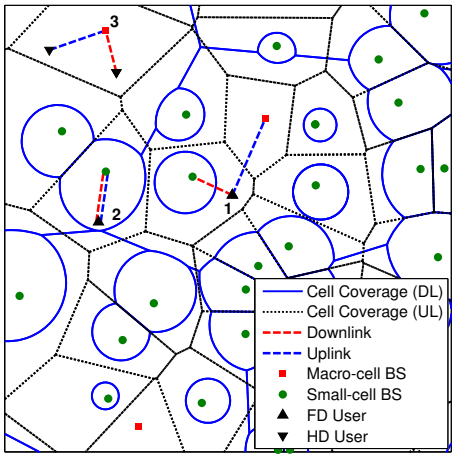

Figure 6.1: A two-tier FD cellular network with a macrocell network tier (red squares) overlaid with lower power and denser small cell BSs (green circles). Solid blue lines show the coverage area of each cell for the downlink transmissions, while the dotted black lines show that of the uplink transmissions.

same channel. To illustrate, without loss of generality, Figure 6.1 shows a realization of a two-tier FD cellular network where a macro-cell network tier is overlaid with a denser and lower power small-cell network tier. It shows that the coverage area of each cell in downlink is different from that in uplink. For example, although user 1 is served by a macro-cell BS in downlink, she is located in uplink coverage area of another small-cell BS, hence, served by two different BSs. On the other hand, user 2 is located in the coverage area of one small-cell BS in both downlink and uplink, hence, served by the same BS. Figure 6.1 also shows an example of 3NT realization where BS 3 serves two HD users simultaneously: one HD user is in downlink and another HD user is in uplink.

I assume a weighted path-loss cell association criterion similar to [42, 94] where each user independently associates with the BS(s) that minimizes the weighted path-loss of uplink and downlink. That is, for a user at y, with a slight abuse of notation,

let x_i, x^{UL}, and x^{DL} denote the BS with minimum path-loss from i-th tier, serving BS in uplink, and serving BS in downlink, respectively. Then, the association criteria for the uplink can be described as

$$x^{\mathrm{UL}} = \underset{x \in \{x_i\}}{\arg\min}\, U_i \|x - y\|^{\alpha} \tag{6.1}$$

where

$$x_i = \underset{x \in \mathbf{\Phi}_i}{\arg\min}\, \|x - y\|^{\alpha}, \quad i = \{1, 2, \ldots, K\}$$

and U_i is the weighting factor for the uplink cell association for a BS belonging to the i-th tier. Similarly, the cell association criteria for the downlink can be described as

$$x^{\mathrm{DL}} = \underset{x \in \{x_i\}}{\arg\min}\, D_i \|x - y\|^{\alpha} \tag{6.2}$$

where D_i is the weighting factor for the downlink cell association for a BS from the i-th tier.

Assumption 6.1. Let $\mu_i = \frac{U_i}{D_i}$ and without loss of generality, let us assume that the network tiers are ordered such that $\mu_1 \leq \mu_2 \leq \cdots \leq \mu_K$.

Note that U_i and D_i are design parameters which are not necessarily equal. Varying the weighting factors can result in different association scenarios. For example, (i) *coupled cell association*: when $U_i = D_i$, each user associates to the same BS for both downlink and uplink, (ii) *minimum-distance cell association*: when $U_i = U$ (or $D_i = D$), each user associates to the nearest BS for uplink (or downlink), (iii) *maximum-received power cell association*: when $D_i = P_i^{-1}$, each user associates to the BS that offers the strongest received power for downlink, and (iv) *minimum-transmit power cell association*: when $U_i = \rho_i$, each user associates to the BS that requires

lowest transmit power for uplink.

6.3.5 Methodology of Analysis

Based on the system model described above, I aim at quantifying the performance of a generic FD link in terms of mean rate in nats/sec/Hz. I first derive the cell association probability and distance distributions based on decoupled and weighted path-loss cell association. Then, I obtain the mean of interference experienced at a typical BS in the uplink and at a typical user in the downlink. Next, I derive the mean rate utility of the network as well as that of uplink and downlink transmissions. I also present some special cases. Finally, I optimize the uplink and downlink cell association weighting factors such that the mean rate of the FD network is maximized.

6.4 Analysis of Distance and Association Probabilities

6.4.1 Analysis of Association Probabilities

Note that, even with DCA, an FD user can associate to the same BS in the k-th tier for both uplink and downlink transmissions with a certain probability. It is worth mentioning that this scenario is different from the CCA as it does not necessitate U_k and D_k to be equal (as in the CCA). That is, although the user still uses two different decision criteria for uplink and downlink cell association (i.e., DCA in (6.1) and (6.2)), one BS meets both criteria. This event occurs depending on the network realization. Let ψ_{jk} denote the *joint association probability* that a user is served by a BS from the j-th tier in the downlink and a BS from the k-th tier in the uplink. The following lemma characterizes this probability.

Lemma 6.1. *(Joint association probability)* The probability that an FD user is served

by the j-th tier for the downlink and k-th tier for the uplink transmissions is

$$\psi_{jk} = \begin{cases} \lambda_j \left(\sum_{i=1}^{K} \max\{\mathcal{D}_{ji}, \mathcal{U}_{ji}\}^{\frac{2}{\alpha}} \lambda_i \right)^{-1}, & j = k \\ \lambda_j \lambda_k \left(\frac{D_j}{U_k} \right)^{\frac{2}{\alpha}} \sum_{l=k}^{j-1} \frac{1}{\Upsilon_l^2(j)} \left(\frac{\mu_{l+1}^{\frac{2}{\alpha}}}{1 + \mu_{l+1}^{\frac{2}{\alpha}} \Omega_l} - \frac{\mu_l^{\frac{2}{\alpha}}}{1 + \mu_l^{\frac{2}{\alpha}} \Omega_l} \right), & k < j \\ 0, & k > j \end{cases} \tag{6.3}$$

where

$$\Upsilon_l(j) = \sum_{i=l+1}^{K} \mathcal{D}_{ji}^{\frac{2}{\alpha}} \lambda_i \tag{6.4}$$

and

$$\Omega_l = \left(\sum_{i=1}^{l} \frac{\lambda_i}{U_i^{\frac{2}{\alpha}}} \right) \left(\sum_{i=l+1}^{K} \frac{\lambda_i}{D_i^{\frac{2}{\alpha}}} \right)^{-1}. \tag{6.5}$$

Proof. See **Appendix E.1.1**. □

Note that the joint association probability ψ_{jk} is different from the *per-tier association probability* which is defined as the probability that a user is served by a BS belonging to a certain tier for downlink (uplink) regardless of the serving uplink (downlink) BS. This probability can be obtained directly from the joint association probability ψ_{jj} when $D_i = U_i$. The following lemma provides expressions for this probability for both downlink and uplink transmissions.

Lemma 6.2. *(Per-tier association probability)* The probability that a user associates to a BS from the j-th tier for either the downlink or uplink is defined, respectively,

as follows

$$\begin{aligned} A_j^{\mathrm{DL}} &= \lambda_j \left(\Lambda_j^{\mathrm{DL}}\right)^{-1} \\ A_j^{\mathrm{UL}} &= \lambda_j \left(\Lambda_j^{\mathrm{UL}}\right)^{-1} \end{aligned}. \tag{6.6}$$

where $\Lambda_j^{\mathrm{DL}} = \sum_{i=1}^{K} \mathcal{D}_{ji}^{\frac{2}{\alpha}} \lambda_i$ and $\Lambda_j^{\mathrm{UL}} = \sum_{i=1}^{K} \mathcal{U}_{ji}^{\frac{2}{\alpha}} \lambda_i$ are the *effective spatial densities* of the j-th tier for downlink and uplink transmissions, respectively.

6.4.2 Analysis of Distance to Serving BS(s)

Based on the system model and cell association criteria described above, for users operating in FD mode, the marginal PDFs of the distances to the serving BSs in downlink and uplink are presented in the following lemma where the proof follows **Appendix D.1**.

Lemma 6.3. *(Marginal distance distributions)* The CDF of the distance between a generic user associated with the j-th tier for the downlink (or uplink) and her serving BS is defined as

$$\mathbb{P}[R_j^m \leq r] = 1 - \exp\left[-\pi \Lambda_j^m r^2\right] \tag{6.7}$$

and its n-th moment is given by

$$\mathbb{E}_{R_j^m}\left[R_j^n\right] = \Gamma\left[\frac{2+n}{2}\right] \left(\pi \Lambda_j^m\right)^{-\frac{n}{2}} \tag{6.8}$$

where $m \in \{\mathrm{DL}, \mathrm{UL}\}$ and Λ_j^m is given in **Lemma 6.2**.

Furthermore, the following lemma provides the joint distance distribution of the distance to the serving BSs for downlink and uplink transmissions for FD users.

Lemma 6.4. *(Joint distance distribution)* The joint PDF of the distance(s) from a

generic FD user and her serving BS(s), when associated with the j-th for downlink and tier k-th for uplink, is

$$f_{\mathbf{R}}(r_j, r_k) = \begin{cases} 2\pi\lambda_j r_j \exp\left[-\pi \sum_{i=1}^{K} \max\{\mathcal{D}_{ji}, \mathcal{U}_{ji}\}^{\frac{2}{\alpha}} \lambda_i r_j^2\right], & j = k, r_k = r_j \\ 4\pi^2\lambda_j\lambda_k r_j r_k \exp\left[-\pi \sum_{i=1}^{K} \max\left\{\mathcal{D}_{ji} r_j^{\alpha}, \mathcal{U}_{ki} r_k^{\alpha}\right\}^{\frac{2}{\alpha}} \lambda_i\right], & k < j, (r_j, r_k) \in \mathcal{A} \end{cases} \tag{6.9}$$

where

$$\mathcal{A} = \left\{(r_j, r_k) : r_j \geq 0, \mathcal{D}_{jk}^{\frac{1}{\alpha}} r_j < r_k < \mathcal{U}_{jk}^{\frac{1}{\alpha}} r_j\right\}$$

and their joint expectation is given by

$$\begin{aligned} \mathbb{E}_{\mathbf{R}}[R_j^m] &= \Gamma\left[\tfrac{2+m}{2}\right] \left(\pi \sum_{i=1}^{K} \max\left\{\mathcal{D}_{ji}, \mathcal{U}_{ji}\right\}^{\frac{2}{\alpha}} \lambda_i\right)^{-\frac{m}{2}}, && j = k \\ \mathbb{E}_{\mathbf{R}}[R_j^m] &= \left(\sum_{l=k}^{j-1} \mathcal{H}_{jl}\left[\mu_l, \mu_{l+1}; 0\right]\right)^{-1} \sum_{l=k}^{j-1} \tfrac{-1}{\Omega_l} \mathcal{H}_{jl}\left[1, 1; m\right], && k < j \\ \mathbb{E}_{\mathbf{R}}[R_k^n] &= \left(\sum_{l=k}^{j-1} \mathcal{H}_{jl}\left[\mu_l, \mu_{l+1}; 0\right]\right)^{-1} \sum_{l=k}^{j-1} \mathcal{H}_{jl}\left[\mu_l, \mu_{l+1}; n\right], && k < j \end{aligned} \tag{6.10}$$

where

$$\mathcal{H}_{jl}\left[a, b; c\right] = \frac{\Gamma\left[\frac{2+c}{2}\right]}{\pi^{\frac{c}{2}} \left(\Upsilon_l(j)\right)^{\frac{4+c}{2}}} \left[\frac{a^{\frac{2+c}{\alpha}}}{\left(1 + \mu_l^{\frac{2}{\alpha}} \Omega_l\right)^{\frac{2+c}{2}}} - \frac{b^{\frac{2+c}{\alpha}}}{\left(1 + \mu_{l+1}^{\frac{2}{\alpha}} \Omega_l\right)^{\frac{2+c}{2}}}\right]. \tag{6.11}$$

Proof. See **Appendix E.1.2**. □

6.4.3 Analysis of Uplink Transmission Power

Based on the described system model, users served in the uplink by a BS from k-th tier are assumed to perform fractional channel inversion with open loop power spectral density ρ_k. Users are also assumed to have a constraint $P_{\max}$ on the transmit power. Thus, I define the required amount of transmit power of a user when she associates with a BS from the k-th tier as

$$\gamma_k = \min\{\rho_k G^{\epsilon} R_k^{\epsilon\alpha}, P_{\max}\} \tag{6.12}$$

where R_k is the distance to the serving BS from tier k for the uplink transmission and its CDF is given in **Lemma 6.3**.

Therefore, I use (6.7) and (6.12) to derive the CDF and the n-th moment of a typical user's transmit power when she associates to the k-th tier as in the following lemma where the proof follows directly from **Lemma 6.3** and **Appendix C.2**.

Lemma 6.5. *(Transmit power distribution)* The CDF of the transmit power of a user associated to tier k in the uplink and performing fractional channel inversion power control is

$$F_{\Gamma_k}(t) = 1 - \exp\left[-\pi\Lambda_k^{\mathrm{UL}}\left(\frac{t}{\rho_k G^{\epsilon}}\right)^{\frac{2}{\epsilon\alpha}}\right] \cdot \mathbf{1}_{\{t<P_{\max}\}} \tag{6.13}$$

and its n-th moment is given by

$$\mathbb{E}[\Gamma_k^n] = \frac{n\epsilon\alpha\rho_k^n G^{n\epsilon}}{2(\pi\Lambda_k^{\mathrm{UL}})^{\frac{n\epsilon\alpha}{2}}}\,\gamma\left[\frac{n\epsilon\alpha}{2}, \pi\Lambda_k^{\mathrm{UL}}\left(\frac{P_{\max}}{\rho_k G^{\epsilon}}\right)^{\frac{2}{\epsilon\alpha}}\right]. \tag{6.14}$$

6.5 Analysis of Rate Coverage

In this section, I characterize the rate coverage for a generic FD link based on the described system model. To evaluate the rate coverage, I assume that during a transmission interval, a receiver (i.e., BS or a user) using a particular channel to communicate with its corresponding transmitter experiences interference from all other BSs as well as users reusing the same channel. I start by defining the SINR received at a typical user and BS. Then, the rate coverage probability is derived for a generic FD link and several special cases in the literature.

6.5.1 Signal-to-Interference-plus-Noise Ratio

For the system model described above, the SINR can be expressed as follows

$$\begin{aligned} \mathrm{SINR}_{jk}^{\mathrm{DL}} &= \frac{P_j h(x^{\mathrm{DL}}, u_\circ)}{G(\mathcal{I}^{\mathrm{DL}} + \mathcal{I}_{\mathrm{SI}}^{\mathrm{DL}} + \sigma^2)\|x^{\mathrm{DL}}\|^{\alpha}} \\ \mathrm{SINR}_{jk}^{\mathrm{UL}} &= \frac{\min\{\rho_k G^{\epsilon}\|x^{\mathrm{UL}}\|^{\epsilon\alpha}, P_{\max}\} g(u_\circ, x^{\mathrm{UL}})}{G(\mathcal{I}^{\mathrm{UL}} + \mathcal{I}_{\mathrm{SI}}^{\mathrm{UL}} + \sigma^2)\|x^{\mathrm{UL}}\|^{\alpha(1-\epsilon)}} \end{aligned} \tag{6.15}$$

where $x^{\mathrm{DL}} \in \mathbf{\Phi}_j$ and $x^{\mathrm{UL}} \in \mathbf{\Phi}_k$ denote the serving BS for downlink and uplink transmissions, respectively, as defined in (6.1)-(6.2). $u_\circ$ is the tagged user, σ^2 is the additive noise power, $h(x, y)$ and $g(x, y)$ are the channel power gains, and $\mathcal{I}^{\mathrm{DL}}$ and $\mathcal{I}^{\mathrm{UL}}$ are the interference received, respectively, at the tagged user (i.e., downlink) and BS (i.e., uplink) from all other BSs and users sharing the same channel. Note that, unlike HD networks, the interference signals received from the downlink and uplink transmissions are correlated due to the relative distance between each user-BS pair and the observation point. In order to characterize the interference, using the fact that each cell has exactly one downlink and one uplink transmissions, I pair each user and her serving BS in the uplink together as an interfering pair. Hence, the aggregate

interference at a typical receiver (i.e., a user or a BS) located at the origin $(0,0)$ can be defined as follows[1]:

$$\mathcal{I}^{\mathrm{DL}} = \sum_{i=1}^{K} \sum_{x \in \mathbf{\Phi}_i \setminus \{x^{\mathrm{DL}}\}} \frac{P_i h(x,0)}{G\|x\|^{\alpha}} + \sum_{y \in \tilde{\mathbf{\Psi}}_i \setminus \{u[x^{\mathrm{UL}}]\}} \frac{\gamma_i(y) g(y,0)}{G_u \|y\|^{\alpha_u}} \tag{6.16}$$

$$\mathcal{I}^{\mathrm{UL}} = \sum_{i=1}^{K} \sum_{x \in \mathbf{\Phi}_i \setminus \{x^{\mathrm{UL}}\}} \frac{P_i h(x,0)}{G_b\|x\|^{\alpha_b}} + \sum_{y \in \tilde{\mathbf{\Psi}}_i \setminus \{u[x^{\mathrm{UL}}]\}} \frac{\gamma_i(y) g(y,0)}{G\|y\|^{\alpha}} \tag{6.17}$$

where $u[x]$ returns the user served by BS x in the uplink, $\gamma_i(y) = \min\{\rho_i G^{\epsilon} \|y - u[y]\|^{\epsilon\alpha}, P_{\max}\}$ is the transmit power of the user, and $\tilde{\mathbf{\Psi}}_i$ is the point process that represents the active users. Note that, due to the correlation between the positions of active users and BSs resulting from the orthogonal time-frequency resource allocations (e.g., OFDMA), this point process does is not a PPP. Instead, the positions of active users can be seen as a Voronoi perturbed lattice process which is not mathematically tractable [78, 95].

Assumption 6.2. The active users from the i-th tier are assumed to form an arbitrary point process $\tilde{\mathbf{\Psi}}_i$ that is (i) stationary with spatial density λ_i, (ii) independent of the point processes of active users from different tiers, and (iii) independent of $\mathbf{\Phi}_i$[2].

6.5.2 Interference Model

For each type of tagged receivers (i.e., BSs or users) and interferers (i.e., BSs or users), I define a pair correlation function $g(r)$ which in turn quantifies the spatial density

[1]Due to the homogeneous PPP assumption, interference statistics are independent of the observation point [28].

[2]Other approximations for $\tilde{\mathbf{\Psi}}_i$ exist in the literature, e.g., non-homogeneous PPP with spatial density $\lambda_i \left(1 - \exp[-\pi \Lambda_i^{\mathrm{UL}} r^2]\right)$ [78], or more generally $\lambda_i g(r)$, where $g(r)$ is a pair correlation function as proposed in [96]. Another approximation is using PPP assumption with exclusion ball of radius $\sqrt{\frac{1}{\pi \Lambda_i^{\mathrm{UL}}}}$ such as in [97] for single-tier networks.

of interfering nodes from i-th tier as $\lambda_i g(r)$.

1. BSs-to-users (downlink-to-downlink): Using (6.2), it is clear that no interfering BS from i-th tier can have less weighted path-loss to a user than her serving BS, hence, $\|x\| > \mathcal{D}_{ji}^{\frac{1}{\alpha}} \|x^{\mathrm{DL}}\|$, where $x \in \mathbf{\Phi}_i$ and $x^{\mathrm{DL}} \in \mathbf{\Phi}_j$ [28, 34, 42, 78, 79]. Therefore, $g_1(r) = \mathbf{1}\{r > \mathcal{D}_{ji}^{\frac{1}{\alpha}} R_j\}$, where $R_j = \|x^{\mathrm{DL}}\|$.

2. Users-to-BS (uplink-to-uplink): There is no exact boundary for the exclusion region around the tagged BS where interfering users can be arbitrarily close. However, using (6.1), it is clear that none of the interfering users associates with that BS, hence, for a user u served by a BS from i-th tier, $\|x^{\mathrm{UL}} - u\| > \mathcal{U}_{ik}^{\frac{1}{\alpha}} \|x - u\|$, where $x \in \mathbf{\Phi}_i$ and $x^{\mathrm{UL}} \in \mathbf{\Phi}_k$ [78, 79, 94, 98]. Therefore, $g_2(r) = \mathbf{1}\{r > \mathcal{U}_{ik}^{\frac{1}{\alpha}} R_i\}$, where $R_i = \|x - u\|$.

3. BSs-to-BS (downlink-to-uplink): Due to the PPP assumption, the BSs can be very close to each other, however, this is not true in practice due to physical constraints, different antenna heights, etc. [91]. Here, I use the approximation proposed in [96] to model interfering BSs from i-th tier as a non-homogeneous point process with $g_3(r) = (1 - \exp[-\pi \frac{\lambda_i}{\beta_b} r^2]) \mathbf{1}\{r > d_b\}$ to model the repulsion between BSs in practical deployments where β_b is the repulsion parameter and d_b is a constraint on the length of an uplink-to-uplink interference link.

4. Users-to-user (uplink-to-downlink): I use a similar approximation to model the interfering users served by the i-th tier of BSs in uplink as a non-homogeneous point process with $g_4(r) = (1 - \exp[-\pi \frac{\lambda_i}{A_i^{\mathrm{UL}}} r^2]) \mathbf{1}\{r > d_u\}$, where A_i^{UL} is the repulsion parameter as in [78] and d_u is the minimum length of an uplink-to-downlink interference link.

6.5.3 Self-Interference

In (6.15), $\mathcal{I}_{\mathrm{SI}}^{\mathrm{DL}}$ is SI resulting from uplink transmission at the user, and $\mathcal{I}_{\mathrm{SI}}^{\mathrm{UL}}$ is SI resulting from downlink transmission at the BS. Since the SI incurred at a given receiver depends on its own transmit power, I define the residual SI power after cancellation as follows:

$$\mathcal{I}_{\mathrm{SI}}^{\mathrm{DL}} = \min\left\{\rho_k G^{\epsilon} \|x^{\mathrm{UL}}\|^{\epsilon\alpha}, P_{\max}\right\} h_u \quad \text{and} \quad \mathcal{I}_{\mathrm{SI}}^{\mathrm{UL}} = P_k h_{b_k} \tag{6.18}$$

where h_{b_k} and h_u represent SI channels such that $\sigma_{b_k} = \mathbb{E}[h_{b_k}]$ and $\sigma_u = \mathbb{E}[h_u]$ are the inverse of SIC capability of BSs from tier k and users, respectively.

6.5.4 Mean Rate Utility

For a given FD link, let us define the rate coverage probability as the probability of uplink (downlink) transmission rate to be higher than a required target rate threshold $\mathcal{R}_{\circ}^{\mathrm{UL}}$ ($\mathcal{R}_{\circ}^{\mathrm{DL}}$). In other words, for the uplink (downlink) transmission to achieve the target rate, the SIRN received at the BS (user) must be greater than a prescribed threshold τ^{UL} (τ^{DL}) that can be given using Shannon's formula as follows

$$\tau^m = \exp[\mathcal{R}_{\circ}^m] - 1, \qquad m \in \{\mathrm{DL}, \mathrm{UL}\}. \tag{6.19}$$

Hence, the rate $\mathcal{R}_{jk}$ of a generic FD link measured in nats/sec/Hz for a user served by a BS from j-th tier for downlink and a BS from k-th tier for uplink is defined as

$$\mathcal{R}_{jk} = \underbrace{\mathbb{P}(\mathrm{SINR}_{jk}^{\mathrm{DL}} > \tau^{\mathrm{DL}}) \ln\left[1+\tau^{\mathrm{DL}}\right]}_{=\mathcal{R}_{jk}^{\mathrm{DL}}} + \underbrace{\mathbb{P}(\mathrm{SINR}_{jk}^{\mathrm{UL}} > \tau^{\mathrm{UL}}) \ln\left[1+\tau^{\mathrm{UL}}\right]}_{=\mathcal{R}_{jk}^{\mathrm{UL}}} \tag{6.20}$$

which corresponds to a fixed data rate transmission (i.e., $\mathcal{R}_{\circ}^{\mathrm{DL}} = \ln[1+\tau^{\mathrm{DL}}]$ and $\mathcal{R}_{\circ}^{\mathrm{UL}} = \ln[1+\tau^{\mathrm{UL}}]$) when the SINR of the downlink and uplink transmissions (i.e., $\mathrm{SINR}_{jk}^{\mathrm{DL}}$ and $\mathrm{SINR}_{jk}^{\mathrm{UL}}$, respectively) exceed the predefined thresholds, otherwise, the transmission rate is zero.

Furthermore, I define the mean rate coverage utility of a generic FD link in the network as:

$$\bar{\mathcal{R}} = \sum_{j=1}^{K}\sum_{k=1}^{K} \psi_{jk} f\big(\mathcal{R}_{jk}^{\mathrm{DL}}, \mathcal{R}_{jk}^{\mathrm{UL}}\big) \tag{6.21}$$

where $f\big(\mathcal{R}_{jk}^{\mathrm{DL}}, \mathcal{R}_{jk}^{\mathrm{UL}}\big)$ is the mean utility of an FD link given that the user is associated with j-th tier for downlink and k-th tier for uplink. In this work, I use $f\big(\mathcal{R}_{jk}^{\mathrm{DL}}, \mathcal{R}_{jk}^{\mathrm{UL}}\big) = \mathbb{E}\left[\ln\left[\mathcal{R}_{jk}^{\mathrm{DL}}\mathcal{R}_{jk}^{\mathrm{UL}}\right]\right] = \mathbb{E}\left[\ln \mathcal{R}_{jk}^{\mathrm{DL}}\right] + \mathbb{E}\left[\ln \mathcal{R}_{jk}^{\mathrm{UL}}\right]$ as the mean utility function [79, 99]. The motivation of considering this utility is to achieve *proportional fairness* among users. This is achieved by improving the rates of links with low rate coverage probability while saturating the rates of links with high rate coverage probability. This performance metric is widely used in the literature to solve the problem of radio resource allocations while achieving fairness via maximizing $\bar{\mathcal{R}}$ [100]. Therefore, hereafter, I derive the following performance metric for a generic user operating in the FD mode:

$$\mathbb{E}[\ln \mathcal{R}_{jk}^{m}] = \ln \mathcal{R}_{\circ}^{m} + \mathbb{E}\left[\ln\left[\mathbb{P}(\mathrm{SINR}_{jk}^{m} > \tau^{m})\right]\right], \qquad m \in \{\mathrm{DL}, \mathrm{UL}\} \tag{6.22}$$

where the expectation is with respect to $\mathbf{R}$, $\mathbf{\Phi}_i$, and $\mathbf{\Psi}_i$.

First, I focus on uplink rate coverage, which can be obtained as follows:

$$\mathbb{E}\left[\ln\left[\mathbb{P}(\mathrm{SINR}_{jk}^{\mathrm{UL}} > \tau^{\mathrm{UL}})\right]\right] \overset{(a)}{=} \mathbb{E}\left[\ln\left[\mathbb{P}\left(g(y,0) > \frac{\tau^{\mathrm{UL}} G\left(\mathcal{I}^{\mathrm{UL}} + \mathcal{I}_{\mathrm{SI}}^{\mathrm{UL}} + \sigma^2\right)}{\min\{\rho_k G^{\epsilon} R_k^{\epsilon\alpha}, P_{\max}\} R_k^{-\alpha}}\right)\right]\right]$$

$$\overset{(b)}{=} -\tau^{\mathrm{UL}} G\, \mathbb{E}_{\mathbf{R}} \left[\frac{\mathbb{E}\left[\mathcal{I}^{\mathrm{UL}}\right] + \mathbb{E}\left[\mathcal{I}_{\mathrm{SI}}^{\mathrm{UL}}\right] + \sigma^2}{\min\{\rho_k G^{\epsilon} R_k^{\epsilon\alpha}, P_{\max}\} R_k^{-\alpha}} \right] \tag{6.23}$$

where (a) follows from (6.15) and (b) follows from the Rayleigh fading assumption. The mean of $\mathcal{I}^{\mathrm{UL}}$ and $\mathcal{I}_{\mathrm{SI}}^{\mathrm{UL}}$ are presented in the following lemma.

Lemma 6.6. *(Mean of uplink interference)* The mean interference power received at a typical BS belonging to the k-th tier is given by

$$\mathbb{E}\left[\mathcal{I}^{\mathrm{UL}}\right] = \sum_{i=1}^{K} 2\pi\lambda_i \left(\frac{\mathcal{K}_1(d_b, \alpha_b, \frac{\lambda_i}{\beta_b})}{G_b} P_i + \frac{\mathcal{U}_{ik}^{\frac{2-\alpha}{\alpha}} \mathcal{K}_2(i)}{G(\alpha-2)} \rho_i \right) \tag{6.24}$$

and the mean of SI is $\mathbb{E}\left[\mathcal{I}_{\mathrm{SI}}^{\mathrm{UL}}\right] = \sigma_{b_k} P_k$, where

$$\begin{aligned} \mathcal{K}_1(d, \alpha, \Lambda) &= \frac{d^{2-\alpha}}{\alpha-2} - \frac{1}{2} (\pi\Lambda)^{\frac{\alpha-2}{2}} \Gamma\left[\frac{2-\alpha}{2}, \pi\Lambda d^2\right] \\ &\overset{\substack{(2<\alpha<4)\\(d\to 0)}}{=} -\frac{1}{2} (\pi\Lambda)^{\frac{\alpha-2}{2}} \Gamma\left[\frac{2-\alpha}{2}\right] \end{aligned} \tag{6.25}$$

and

$$\begin{aligned} \mathcal{K}_2(i) = (\pi\Lambda_i^{\mathrm{UL}})^{\frac{\alpha(1-\epsilon)-2}{2}} &\Gamma\left[\frac{4-\alpha(1-\epsilon)}{2}, \pi\Lambda_i^{\mathrm{UL}} d_{\circ}^2, \pi\Lambda_i^{\mathrm{UL}} \left(\frac{P_{\max}}{\rho_i G^{\epsilon}}\right)^{\frac{2}{\epsilon\alpha}}\right] \\ &+ (\pi\Lambda_i^{\mathrm{UL}})^{\frac{\alpha-2}{2}} \frac{P_{\max}}{\rho_i G^{\epsilon}} \Gamma\left[\frac{4-\alpha}{2}, \pi\Lambda_i^{\mathrm{UL}} \left(\frac{P_{\max}}{\rho_i G^{\epsilon}}\right)^{\frac{2}{\epsilon\alpha}}\right] \\ \overset{(P_{\max}\to\infty)}{=} (\pi\Lambda_i^{\mathrm{UL}})^{\frac{\alpha(1-\epsilon)-2}{2}} &\Gamma\left[\frac{4-\alpha(1-\epsilon)}{2}, \pi\Lambda_i^{\mathrm{UL}} d_{\circ}^2\right]. \end{aligned} \tag{6.26}$$

in which $d_{\circ}$ is the minimum distance between users and BSs [91].

Proof. See **Appendix E.2.1**. □

Note that in (6.26), the first term represents interference from users that are able to perform channel inversion power control without exceeding the power budget where

the second term represents the interference from users who are transmitting with the maximum power $P_{\max}$.

Next, similar to uplink, the rate coverage for downlink can be obtained as follows:

$$\mathbb{E}\left[\ln\left[\mathbb{P}(\mathrm{SINR}_{jk}^{\mathrm{DL}} > \tau^{\mathrm{DL}})\right]\right] = -\tau^{\mathrm{DL}} G\, \mathbb{E}_{\mathbf{R}}\left[\frac{\mathbb{E}\left[\mathcal{I}^{\mathrm{DL}}\right] + \mathbb{E}\left[\mathcal{I}_{\mathrm{SI}}^{\mathrm{DL}}\right] + \sigma^2}{P_j R_j^{-\alpha}}\right] \tag{6.27}$$

where the mean of $\mathcal{I}^{\mathrm{DL}}$ and $\mathcal{I}_{\mathrm{SI}}^{\mathrm{DL}}$ are presented in the following lemma.

Lemma 6.7. *(Mean of downlink interference)* The mean interference power received at a typical user served in downlink by the j-th tier and in uplink by the k-th tier is given by

$$\mathbb{E}\left[\mathcal{I}^{\mathrm{DL}}\right] = \sum_{i=1}^{K} 2\pi\lambda_i \left(\frac{\mathcal{D}_{ji}^{\frac{2-\alpha}{\alpha}} R_j^{2-\alpha}}{G(\alpha-2)} P_i + \frac{\mathcal{K}_1(d_u, \alpha_u, \Lambda_i^{\mathrm{UL}})}{G_u}\mathbb{E}\left[\Gamma_i\right]\right) \tag{6.28}$$

where $\mathbb{E}\left[\Gamma_i\right]$ is given in **Lemma 6.5** and the mean of SI power is

$$\mathbb{E}\left[\mathcal{I}_{\mathrm{SI}}^{\mathrm{DL}}\right] = \frac{\sigma_u \epsilon\alpha\rho_k G^{\epsilon}}{2(\pi\Lambda_k^{\mathrm{UL}})^{\frac{\epsilon\alpha}{2}}}\, \gamma\left[\frac{\epsilon\alpha}{2}, \pi\Lambda_k^{\mathrm{UL}}\left(\frac{P_{\max}}{\rho_k G^{\epsilon}}\right)^{\frac{2}{\epsilon\alpha}}\right]. \tag{6.29}$$

Proof. See **Appendix E.2.2**. □

The following theorem presents closed-form expressions for the mean rate coverage in (6.21) for a generic FD link when a user associates with the same tier j with probability ψ_{jj} and when a user associates with tier j for downlink transmission and tier k for uplink transmission with probability ψ_{jk}.

Theorem 6.1. *(Mean of logarithm of rate coverage)* The mean rate utility of the FD

network model described above is given by

$$\bar{\mathcal{R}} = \bar{\mathcal{R}}_{\circ} - \sum_{j=1}^{K}\sum_{k=1}^{K}\psi_{jk}G\left(\frac{\tau^{\mathrm{DL}}}{P_j}\left(\frac{\mathcal{A}_1(j)}{\pi\Lambda_j^{\mathrm{DL}}}+\frac{\Gamma\left[\frac{2+\alpha}{2}\right]\mathcal{A}_2}{(\pi\Lambda_j^{\mathrm{DL}})^{\frac{\alpha}{2}}}+\frac{\sigma_u\mathbb{E}[\Gamma_k]}{\mathcal{K}_3(j,k)}\right)+\frac{\tau^{\mathrm{UL}}}{\rho_k}\frac{\sigma_{b_kP_k}+\mathcal{A}_3(k)}{G^{\epsilon}(\pi\Lambda_k^{\mathrm{UL}})^{\frac{\alpha}{2}}}\mathcal{K}_4(k)\right) \tag{6.30}$$

where $\bar{\mathcal{R}}_{\circ} = \ln\mathcal{R}_{\circ}^{\mathrm{DL}} + \ln\mathcal{R}_{\circ}^{\mathrm{UL}}$ and

$$\begin{aligned}\mathcal{A}_1(j) &= \sum_{i=1}^{K}\frac{2\pi\lambda_i\mathcal{D}_{ji}^{\frac{2-\alpha}{\alpha}}}{G(\alpha-2)}P_i, \quad \mathcal{A}_2 = \sigma^2+\sum_{i=1}^{K}\frac{2\pi\lambda_i\mathcal{K}_1(d_u,\alpha_u,\Lambda_i^{\mathrm{UL}})}{G_u}\mathbb{E}\left[\Gamma_i\right]\\ \mathcal{A}_3(k) &= \sigma^2+\sum_{i=1}^{K}2\pi\lambda_i\left(\frac{\mathcal{K}_1(d_b,\alpha_b,\frac{\lambda_i}{\beta_b})}{G_b}P_i+\frac{\mathcal{U}_{ik}^{\frac{2-\alpha}{\alpha}}\mathcal{K}_2(i)}{G(\alpha-2)}\rho_i\right).\end{aligned} \tag{6.31}$$

and

$$\mathcal{K}_3(j,k) = \begin{cases}\frac{1}{\Gamma\left[\frac{2+\alpha}{2}\right]}\left(\pi\sum_{i=1}^{K}\max\left\{\mathcal{D}_{ji},\mathcal{U}_{ji}\right\}^{\frac{2}{\alpha}}\lambda_i\right)^{\frac{\alpha}{2}}, & j=k\\ \left(\sum_{l=k}^{j-1}\frac{-1}{\Omega_l}\mathcal{H}_{jl}\left[1,1;\alpha\right]\right)^{-1}\sum_{l=k}^{j-1}\mathcal{H}_{jl}\left[\mu_l,\mu_{l+1};0\right], & k<j\end{cases} \tag{6.32}$$

$$\begin{aligned}\mathcal{K}_4(k) &= (\pi\Lambda_k^{\mathrm{UL}})^{\frac{\epsilon\alpha}{2}}\gamma\left[\frac{2+\alpha(1-\epsilon)}{2},\pi\Lambda_k^{\mathrm{UL}}\left(\frac{P_{\max}}{\rho_kG^{\epsilon}}\right)^{\frac{2}{\epsilon\alpha}}\right]\\ &\quad+\frac{\rho_kG^{\epsilon}}{P_{\max}}\Gamma\left[\frac{2+\alpha}{2},\pi\Lambda_k^{\mathrm{UL}}\left(\frac{P_{\max}}{\rho_kG^{\epsilon}}\right)^{\frac{2}{\epsilon\alpha}}\right]\\ &\overset{(P_{\max}\to\infty)}{=}(\pi\Lambda_k^{\mathrm{UL}})^{\frac{\epsilon\alpha}{2}}\Gamma\left[\frac{2+\alpha(1-\epsilon)}{2}\right].\end{aligned} \tag{6.33}$$

Proof. See **Appendix E.3**. □

Note that in (6.33), the first term represents the mean of the inverse of the useful signal power received at a typical BS from a user being served that is able to perform channel inversion power control without exceeding the power budget. On the other hand, the second term represents the mean of the inverse of the useful signal power received from a user that is transmitting with the maximum power $P_{\max}$.

6.5.5 Special Cases

Using the lemmas derived above and **Theorem 6.1**, the performance of (i) a network tier that consists only of legacy HD BSs with uplink transmissions and (ii) a typical legacy HD user with downlink transmissions is presented in the following two corollaries where the proofs follow directly from (6.30). It is worth mentioning that if SI is added at FD BSs and FD users, the expressions for mean rate in **Corollaries 6.1** and **6.2**, respectively, will be equivalent to the mean rate of uplink and downlink transmissions in an FD network.

Corollary 6.1. *(Mean rate of legacy uplink transmissions)* The mean rate by the k-th tier that consists only of HD BSs in an FD cellular network to its users is given by

$$\ln \mathcal{R}_k^{\mathrm{UL}} = \ln \mathcal{R}_\circ^{\mathrm{UL}} - \frac{\tau^{\mathrm{UL}}}{\rho_k} G^{1-\epsilon} \left(\sigma^2 + \sum_{i=1}^{K} 2\pi\lambda_i \left(\frac{\mathcal{K}_1(d_b, \alpha_b, \frac{\lambda_i}{\beta_b}) \mathbf{1}\{i \neq k\}}{G_b} P_i + \frac{\mathcal{U}_{ik}^{\frac{2-\alpha}{\alpha}} \mathcal{K}_2(i)}{G(\alpha-2)} \rho_i \right) \right) \frac{\mathcal{K}_4(k)}{(\pi\Lambda_k^{\mathrm{UL}})^{\frac{\alpha}{2}}}. \tag{6.34}$$

Corollary 6.2. *(Mean rate of legacy downlink transmissions)* The mean rate coverage

offered by an FD network to a legacy HD user served by the j-th tier is given by

$$\ln \mathcal{R}_j^{\mathrm{DL}} = \ln \mathcal{R}_\circ^{\mathrm{DL}} - \frac{\tau^{\mathrm{DL}}}{P_j} G \left(\frac{\Gamma\left[\frac{2+\alpha}{2}\right]}{(\pi \Lambda_j^{\mathrm{DL}})^{\frac{\alpha}{2}}} \sigma^2 + \sum_{i=1}^{K} 2\pi\lambda_i \left(\frac{\mathcal{D}_{ji}^{\frac{2-\alpha}{\alpha}}}{\pi \Lambda_j^{\mathrm{DL}} G(\alpha-2)} P_i + \frac{\Gamma\left[\frac{2+\alpha}{2}\right] \mathcal{K}_1(d_u, \alpha_u, \Lambda_i^{\mathrm{UL}})}{G_u (\pi \Lambda_j^{\mathrm{DL}})^{\frac{\alpha}{2}}} \mathbb{E}\left[\Gamma_i\right] \right) \right). \tag{6.35}$$

In addition, the performance of HD uplink networks and HD downlink networks can be obtained as presented in the following corollaries where the proofs follow directly from (6.30).

Corollary 6.3. *(Half-duplex uplink networks)* The mean rate of HD uplink networks with weighted path-loss cell association is given by

$$\bar{\mathcal{R}} = \ln \mathcal{R}_\circ^{\mathrm{UL}} - \sum_{k=1}^{K} A_k^{\mathrm{UL}} \frac{\tau^{\mathrm{UL}}}{\rho_k} G^{1-\epsilon} \left(\sigma^2 + \sum_{i=1}^{K} \frac{2\pi\lambda_i \, \mathcal{U}_{ik}^{\frac{2-\alpha}{\alpha}} \mathcal{K}_2(i)}{G(\alpha-2)} \rho_i \right) \frac{\mathcal{K}_4(k)}{(\pi \Lambda_k^{\mathrm{UL}})^{\frac{\alpha}{2}}} \tag{6.36}$$

$$\overset{\substack{(P_{\max}\to\infty)\\(\sigma^2=0)}}{=} \ln \mathcal{R}_\circ^{\mathrm{UL}} - \sum_{k=1}^{K} A_k^{\mathrm{UL}} \frac{\tau^{\mathrm{UL}}}{\rho_k} \Gamma\left[\frac{2+\alpha(1-\epsilon)}{2}\right] \Gamma\left[\frac{4-\alpha(1-\epsilon)}{2}\right] \sum_{i=1}^{K} \frac{2\rho_i \, \mathcal{U}_{ik}^{\frac{2-\alpha}{\alpha}}}{G^{\epsilon}(\alpha-2)} A_i^{\mathrm{UL}} \tag{6.37}$$

$$\overset{\substack{(U_i=\rho)\\(P_{\max}\to\infty)\\(\sigma^2=0)}}{=} \ln \mathcal{R}_\circ^{\mathrm{UL}} - \frac{2\tau^{\mathrm{UL}}}{G^{\epsilon}(\alpha-2)} \Gamma\left[\frac{2+\alpha(1-\epsilon)}{2}\right] \Gamma\left[\frac{4-\alpha(1-\epsilon)}{2}\right]. \tag{6.38}$$

Corollary 6.4. *(Half-duplex downlink networks)* The mean rate of HD downlink networks with weighted path-loss cell association is given by

$$\bar{\mathcal{R}} = \ln \mathcal{R}_\circ^{\mathrm{DL}} - \sum_{j=1}^{K} A_j^{\mathrm{DL}} \frac{\tau^{\mathrm{DL}}}{P_j} G \left(\frac{\Gamma\left[\frac{2+\alpha}{2}\right]}{(\pi \Lambda_j^{\mathrm{DL}})^{\frac{\alpha}{2}}} \sigma^2 + \sum_{i=1}^{K} \frac{2\pi\lambda_i \mathcal{D}_{ji}^{\frac{2-\alpha}{\alpha}}}{\pi \Lambda_j^{\mathrm{DL}} G(\alpha-2)} P_i \right) \tag{6.39}$$

$$\overset{(\sigma^2=0)}{=} \ln \mathcal{R}_{\circ}^{\mathrm{DL}} - \sum_{j=1}^{K} A_j^{\mathrm{DL}} \frac{\tau^{\mathrm{DL}}}{P_j} \sum_{i=1}^{K} \frac{2P_i \, \mathcal{D}_{ij}}{\alpha - 2} A_i^{\mathrm{DL}} \tag{6.40}$$

$$\overset{\substack{(D_i=P_i^{-1}) \\ (\sigma^2=0)}}{=} \ln \mathcal{R}_{\circ}^{\mathrm{DL}} - \frac{2\tau^{\mathrm{DL}}}{\alpha - 2}. \tag{6.41}$$

The results presented in (6.37) and (6.40) are consistent with the previous results in [79] on cell association in multi-tier HD cellular networks. Furthermore, from (6.38) and (6.41), it can be seen that the performance of an interference-limited network is independent of the spatial density, receiver sensitivity, and transmit power of BSs, which is consistent with the results in existing literature [34, 42, 78, 79, 94].

In addition, by comparing the results in **Corollaries 6.1** and **6.2** with those in **Corollaries 6.3** and **6.4**, respectively, it can be seen that the mean rates of both uplink and downlink transmissions in FD networks are lower than those in HD networks. This degradation is due to the additional interference resulting from FD transmissions and SI. It can be seen that for uplink transmissions, downlink-to-uplink interference can be reduced by increasing the isolation of BSs. This can achieved by increasing SIC capability of BSs or using directional antennas where both vertical and horizontal patterns are designed such that the BSs are not in the main-lobe of each other. For downlink, the effect of uplink-to-downlink interference can be seen to be less severe because of the low transmit power of users compared to that of BSs.

Furthermore, the performance of FD networks with CCA and FD networks with 3NT are presented in the following two corollaries where the proofs follow directly from (6.30).

Corollary 6.5. *(Coupled cell association)* The mean rate utility of FD networks with

CCA is given by

$$\bar{\mathcal{R}} = \bar{\mathcal{R}}_{\circ} - \sum_{k=1}^{K} A_k^{\mathrm{DL}} \left(\frac{\tau^{\mathrm{DL}}}{P_k} G \left(\frac{\mathcal{A}_1(k)}{\pi \Lambda_k^{\mathrm{DL}}} + \Gamma\left[\frac{2+\alpha}{2}\right] \frac{\sigma_u \mathbb{E}[\Gamma_k] + \mathcal{A}_2}{(\pi \Lambda_k^{\mathrm{DL}})^{\frac{\alpha}{2}}} \right) + \frac{\tau^{\mathrm{UL}}}{\rho_k} G^{1-\epsilon} \frac{\sigma_{b_k} P_k + \mathcal{A}_3(k)}{(\pi \Lambda_k^{\mathrm{DL}})^{\frac{\alpha}{2}}} \mathcal{K}_4(k) \right). \tag{6.42}$$

Corollary 6.6. *(3-node topology)* The mean rate of FD networks with 3NT for a user served by j-th tier in downlink in given by (6.35) where that for a user served by k-th tier in uplink is given by

$$\ln \mathcal{R}_k^{\mathrm{UL}} = \ln \mathcal{R}_{\circ}^{\mathrm{UL}} - \frac{\tau^{\mathrm{UL}}}{\rho_k} G^{1-\epsilon} \left(\sigma^2 + \sigma_{b_k} P_k + \sum_{i=1}^{K} 2\pi\lambda_i \left(\frac{\mathcal{K}_1(d_b, \alpha_b, \frac{\lambda_i}{\beta_b})}{G_b} P_i + \frac{\mathcal{U}_{ik}^{\frac{2-\alpha}{\alpha}} \mathcal{K}_2(i)}{G(\alpha-2)} \rho_i \right) \right) \frac{\mathcal{K}_4(k)}{(\pi \Lambda_k^{\mathrm{UL}})^{\frac{\alpha}{2}}}. \tag{6.43}$$

Proof. The proof follows from **Corollaries 6.1** and **6.2** while considering SI affecting uplink transmissions at BSs. □

6.6 Rate Maximization in FD Networks by Optimal Cell Association

In this section, for optimal cell association, I derive closed-form expressions for the weighting factors that maximize the overall mean rate of FD cellular networks given in **Theorem 6.1**. For analytical tractability, I assume that (i) all BSs have the same receiver sensitivity (i.e., $\rho_k = \rho$), (ii) there is no constraint on the maximum

transmit power of users (i.e., $P_{\max} \to \infty$), and (iii) SI at BSs is modeled as noise such that $\sigma_{b_k} P_k = \sigma_b$. The last assumption implies that the SIC capability of a BS is proportional to its transmit power (i.e., $\sigma_{b_k} \propto \frac{1}{P_k}$), that is, the cancellation capability of BSs with higher transmit power such as macrocell BSs is better than that of BSs with lower transmit power such as picocell or femtocell BSs. Following a similar procedure as in [79], I first derive the optimal effective spatial density $\Lambda_k^{*\mathrm{UL}}$ and $\Lambda_j^{*\mathrm{DL}}$, then the optimal weighting factors is retrieved such that $U_k^* \leftarrow a_1(\Lambda_k^{*\mathrm{UL}})^{\frac{\alpha}{2}}$ and $D_j^* \leftarrow a_2(\Lambda_j^{*\mathrm{DL}})^{\frac{\alpha}{2}}$ which satisfy $\sum_{j=1}^{K} \frac{\lambda_j}{\Lambda_j^{*\mathrm{DL}}} = 1$ and $\sum_{k=1}^{K} \frac{\lambda_k}{\Lambda_k^{*\mathrm{UL}}} = 1$ for any positive constants a_1 and a_2 (cf. **Lemma 6.2**).

After some mathematical manipulations, maximizing (6.30) is equivalent to solving the following set of concave optimization sub-problem simultaneously:

$$\text{P1:} \min_{\Lambda_j^{\mathrm{DL}}, \Lambda_j^{\mathrm{UL}}} \sum_{j=1}^{K} \frac{c_1 \lambda_j}{P_j (\Lambda_j^{\mathrm{DL}})^{\frac{2+\alpha}{2}}} \sum_{i=1}^{K} \frac{P_i \lambda_i}{(\Lambda_i^{\mathrm{DL}})^{\frac{2-\alpha}{2}}} + \sum_{j=1}^{K} \frac{c_2 \lambda_j}{P_j (\Lambda_j^{\mathrm{DL}})^{\frac{2+\alpha}{2}}} \sum_{i=1}^{K} \frac{\rho_i \lambda_i \mathcal{K}_1(d_u, \alpha_u, \Lambda_i^{\mathrm{UL}})}{(\Lambda_i^{\mathrm{UL}})^{\frac{\epsilon\alpha}{2}}}$$

$$\text{P2:} \min_{\Lambda_j^{\mathrm{DL}}, \Lambda_j^{\mathrm{UL}}} \sum_{j=1}^{K} \frac{c_3 \lambda_j}{\rho_j (\Lambda_j^{\mathrm{UL}})^{\frac{2+\alpha}{2}}} \sum_{i=1}^{K} \rho_i \lambda_i \left(\Lambda_i^{\mathrm{UL}}\right)^{\frac{\epsilon\alpha}{2}} + \sum_{j=1}^{K} \frac{c_4 \lambda_j}{P_j (\Lambda_j^{\mathrm{DL}})^{\frac{2+\alpha}{2}}} \sum_{i=1}^{K} \frac{\rho_i \lambda_i}{(\Lambda_i^{\mathrm{UL}})^{\frac{2+\epsilon\alpha}{2}}}$$

$$\text{subject to} \quad \sum_{j=1}^{K} \frac{\lambda_j}{\Lambda_j^{\mathrm{DL}}} = 1, \quad \sum_{j=1}^{K} \frac{\lambda_j}{\Lambda_j^{\mathrm{UL}}} = 1, \quad \text{and} \quad \Lambda_j^{\mathrm{DL}}, \Lambda_j^{\mathrm{UL}} \geq 0, \quad \forall j$$

where c_i is an arbitrary positive constant for $i \in \{1, 2, 3, 4\}$.

Using Lagrangian relaxation and taking the first order partial derivatives with respect to Λ_j^{DL} and Λ_j^{UL}, the optimal cell association probability can be obtained as follows:

$$\Lambda_j^{*\mathrm{DL}} = P_j^{-\frac{2}{\alpha}} \sum_{i=1}^{K} P_i^{\frac{2}{\alpha}} \lambda_i \quad \text{and} \quad \Lambda_j^{*\mathrm{UL}} = \sum_{i=1}^{K} \lambda_i \tag{6.44}$$

which are equivalent to $D_j^* = \frac{D}{P_j}$ and $U_j^* = U$ for arbitrary positive constants D and U. This result is presented in the following theorem.

Theorem 6.2. *(Optimal cell association in multi-tier FD networks)* For an FD network, the mean transmission rate is maximized when cell association is based on maximum received power in downlink and on minimum distance in uplink.

It is worth mentioning that the result in **Theorem 6.2** shows the importance of DCA in FD cellular networks in order to maximize the overall mean rate of the network. The reason that a user prefers to be served based on the maximum received SINR for downlink and the minimum distance for uplink can be explained as follows. From the downlink perspective: (i) the received signal power at the user from her serving BS is maximized, (ii) the received interference power at the user from other BSs is minimized, and (iii) the SI power at the user is minimized when transmitting to the nearest BS in uplink. From the uplink perspective: (i) the received signal power from the user at her serving BS is maximized, (ii) the received interference power from other users at the serving BS is minimized when all users transmit with the minimum power, and (iii) since all BSs transmit with fixed power, the network tier of the serving BS for downlink (or downlink weighting factors) has no effect on the mean uplink rate. The result above also shows the superiority of DCA compared to CCA in the FD network under consideration. That is, as shown in **Theorem 6.1**, two different association criteria are required for uplink and downlink cell association to maximize the mean rate of FD networks. Clearly, this is possible only with DCA but not possible in general under any CCA criterion where the users are forced to associate with the same BS for both uplink and downlink. This result is also intuitive since CCA is a special case of DCA implying that the maximum performance of CCA can be always achieved by DCA.

6.7 Numerical Results and Discussions

6.7.1 System Parameters

I use the results obtained above in closed-form to evaluate system performance in different scenarios. I consider the following cases: (i) FD networks with both CCA and DCA, (ii) FD networks with 3NT, (iii) HD downlink networks (i.e., only downlink transmissions), (iv) HD uplink networks (i.e., only uplink transmissions), (v) legacy downlink transmissions (i.e., HD users with downlink transmissions in an FD network), and (vi) legacy uplink transmissions (i.e., HD BSs with uplink transmissions in an FD network). For simulation and numerical evaluation, unless otherwise stated, I consider a two-tier network with spatial densities $\lambda_2 = 4\lambda_1$. The transmit powers of BSs are $\{P_1, P_2\} = \{37, 33\}$ dBm and the maximum transmit power of users is $P_{\max} = 23$ dBm. The path-loss exponents are $\{\alpha, \alpha_b, \alpha_u\} = \{4, 3.7, 4\}$, path-loss constants are $\{G, G_b, G_u\} = \{0, 30, 0\}$ dB, and the minimum distances for the pair correlation functions are $\{d_\circ, d_b, d_u\} = \{1, 40, 1\}$ m. For uplink transmissions, the power control factor is $\epsilon = 0.9$ and all BSs have the same receiver sensitivity $\rho_1 = \rho_2 = -40$ dBm. The SIC capabilities of BSs and users are $\{\frac{1}{\sigma_{b_k}}, \frac{1}{\sigma_u}\} = \{70, 70\}$ dB and the noise power is $\sigma = -104$ dBm. For the evaluation of mean rate utility, SINR thresholds τ^{DL} and τ^{UL} are set to 0, i.e., $\mathcal{R}_\circ^{\mathrm{DL}} = \mathcal{R}_\circ^{\mathrm{UL}} = \ln(2)$ nats/sec/Hz.

6.7.2 Validation of Analytical Results

I validate the expressions derived in **Lemmas 6.6** and **6.7** for the mean interference received at a BS and a user, respectively. These two expressions are the keys to deriving all the following results including **Theorem 6.1** and they include all assumptions made throughout the analysis of the mean transmission rate. The curves in Figures

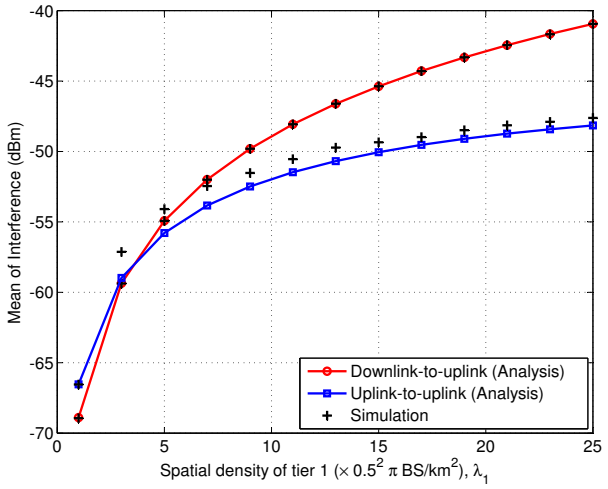

Figure 6.2: Analysis (**Lemmas 6.6** vs. simulation: Mean of interference resulting from downlink and uplink transmissions at a typical BS. Network parameters are $K = 2$, $\lambda_2 = 4\lambda_1$, $\{P_1, P_2\} = \{37, 33\}$ dBm, and $\rho_1 = \rho_2 = -40$ dBm.

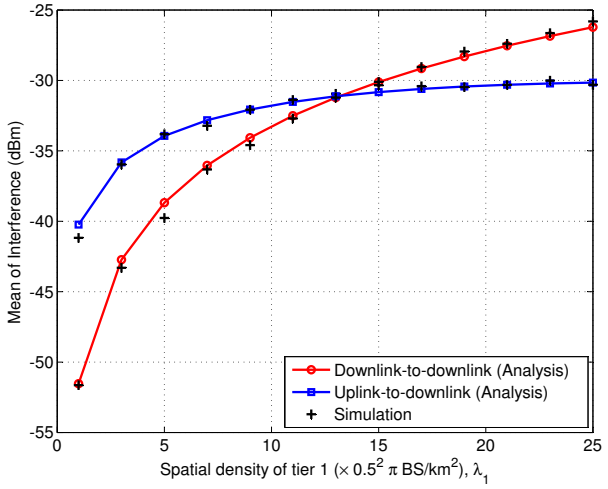

Figure 6.3: Analysis (**Lemmas 6.7** vs. simulation: Mean of interference resulting from downlink and uplink transmissions at a typical user. Network parameters are $K = 2$, $\lambda_2 = 4\lambda_1$, $\{P_1, P_2\} = \{37, 33\}$ dBm, and $\rho_1 = \rho_2 = -40$ dBm.

6.2 and 6.3 compare the results obtained from simulations and analysis as a function of the spatial density of tier 1. For Monte Carlo simulations, the locations of the BSs simulated as independent PPPs over a 10×10 km^2 area with a typical user or

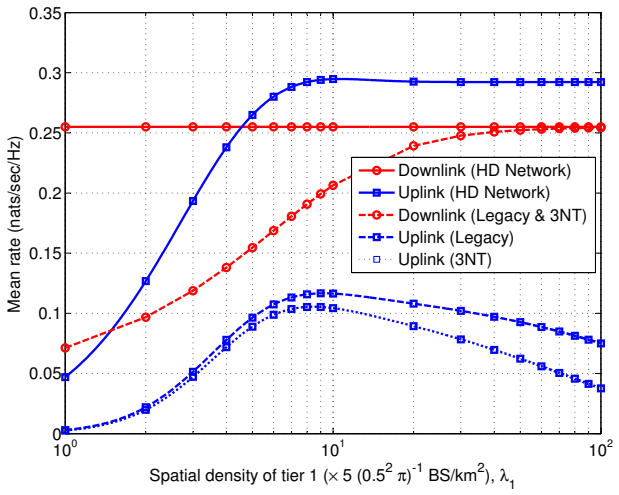

Figure 6.4: Mean rate (in nats/sec/Hz) of downlink and uplink transmissions vs. spatial density of tier 1 (in BS/km^2). Network parameters are $K = 2$, $\lambda_2 = 4\lambda_1$, $\{P_1, P_2\} = \{37, 33\}$ dBm, and $\rho_1 = \rho_2 = -40$ dBm.

BS at the origin. To simulate the active users that are causing uplink-to-uplink and uplink-to-downlink interference, the users are first dropped as a PPP with high spatial density, then the users associate with BSs based on the defined association criteria for uplink. Then, each BS randomly selects one user for uplink transmission. Hence, **Assumption 6.2** is not retained in the simulation. The mean interference power for various links is averaged over $10,000$ iterations. The results in Figures 6.2 and 6.3 validate the accuracy of the proposed approach to derive the mean interference and show that the assumptions made above have a minor effect on the accuracy of the proposed analytical model.

6.7.3 Effect of Spatial Density

Figures 6.4 and 6.5 show the effect of varying the density of BSs on the mean rate for three different networks: (i) HD downlink network, (ii) HD uplink network, and (iii) FD network including both legacy downlink and uplink transmissions, and (iv)

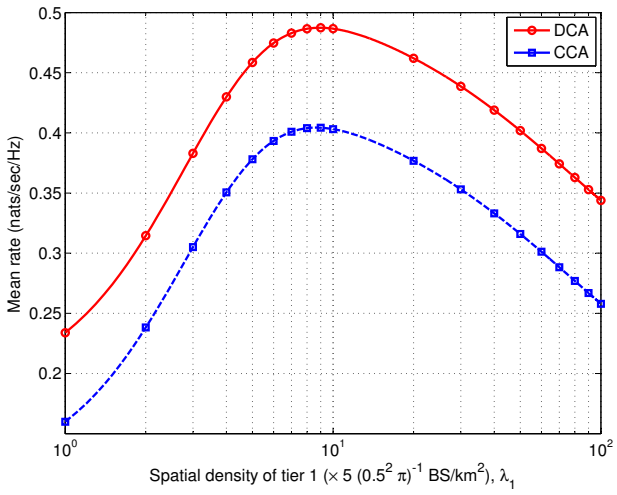

Figure 6.5: Mean rate (in nats/sec/Hz) of FD networks vs. spatial density of tier 1 (in BS/km^2). Network parameters are $K = 2$, $\lambda_2 = 4\lambda_1$, $\{P_1, P_2\} = \{37, 33\}$ dBm, and $\rho_1 = \rho_2 = -40$ dBm. Results are shown for both DCA and CCA in FD networks.

3NT. For HD downlink networks (i.e., **Corollary 6.4**) in Figure 6.4, the mean rate of downlink transmissions is *almost* independent of the density of BSs. This can be explained as increasing λ results in increasing the power of both the useful signal and interference and the SINR remains unchanged. For HD uplink networks (i.e., **Corollary 6.3**), the performance results can be explained as follows. In sparse networks with low density, the distances between users and their serving BSs become large and the users transmit with their maximum power with high probability. Consequently, the useful received signal power decreases and the interference power is increased at the serving BS. Increasing the BS density improves the mean rate by making users closer to their serving BSs which in turn increases their ability to perform channel inversion without exceeding the maximum power budget. This increases the useful signal power and decreases interference power. With a very high BS density, the network becomes interference-limited and *almost* all users are able to invert their channel towards the serving BS, hence, the mean rate becomes independent of the

spatial density of BSs.

Figure 6.4 shows that increasing the density of FD networks has two different effects on the mean rate of legacy transmissions. For legacy downlink transmissions (i.e., **Corollary 6.2**), the mean rate is lower compared to HD downlink networks where the difference is due to the extra interference resulting from uplink transmissions sharing the same spectrum in the FD network. However, increasing the density of BSs (i) decreases the transmit power of users, hence, decreases uplink-to-downlink interference, (ii) increases the useful signal power which is counteracted by the increase in downlink-to-downlink interference. Overall, this improves the mean rate of legacy downlink transmissions and the performance approaches that of HD downlink networks in very dense networks. On the other hand, the mean rate of legacy uplink BSs (i.e., **Corollary 6.1**) degrades with increasing spatial density of BSs. Compared to HD uplink networks, the difference is due to the extra interference resulting from downlink transmissions. With increasing spatial density, the BSs become closer to each other which increases the downlink-to-uplink interference power received at all BSs. At the same time, the useful signal power received at any BS is upper bounded by ρ. Therefore, the SINR becomes very low and the mean uplink rate approaches zero with increasing BS density. A similar behavior is evident for 3NT as shown in Figure 6.4. The mean downlink rate is identical to that of legacy downlink because both rates are evaluated at an HD user. On the other hand, the difference between the mean uplink rate in 3NT with FD BS and legacy uplink with HD BS is due to the SI experienced at the FD BS in 3NT.

Figure 6.5 elaborates more on the effect of spatial density in FD networks by showing the mean rate of a generic FD link for different cell association criteria (i.e., **Theorem 6.1** and **Corollary 6.5**). Overall, it can be seen that the spatial density

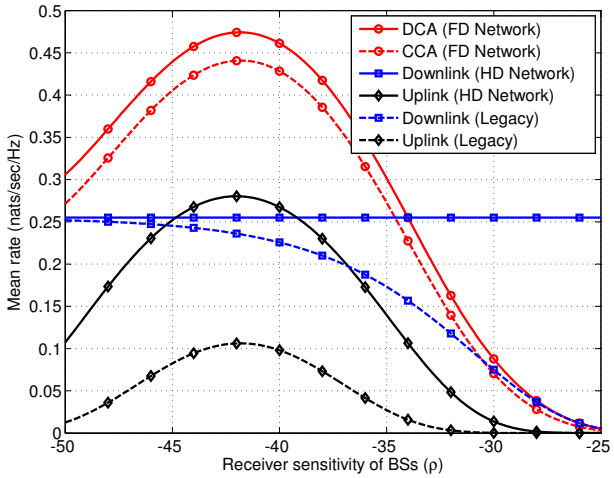

Figure 6.6: Mean rate (in nats/sec/Hz) vs. the sensitivity of BS receivers ρ (in dBm). Network parameters are $K = 2$, $\lambda_2 = 4\lambda_1$, $\{P_1, P_2\} = \{37, 33\}$ dBm, and $\rho_1 = \rho_2$. Results are shown for both CCA and DCA in FD networks, legacy downlink and uplink users, and HD downlink and HD uplink networks.

should be adjusted to balance the trade-off between the rates of downlink and uplink transmissions in FD networks. As shown in Figure 6.4, in dense FD networks, uplink transmissions become more susceptible to high downlink-to-uplink interference. On the other hand, low spatial density of BSs degrades the performance of both downlink and uplink transmissions, respectively, due to high uplink-to-downlink interference and the maximum power budget constraint. Therefore, as shown in Figure 6.5, as the spatial density of BSs increases, the overall mean rate of the FD network increases up to a maximum value due to the improvement in both downlink and uplink transmissions, then it starts to decrease due to the degradation in the mean uplink rate.

6.7.4 Effect of Power Control

Figure 6.6 shows the effect of varying ρ on the mean rate of different networks. In general, decreasing the sensitivity of the receiver (i.e., increasing ρ) increases the amount of transmit power required by each user to perform channel inversion towards the serving BS (i.e., **Lemma 6.5**). This, in turn, increases the power of useful signal, uplink-to-uplink interference, and uplink-to-downlink interference (cf., **Lemmas 6.6** and **6.7**). Hence, as shown in Figure 6.6, the mean rate of downlink transmissions in the FD network deteriorates with increasing ρ because of uplink-to-downlink interference compared to the HD downlink scenario. For uplink transmissions in both HD uplink and FD networks, the mean uplink transmission rate increases due to increased useful signal power. This happens up to a maximum value, then the rate starts to decrease because the transmit power of users becomes limited by the power budget $P_{\max}$. Overall, there exists an optimal value of ρ that maximizes the mean rate of FD networks and splits the performance into two regimes. That is, as ρ increases, the mean rate of FD networks increases up to a maximum value, then it starts to decrease. This behavior can be explained as follows. When ρ is very low (the left side of the optimal point), while downlink transmissions experience low interference from uplink transmissions, the interference at the BSs is very high compared to the useful signal power and thus the mean uplink transmission rate is almost 0. As ρ increases, the mean downlink transmission rate of downlink transmissions starts to degrade while the mean rate of uplink transmissions improves where this improvement dominates the overall mean rate performance. This happens until achieving the maximum mean rate. After this point, as ρ increases (the right side of the optimal point), the mean rates of both downlink and uplink transmissions start to fall. Hence, the overall mean rate of the FD network start to decrease. A similar behavior is observed in Figure 6.7

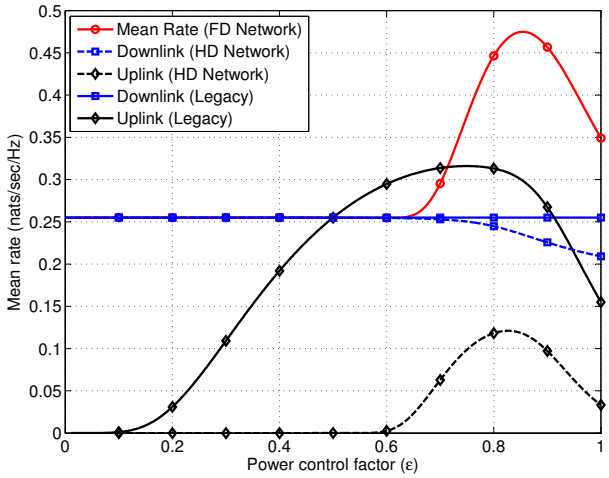

Figure 6.7: Mean rate (in nats/sec/Hz) vs. the power control factor ϵ. Network parameters are $K = 2$, $\lambda_2 = 4\lambda_1$, $\{P_1, P_2\} = \{37, 33\}$ dBm, and $\rho_1 = \rho_2 = -40$ dBm. Results are shown for FD networks, legacy downlink and uplink users, and HD downlink and HD uplink networks.

for varying the power control factor ϵ which can be justified using the same line of arguments as that for varying ρ. It is worth mentioning that Figures 6.5 and 6.6 show that DCA is always superior to CCA for all ranges of λ and ρ, which is in agreement with the analytical results in Section 6.6.

6.7.5 Effect of Weighting Factors

Figure 6.8 shows the mean rate of FD and HD downlink networks as a function of downlink weighting factors for different transmit power settings. For both networks, it can be clearly seen that the maximum mean rate is achieved when the ratio of the weighting factors is equal to the inverse of the transmit power ratio. For example, when $\frac{P_2}{P_1} = 0.2$ (i.e., $\{P_1, P_2\} = \{33, 26\}$ dBm), the rate of FD transmissions and HD downlink transmissions are maximized when $\frac{D_2}{D_1} = \frac{P_1}{P_2} = 5$. Similar remark can be made for different cases when the ratio $\frac{P_2}{P_1}$ is 1, 0.5, and 0.1. For these values of $\frac{P_2}{P_1}$,

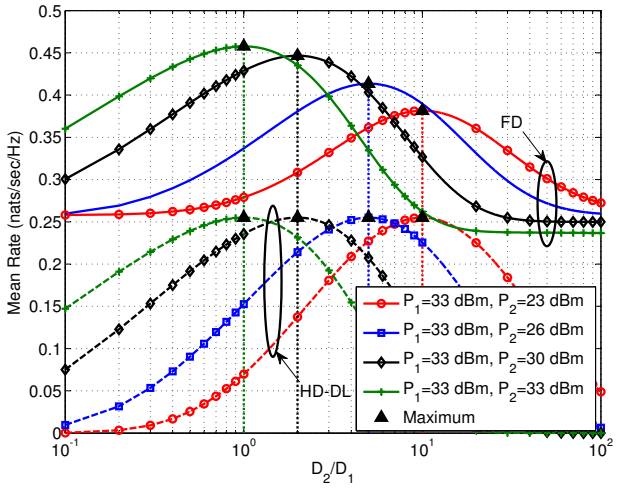

Figure 6.8: Mean rate (in nats/sec/Hz) vs. the ratio of downlink weighting factors $\frac{D_2}{D_1}$. Network parameters are $K = 2$, $\lambda_2 = 4\lambda_1$, $\{U_1, U_2\} = \{1, 1\}$, $\rho_1 = \rho_2 = -40$ dBm. Results are shown for FD, HD downlink, and HD uplink networks.

the rate is maximized when $\frac{D_2}{D_1}$ is set to 1, 2, and 10, respectively. This behavior is consistent with **Theorem 6.2** and can be explained as follows. For HD downlink networks, intuitively, the power of the useful signal at the user is maximized while the power of interference from other BSs is minimized when $D_j^{*\mathrm{HD}} = P_j^{-1}$. Consequently, both the SINR and mean rate are maximized. For FD networks, same argument holds for downlink transmissions as shown in **Corollary 6.2**. On the other hand, the mean uplink transmission rate in an FD network is independent of downlink weighting factors as shown in **Theorem 6.1** and **Corollary 6.1**. Hence, the mean rate of FD transmissions is maximized by maximizing the rate of downlink transmissions by setting $D_j^{*\mathrm{FD}} = P_j^{-1}$.

On the other hand, Figure 6.9 shows the mean rate of FD and HD uplink networks as a function of uplink weighting factors for different receiver sensitivity settings. In contrast to Figure 6.8, the maximum rate for both FD and HD networks is achieved when the ratio of the weighting factors is equal 1. This behavior is evident for different

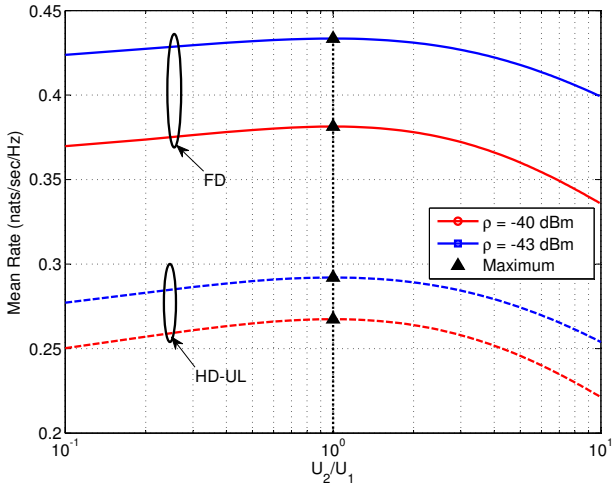

Figure 6.9: Mean rate (in nats/sec/Hz) vs. the ratio of uplink weighting factors $\frac{U_2}{U_1}$. Network parameters are $K = 2$, $\lambda_2 = 4\lambda_1$, $\{P_1, P_2\} = \{37, 33\}$ dBm, $\{D_1, D_2\} = \{\frac{1}{P_1}, \frac{1}{P_2}\}$, $\rho_1 = \rho_2$. Results are shown for FD, HD downlink, and HD uplink networks.

values of ρ and can be explained as follows. For HD uplink networks, when the users associate with their nearest BSs, the aggregate interference power is minimized as the users transmit with the minimum power required to perform channel inversion power control. In addition, the useful signal power is maximized as the probability of a user to perform channel inversion without exceeding $P_{\max}$ increases as the distance to the serving BS decreases. Therefore, both SINR and mean rate are maximum when $U_k^{*\mathrm{HD}} = U$ for some constant U. For FD networks, same argument holds for uplink transmissions as given in **Corollary 6.1**. For downlink transmissions in an FD network, uplink-to-downlink interference is minimized when all the users transmit with the minimum transmit power as given in **Theorem 6.1** and **Corollary 6.2**. Hence, the mean rate of FD transmissions is maximized by simultaneously maximizing the rate of uplink transmissions and minimizing the uplink-to-downlink interference where both are achieved by setting $U_k^{*\mathrm{FD}} = U$. Therefore, it is clear that the maximum rate offered by an FD network is achieved for $\frac{D_j}{D_k} = \frac{P_k}{P_j}$ and $\frac{U_j}{U_k} = 1$. In other words,

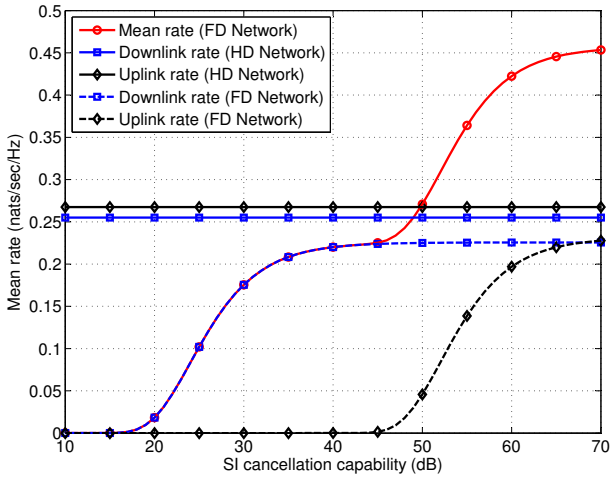

Figure 6.10: Mean rate (in nats/sec/Hz) vs. the SIC capability of BSs and users $\frac{1}{\sigma_{b_k}}$ and $\frac{1}{\sigma_u}$. Network parameters are $K = 2$, $\lambda_2 = 4\lambda_1$, $\{P_1, P_2\} = \{37, 33\}$ dBm, $\rho_1 = \rho_2 = -40$ dBm.

thanks to DCA, the mean rate can be maximized by simultaneously optimizing both downlink and uplink weighting factors which is not generally possible with CCA.

6.7.6 Effect of Imperfect Self-Interference Cancellation

Figure 6.10 shows the effect of SI on the performance of FD networks. It shows that the mean rates of downlink and uplink transmissions in FD networks are highly impacted with increasing σ_u and σ_b, respectively. It is clear that the effect of SI is more severe for uplink transmissions as it occurs at the FD BS where the transmit power is generally high compared to the power of the signal received from uplink user. Figure 6.10 also shows that, based on SIC capability of users and BSs, HD transmissions may be preferable to FD transmissions. Figure 6.11 shows the minimum required SIC capabilities of the users and BSs so that the rate offered by an FD network is higher than that of its HD counterpart. For example, the rate offered by an HD network is higher than that offered by an FD network when the SIC capabilities of

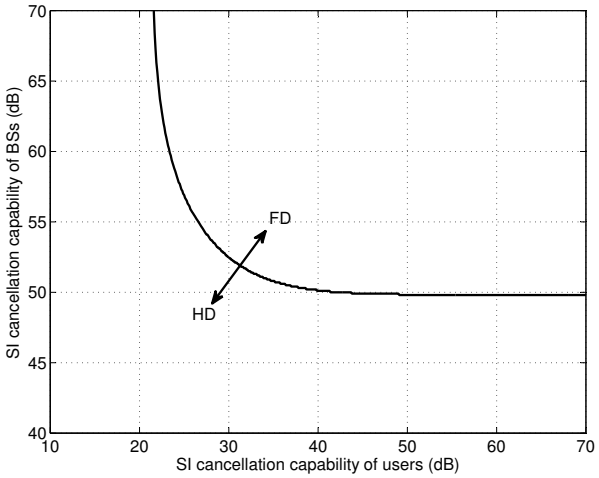

Figure 6.11: Minimum required SIC capability for FD networks vs. the SIC capability of BSs and users $\frac{1}{\sigma_{b_k}}$ and $\frac{1}{\sigma_u}$. Network parameters are $K = 2$, $\lambda_2 = 4\lambda_1$, $\{P_1, P_2\} = \{37, 33\}$ dBm, $\rho_1 = \rho_2 = -40$ dBm.

users and BSs are less than 40 and 50 dBm, respectively. From Figure 6.11, it can be seen that the SIC capability of users does not have to be as high as that of BSs to achieve the same performance. This is mainly because the transmit power of FD users is not very high compared to the transmit power BSs.

6.8 Chapter Summary

I have presented a comprehensive framework for cell association in multi-tier FD cellular networks. For both uplink and downlink transmissions, I have considered different cell association criteria including both coupled and decoupled cell association.. I have used stochastic geometry to model, analyze, and evaluate the performance of the proposed system in terms of mean rate of full-duplex, uplink, and downlink transmissions. Using weighted path-loss cell association, I have derived the optimal weighting factors that maximize the mean rate of FD transmissions in the presence of downlink-to-downlink, downlink-to-uplink, uplink-to-uplink, and uplink-to-downlink

interferences. In addition, I have shown that, in order to maximize the mean rate of FD networks, the users should associate with their nearest BSs in uplink and to the BSs that result in the maximum received power in downlink. This shows the advantage of using DCA over CCA. I have also shown that FD networks may be preferable to HD networks based on the level of SIC at users and BSs.

Chapter 7

Conclusion

7.1 Summary

The deployment of multi-tier cellular networks is seen as a main solution in order to meet the ever-increasing users demand for higher data rates and better coverage. Different from traditional single-tier networks, multi-tier cellular networks consist of different classes of BSs such as macrocell, femtocell, and picocell BSs. These BSs operate simultaneously in the same geographical area and differ in transmit power, coverage range, and spatial density. Small cells such as femtocell BSs are deployed by the end user in unplanned manner which introduces an increase to the randomness in the locations of BSs. Recently, stochastic geometry has attracted attention as an effective tool to model and analyze multi-tier cellular networks while capturing the uncertainties in the deployment of BSs. This in turn enables us to better understand different tradeoffs in the network and optimize fundamental design parameters to improve certain performance metrics. Therefore, in this thesis, I adopted stochastic geometry-based analytical approaches to model multi-tier cellular networks under several setups and technologies. The key contributions and conclusions of this thesis

are summarized below.

In Chapter 2, I proposed the concept of location-aware cross-tier cooperation in multi-tier cellular networks. In the proposed scheme, downlink CoMP transmission are used depending on the locations of the users and their nearest macrocell and small cell BSs. I used stochastic geometry to analyze the outage probability, average rate, and load per BS for the proposed scheme. I showed that the proposed scheme outperforms several schemes in the literature such as non-cooperative transmissions and range expansion in terms of outage probability and average ergodic rate. In addition, I showed that the performance of the proposed scheme approaches that of networks with full cooperation for sufficiently high cooperation threshold. Finally, I demonstrated that the proposed scheme provides a tradeoff between improved outage probability and load per BS.

In Chapter 3, I used stochastic geometry to model cognitive D2D communication in multi-channel downlink-uplink cellular network with energy harvesting. I proposed different spectrum access policies for the cellular network in order to allow D2D users to coexist in uplink and downlink channels. I evaluated the performance of the proposed framework in terms of transmission probability and outage probabilities for D2D and cellular users. I showed that prioritized spectrum access for cellular transmissions outperforms random spectrum access method. Furthermore, I demonstrated that the effects on cellular transmissions are negligible. I proved that uplink channels are preferable to downlink channels for D2D transmissions in dense cellular networks and vice versa. Finally, I illustrated how to tune network design parameters so that energy harvesting can be used along with cognitive D2D transmission to provide an acceptable quality of service performance of D2D communication while protecting cellular transmissions.

In Chapter 4, I studied multi-tier uplink cellular networks with energy harvesting. I used stochastic geometry along with a Markov chain to model to capture the randomness in the network topology and the battery dynamics. I derived simple expressions for the coverage probability, transmission probability, and success probability. Furthermore, I presented several guidelines to design energy harvesting-based multi-tier cellular networks and optimize their performance. I also showed that the performance of cellular users in uplink is optimized when carefully tuning network design parameters such as receiver sensitivity and spatial densities of the BSs.

Unlike Chapter 4 in which uplink users associate with the nearest BS, I considered the case with flexible cell association in Chapter 5. I used stochastic geometry to show that energy harvesting can be a viable technology to power cellular devices especially those with short-range transmissions such as femtocell users.

In Chapter 6, I presented a comprehensive framework to model and analyze cell association in multi-tier FD cellular networks. I considered different cell association criteria including coupled and decoupled cell association for uplink and downlink transmissions. I used stochastic geometry to evaluate the performance in terms of mean rate of FD, uplink, and downlink transmissions. I derived optimal weighting factors that maximize the mean rate of of the network in the presence of interference resulting from FD transmissions. I showed that there exist minimum required SIC capabilities for BSs and users for which FD networks are preferable to HD networks. Finally, I concluded that decoupled cell association outperforms coupled cell association for wide range of weighting factors.

7.2 Future Directions

Here, I present two future directions to extend the work in this thesis. First is to use stochastic geometry-based analysis to evaluate the performance of new emerging technologies for multi-tier cellular networks. Another direction is to explore new tractable point processes that capture the dependencies between the locations of different network elements such as BSs and users. A brief discussion on future directions is presented below.

7.2.1 Performance Evaluation of New Technologies

In this thesis, I have presented several analytical frameworks to evaluate the performance of some of the emerging technologies such as cross-tier cooperation, energy harvesting, D2D communication, and FD communication. However, the need for higher data rates is growing exponentially which in turn motivates research community to propose new technologies to satisfy this ever-increasing demand.

In general, improving the data rate supported by a cellular network can be achieved either by increasing the bandwidth or SINR as dictated by Shannon's formula. To achieve this, two new technologies have been proposed for rate improvement in multi-tier cellular networks. First is to increase bandwidth by utilizing the millimeter wave (mmWave) spectrum (i.e., 30-300 GHz). This can be achieved by deploying additional class(s) of BSs that support communication in this frequency band. Another solution is to increase spectral efficiency (or equivalently SINR) through massively increase the number of antennas per BS which is known as massive MIMO.

Both technologies add more challenges on modeling cellular networks using tools from stochastic geometry. For example, some of the challenges to model massive MIMO-based networks are pilot contamination, new channel models, and coexistence

with small cells. On the other hand, modeling mmWave-based networks should take into account the different nature of mmWave signals and their propagation in this frequency range. Furthermore, both technologies are expected to coexist together since mmWave communication requires very high number of antennas for beam steering. Another possible application is to use massive MIMO and mmWave communication to provide small cell with wireless backhaul links which is a cost-efficient alternative compared to the prohibitively expensive wired backhaul networks.

7.2.2 More Realistic Point Processes

Throughout this thesis, the main assumption is that locations of BSs are independent from each other, hence, an independent PPP is used to model each network tier with certain spatial density. Although this assumption provides a good approximation for the unplanned deployment of small cells, not all network tiers are deployed randomly. For example, macrocell BSs are deployed by the operator, hence, the location of a BS is correlated with and dependent on locations of other BSs in the network. Another example is D2D communication in which users are expected to form clusters rather than being randomly located. Since PPP cannot capture these factors, there has been a rising need for new point processes to better model cellular networks while being tractable.

Bibliography

[1] "More Than 50 Billion Connected Devices," Ericsson White Paper, February 2011.

[2] A. Damnjanovic, J. Montojo, Y. Wei, T. Ji, T. Luo, M. Vajapeyam, T. Yoo, O. Song, and D. Malladi, "A survey on 3GPP heterogeneous networks," *IEEE Wireless Commun.,* vol. 18, no. 3, pp. 10–21, 2011.

[3] D. Gesbert, S. Hanly, H. Huang, S. Shamai Shitz, O. Simeone, and W. Yu, "Multi-cell MIMO cooperative networks: A new look at interference," *IEEE J. Select. Areas in Commun.,* vol. 28, no. 9, pp. 1380–1408, 2010.

[4] O. Simeone, O. Somekh, H. V. Poor, and S. Shamai, "Local base station cooperation via finite-capacity links for the uplink of linear cellular networks," *IEEE Trans. Inf. Theory*, vol. 55, no. 1, pp. 190–204, 2009.

[5] D. Lee, H. Seo, B. Clerckx, E. Hardouin, D. Mazzarese, S. Nagata, and K. Sayana, "Coordinated multipoint transmission and reception in LTE-Advanced: deployment scenarios and operational challenges," *IEEE Commun. Mag.*, vol. 50, no. 2, pp. 148–155, 2012.

[6] S. Venkatesan, A. Lozano, and R. Valenzuela, "Network MIMO: Overcoming intercell interference in indoor wireless systems," in *Conf. Rec. of the 41st Asilomar Conference on Signals, Systems and Computers,* 2007, pp. 83–87.

[7] G. Foschini, K. Karakayali, and R. Valenzuela, "Coordinating multiple antenna cellular networks to achieve enormous spectral efficiency," *IEE Proc. Commun.,* vol. 153, no. 4, pp. 548–555, Aug. 2006.

[8] R. Irmer, H. Droste, P. Marsch, M. Grieger, G. Fettweis, S. Brueck, H.-P. Mayer, L. Thiele, and V. Jungnickel, "Coordinated multipoint: Concepts, performance, and field trial results," *IEEE Commun. Mag.,* vol. 49, no. 2, pp. 102–111, 2011.

[9] K. Doppler, M. Rinne, C. Wijting, C. B. Ribeiro, and K. Hugl, "Device-to-device communication as an underlay to LTE-advanced networks," *IEEE Commun. Mag.,* vol. 47, no. 12, pp. 42–49, Dec. 2009.

[10] D. Feng, L. Lu, Y. Yuan-Wu, G. Y. Li, S. Li, and G. Feng, "Device-to-device communications in cellular networks," *IEEE Commun. Mag.,* vol. 52, no. 4, pp. 49–55, Apr. 2014.

[11] L. Song, D. Niyato, Z. Han, and E. Hossain, *Wireless Device-to-Device Communications and Networks*, Cambridge University Press, 2015.

[12] A. Sabharwal, P. Schniter, D. Guo, D. Bliss, S. Rangarajan, and R. Wichman,"In-band full-duplex wireless: Challenges and opportunities" *IEEE J. Select. Areas Commun.,* vol. 32, no. 9, pp. 1637–1652, Sept. 2014.

[13] H. Tabassum, A. H. Sakr , and E. Hossain, "Analysis of massive MIMO-enabled downlink wireless backhauling for full-duplex small cells," *IEEE Trans. Commun.,* vol. 64, no. 6, pp. 2354–2369, April 2016.

[14] I. Randrianantenaina, H. ElSawy, and M.-S. Alouini, "Limits on the capacity of in-band full duplex communication in uplink cellular networks" in *Proc. of 2015 IEEE Global Telecommunications Conference (GLOBECOM),* 2015.

[15] S. Hong, J. Brand, J. Choi, M. Jain, J. Mehlman, S. Katti, and P. Levis, "Applications of self-interference cancellation in 5G and beyond," *IEEE Commun. Mag.,* vol. 52, no. 2, pp. 114–121, Feb. 2014.

[16] A. D. Wyner, "Shannon-theoretic approach to a Gaussian cellular multiple-access channel," *IEEE Trans. on Info. Theory,* vol. 40, no. 6, pp. 1713–1727, Nov. 1994.

[17] F. Baccelli and B. Blaszczyszyn, *Stochastic Geometry and Wireless Networks: Volume I Theory*. Now Publishers Inc, 2010, vol. 1.

[18] F. Baccelli and B. Blaszczyszyn, *Stochastic Geometry and Wireless Networks: Volume I Theory*. Now Publishers Inc, 2010, vol. 2.

[19] J. G. Andrews, F. Baccelli, R. K. Ganti, "A tractable approach to coverage and rate in cellular networks," in *IEEE Trans. Commun.,* vol. 59, no. 11, pp. 3122–3134, Nov. 2011.

[20] H. S. Dhillon, R. K. Ganti, F. Baccelli, and J. G. Andrews, "Modeling and analysis of k-tier downlink heterogeneous cellular networks," in *IEEE J. Select. Areas Commun,* vol. 30, no. 3, pp. 550–560, 2012.

[21] H. ElSawy, E. Hossain, and M. Haenggi, "Stochastic geometry for modeling, analysis, and design of multi-tier and cognitive cellular wireless networks: A survey," *IEEE Commun. Surveys Tuts.,* vol. 15, no. 3, pp. 996–1019, July 2013.

[22] D. Stoyan, W. S. Kendall, and J. Mecke, *Stochastic Geometry and its Applications*. John Wiley & Sons, 1995.

[23] A. J. Baddeley, "Spatial Point Processes and their Applications," in *Lecture Notes in Mathematics: Stochastic Geometry*. Springer Verlag , Berlin Heidelberg, 2007, pp. 1–75.

[24] M. Haenggi, J. G. Andrews, F. Baccelli, O. Dousse, and M. Franceschetti, "Stochastic geometry and random graphs for the analysis and design of wireless networks," *IEEE Journal on Selected Areas of Communications*, Sept. 2009.

[25] P. Cardieri, "Modeling interference in wireless ad Hoc networks," *IEEE Communications Surveys & Tutorials*, vol.12, no. 4, pp. 551–572, Fourth Quarter 2010.

[26] S. Weber and J. G. Andrews, *Transmission Capacity of Wireless Networks* in *Foundations and Trends in Networking*, NOW Publishers, February 2012.

[27] M. Haenggi, *Stochastic Geometry for Wireless Networks*. Cambridge University Press, 2013.

[28] M. Haenggi and R. K. Ganti, *Interference in Large Wireless Networks,* Now Publishers Inc, 2009.

[29] E. Hossain, L. B. Le, and D. Niyato, *Radio Resource Management in Multi-Tier Cellular Wireless Networks*, Wiley, 2013.

[30] E. Hossain, V. K. Bhargava, and G. Fettweis, *Green Radio Communication Networks*, (edited volume), Cambridge University Press, 2012.

[31] A. Harb, "Energy harvesting: State-of-the-art," *Renewable Energy,* vol. 36, no. 10, pp. 2641–2654, Oct. 2011.

[32] J. A. Paradiso and T. Starner, "Energy scavenging for mobile and wireless electronics," *IEEE Pervasive Computing*, vol. 4, no. 1, pp. 18–27, Jan.-Mar. 2005.

[33] D. Bouchouicha, F. Dupont, M. Latrach, and L. Ventura, "Ambient RF energy harvesting," in Proc. of *IEEE Int. Conf. Renewable Energies Power Quality (ICREPQ'10)*, Mar. 2010, pp. 486–495.

[34] A. H. Sakr and E. Hossain, "Location-aware cross-tier coordinated multipoint transmission in two-tier cellular networks," *IEEE Trans. Wireless Commun.,* vol. 13, no. 11, pp. 6311–6325, 2014.

[35] A. H. Sakr and E. Hossain, "Analysis of K-tier uplink cellular networks with ambient RF energy harvesting," *IEEE J. Select. Areas Commun.,* vol. 33, no. 10, pp. 2226–2238, Oct. 2015.

[36] A. H. Sakr and E. Hossain, "Cognitive and energy harvesting-based D2D communication in cellular networks: Stochastic geometry modeling and analysis," *IEEE Trans. Commun.,* vol. 63, no. 5, pp. 1867–1880, May 2015.

[37] A. H. Sakr , H. Tabassum, E. Hossain, and D. I. Kim, "Cognitive spectrum access in device-to-device (D2D)-enabled cellular networks," *IEEE Commun. Mag.,* vol. 53, no. 7, pp. 126–133, July 2015.

[38] A. H. Sakr and E. Hossain, "On cell association in multi-tier full-duplex cellular networks," under submission, [Available Online:] arXiv:1607.01119.

[39] P. Marsch and G. Fettweis, "On base station cooperation schemes for downlink network MIMO under a constrained backhaul," in *Proc. of IEEE Global Telecommunications Conference (GLOBECOM),* 2008, pp. 1–6.

[40] K. Okino, T. Nakayama, C. Yamazaki, H. Sato, and Y. Kusano, "Pico cell range expansion with interference mitigation toward LTE-Advanced heterogeneous networks," in *Proc. of IEEE Int. Conf. on Communications Workshops (ICC)*, 2011, pp. 1–5.

[41] D. López-Pérez, I. Guvenc, G. De La Roche, M. Kountouris, T. Q. Quek, and J. Zhang, "Enhanced intercell interference coordination challenges in heterogeneous networks," *IEEE Wireless Commun.*, vol. 18, no. 3, pp. 22–30, 2011.

[42] H.-S. Jo, Y. J. Sang, P. Xia, and J. Andrews, "Heterogeneous cellular networks with flexible cell association: A comprehensive downlink SINR analysis," *IEEE Trans. Wireless Commun.,* vol. 11, no. 10, pp. 3484–3495, Aug. 2012.

[43] G. Nigam, P. Minero, and M. Haenggi, "Coordinated multipoint in heterogeneous networks: A stochastic geometry approach," *IEEE GLOBECOM Workshop on Emerging Technologies for LTE-Advanced and Beyond 4G (GLOBECOM-B4G'13),* 2013, pp. 145–150.

[44] A. Giovanidis and F. Baccelli, "A stochastic geometry framework for analyzing pairwise-cooperative cellular networks," *arXiv preprint arXiv:1305.6254*, 2013.

[45] S. Akoum and R. Heath, "Interference coordination: Random clustering and adaptive limited feedback," *IEEE Trans. Signal Process.,* vol. 61, no. 7, pp. 1822–1834, 2013.

[46] P. Xia, C.-H. Liu, and J. G. Andrews, "Downlink coordinated multi-point with overhead modeling in heterogeneous cellular networks," *IEEE Trans. Wireless Commun,* vol. 12, no. 8, pp. 4025–4037, Aug. 2013.

[47] C. Lima, M. Bennis, and M. Latva-aho, "Coordination mechanisms for self-organizing femtocells in two-tier coexistence scenarios," *IEEE Trans. Wireless Commun,* vol. 11, no. 6, pp. 2212–2223, June 2012.

[48] D. López-Pérez, X. Chu, and I. Guvenc, "On the expanded region of picocells in heterogeneous networks," *IEEE J. Sel. Top. Signal Process.,* vol. 6, no. 3, pp. 281–294, Jun. 2012.

[49] F. Pantisano, M. Bennis, W. Saad, M. Debbah, M. Latva-aho, "On the impact of heterogeneous backhauls on coordinated multipoint transmission in femtocell networks," in *Proc. of IEEE Int. Conf. on Communications (ICC)*, 2012, pp. 5064–5069.

[50] A. H. Sakr and E. Hossain, "Energy-efficient downlink transmission in two-tier network MIMO OFDMA networks," in *Proc. of IEEE Int. Conf. on Communications (ICC)*, 2014, pp. 3652–3657.

[51] A. H. Sakr, H. ElSawy, and E. Hossain, "Location-aware coordinated multipoint transmission in OFDMA networks," in *Proc. of IEEE Int. Conf. on Communications (ICC)*, 2014, pp. 5517–5182.

[52] H. ElSawy and E. Hossain, "Two-tier HetNets with cognitive femtocells: Downlink performance modeling and analysis in a multi-channel environment," *IEEE Trans. Mobile Comput.,* vol. 13, no. 3, pp. 649–663, Mar. 2014.

[53] E. Hossain, D. Niyato, and Z. Han, *Dynamic Spectrum Access and Management in Cognitive Radio Networks*, Cambridge University Press, 2009.

[54] H. ElSawy and E. Hossain, "On cognitive small cells in two-tier heterogeneous networks," in *11th Intl. Symposium on Modeling and Optimization in Mobile, Ad Hoc, and Wireless Networks (WiOpt 2013)*, 2013, pp. 75–82.

[55] K. Huang and V. K. N. Lau, "Enabling wireless power transfer in cellular networks: Architecture, modeling and deployment," *IEEE Trans. Wireless Commun.,* vol. 13, no. 2, pp. 902–912, Feb. 2014.

[56] S. Lee, R. Zhang and K. Huang, "Opportunistic wireless energy harvesting in cognitive radio networks," *IEEE Trans. Wireless Commun.,* vol. 12, no. 9, pp. 4788–4799, Sep. 2013.

[57] I. Flint, X. Lu, N. Privault, D. Niyato, and P. Wang, "Performance analysis of ambient RF energy harvesting: A stochastic geometry approach," in *Proc. of 2014 IEEE Global Telecommunications Conference (GLOBECOM)*, 2014, pp. 1448–1453.

[58] I. Krikidis, "Simultaneous information and energy transfer in large-scale networks with/without relaying," *IEEE Trans. on Commun.,* vol. 62, no. 3, pp. 900–912, Mar. 2014.

[59] C. Huang, R. Zhang, and S. Cui, "Optimal power allocation for outage probability minimization in fading channels with energy harvesting constraints," *IEEE Trans. Wireless Commun.,* vol. 13, no. 2, pp. 1074–1087, Feb. 2014.

[60] L. Liu, R. Zhang, and K. C. Chua, "Wireless information transfer with opportunistic energy harvesting," *IEEE Trans. Wireless Commun.,* vol. 12, no. 1, pp. 288–300, Jan. 2013.

[61] D. W. K. Ng, E. S. Lo, and R. Schober, "Wireless information and power transfer: Energy efficiency optimization in OFDMA systems," *IEEE Trans. Wireless Commun.,* vol. 12, pp. 6352–6370, Dec. 2013.

[62] X. Lin, J. G. Andrews, and A. Ghosh, "Spectrum sharing for device-to-device communication in cellular networks," *IEEE Trans. Wireless Commun.,* vol. 13, no. 12, pp. 6727–6740, Dec. 2014.

[63] H. ElSawy and E. Hossain, "Analytical modeling of mode selection and power control for underlay D2D communication in cellular networks," *IEEE Trans. Commun.*, vol. 62, no. 11, pp. 4147–4161, Nov. 2014.

[64] M. Zulhasnine, C. Huang, and A. Srinivasan, "Efficient resource allocation for device-to-device communication underlaying LTE network," in Proc. of *IEEE WiMob,* Oct. 2010, pp. 368–375.

[65] C.-H. Yu, K. Doppler, C. B. Ribeiro, and O. Tirkkonen, "Resource sharing optimization for device-to-device communication underlaying cellular networks," *IEEE Trans. Wireless Commun.,* vol. 10, no. 8, pp. 2752–2763, Aug. 2011.

[66] P. Phunchongharn, E. Hossain, D. I. Kim, "Resource allocation for device-to-device communications underlaying LTE-advanced networks," *IEEE Wireless Commun.,* vol. 20, no. 4, pp. 91–100, Aug. 2013.

[67] X. Zhang and J. G. Andrews, "Downlink cellular network analysis with multi-slope path moss models," Available [Online]: arXiv:1408.0549.

[68] S. Weber, J. Andrews, and N. Jindal, "The effect of fading, channel inversion, and threshold scheduling on ad hoc networks," *IEEE Trans. Inf. Theory,* vol. 53, no. 11, pp. 4127–4149, Nov. 2007.

[69] C. H. Lee and M. Haenggi, "Interference and outage in Poisson cognitive networks," *IEEE Trans. Wireless Commun.*, vol. 11, no. 4, pp. 1392–1401, Apr. 2012.

[70] A. Ghosh, J. G. Andrews, N. Mangalvedhe, R. Ratasuk, B. Mondal, M. Cudak, E. Visotsky, T. A. Thomas, P. Xia, H. S. Jo, H. S. Dhillon, and T. D. Novlan, "Heterogeneous cellular networks: From theory to practice," *IEEE Commun. Mag.,* Jun. 2012.

[71] N. Saquib, E. Hossain, L. B. Le, and D. I. Kim, "Interference management in OFDMA femtocell networks: Issues and approaches," *IEEE Wireless Commun.*, vol. 19, no. 3, pp. 86–95, 2012.

[72] K. Huang, "Spatial throughput of mobile ad hoc network with energy harvesting," *IEEE Trans. Inf. Theory,* vol. 59, no. 11, pp. 7597–7612, Nov. 2013.

[73] X. Lu, P. Wang, D. Niyato, D. I. Kim, and Z. Han, "Wireless networks with RF energy harvesting: A contemporary survey," *IEEE Commun. Surveys Tuts.,* Available [Online]: arXiv:1406.6470

[74] T. D. Novlan, H. S. Dhillon, and J. G. Andrews,"Analytical modeling of uplink cellular networks," *IEEE Trans. Wireless Commun.,* vol. 12, no. 6, pp. 2669–2679, 2013.

[75] H. ElSawy and E. Hossain, "On stochastic geometry modeling of cellular uplink transmission with truncated channel inversion power control," to appear in *IEEE Trans. Wireless Commun.,* vol. 13, no. 8, pp. 4454–4469, 2014.

[76] T. J. Sheskin, *A Markov chain partitioning algorithm for computing steady state probabilities,* Operations Research 33, 1985, pp. 228–235.

[77] H. Elshaer, F. Boccardi, M. Dohler, and R. Irmer, "Downlink and uplink decoupling: A disruptive architectural design for 5G networks," in *Proc. of 2014 IEEE Global Telecommunications Conference (GLOBECOM),* 2014, pp. 1798–1803.

[78] S. Singh, X. Zhang, J. G. Andrews, "Joint rate and SINR coverage analysis for decoupled uplink-downlink biased cell associations in HetNets," *IEEE Trans. Wireless Commun.,* vol. 14, no. 10, pp. 5360–373, May 2015.

[79] Y. Lin, W. Bao, W. Yu, and B. Liang, "Optimizing user association and spectrum allocation in HetNets: A utility perspective," *IEEE J. Select. Areas Commun.,* vol. 33, no. 6, pp. 1025–1039, June 2015.

[80] K. Smiljkovikj, H. Elshaer, P. Popovski, F. Boccardi, M. Dohler, L. Gavrilovska, and R. Irmer, "Capacity analysis of decoupled downlink and uplink access in 5G heterogeneous systems," Available [Online]: arXiv:1410.7270 (2015).

[81] S. Sekander, H. Tabassum, and E. Hossain, "A matching game for decoupled uplink-downlink user association in full-duplex small cell networks," in *Proc. of 2015 IEEE Global Telecommunications Conference (GLOBECOM),* 2015.

[82] Z. Tong and M. Haenggi, "Throughput analysis for full-duplex wireless networks with imperfect self-interference cancellation," *IEEE Trans. Commun.,* vol. 63, no. 11, pp. 4490–4500, Nov. 2015.

[83] A. Munari, P. Mähönen, and M. Petrova, "A stochastic geometry framework for asynchronous full-duplex networks." Available [Online]: arXiv:1512.01478 (2015).

[84] A. AlAmmouri, H. ElSawy, and M.-S. Alouini, "Flexible design for α-duplex communications in multi-tier cellular networks," Available [Online]: arXiv:1511.07903 (2015).

[85] J. Lee and T. Q. S. Quek, "Hybrid full-/half-duplex system analysis in heterogeneous wireless networks," *IEEE Trans. Wireless Commun.,* vol. 14, no. 5, pp. 2883–2895, May. 2015.

[86] M. Mohammadi, H. A. Suraweera, I. Krikidis, and C. Tellambura, "Full-duplex radio for uplink/downlink transmission with spatial randomness," in *Proc. of IEEE Int. Conf. on Communications (ICC'15),* 2015, pp. 1908–1913.

[87] J. H. Yun, "Intra and inter-cell resource management in full-duplex heterogeneous cellular networks," *IEEE Trans. Mobile Comput.,* vol. 15, no. 2, pp. 392–405, Feb. 2016.

[88] C. Nam, C. Joo, and S. Bahk, "Joint subcarrier assignment and power allocation in full-duplex OFDMA networks," *IEEE Trans. Wireless Commun.,* vol. 14, no. 6, pp. 3108–3119, June 2015.

[89] S. Goyal, P. Liu, S. Panwar, R. Yang, R. A. DiFazio, and E. Bala, "Full duplex operation for small cells," Available [Online]: arXiv:1412.8708 (2015).

[90] W. Choi, H. Lim, and A. Sabharwal, "Power-controlled medium access control protocol for full-duplex WiFi networks," *IEEE Trans. Wireless Commun.,* vol. 14, no. 7, pp. 3601–3613, July 2015.

[91] 3GPP, "TR 36.814 v.9.0.0: Further advancements for E-UTRA," Mar. 2010.

[92] F. J. Martin-Vega, G. Gomez, M. C. Aguayo-Torres, and M. Di Renzo,"Analytical modeling of interference aware power control for the uplink of heterogeneous cellular networks," *IEEE Trans. Wireless Commun.,* vol. 15, no. 10, pp. 6742–6757, Oct. 2016.

[93] A. Shojaeifard, K. Wong, M. Di Renzo, G. Zheng, K. A. Hamdi, and J. Tang, "Massive MIMO-enabled full-duplex cellular networks," Available [Online]: arXiv:1611.03854 (2016).

[94] A. H. Sakr and E. Hossain, "Analysis of multi-tier uplink cellular networks with energy harvesting and flexible cell association," in *Proc. of 2014 IEEE Global Telecommunications Conference (GLOBECOM)*, 2014, pp. 4712–4717.

[95] B. Blaszczyszyn and D. Yogeshwaran, "Clustering comparison of point processes with applications to random geometric models," Available [Online]: arXiv:1212.5285 (2014).

[96] M. Haenggi, "User point processes in cellular networks," Available [Online]: arXiv:1611.08560 (2016).

[97] T. Bai and R. W. Heath, "Analyzing uplink SINR and rate in massive MIMO systems using stochastic geometry," *IEEE Trans. Commun.,* vol. 64, no. 11, pp. 4592–4606, Nov. 2016.

[98] A. H. Sakr and E. Hossain, "Analysis of K-tier uplink cellular networks with ambient RF energy harvesting," *IEEE J. Select. Areas Commun.,* vol. 33, no. 10, pp. 2226–2238, Oct. 2015.

[99] F. Baccelli, B. Blaszczyszyn, and C. Singh, "Analysis of a proportionally fair and locally adaptive spatial aloha in Poisson networks," in *Proc. IEEE Int. Conf. Comput. Commun. (INFOCOM),* 2014, pp. 2544–2552.

[100] F. Kelly, A. Maulloo, and D. Tanm "Rate control in communication networks: shadow prices, proportional fairness and stability," *Journal of the Operational Research Society,* vol. 49, no. 3, pp. 237–252, Mar. 1998.

[101] [Online] http://home.cc.umanitoba.ca/~sakra/publications.html

[102] L. C. Andrews, *Special Functions for Engineers and Applied Mathematicians.* New York: MacMillan, 1985.

[103] A. M. Cohen, *Numerical Methods for Laplace Transform Inversion.* Springer, 2007.

Appendix A

A.1 Proof of Lemma 2.1

Firstly, I derive the probability for a typical user to operate in a certain mode. By definition,

$$q_M = \mathbb{E}_{R_1}\left[\mathbb{P}\left[\mathcal{B} = x_1\right]\right] = \mathbb{E}_{R_1}\left[\mathbb{P}\left[\frac{P_1 R_1^{-\alpha_1}}{P_2 R_2^{-\alpha_2}} \geq \beta\right]\right] \tag{A.1}$$

and

$$q_P = \mathbb{E}_{R_2}\left[\mathbb{P}\left[\mathcal{B} = x_2\right]\right] = \mathbb{E}_{R_2}\left[\mathbb{P}\left[\frac{P_1 R_1^{-\alpha_1}}{P_2 R_2^{-\alpha_2}} < 1\right]\right]. \tag{A.2}$$

Using (A.1) and (A.2) and following the proof in [42, Lemma 1] with the proper changes, q_M, q_P, and q_C can be obtained.

For the joint PDF $f_{R_C}(\mathbf{r})$ of a typical CoMP user's distances to the cooperating macrocell BS and picocell BS, it is known for sure that if the distance to the macrocell BS is R_1, the distance to the picocell BS R_2 is bounded as follows

$$\left(\frac{P_2}{P_1}\right)^{\frac{1}{\alpha_2}} R_1^{\frac{\alpha_1}{\alpha_2}} < R_2 < \left(\frac{\beta P_2}{P_1}\right)^{\frac{1}{\alpha_2}} R_1^{\frac{\alpha_1}{\alpha_2}} \tag{A.3}$$

as can be obtained from (2.2) when $\mathcal{B} = \{x_1, x_2\}$.

Therefore, the conditional probability of $R_1 > r_1$ and $R_2 > r_2$ given that the user operates in the CoMP mode can be written as

$$\begin{aligned}
&\mathbb{P}[R_1 > r_1, R_2 > r_2 | \mathcal{B} = \{x_1, x_2\}] \\
&\qquad \overset{(a)}{=} \frac{1}{q_C} \mathbb{P}\left[R_1 > r_1, R_2 > \max\left(r_2, \left(\frac{P_2}{P_1}\right)^{\frac{1}{\alpha_2}} R_1^{\frac{\alpha_1}{\alpha_2}} \right) \right] \\
&\qquad - \frac{1}{q_C} \mathbb{P}\left[R_1 > r_1, R_2 > \max\left(r_2, \left(\frac{\beta P_2}{P_1}\right)^{\frac{1}{\alpha_2}} R_1^{\frac{\alpha_1}{\alpha_2}} \right) \right] \\
&\qquad \overset{(b)}{=} \frac{1}{q_C} \int\limits_{r > r_1} \left(\mathbb{P}\left[R_2 > \max\left(r_2, \left(\frac{P_2}{P_1}\right)^{\frac{1}{\alpha_2}} R_1^{\frac{\alpha_1}{\alpha_2}} \right) \right] \right. \\
&\qquad\qquad \left. - \mathbb{P}\left[R_2 > \max\left(r_2, \left(\frac{\beta P_2}{P_1}\right)^{\frac{1}{\alpha_2}} R_1^{\frac{\alpha_1}{\alpha_2}} \right) \right] \right) f'_{R_1}(r)\, \mathrm{d}r \qquad \text{(A.4)}
\end{aligned}$$

where (a) follows the bound on R_2 given in (A.3) and $f'_{R_i}(r)$ in (b) is the distribution of the distance to the nearest point in a homogeneous PPP $\mathbf{\Phi}_k \in \mathbb{R}^2$ which can be derived using (1.1) as follows

$$\begin{aligned}
\mathbb{P}\left[R_k > r\right] &= \mathbb{P}\left[\text{There are no BSs in a disc of radius } r\right] \\
&= \exp\left[-\pi \lambda_k r^2\right]. \qquad \text{(A.5)}
\end{aligned}$$

Therefore,

$$\begin{aligned}
f'_{R_i}(r) &= \frac{\mathrm{d}}{\mathrm{d}r}\left(1 - \mathbb{P}\left[R_i > r\right]\right) \\
&= 2\pi\lambda_i\, r \exp\left[-\pi\lambda_i r^2\right]. \qquad \text{(A.6)}
\end{aligned}$$

After plugging (A.6) into (A.4), I use the resulting cumulative CDF (CCDF), i.e.,

$\mathbb{P}\left[R_1 > r_1, R_2 > r_2 | \mathcal{B} = \{x_1, x_2\}\right]$, to obtain the joint PDF $f_{R_C}(\mathbf{r})$ of R_1 and R_2 of a user who operates in the CoMP mode as follows

$$\begin{aligned} f_{R_C}(\mathbf{r}) &= \frac{\partial^2}{\partial r_1 \partial r_2} \left(1 - \mathbb{P}\left[R_1 > r_1, R_2 > r_2 | \mathcal{B} = \{x_1, x_2\}\right]\right) \\ &= \begin{cases} \frac{4\pi^2 \lambda_1 \lambda_2}{q_C} r_1 r_2 \exp\left[-\pi\left(\lambda_1 r_1^2 + \lambda_2 r_2^2\right)\right], & (r_1, r_2) \in \mathcal{A} \\ 0, & \text{otherwise} \end{cases} \end{aligned} \tag{A.7}$$

where

$$\mathcal{A} = \left\{(r_1, r_2) : r_1 \geq 0 \text{ and } \left(\frac{P_2}{P_1}\right)^{\frac{1}{\alpha_2}} r_1^{\frac{\alpha_1}{\alpha_2}} < r_2 < \left(\frac{\beta P_2}{P_1}\right)^{\frac{1}{\alpha_2}} r_1^{\frac{\alpha_1}{\alpha_2}}\right\}. \tag{A.8}$$

For $f_{R_1}(r)$, using the event of $R_1 > r$ given that the macrocell user operates in the non-CoMP mode, i.e., $\mathcal{B} = \{x_1\}$, the probability of this event is given by

$$\begin{aligned} \mathbb{P}[R_1 > r_1 | \mathcal{B} = \{x_1\}] &= \frac{1}{q_M} \mathbb{P}\left[R_1 > r_1, \frac{P_1 R_1^{-\alpha_1}}{P_2 R_2^{-\alpha_2}} > \beta\right] \\ &= \frac{1}{q_M} \int\limits_{r > r_1} \mathbb{P}\left[R_2 > \left(\frac{\beta P_2}{P_1}\right)^{\frac{1}{\alpha_2}} r^{\frac{\alpha_1}{\alpha_2}}\right] f'_{R_1}(r)\, \mathrm{d}r. \end{aligned} \tag{A.9}$$

Then, I follow the same procedure by plugging (A.6) into (A.9) and taking the derivative of the CDF, i.e., $1 - \mathbb{P}\left[R_1 > r_1 | \mathcal{B} = \{x_1\}\right]$, with respect to r_1. Hence, (A.9) reduces to (2.4). Similarly, the PDF of R_2 can be obtained as in (2.5).

A.2 Proof of Theorem 2.1

Firstly, I derive the outage probability of a randomly located non-CoMP macrocell user. Using the definition of the outage probability in (2.13) for a non-CoMP macro-

cell user,

$$\mathcal{O}_M(\tau) = 1 - \int_{\mathbb{R}_+} \mathbb{P}\left[\text{SINR}(\mathcal{B} = \{x_1\}) > \tau\right] f_{R_1}(r)\, \mathrm{d}r \tag{A.10}$$

where the SINR in (2.11) can be rewritten as

$$\text{SINR}(\mathcal{B} = \{x_1\}) = \frac{P_1 |h(x_1, 0)|^2 r_1^{-\alpha_1}}{\mathcal{I} + \sigma^2} \tag{A.11}$$

in which

$$\mathcal{I} = \mathcal{I}_1 + \mathcal{I}_2 \tag{A.12}$$

such that

$$\begin{aligned} \mathcal{I}_1 &= P_1 \sum_{x_i \in \mathbf{\Phi}_1 \setminus x_1} |h(x_i, 0)|^2 \|x_i\|^{-\alpha_1} \\ \mathcal{I}_2 &= P_2 \sum_{x_i \in \mathbf{\Phi}_2} |h(x_i, 0)|^2 \|x_i\|^{-\alpha_2} \end{aligned} \tag{A.13}$$

where $\mathcal{I}_i$ ($i \in \{1, 2\}$) is the total interference power received from the i-th tier and $f_{R_1}(r)$ is the PDF of distance given in **Lemma 2.1**.

After rewriting the SINR of the non-CoMP macrocell user, I calculate the CCDF following a similar procedure as in Section 1.5.2 as follows

$$\begin{aligned} \mathbb{P}\left[\text{SINR} > \tau\right] &= \mathbb{P}\left[|h(x_1, 0)|^2 > \frac{\tau(\mathcal{I} + \sigma^2)}{P_1 r_1^{-\alpha_1}}\right] \\ &\overset{(c)}{=} \int_{\mathbb{R}_+} \exp\left[-\frac{\tau(i + \sigma^2)}{P_1 r_1^{-\alpha_1}}\right] f_I(i) di \\ &= \mathbb{E}_{\mathcal{I}}\left[\exp\left[-\frac{\tau(i + \sigma^2)}{P_1 r_1^{-\alpha_1}}\right]\right] \end{aligned}$$

$$\stackrel{(d)}{=} \exp\left[\frac{-\tau\sigma^2}{P_1 r_1^{-\alpha_1}}\right] \prod_{j=1}^{2} \mathcal{L}_{I_j}\left(\frac{\tau}{P_1 r_1^{-\alpha_1}}\right) \tag{A.14}$$

where (c) follows because the channel fading power $|h(x_1,0)|^2 \sim \text{Exp}(1)$, and (d) follows from the definition of Laplace transform. Without loss of generality, I calculate the Laplace transform of the PDF of $\mathcal{I}_1$ and the calculation of the Laplace transform of the PDF of $\mathcal{I}_2$ follows the same procedure.

$$\begin{aligned}
\mathcal{L}_{\mathcal{I}_1}(s) &= \mathbb{E}_{\mathcal{I}_1}\left[\exp\left[-s\mathcal{I}_1\right]\right] \\
&= \mathbb{E}_{\mathbf{\Phi}_1,\{h(x_i,0)\}}\left[\exp\left[-sP_1 \sum_{x_i\in\mathbf{\Phi}_1\setminus x_1} |h(x_i,0)|^2 R_i^{-\alpha_1}\right]\right] \\
&\stackrel{(e)}{=} \mathbb{E}_{\mathbf{\Phi}_1}\left[\prod_{x_i\in\mathbf{\Phi}_1\setminus x_1} \mathbb{E}_{\{h(x_i,0)\}}\left[\exp\left[-sP_1|h(x_i,0)|^2 R_i^{-\alpha_1}\right]\right]\right] \\
&\stackrel{(f)}{=} \mathbb{E}_{\mathbf{\Phi}_1}\left[\prod_{x_i\in\mathbf{\Phi}_1\setminus x_1} \frac{1}{1+sP_1 R_i^{-\alpha_1}}\right] \\
&\stackrel{(g)}{=} \exp\left[-2\pi\lambda_1 \int_{r_1}^{\infty}\left(1-\frac{1}{1+sP_1 r^{-\alpha_1}}\right) r\,\mathrm{d}r\right].
\end{aligned} \tag{A.15}$$

In the above, (e) follows from the independence assumption between $\{h(x_i,0)\}$, (f) follows from the moment generating function of an exponential random variable with parameter μ is $\frac{\mu}{\mu-t}$, while (g) follows from (i) the probability generating functional of a PPP and (ii) the fact that an interfering macrocell BS cannot be closer to the user than her serving macrocell BS, i.e., r_1. Now, let $u^{\alpha_1} = (sP_1)^{-1} r^{\alpha_1}$ and replacing s with $\frac{\tau}{P_1 r_1^{-\alpha_1}}$, I obtain

$$\mathcal{L}_{\mathcal{I}_1}\left(\frac{\tau}{P_1 r_1^{-\alpha_1}}\right) = \exp\left[-2\pi\lambda_1 \tau^{\frac{2}{\alpha_1}} r_1^2 \mathcal{F}\left(\left(\frac{1}{\tau}\right)^{\frac{1}{\alpha_1}}, \alpha_1\right)\right] \tag{A.16}$$

where $\mathcal{F}(y,\alpha)$ is defined in (2.20). Similarly, I can obtain the Laplace transform of PDF of $\mathcal{I}_2$ as

$$\mathcal{L}_{\mathcal{I}_2}\left(\frac{\tau}{P_1 r_1^{-\alpha_1}}\right) = \exp\left[-2\pi\lambda_2\left(\tau\frac{P_2}{P_1}\right)^{\frac{2}{\alpha_2}} r_1^{\frac{2\alpha_1}{\alpha_2}}\mathcal{F}\left(\left(\frac{\beta}{\tau}\right)^{\frac{1}{\alpha_1}},\alpha_2\right)\right] \tag{A.17}$$

where the closest interferer in this case is at least at a distance $z = \left(\frac{\beta P_2}{P_1}\right)^{\frac{1}{\alpha_2}} r_1^{\frac{\alpha_1}{\alpha_2}}$ instead of r_1 which was used to obtain the Laplace transform $\mathcal{L}_{\mathcal{I}_2}(\cdot)$. The distance to the closest interfering picocell BS, i.e., z, is obtained from the fact that $P_1 r_1^{-\alpha} \geq \beta P_2 z^{-\alpha}$ for a non-CoMP macrocell user. By combining (A.16) and (A.17) with (A.14) and then substituting in (A.10), (2.17) can be obtained. The outage probability of a non-CoMP picocell user can be easily obtained as in (2.18) by following the same procedure.

For a randomly located CoMP user, given that $\mathcal{B} = \{x_1, x_2\}$, the outage probability is given by

$$\mathcal{O}_C(\tau) = 1 - \int_{\mathcal{A}} \mathbb{P}\left[\text{SINR}(\mathcal{B} = \{x_1, x_2\}) > \tau\right] f_{R_c}(\mathbf{r})\,\mathrm{d}\mathbf{r} \tag{A.18}$$

where $f_{R_c}(\mathbf{r})$ is the joint PDF of the distance to the nearest two BSs (one from each tier) to the typical user, i.e., x_1 and x_2, given in **Lemma 2.1**. Then, the SINR in (2.11) can be rewritten as

$$\text{SINR}(\mathcal{B}) = \frac{\left|\sqrt{P_1}h(x_1,0)r_1^{-\frac{\alpha_1}{2}} + \sqrt{P_2}h(x_2,0)r_2^{-\frac{\alpha_2}{2}}\right|^2}{\mathcal{I}+\sigma^2} \tag{A.19}$$

where

$$\mathcal{I} = \mathcal{I}_1 + \mathcal{I}_2 \tag{A.20}$$

such that

$$\mathcal{I}_1 = P_1 \sum_{x_i \in \mathbf{\Phi}_1 \setminus x_1} |h(x_i,0)|^2 \|x_i\|^{-\alpha_1}$$
$$\mathcal{I}_2 = P_2 \sum_{x_i \in \mathbf{\Phi}_2 \setminus x_2} |h(x_i,0)|^2 \|x_i\|^{-\alpha_2}. \tag{A.21}$$

Before calculating the CCDF of the SINR, I define a new variable θ_i such that

$$\theta_k = \sqrt{P_k}\|x_k\|^{-\frac{\alpha_k}{2}}.$$

Then, the CCDF of the SINR can be rewritten as

$$\mathbb{P}\left[\text{SINR} > \tau\right] = \mathbb{P}\left[|\theta_1 h(x_1,0) + \theta_2 h(x_2,0)|^2 > \tau(\mathcal{I} + \sigma^2)\right]. \tag{A.22}$$

Since $\{h(x,y)\}$ are i.i.d. and follows a $\mathcal{CN}(0,1)$, I obtain

$$|\theta_1 h(x_1,0) + \theta_2 h(x_2,0)|^2 \sim \text{Exp}\left(\frac{1}{\sum_{k=1}^{2} \theta_k^2}\right)$$

which means that the CCDF of the SINR can be written as

$$\begin{aligned}\mathbb{P}\left[\text{SINR} > \tau\right] &= \mathbb{E}_{\mathcal{I}}\left[\exp\left[-\frac{\tau(i+\sigma^2)}{\sum_{k=1}^{2}\theta_k^2}\right]\right] \\ &\overset{(h)}{=} \exp\left[\frac{-\tau\sigma^2}{\sum_{k=1}^{2}\theta_k^2}\right] \prod_{j=1}^{2} \mathcal{L}_{\mathcal{I}_j}\left(\frac{\tau}{\sum_{k=1}^{2}\theta_k^2}\right)\end{aligned} \tag{A.23}$$

where (h) follows from the definition of the Laplace transform of the PDF of $\mathcal{I}_j$. By

following the same steps in deriving (A.15), I get

$$\mathcal{L}_{\mathcal{I}_j}(s) = \exp\left[-2\pi\lambda_j (sP_j)^{\frac{2}{\alpha_j}} \mathcal{F}\left(\left(\frac{1}{sP_j}\right)^{\frac{1}{\alpha_j}} r_j, \alpha_j\right)\right]. \tag{A.24}$$

By combining (2.3), (A.23), and (A.24), and then substituting in (A.18), the outage probability of a randomly located CoMP user is obtained as given in (2.19).

A.3 $\mathcal{F}(y, \alpha)$ Special Cases

The function $\mathcal{F}(\cdot)$, given in (2.20), has a semi-open integral and does not give a closed-form solution in general. However, this function yields a closed-form expression for some values of α. For example, if α is a rational number and can be expressed as

$$\alpha = \frac{2n}{n-m}, \qquad n > m$$

where n and m are any two positive integer numbers, the function $\mathcal{F}(\cdot)$ reduces to

$$\mathcal{F}(y, \alpha) = \frac{(-1)^{\frac{2}{\alpha}}}{\alpha} \sum_{k=0}^{n-1} \frac{\ln\left[1 - \sqrt[n]{-y^{-\alpha}} \exp\left[\frac{2\pi i k}{n}\right]\right]}{\exp\left[\frac{2\pi i k(\alpha-2)}{\alpha}\right]} \tag{A.25}$$

where $i = \sqrt{-1}$ is the imaginary unit number.

This expression reduces to even simpler expressions for specific values of α. For example, if $\alpha = 4$, i.e., $m = 1$ and $n = 2$, $\mathcal{F}(y^{\frac{-1}{4}}, 4)$ reduces to

$$\mathcal{F}(y^{\frac{-1}{\alpha}}, \alpha) = \frac{1}{2} \arctan(\sqrt{y}).$$

For $\alpha = 3$, i.e., $m = 1$ and $n = 3$, $\mathcal{F}(y^{\frac{-1}{3}}, 3)$ reduces to

$$\mathcal{F}(y^{\frac{-1}{\alpha}}, \alpha) = \frac{1}{\sqrt{3}} \arctan\left(\frac{\sqrt{3}\sqrt[3]{y}}{\sqrt[3]{y}+2}\right) + \frac{1}{6}\ln\left[1 + \frac{3\sqrt[3]{y}}{\sqrt[3]{y^2}-\sqrt[3]{y}+1}\right].$$

Appendix B

B.1 Proof of Access Probabilities

B.1.1 Proof of ***Lemma 3.1***

Since the number of used channels by a BS is $\min\{N_u, |\mathcal{S}|\}$, by conditioning on the number of users served by a generic BS such that $N_u = n$, the conditional probability that a BS has at least one free channel to assign for a generic cellular user is given by

$$q_{f|n} = \begin{cases} 1, & 0 \leq n \leq |\mathcal{S}| \\ \dfrac{|\mathcal{S}|}{n}, & n > |\mathcal{S}| \end{cases}. \tag{B.1}$$

Therefore, the unconditional probability can be obtained as

$$q_f = \sum_{n=0}^{\infty} q_{f|n} \mathbb{P}\{N_u = n\} = \sum_{n=0}^{|\mathcal{S}|} \mathbb{P}\{N_u = n\} + \sum_{n=|\mathcal{S}|+1}^{\infty} \frac{|\mathcal{S}|}{n} \mathbb{P}\{N_u = n\}. \tag{B.2}$$

Using the fact that $\sum_{n=0}^{\infty} \mathbb{P}\{N_u = n\} = 1$, the expression of q_f in (3.7) can be obtained.

B.1.2 Proof of ***Lemma 3.2***

By conditioning on the number of users served by a generic BS such that $N_u = n$, when using RSA, the conditional probability that a BS uses any channel $s_i \in \mathcal{S}$ is

$$q_{c|n} = \frac{\binom{|\mathcal{S}|-1}{n-1}}{\binom{|\mathcal{S}|}{n}} = \begin{cases} \dfrac{n}{|\mathcal{S}|}, & n < |\mathcal{S}| \\ 1, & n \geq |\mathcal{S}|. \end{cases} \tag{B.3}$$

Therefore, the unconditional probability can be obtained as

$$q_c = \sum_{n=0}^{\infty} q_{c|n} \mathbb{P}\{N_u = n\} = \sum_{n=0}^{|\mathcal{S}|-1} \frac{n}{|\mathcal{S}|} \mathbb{P}\{N_u = n\} + \sum_{n=|\mathcal{S}|}^{\infty} \mathbb{P}\{N_u = n\}. \tag{B.4}$$

Using $\sum_{n=0}^{\infty} \mathbb{P}\{N_u = n\} = 1$ and since all channels are used with the same probability when adopting the RSA policy, the expressions of q_c^{RSA} and q_d^{RSA} in (3.8) can be easily verified.

B.1.3 Proof of ***Lemma 3.3***

When using PSA, each BS randomly and independently uses any channel $s_i \in \mathcal{S} \backslash \{s_d\}$ with the same probability. By following the same proof of **Lemma 3.2** in **Appendix B.1.2** while using the number of available channels to be $|\mathcal{S}| - 1$ instead of $|\mathcal{S}|$, the expression for the unconditional probability q_c in (3.9) can be easily obtained. Note that, the last term of the summation is zero when $n = |\mathcal{S}| - 1$.

Channel s_d is used only when the BS has no other channels to use, i.e., when the number of cellular users associated to that BS is greater than $|\mathcal{S}| - 1$. Hence,

$$q_d = \mathbb{P}\{N_u \geq |\mathcal{S}|\} \tag{B.5}$$

which is equivalent to (3.10).

B.2 Proof of Lemma 3.4

Here, I present the proof when s_d is a downlink channel where the same proof follows for the uplink case. For a generic D2D transmitter in the origin $(0,0) \in \mathbb{R}^2$, firstly, I obtain the distribution of the number of BSs that use s_d in the protection region $\mathcal{R}(\zeta)$ defined in (3.2). Using the thinning operation on the PPP of the BSs $\mathbf{\Phi}$, the BSs that use the D2D channel s_d can be modeled by a homogenous PPP $\tilde{\mathbf{\Phi}}(s_d)$ with spatial density $\lambda_b' = q_d \lambda_b$. Let $N_{\mathcal{R}(\zeta)}$ be defined as the number of BSs that use s_d in the protection region $\mathcal{R}(\zeta)$.

Since the BSs that use the D2D channel constitute a PPP, the number of BSs in $\mathcal{R}(\zeta)$ from $\tilde{\mathbf{\Phi}}(s_d)$ is a Poisson-distributed random variable with parameter $\lambda_b' \times L(\mathcal{R}(\zeta))$ as presented in (1.1), i.e., $N_{\mathcal{R}(\zeta)} \sim \text{Poisson}(\lambda_b' \times L(\mathcal{R}(\zeta))$, where

$$L(\mathcal{R}(\zeta)) = \mathbb{E}\left[\pi r_P^2\right] = \pi \left(\frac{P_b}{\zeta}\right)^{\frac{2}{\alpha}} \zeta \left(\frac{\alpha+2}{\alpha}\right). \tag{B.6}$$

By definition, I obtain

$$p_f = \mathbb{P}\{N_{\mathcal{R}(\zeta)} = 0\} = \exp[-\lambda_b' \, \nu(\mathcal{R}(\zeta))]. \tag{B.7}$$

For the uplink case, p_f follows by using the $\frac{2}{\alpha}$-th moment of the transmit power of a cellular user, i.e., $\mathbb{E}\left[P_u^{\frac{2}{\alpha}}\right] = \frac{\rho_b^{\frac{2}{\alpha}}}{\pi \lambda_b}$ when using channel inversion uplink power control which will be derived in Chapter 4.

B.3 Proof of Lemma 3.5

Here, I derive the distribution of the aggregate interference power received at a generic D2D transmitter located at the origin $(0,0) \in \mathbb{R}^2$ by calculating its Laplace transform. That is,

$$\mathcal{L}_{P_{\mathrm{H}}}(s) = \mathcal{L}^{\mathrm{D}}_{P_{\mathrm{H}}}(s)\, \mathcal{L}^{\mathrm{U}}_{P_{\mathrm{H}}}(s) \tag{B.8}$$

where the superscripts D and U refer to the downlink and uplink channels as presented in (3.1) by the first and second terms, respectively.

Firstly, I start by obtaining $\mathcal{L}^{\mathrm{D}}_{P_{\mathrm{H}}}(s)$ for the downlink subset of channels $\mathcal{S}^{\mathrm{D}}$ as

$$\begin{aligned}\mathcal{L}^{\mathrm{D}}_{P_{\mathrm{H}}}(s) &= \mathbb{E}_{\tilde{\mathbf{\Phi}},\{h\}}\left[\exp\left[-saP_b \sum_{x\in\tilde{\mathbf{\Phi}}}\sum_{s\in\int_{\Gamma}} h(x,0) R_i^{-\alpha}\right]\right] \\ &\overset{(a)}{=} \mathbb{E}_{\tilde{\mathbf{\Phi}}}\left[\prod_{x\in\tilde{\mathbf{\Phi}}}\left(\frac{1}{1+saP_bR_i^{-\alpha}}\right)^{|\mathcal{S}^{\mathrm{D}}|}\right]\end{aligned} \tag{B.9}$$

where (a) follows because of the independence assumption of Rayleigh fading and by using the moment generating function of an exponential random variable. By using the probability generating functional of a PPP, I obtain

$$\begin{aligned}\mathcal{L}^{\mathrm{D}}_{P_{\mathrm{H}}}(s) &= \exp\left[-2\pi q_c^{\mathrm{D}}\lambda_b \int_0^{\infty}\left(1-\left(\frac{1}{1+saP_br^{-\alpha}}\right)^{|\mathcal{S}^{\mathrm{D}}|}\right) r\,\mathrm{d}r\right] \\ &\overset{(b)}{=} \exp\left[-\frac{2\pi q_c^{\mathrm{D}}\lambda_b}{\alpha}(saP_b)^{\frac{2}{\alpha}}\int_0^1 \frac{1-u^{|\mathcal{S}^{\mathrm{D}}|}}{(1-u)^{1+\frac{2}{\alpha}}}u^{\frac{2}{\alpha}-1}\,\mathrm{d}u\right] \\ &\overset{(c)}{=} \exp\left[-\kappa_1 s^{\frac{2}{\alpha}}\right]\end{aligned} \tag{B.10}$$

where κ_1 is defined in (3.18) and q_c^{D} is given in (3.8) and (3.9) for the RSA and PSA

policies, respectively, by using $|\mathcal{S}^{\mathrm{D}}|$. In addition, (b) follows by replacing $u = \frac{1}{1+sP_b r^{-\alpha}}$ and (c) follows from the definition of Gamma function.

Unlike the downlink network in which a BS can establish up to $|\mathcal{S}^{\mathrm{D}}|$ transmissions over many channel, each user in the uplink network can establish only one connection using only one of the $\mathcal{S}^{\mathrm{U}}$ channels. Therefore, I define a point process $\hat{\mathbf{\Psi}} = \bigcup_{s\in\mathcal{S}^{\mathrm{U}}} \tilde{\mathbf{\Psi}}(s)$ with spatial density $q_c^{\mathrm{U}}|\mathcal{S}^{\mathrm{U}}|\lambda_b$ that represents all the transmitting cellular users. Note that the spatial density of this point process is calculated based on the fact that each BS receives only up to $|\mathcal{S}^{\mathrm{U}}|$ transmissions at any time. Hence, the average number of uplink transmissions received by a BS is equal to $\sum_{n=0}^{\infty} \min\{n, |\mathcal{S}^{\mathrm{U}}|\}\mathbb{P}\{N_u = n\} = q_c^{\mathrm{U}}|\mathcal{S}^{\mathrm{U}}|$ where q_c^{U} is obtained by **Lemma 3.2** (or **3.3**) after replacing $|\mathcal{S}|$ by $|\mathcal{S}^{\mathrm{U}}|$. Now, I obtain $\mathcal{L}^{\mathrm{U}}_{P_{\mathrm{H}}}(s)$ for the uplink subset of channels $\mathcal{S}^{\mathrm{U}}$ as follows

$$\begin{aligned}
\mathcal{L}^{\mathrm{U}}_{P_{\mathrm{H}}}(s) &= \mathbb{E}_{\hat{\mathbf{\Psi}}}\left[\prod_{u\in\hat{\mathbf{\Psi}}} \mathbb{E}_{P_u}\left[\frac{1}{1+saP_u R_i^{-\alpha}}\right]\right] \\
&\overset{(d)}{=} \exp\left[-2\pi q_c^{\mathrm{U}}|\mathcal{S}^{\mathrm{U}}|\lambda_b \int_0^{\infty} \mathbb{E}_{P_u}\left[\frac{r}{1+\frac{1}{saP_u}r^{\alpha}}\right] \mathrm{d}r\right] \\
&\overset{(e)}{=} \exp\left[-2\pi q_c^{\mathrm{U}}|\mathcal{S}^{\mathrm{U}}|\lambda_b a^{\frac{2}{\alpha}} s^{\frac{2}{\alpha}} \mathbb{E}_{P_u}\left[P_u^{\frac{2}{\alpha}}\right] \int_0^{\infty} \frac{u}{1+u}\,\mathrm{d}u\right] \\
&\overset{(f)}{=} \exp\left[-\frac{2\pi q_c^{\mathrm{U}}|\mathcal{S}^{\mathrm{U}}|(a\rho_b)^{\frac{2}{\alpha}}}{\alpha \sin\left(\frac{2\pi}{\alpha}\right)} s^{\frac{2}{\alpha}}\right] \\
&= \exp\left[-\kappa_2 s^{\frac{2}{\alpha}}\right] \qquad \text{(B.11)}
\end{aligned}$$

where κ_2 is defined in (3.19) and (d) follows by using the probability generating functional of a PPP and the m-th moment of the user's transmit power. Note that $\hat{\mathbf{\Psi}}$ is not a PPP where this assumption will be validated by simulations in Section 3.6. (e) follows by replacing $u = \frac{1}{1+sP_b r^{-\alpha}}$ and (f) follows by the $\frac{2}{\alpha}$-th moment of the transmit power of a cellular user.

Using (B.8), (B.10), and (B.11), I obtain the Laplace transform of the PDF of the aggregate received interference as

$$\mathcal{L}_{P_{\mathrm{H}}}(s) = \exp[-\kappa_3 s^{\frac{2}{\alpha}}]$$

where

$$\kappa_3 = \kappa_1 + \kappa_2.$$

Now, I derive the CDF of the harvested power using the inverse Laplace transform method. Specifically, I use the Bromwich inversion theorem with the modified contour defined in [103, Chapter 2]. Hence,

$$\begin{aligned} F_{P_{\mathrm{H}}}(t) &\overset{(g)}{=} \frac{1}{2\pi i} \lim_{T\to\infty} \int_{\zeta-iT}^{\zeta+iT} \exp\left[st - \kappa_3 s^{\frac{2}{\alpha}}\right] \frac{\mathrm{d}s}{s} \\ &\overset{(h)}{=} 1 - \frac{1}{2\pi i} \int_0^{\infty} e^{-ut} \left(e^{\kappa_3(-u)^{\frac{2}{\alpha}}} - e^{-\kappa_3(-u)^{\frac{2}{\alpha}}}\right) \frac{\mathrm{d}u}{u} \end{aligned} \tag{B.12}$$

where (h) follows because the integrand in (g) has a branch point at the origin. Then, according to the definition of p_s and by using the expression for P_d, (3.20) can be easily verified. For the detailed derivations of (h) refer to the auxiliary appendix in [101].

B.4 Proof of Theorem 3.1

By definition, I obtain the complementary CDF of the SINR_D as

$$\begin{aligned} \mathbb{P}\left[\mathrm{SINR}_D > \tau\right] &= \mathbb{P}\left[h_{y_0} > \tau \frac{\mathcal{I}_C + \mathcal{I}_D + \sigma^2}{\rho_d}\right] \\ &\overset{(i)}{=} \exp\left[\frac{-\tau\sigma^2}{\rho_d}\right] \mathcal{L}_{\mathcal{I}_C}\left(\frac{\tau}{\rho_d}\right) \mathcal{L}_{\mathcal{I}_D}\left(\frac{\tau}{\rho_d}\right) \end{aligned} \tag{B.13}$$

where (i) follows because the channel fading coefficient $h(y_\circ, 0) \sim \text{Exp}(1)$ while $\mathcal{L}_{\mathcal{I}_C}$ and $\mathcal{L}_{\mathcal{I}_D}$ are the Laplace transforms of the PDF of the aggregate interference resulting from, respectively, the cellular and D2D transmissions, evaluated at $\frac{\tau}{\rho_d}$.

For the Laplace transform of the PDF of $\mathcal{I}_D$, by following the proof of **Lemma** 3.5 in **Appendix B.3** when $|\mathcal{S}| = 1$, I obtain

$$\mathcal{L}_{\mathcal{I}_D}\left(\frac{\tau}{\rho_d}\right) = \exp\left[-\frac{2\pi^2 d_0^2 p_s p_f \lambda_d}{\beta \sin\left(\frac{2\pi}{\beta}\right)} \tau^{\frac{2}{\beta}}\right]. \tag{B.14}$$

For $\mathcal{I}_C$, since the D2D transmitters use spectrum sensing before transmission, the nearest interfering macrocell BS (or cellular user) when s_d is a downlink (or uplink) channel is at least at a distance of $\bar{r}_P$ from the intended D2D receiver where $\bar{r}_P$ is given in (3.4) (or (3.5)). Note that in order to protect the D2D transmissions, the protection region should be centered around the receiver rather than the transmitter. However, for simplicity, I assume that the protection region is centered around the D2D transmitter while the maximum separation between the transmitter and the receiver $d_\circ << \bar{r}_P$ so that the D2D receiver is well protected by the cognition performed by its corresponding transmitter. Hence, by following (B.9) I obtain

$$\mathcal{L}_{\mathcal{I}_C}(s) = \exp\left[-2\pi q_d \lambda_b \int_{\bar{r}_P}^{\infty} \mathbb{E}_P\left[\frac{r}{1+\frac{1}{sP} r^\alpha}\right] \mathrm{d}r\right] \tag{B.15}$$

where P is the transmit power P_b of a BS, when s_d is a downlink channel, otherwise, P is the transmit power P_u of a cellular user.

Now, by replacing $\frac{1}{sP} r^\alpha$ with u^α and $\bar{r}_P = \left(\frac{P}{\zeta}\right)^{\frac{1}{\alpha}} \zeta\left(1+\frac{1}{\alpha}\right)$, I obtain

$$\mathcal{L}_{\mathcal{I}_C}(s) = \exp\left[-2\pi q_d \lambda_b \mathbb{E}[P^{\frac{2}{\alpha}}] s^{\frac{2}{\alpha}} \int_{\left(\frac{1}{\zeta s}\right)^{\frac{1}{\alpha}} \zeta\left(1+\frac{1}{\alpha}\right)}^{\infty} \frac{u}{1+u^\alpha}\right] \mathrm{d}u. \tag{B.16}$$

By combining (B.13), (B.14), and (B.16), I obtain the SINR outage probability $\mathcal{O}_D(\tau)$ of a typical D2D receiver.

B.5 Proof of Theorem 3.2

To calculate the outage of cellular downlink and uplink transmissions, I use an approach similar to that in **Appendix B.4** for the proof of **Theorem 3.1**. Note that for $\mathcal{I}_D$, the interfering D2D transmitters can be arbitrarily close to the tagged receiver (macrocell BS in uplink or cellular user in downlink) and there is no protection region. For the cellular interference in downlink, since each user associates with the closest BS, no interfering BS can be closer to the tagged user than the serving BS. For the interference in the uplink, with the channel inversion power control, the closest interferer to the tagged BS is at lease at a distance $(\frac{P_u}{\rho_b})^{\frac{1}{\alpha}}$. Based on the aforementioned facts, the Laplace transform of the PDF of $\mathcal{I}_D$ is the same as in (B.14) and evaluated at $\frac{\tau}{P_b r^{-\alpha}}$ for downlink and at $\frac{\tau}{\rho_b}$ for uplink. On the other hand, that of $\mathcal{I}_C$ can be obtained by following **Appendices B.3** and **B.4** while using the protection radius defined earlier.

Then, knowing that the distribution of the distance between a generic cellular user and her serving BS is Rayleigh, i.e., $f_R(r) = 2\pi\lambda_b\, r \exp\left[-\pi\lambda_b r^2\right]$, using (3.30), the outage probability can be easily verified.

Appendix C

C.1 Proof of Lemma 4.1

Here, I derive the distribution of the amount of power received at a user device located at the origin $(0,0) \in \mathbb{R}^2$ by calculating its Laplace transform. This approach is similar to **Appendix B.3**. Firstly, I redefine the amount of power harvested at the typical user as

$$P_{\mathrm{H}} = \sum_{k=1}^{K} \mathcal{P}_k \tag{C.1}$$

where $\mathcal{P}_k$ is the amount of power harvested from the k-th tier as given by

$$\mathcal{P}_k = a \sum_{x \in \Psi_k} P_k h(x,0) \|x\|^{-\alpha}. \tag{C.2}$$

Then, I obtain the Laplace transform of the PDF of P_{H} so that its CDF can be obtained by inverse Laplace transform. The Laplace transform of the PDF of P_{H} using that of the PDF of $\mathcal{P}_k$ as follows.

$$\mathcal{L}_{P_{\mathrm{H}}}(s) = \prod_{k=1}^{K} \mathcal{L}_{\mathcal{P}_k}(s). \tag{C.3}$$

By definition,

$$\begin{aligned}\mathcal{L}_{\mathcal{P}_k}(s) &= \mathbb{E}\left[\exp\left[-s\mathcal{P}_k\right]\right] \\ &\overset{(a)}{=} \mathbb{E}_{\mathbf{\Phi}_k}\left[\prod_{x\in\mathbf{\Phi}_k}\mathbb{E}_{\{h\}}\left[\exp\left[-saP_k h(x,0)R_i^{-\alpha}\right]\right]\right] \\ &\overset{(b)}{=} \mathbb{E}_{\mathbf{\Phi}_k}\left[\prod_{x\in\mathbf{\Phi}_k}\frac{1}{1+saP_kR_i^{-\alpha}}\right] \\ &\overset{(c)}{=} \exp\left[-2\pi\lambda_k\int_0^\infty \frac{r}{1+\frac{1}{saP_k}r^\alpha}\,\mathrm{d}r\right] \end{aligned} \tag{C.4}$$

where (a) follows because of the independence assumption of small-scale fading, while (b) follows from the use of the moment generating function of exponentially-distributed random variables, and (c) follows by using the probability generating functional of PPPs.

After some mathematical manipulations and substituting $u^\alpha = \frac{1}{saP_k}r^\alpha$, I get

$$\mathcal{L}_{\mathcal{P}_k}(s) = \exp\left[-\frac{2\pi^2\lambda_k}{\alpha\sin\left(\frac{2\pi}{\alpha}\right)}(aP_k)^{\frac{2}{\alpha}}s^{\frac{2}{\alpha}}\right]. \tag{C.5}$$

Hence,

$$\mathcal{L}_{P_{\mathrm{H}}}(s) = \exp\left[-\frac{2\pi^2\xi a^{\frac{2}{\alpha}}}{\alpha\sin\left(\frac{2\pi}{\alpha}\right)}s^{\frac{2}{\alpha}}\right] \tag{C.6}$$

where

$$\xi = \sum_{k=1}^{K}\lambda_k P_k^{\frac{2}{\alpha}}.$$

In order to obtain the CDF, the inverse Laplace transform $\mathcal{L}_{P_{\mathrm{H}}}(s)$ is required. I use the complex inversion integral formula for Laplace transforms with $s = 0$ as a branch point of the integrand and the proper Bromwich contour that does not contain

this branch point. After some mathematical manipulations, the the expression for $F_{P_{\mathrm{H}}}(t)$ in (4.5) is obtained.

C.2 Proof of Lemma 4.2

By definition, the CDF of the user's transmit power can be obtained as

$$\begin{aligned} F_{\Gamma_k}(t) &= 1 - \mathbb{P}\left[\gamma_k > t\right] \\ &= 1 - \mathbb{P}\left[r_k > \left(\frac{t}{\rho_k}\right)^{\frac{1}{\alpha}}\right] \\ &\overset{(d)}{=} 1 - \exp\left[-\pi\Lambda\left(\frac{t}{\rho_k}\right)^{\frac{2}{\alpha}}\right], \quad t \geq 0 \end{aligned} \tag{C.7}$$

where (d) follows from (4.10). Then, the PDF of the uplink transmit power can be obtained by differentiation as follows

$$f_{\Gamma_k}(t) = \frac{\mathrm{d}}{\mathrm{d}t}[1 - \mathbb{P}\left[\gamma_k > t\right]]. \tag{C.8}$$

Finally, the $\frac{2}{\alpha}$-moment can be obtained using the definition of expectation of a random variable.

C.3 Proof of Theorem 4.1

By definition, I obtain the complementary CDF of the SIR_k as

$$\begin{aligned} \mathbb{P}\left[\mathsf{SIR}_k > \tau_k\right] &= \mathbb{E}\left[\mathbb{P}\left[h(u_\circ, 0) > \frac{\tau_k}{\rho_k}\sum_{j=1}^{K}\mathcal{I}_j\right]\right] \\ &\overset{(e)}{=} \prod_{j=1}^{K}\mathcal{L}_{\mathcal{I}_j}\left(\frac{\tau_k}{\rho_k}\right) \end{aligned} \tag{C.9}$$

where (e) follows the definition of Laplace transform and $\mathcal{I}_j$ is the aggregate interference resulting from users served by the j-th tier such that

$$\mathcal{I}_j = \sum_{u \in \tilde{\mathbf{\Psi}}_j \setminus \{u_\circ\}} \gamma_j h(u,0) \|u\|^{-\alpha}.$$

Let the distance between the closest interfering user from j-th tier $\tilde{\mathbf{\Psi}}_j$ to a generic BS from k-th tier $\mathbf{\Phi}_k$ be denoted by z and her transmit power is γ_j. It is known for sure that the average interference received at the BS from tier k is strictly less than ρ_j. Hence,

$$z > \left(\frac{\gamma_j}{\rho_j}\right)^{\frac{1}{\alpha}}. \tag{C.10}$$

Now, I use an approach similar to that presented in Section 1.5.2 to obtain the Laplace transform of the PDF of the interference from the j-th tier. By definition,

$$\begin{aligned}
\mathcal{L}_{\mathcal{I}_j}(s) &= \mathbb{E}_{\tilde{\mathbf{\Psi}}_j,\{h\},\gamma_j}\left[\exp\left[-s \sum_{u \in \tilde{\mathbf{\Psi}}_j \setminus \{u_\circ\}} \gamma_j h(u,0) R_i^{-\alpha}\right]\right] \\
&= \mathbb{E}_{\tilde{\mathbf{\Psi}}_j,\{h\},\gamma_j}\left[\prod_{u \in \tilde{\mathbf{\Psi}}_j \setminus \{u_\circ\}} \exp\left[-s\gamma_j h(u,0) R_i^{-\alpha}\right]\right] \\
&= \mathbb{E}_{\tilde{\mathbf{\Psi}}_j}\left[\prod_{u_i \in \tilde{\mathbf{\Psi}}_j \setminus \{u_\circ\}} \mathbb{E}_{\gamma_j}\left[\frac{1}{1+s\gamma_j R_i^{-\alpha}}\right]\right] \\
&= \exp\left[-2\pi\eta_j\lambda_j \int_z^\infty \mathbb{E}_{\gamma_j}\left[\frac{r}{1+\frac{1}{s\gamma_j}r^\alpha}\,\mathrm{d}r\right]\right]
\end{aligned} \tag{C.11}$$

where z is the distance to the closest interfering user defined in (C.10). Now, letting

$u^{\alpha_k} = \frac{1}{s\gamma_j} r^{\alpha_k}$, I obtain

$$\mathcal{L}_{\mathcal{I}_j}(s) = \exp\left[-2\pi\eta_j\lambda_j s^{\frac{2}{\alpha}}\mathbb{E}_{\gamma_j}\left[\gamma_j^{\frac{2}{\alpha}}\right]\int_{\left(\frac{1}{s\rho_j}\right)^{\frac{1}{\alpha}}}^{\infty}\frac{u}{1+u^{\alpha}}\,\mathrm{d}u\right]. \tag{C.12}$$

Note that the $\frac{2}{\alpha}$-moment is presented in 4.14.

By plugging (4.14) and (C.12) into (C.9), the expression for the coverage probability in 4.34 can obtain.

Appendix D

D.1 Proof of Lemma 5.1

For each tier k, I define $\tilde{\mathbf{\Phi}}_k = \{\beta_k^{\frac{2}{\alpha}} x : x \in \mathbf{\Phi}_k\}$. Using the mapping theorem [27, Theorem 2.34 and Corollary 2.35], I conclude that $\tilde{\mathbf{\Phi}}_k$ is a homogeneous PPP with spatial density $\beta_k^{-\frac{2}{\alpha}} \lambda_k$ since β_k is scalar. Using the superposition property of PPPs, I define the PPP $\hat{\mathbf{\Phi}}_k = \bigcup_{k=1}^{K} \tilde{\mathbf{\Phi}}_k$ which is homogeneous with spatial density $\sum_{j=1}^{K} \lambda_j \beta_j^{\frac{2}{\alpha}}$. Note that the association criterion defined in (5.2) is equivalent to associate with the nearest point in $\hat{\mathbf{\Phi}}_k$, hence, the distance distribution can be obtained by the null probability from a PPP with spatial density

$$\Lambda_k = \beta_k^{-\frac{2}{\alpha}} \sum_{j=1}^{K} \lambda_j \beta_j^{\frac{2}{\alpha}}$$

which is Rayleigh-distributed as given in (4.10).

D.2 Proof of Theorem 5.1

By definition of η_k given in (5.12), I have

$$\eta_k = \int_0^{\infty} F_{\Gamma_k}(t) f_{P_{\mathrm{H}}}(t) \, \mathrm{d}t \tag{D.1}$$

where $F_{\Gamma_k}(t)$ and $f_{P_{\mathrm{H}}}(t)$ can be obtained from (5.9) and (5.4), respectively. Given that $\alpha = 4$, after substitution I get

$$\begin{aligned}\eta_k &= 1 - \kappa_1 \int_0^\infty \frac{1}{\sqrt{t^3}} \exp\left[-\frac{\kappa_2}{t}\right] \exp\left[-\kappa_3\sqrt{t}\right] \mathrm{d}t \\ &\overset{(a)}{=} 1 - \kappa_1\kappa_3^3 \int_0^\infty G_{1,0}^{0,1}\Big(\frac{t}{\kappa_2}\Big|1\Big) G_{0,1}^{1,0}\Big(\kappa_3\sqrt{t}\Big| - 3\Big)\,\mathrm{d}t \end{aligned} \tag{D.2}$$

where

$$\begin{aligned}\kappa_1 &= \frac{\pi\sqrt{\pi a}\xi}{4} \\ \kappa_2 &= a\xi^2\left(\frac{\pi}{2}\right)^4 \\ \kappa_3 &= \frac{\pi\Lambda_k}{\sqrt{\rho_k}}.\end{aligned}$$

G is the Meijer G-function defined in [102]. (a) follows from

(i)

$$\exp(-u) = G_{0,1}^{1,0}(u|0).$$

(ii)

$$G_{0,1}^{1,0}(u|c) = G_{1,0}^{0,1}(u^{-1}|1-c).$$

(iii)

$$u^h G_{0,1}^{1,0}(u|c) = G_{0,1}^{1,0}(u|c+h).$$

By replacing $u = \kappa_3\sqrt{t}$ I get

$$\begin{aligned}\eta_k &= 1 - 2\kappa_1\kappa_3 \int_0^\infty G_{1,0}^{0,1}\Big(\frac{u^2}{\kappa_2\kappa_3^2}\Big|1\Big) G_{0,1}^{1,0}\Big(u\Big| - 2\Big)\,\mathrm{d}u \\ &\overset{(b)}{=} 1 - \frac{\kappa_1\kappa_3}{2\sqrt{\pi}} \int_0^\infty G_{1,0}^{0,1}\Big(\frac{u^2}{\kappa_2\kappa_3^2}\Big|1\Big) G_{0,2}^{2,0}\Big(\frac{u^2}{4}\Big| - 1, -\frac{1}{2}\Big)\,\mathrm{d}u\end{aligned}$$

$$\stackrel{(c)}{=} 1 - \frac{\kappa_1}{\sqrt{\pi\kappa_2}} G_{3,0}^{0,3}\Big(\frac{\kappa_2\kappa_3^2}{4}\Big|\, 0, \frac{1}{2}, \frac{1}{2}\Big) \tag{D.3}$$

where (b) follows from

$$G_{0,1}^{1,0}(u|c) = \frac{1}{4\sqrt{\pi}} G_{0,2}^{2,0}(\frac{u^2}{4}|\frac{c}{2}, \frac{c+1}{2})$$

and (c) follows from

$$\int_0^\infty G_{1,0}^{0,1}(hu|c) G_{0,2}^{2,0}(gu|m,n)\,\mathrm{d}u = \frac{1}{h} G_{0,3}^{3,0}(\frac{g}{h}|-c, m, n).$$

After minor mathematical manipulations, the results in (5.13) can be verified.

Appendix E

E.1 Proof of Association Probabilities and Distance Distribution

E.1.1 Proof of ***Lemma 6.1***

Firstly, I consider the case when a user associates to different BSs for downlink and uplink. A user associates to different BSs ($x^{\mathrm{DL}} \in \mathbf{\Phi}_j$ for downlink and $x^{\mathrm{UL}} \in \mathbf{\Phi}_k$ for uplink where $j \neq k$) under the following four conditions:

1. x^{UL} meets the criterion in (6.1) for the uplink, i.e.,

$$U_k \|x^{\mathrm{UL}}\|^{\alpha} < \min_{x \in \mathbf{\Phi}_i} U_i \|x\|^{\alpha} \quad \forall i \neq j, k.$$

2. x^{DL} meets the criterion in (6.2) for the downlink, i.e.,

$$D_j \|x^{\mathrm{DL}}\|^{\alpha} < \min_{x \in \mathbf{\Phi}_i} D_i \|x\|^{\alpha} \quad \forall i \neq j, k.$$

3. x^{DL} does not meet the criteria defined for the uplink in (6.1), i.e.,

$$U_j \|x^{\mathrm{DL}}\|^{\alpha} > U_k \|x^{\mathrm{UL}}\|^{\alpha}.$$

4. x^{UL} does not meet the criteria defined for the downlink in (6.2), i.e.,

$$D_k\|x^{\mathrm{UL}}\|^{\alpha} > D_j\|x^{\mathrm{DL}}\|^{\alpha}.$$

Using these four conditions and letting $R_j = \|x^{\mathrm{DL}}\|$ and $R_k = \|x^{\mathrm{UL}}\|$, the event that $j \neq k$ can be expressed as

$$\bigcap_{\substack{i=1\\ i\neq j,k}}^{K} \left\{ \min_{x\in\mathbf{\Phi}_i} \|x\| > \max\left\{\mathcal{D}_{ji}R_j^{\alpha}, \mathcal{U}_{ki}R_k^{\alpha}\right\}^{\frac{1}{\alpha}} \middle| \mathcal{D}_{jk}^{\frac{1}{\alpha}}R_j < R_k < \mathcal{U}_{jk}^{\frac{1}{\alpha}}R_j \right\}. \tag{E.1}$$

Hence,

$$\begin{aligned}
\psi_{jk} &\overset{(a)}{=} \mathbb{E}\left[\exp\left[-\pi \sum_{\substack{i=1\\ i\neq j,k}}^{K} \max\left\{\mathcal{D}_{ji}R_j^{\alpha}, \mathcal{U}_{ki}R_k^{\alpha}\right\}^{\frac{2}{\alpha}} \lambda_i \right] \middle| \mathcal{D}_{jk}^{\frac{1}{\alpha}}R_j < R_k < \mathcal{U}_{jk}^{\frac{1}{\alpha}}R_j \right] \\
&\overset{(b)}{=} 4\pi^2\lambda_j\lambda_k \int_0^{\infty} \int_{\mathcal{D}_{jk}^{\frac{1}{\alpha}}u}^{\mathcal{U}_{jk}^{\frac{1}{\alpha}}u} uv \exp\left[-\pi \sum_{i=1}^{K} \max\{\mathcal{D}_{ji}u^{\alpha}, \mathcal{U}_{ki}v^{\alpha}\}^{\frac{2}{\alpha}} \lambda_i \right] \mathrm{d}v\, \mathrm{d}u \\
&= 2\lambda_j\lambda_k \int_{\mathcal{D}_{jk}^{\frac{1}{\alpha}}}^{\mathcal{U}_{jk}^{\frac{1}{\alpha}}} x \left(\sum_{i=1}^{K} \lambda_i \max\left(\mathcal{D}_{ji}^{\frac{2}{\alpha}}, \mathcal{U}_{ki}^{\frac{2}{\alpha}}x^2 \right) \right)^{-2} \mathrm{d}x
\end{aligned} \tag{E.2}$$

where (a) follows from: (i) the fact that the minimum distance to a BS from a PPP $\mathbf{\Phi}_i$ is Rayleigh-distributed with CDF $\mathbb{P}\left[\min_{x\in\mathbf{\Phi}_i}\|x\| \leq t\right] = 1 - \exp[-\pi\lambda_i t^2]$ and (ii) independence assumption for network tiers, (b) follows since the expectation in (a) is with respect to R_j and R_k which denote the distances to the serving BSs. Note also that $\psi_{jk} = 0$ when $k > j$ due to **Assumption 6.1** where network tiers are ordered such that $\mu_i < \mu_{i+1}$.

For the case when $j = k$, using (6.1) and (6.2) and following a similar procedure, the probability of the event where $x^{\mathrm{DL}} = x^{\mathrm{UL}} = x_{\circ}$ given that $x_{\circ}$ belongs to the j-th

tier can be expressed as

$$\psi_{jj} = \mathbb{E}\left[\exp\left[-\pi \sum_{\substack{i=1 \\ i\neq j}}^{K} \max\{\mathcal{D}_{ji}, \mathcal{U}_{ji}\}^{\frac{2}{\alpha}} \lambda_i R_j^2\right]\right]. \tag{E.3}$$

Hence, the result in (6.3) can be then verified.

E.1.2 Proof of ***Lemma 6.4***

Following the procedure in **Lemma 6.1**, the joint CDF of the distance can be obtained by adding two more conditions such that $R_j > r_j$ and $R_k > r_k$. Then, the joint PDF can be obtained by differentiation. $\mathbb{E}[R_j^m R_k^n]$ follows the definition of the expected value.

E.2 Proof of Mean Interference

E.2.1 Proof of ***Lemma 6.6***

Following the definition in (6.17), $g_2(r)$, and $g_3(r)$, I have

$$\begin{aligned}
&\mathbb{E}\left[\mathcal{I}^{\mathrm{UL}}\right] \\
&\overset{(c)}{=} \sum_{i=1}^{K} 2\pi\lambda_i \left(\frac{P_i}{G_b}\int_{d_b}^{\infty} \frac{1-\exp\left[-\pi\Lambda_i^{\mathrm{DL}} r^2\right]}{r^{\alpha_b - 1}}\,\mathrm{d}r + \mathbb{E}_{R_i}\left[\frac{\min\{\rho_i G^{\epsilon} R_i^{\epsilon\alpha}, P_{\max}\}}{G}\int_{\mathcal{U}_{ik}^{\frac{1}{\alpha}} R_i}^{\infty} r^{1-\alpha}\,\mathrm{d}r\right]\right) \\
&= \sum_{i=1}^{K} 2\pi\lambda_i \left(\frac{\mathcal{K}_1(d_b, \alpha_b, \Lambda_i^{\mathrm{DL}})}{G_b} P_i + \frac{\mathcal{U}_{ik}^{\frac{2-\alpha}{\alpha}}}{G(\alpha-2)} \mathbb{E}_{R_i}\left[\min\left\{\rho_i R_i^{\epsilon\alpha}, P_{\max}\right\} R_i^{2-\alpha}\right]\right)
\end{aligned} \tag{E.4}$$

where (c) follows from Campbell's Theorem [28] knowing that the distance R from the tagged BS to the closest interfering user from tier i is greater than $\mathcal{U}_{ik}^{\frac{1}{\alpha}} R_i$ (i.e.,

$U_i R_i^{\alpha} < U_k R^{\alpha}$). Following **Lemma 6.3**, I obtain

$$\mathbb{E}_{R_i}\left[\min\left\{\rho_i G^{\epsilon} R_i^{\epsilon\alpha}, P_{\max}\right\} R_i^{2-\alpha}\right] = \rho_i \mathcal{K}_2(i) \tag{E.5}$$

E.2.2 Proof of ***Lemma 6.7***

Following the definition in (6.16), $g_1(r)$, and $g_4(r)$, I have

$$\mathbb{E}\left[\mathcal{I}^{\mathrm{DL}}\right] \overset{(d)}{=} \sum_{i=1}^{K} 2\pi\lambda_i \left(\frac{P_i}{G} \int_{\mathcal{D}_{ji}^{\frac{1}{\alpha}} R_j}^{\infty} r^{1-\alpha}\, \mathrm{d}r + \frac{\mathbb{E}_{R_i}\left[\Gamma_i\right]}{G_u} \int_{d_u}^{\infty} \frac{1-\exp\left[-\pi\Lambda_i^{\mathrm{UL}} r^2\right]}{r^{\alpha_u - 1}}\, \mathrm{d}r \right) \tag{E.6}$$

where (d) follows from the fact that $D_i R^{\alpha} > D_j R_j^{\alpha}$ and the spatial density of interfering users is $\lambda_i(1-\exp[-\pi\frac{\lambda_i}{A_i^{\mathrm{UL}}} r^2])$. Moreover, (6.29) is obtained from (6.18) such that $\mathbb{E}\left[\mathcal{I}_{\mathrm{SI}}^{\mathrm{DL}}\right] = \varepsilon_u \mathbb{E}\left[\Gamma_k\right]$.

E.3 Proof of Theorem 6.1

By combining (6.22), (6.23), (6.27), **Lemma 6.6**, and **Lemma 6.7** and rearranging all terms, I have

$$\bar{\mathcal{R}} = \sum_{j=1}^{K}\sum_{k=1}^{K} \psi_{jk}\left(\mathbb{E}_{\mathbf{R}}[\ln \mathcal{R}_{jk}^{\mathrm{UL}}] + \mathbb{E}_{\mathbf{R}}[\ln \mathcal{R}_{jk}^{\mathrm{DL}}]\right) \tag{E.7}$$

$$\begin{aligned} &= \ln \mathcal{R}_o^{\mathrm{DL}} + \ln \mathcal{R}_o^{\mathrm{UL}} - \tau^{\mathrm{UL}} G \sum_{k=1}^{K} \frac{\sigma_{b_k} P_k + \mathcal{A}_3(k)}{\rho_k G^{\epsilon}} \sum_{j=1}^{K} \psi_{jk} \mathbb{E}_{\mathbf{R}}\left[\frac{R_k^{\alpha}}{\min\{R_k^{\epsilon\alpha}, \frac{P_{\max}}{\rho_k G^{\epsilon}}\}}\right] \\ &- \tau^{\mathrm{DL}} G \sum_{j=1}^{K} \frac{\mathcal{A}_1(j)}{P_j} \sum_{k=1}^{K} \psi_{jk} \mathbb{E}_{\mathbf{R}}\left[R_j^2\right] - \tau^{\mathrm{DL}} G \sum_{j=1}^{K} \frac{1}{P_j} \sum_{k=1}^{K} \psi_{jk}(\sigma_u \mathbb{E}[\Gamma_k] + \mathcal{A}_2) \mathbb{E}_{\mathbf{R}}\left[R_j^{\alpha}\right] \end{aligned} \tag{E.8}$$

where the expectation is with respect to the distance to the serving BS(s) (i.e., downlink and uplink). Hence, using **Lemmas 6.3** and **6.4**, the expressions in **Theorem 6.1** can be verified.